Organisation of the

Initiation of DNA Replication

Rosemary Helen Clare Wilson

Thesis submitted for the degree of PhD

The University of York

Department of Biology

July 2013

Abstract

Multiple lines of evidence show that DNA replication and the proteins involved with its preparation reside at the nuclear matrix (NM). Some of these, such as cyclin E, are recruited to the NM during differentiation, implying that NM attachment may help to fix cell-type specific replication programmes, and potentially therefore restrict plasticity. However, our understanding of the interplay between the NM, the cell cycle and cell type is still limited. The aim of this PhD is to develop our understanding of the NM in relation to the preparation for DNA replication.

The function of the replication-promoting and cancer-associated NM protein CIZ1 was investigated using cells derived from a CIZ1-/- mouse. Dysregulated cyclin and CDKi expression and immobilisation suggest that CIZ1 has a widespread role as a cell cycle regulator with an exchange function that is consistent with previous analysis of its interaction with cyclin E and A. More importantly, in the absence of CIZ1, the DNA damage response is activated as cells receive growth inhibition signals, leading to the formation of foci outgrowths (and lymphoid malignancies in the animal). Together with published data, this suggests a tumour suppressor role for CIZ1. This also implies that different forms of CIZ1 have tumour suppressor or promoting roles and that the balance between these may be critically important for proper integration of growth control signals.

CIZ1 has also previously been implicated in chromatin loop organisation during G1-phase. My analysis of NM attached chromatin loops during cell cycle re-entry from quiescence shows that average chromatin loop size is smaller in quiescence but recovers in size in a very early, growth factor-independent step during G1. Moreover, chromatin loops were also found to become larger and more unstable following controlled transformation, correlating with changes in CIZ1 expression. This suggests weaker attachment of DNA in cancer cells and mirrors the lack of attachment of cyclin E and CIZ1.

These data support the hypothesis that loss of NM attachment is a feature of cancer cells and were collected using novel methods developed and validated during this project that allow rapid, non-subjective computer measurement of chromatin loops.

Table of Contents

List of Figures

Chapter 1

Chapter 3

Chapter 4

Chapter 5

Chapter 6

List of Tables

Chapter 1

Chapter 2

Chapter 3

List of Appendices

Acknowledgements

Firstly I want to thank my supervisor Dawn Coverley for taking me on as a PhD student and for her constant support, encouragement, advice and inspiration. I also want to thank Justin Ainscough for involving me in his CIZ1 knock-out project, my TAP panel members Debbie Smith and James Chong for their help and support, and all the past and present members of the Coverley lab, especially Gill, Nik, Jenny, Katherine and Emma for their wise suggestions and ideas, and for giggles and cake. Thanks also to other York PhD students, friends elsewhere, and particularly my housemates; Ed, Adam and Noelía, for keeping me sane – much appreciated!

I would like to thank the BBSRC for funding this research, the BSCB for grants to attend conferences, Celina Walley and Peter Ashton from the Genomics facility for invaluable help with preparation and analysis of MAR samples, Peter O'Toole, Karen Hodgkinson, Karen Hogg and Graeme Park from the Imaging & Cytometry facility for invaluable advice with flow cytometry, Phil Roberts for making some lovely chromatin loop pictures, Nick Grayson, Roger Leigh and Nick McEntyre for help with writing the HIM ImageJ macro, Juan Méndez for providing a protocol for DAPI halo, Fiona Frame and Jenny Hinley for advice and help with reagents, Elizabeth Klakus and Amanda Collier, two summer students I supervised, who helped with some experiments and Jenny Munkley, John Knight, Vicki Moignard and Laura Knight for discussion of their unpublished data.

I would also like to thank the following people for kindly providing cells and cell lines for this work; Justin Ainscough, University of Leeds, Juan Funes and Chris Boshoff, University College London, Yan Geng and Peter Sicinski, Dana-Farber Cancer Institute, Harvard, Ian Wood, University of Leeds, Jo Milner, William Brackenbury, Dimitris Lagos, Edward Bowen and Jenny Southgate, University of York and Ronald Laskey, Hutchinson/MRC Research Centre, Cambridge.

Last but not least, I would like to thank my parents for their unending encouragement and support in everything I do and to my boyfriend Nick for just generally being lovely and for making me smile.

Declaration

All the research in this thesis is my own with the following exceptions:

Figures 1.5, 6.1 and 6.2 were designed by me but drawn by Phil Roberts, Biology Graphics department, University of York and published in Wilson and Coverley, 2013.

Figure 3.3 A: transfection of cells with EGFP-CIZ1 C-term274 performed by Nikki Copeland.

Figure 3.8 C: raw MFHR images were previously collected by Laura Knight.

Figure 3.15 H: Bioanalyzer analysis undertaken by Celina Walley.

Figure 3.16: generated in collaboration with Peter Ashton, Genomics department, University of York.

Figure 4.4/6: MFHR of RT4, RT112, EJ and MCF7 cells undertaken with Amanda Collier.

Chapter 5: CIZ1+/+, -/- cells generated by Justin Ainscough, University of Leeds.

Appendix A: Data generated by Laura Knight.

Appendix B: Map and data generated by Justin Ainscough, University of Leeds.

Appendix D: Data and manuscript generated by Jennifer Munkley, myself, Emma Hesketh, Heather Sercombe, Elizabeth Klakus, Jennifer Southgate, Justin Ainscough and Dawn Coverley.

Published sections

- The following sections have previously been published within a review, which is included at the end of the thesis, entitled;

  Wilson, R.H., and Coverley, D. (2013). Relationship between DNA replication and the nuclear matrix. Genes Cells *18*, 17-31.

  Sections 1.1.7, 1.2, 1.3 (1.3.1-1.3.4), 1.4 (1.4.1-1.4.10), 1.5, 6.2.1-6.2.3
  Figures 1.4, 1.5, 6.1, 6.2.

- A detailed description of methods for nuclear matrix fractionation for immunofluorescence and immunoblot analysis, referenced within Chapter 2: Materials and Methods, is also included at the end of this thesis. This has been submitted as an invited chapter for a Cold Spring Harbour Press book entitled Subnuclear Fractionation. The chapter comprises a topic introduction and protocol that will also be published separately in Cold Spring Harbour Protocols.

  Wilson, R.H.C., Hesketh, E.L., and Coverley, D. The nuclear matrix: preparation for microscopy and biochemical analysis

  Wilson, R.H.C., Hesketh, E.L., and Coverley, D The nuclear matrix: fractionation techniques and analysis (Topic introduction)

  Wilson, R.H.C., Hesketh, E.L., and Coverley, D The nuclear matrix: preparation protocol for parallel microscopy and biochemical analysis (Protocol)

1 Introduction

1 Introduction

The overall aim of my project was to increase the understanding of events during the preparation for initiation of DNA replication, with particular attention to the nuclear matrix (NM) and the NM binding protein CIZ1.

The importance of accurate cell cycle progression and high fidelity of DNA replication is evidenced by their multiple links with the development of cancer. Despite a dramatic increase in the understanding of the cell cycle and its control during the 30 years since its discovery (Evans et al., 1983; Pines and Hunt, 1987), many questions remain. Numerous reviews have been published concerning features of the cell cycle (for example, Bell and Dutta, 2002; Blow, 2001; Diffley and Labib, 2002; Murray, 2004; Sclafani and Holzen, 2007; Sherr and Roberts, 1995, 1999; Vermeulen et al., 2003). By increasing our understanding of mechanisms occurring within the 'normal' cell cycle we have a greater chance of understanding the changes that occur in cancer cells and in doing so, discover new ways to detect or treat disease.

Many nuclear processes, including DNA replication, appear to occur at the NM, though probably not in all cell types. The notion that this may help to restrict processes to specific areas of the nucleus making them more efficient by creating locally high concentrations of required factors is attractive. However, despite an initial burst of papers in the 1970-80s, the NM has been an under-researched area of cell biology marred by strongly held but conflicting opinions.

Evidence suggests that cancer cells exhibit changes in their NM. The potential impact of this on the cell, including the effect on the cell cycle, is largely still unknown but warrants some detailed attention. This introduction will cover the relevant features of the cell cycle, the NM and attachment of DNA and replication proteins to the NM. Information that is more relevant to specific chapters can be found in their individual introductions. The majority of this introduction has been published as a review entitled 'Relationship between DNA replication and the nuclear matrix' (Wilson and Coverley, 2013).

1.1 The cell cycle

The cell cycle consists of four phases (fig 1.1): growth 1 (G1-phase) during which the cell receives signals from its environment and prepares for DNA replication, DNA synthesis (S-phase) when the cell replicates its entire DNA content, growth 2 (G2-phase) with further protein synthesis and preparation for division and finally mitosis (M-phase), when the cell divides into two identical daughter cells. Each daughter cell then proceeds into G1-phase again. Cells which are constantly dividing, albeit at different rates, include cells of the embryo and some stem cells such as those at the base of intestinal crypts and in hair follicles. However, the majority of the cells in adult animals are said to be in quiescence (G0). This is a state somewhat similar to G1, usually with 2n DNA content. However, the cell is not actively dividing but crucially, can be stimulated to return to a dividing state. The transition from quiescence, through G1-phase to S-phase will be the focus of this project.

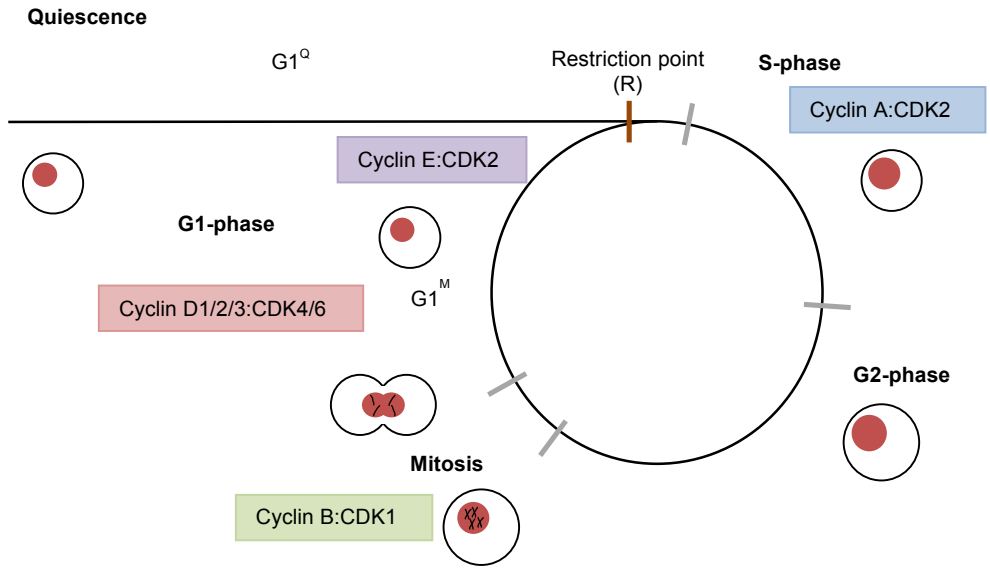

Figure 1.1: Schematic showing phases of the cell cycle including quiescence. Highlighted are the state of the cell at each phase and key cyclin:CDK complexes.

1.1.1 Key features of the cell cycle

The established view of the cell cycle is that cyclins are periodically and sequentially expressed (Evans et al., 1983; and reviewed in Pines, 1991), and when present bind to and activate constitutively expressed cyclin-dependent kinases (CDKs). Cyclin-CDK complexes can then phosphorylate substrates at serines and/or threonines on target proteins activating or inhibiting their function and influencing cell cycle progression (reviewed in Bloom and Cross, 2007; Hochegger et al., 2008; Moroy and Geisen, 2004). Cyclins are believed to target CDK activity temporally, spatially and in terms of substrate specificity (reviewed in Darzynkiewicz et al., 1996; Pines, 1999), offering refined and precise levels of control.

Mitogen signalling from extracellular growth factors stimulates cyclin D expression, which is transported into the nucleus during G1 phase (Baldin et al., 1993). Cyclin D1/2/3 interact with CDK4/6, and the phosphorylation of their targets helps to de-repress expression of genes required for cell cycle progression. For example, a major target is the pocket protein, retinoblastoma (RB), which in its hypophosphorylated state at the beginning of G1 binds to and inhibits the transcriptional promoting activity of E2F proteins (Buchkovch et al., 1989; Honda et al., 2005; Kato et al., 1993 and reviewed in Assoian and Zhu, 1997; Moroy and Geisen, 2004). Phosphorylation of Rb and de-repression of E2F leads to expression of cyclin E; levels rise during mid G1, at the time of the restriction point (R) (Ekholm et al., 2001; Ohtsubo et al., 1995). At R, cells commit to DNA replication, and are then no longer dependent on mitogenic signalling (Pardee, 1974). Cyclin E interacts with CDK2 and helps to de-repress gene expression as well as interacting with the pre-replication complex (pre-RC) at origins of replication (Ekholm et al., 2001; Koff et al., 1991; Ohtsubo et al., 1995). Cyclin A is expressed after cyclin E, immediately before and during S-phase, followed by cyclin B, which acts with its partner CDK1 to progress the cell through mitosis.

1.1.2 Complexities of cell cycle components

However, this is a very simple view of the cell cycle, and the reality is much more complex. Firstly, several more cyclins exist, that are not mentioned here. Secondly, cyclins and CDKs have some promiscuity in their partnerships, for example both

cyclin A and E can activate CDK2, and cyclin A also activates CDK1. Different pairings likely have an effect on substrate specificity and allow for fine regulation of cell cycle control. Thirdly and perhaps not surprising given the promiscuity, there exists a high degree of redundancy within the cell cycle. This is evidenced by the fact that cyclin E, once thought to be essential, is almost completely unnecessary during murine development (Geng et al., 2003). Cyclin A appears to compensate for the majority of its normal roles, for example, cyclin E1-/- E2-/- cells had normal levels of phosphorylated RB. Defects were only observed in cardiovascular development, and spermatogenesis, placental trophoblasts, hepatic megakaryocytes and re-entry to the cell cycle from quiescence, which all experience a G1 not directly preceded by mitosis (Geng et al., 2003). This redundancy is also true for other cell cycle components including cyclin A1/2, cyclin D1/2/3, CDK2/4/6, $p21^{CIP1}$ and $p27^{KIP1}$ (reviewed in Hochegger et al., 2008; Malumbres and Barbacid, 2009; Murray, 2004).

Lastly, non-canonical roles are also being found for several of the cyclins and other cell cycle factors, which include CDK-independent roles and links with development. For example, cyclin E ablation causes cardiovascular abnormalities (Geng et al., 2003), and also reveals more developmental defects than the CDK2-/- mouse, which is not embryonic lethal, and *ex vivo* cells are able to re-enter the cell cycle normally, suggesting CDK-independent roles for cyclin E (Berthet et al., 2003; Ortega et al., 2003). In spite of the promiscuity previously mentioned, there was no kinase activity found to be associated with cyclin E in CDK2-/- cells (Berthet et al., 2003) and a cyclin E mutant defective in kinase activation can partially rescue cyclin E1-/- E2-/- phenotypes (Geng et al., 2007). Association of CDK-independent cyclins A and E has also been described for centrosomes (Honda et al., 2005; Matsumoto and Maller, 2004; Pascreau et al., 2010) as well as a connection between CDK-independent cyclin D1 and transcription (Emmerich et al., 2004; Fu et al., 2005; Geng et al., 1999; Trent et al., 2007; Wang et al., 2003; Zwijsen et al., 1997 and reviewed in Fu et al., 2004). These non-canonical roles can lead to complications when interpreting results, and apparently conflicting conclusions between biochemical analysis of functional specificity and knock-out mouse models.

1.1.3 Cell cycle control

Cell cycle progression is normally restrained by small inhibitory molecules called CDK-inhibitors (CDKi), for example, the INK4 (Inhibitor of CDK4) and CIP (CDK-interacting protein) families of inhibitors. INK4 members inhibit cyclin D:CDK4/6 complex and the CIP family members $p21^{CIP1}$ and $p27^{KIP1}$ inhibit cyclin E/cyclin A:CDK2 complexes. As with cyclins, CIP family proteins also have additional roles, including facilitating the interaction of cyclin D with CDK4/6 and roles in senescence and quiescence respectively (reviewed in Sherr and Roberts, 1995, 1999). Other mechanisms for control include phosphorylation and dephosphorylation of specific residues to enhance or inhibit the activity of a protein (reviewed in Moroy and Geisen, 2004), such as the opposing roles of CDK-activating kinase (CAK) and the phosphatase CDK-inhibitor 3 (CDKN3 or KAP), and the inhibiting kinases WEE1 and MIK1 versus the activating phosphatases in the CDC25 family (reviewed in Pines, 1999).

1.1.4 Quiescence

As previously mentioned, cells can exist in the non-cycling state of quiescence. Quiescence (G0) was first described in 1962 as a 'growth fraction' or a proportion of cells not cycling (Mendelsohn, 1962) due to a variety of 'suboptimal' growth cues (Pardee, 1974). Critically, quiescence is a state of no cell division, but unlike senescence, in which cells have permanently exited from the cell cycle, cells may return to the cell cycle in response to signals. For cells to be quiescent, pathways triggering senescence, apoptosis and further differentiation must be inhibited. After some debate, quiescence is now generally accepted to be a distinct state rather than simply a pause in G1 (reviewed in Coller, 2007) (fig 1.1).

Cycling cell cultures consist of cells in all phases of the cell cycle, so called asynchronous populations. To study a particular part of the cell cycle cells must be halted at a particular point before being released. The cells will then transverse subsequent phases and events will occur in sequence and synchronously. Synchronising cells in quiescence followed by their release back into the cell cycle is a useful method to study discrete points of the cell cycle without the use of non-physiological chemical inhibition. During re-entry, cells pass through a G1 period,

during which they prepare for DNA replication. It is important to note that this G1-phase (referred to hereafter as $G1^{Q}$) is subtly different from the G1 following mitosis ($G1^{M}$). It is important to study $G1^{Q}$ as inappropriate re-entry to the cell cycle may play a role in the formation of some cancers.

1.1.5 Characteristics of quiescence

Published literature favours quiescence being an actively maintained and specific state with the induction of specific genes as cells exit the cell cycle, rather than just a total reduction in gene expression (reviewed in Fox et al., 2005). In support of an actively maintained state, many known and several unknown genes were identified as upregulated through gene-trap or microarray methods (Coller et al., 2006; Sambasivan et al., 2008). Quiescence also does not necessarily result in reduced metabolism. A reduction in metabolism has been recorded for yeast and lymphocytes (Bauer et al., 2004; Frauwirth et al., 2002; Fuge et al., 1994), however, quiescent fibroblasts do not show much decrease in overall metabolism although there does appear to be some shifts in the comparative usage of pathways (Lemons et al., 2010). Indeed, cardiomyocytes, neurons and renal tubular epithelial cells, all quiescent, are high energy consumers *in vivo* (Lemons et al., 2010). Proposed energy usage in quiescent cells (as DNA replication does not occur) are i) recycling of macromolecules, ii) detoxification of free radicals and iii) cell type specific functions such as secretion of extracellular matrix by fibroblasts and contraction by cardiomyocyctes (Lemons et al., 2010).

Recently, the method employed for generating quiescent cells *in vitro* has been shown to have an impact on cellular characteristics (Coller et al., 2006; Lemons et al., 2010). Laboratory models of quiescence include anchorage-dependent arrest (adherent cells are prevented from making surface contacts by suspension in a semi-solid medium or in non-tissue culture treated flasks), removal of growth factors, contact inhibition or a combination of these methods. Coller et al. (2006) compared gene expression from primary human fibroblasts induced into quiescent states by these methods, recording up or down regulation of genes relative to G1 cells. Differences in gene expression after only 14 hrs, confirms quiescence to be a distinct state (G0) rather than G1 arrest. However, each method for driving cells to

quiescence produced its own 'signature' of gene expression changes suggesting quiescence to be in fact a collection of states.

In spite of differences between quiescent methods, there does appear to be a core "quiescent programme of gene expression" (Coller et al., 2006). This becomes stronger over time especially for up-regulated genes. Many of the genes within this defined programme are involved in negative regulation of cell growth and division, apoptosis or differentiation, and may play a roll in cell-cell communication suggesting this to be important for keeping cells under reversible arrest. It is also important to note that overexpression of the CDK inhibitors, $p21^{CIP1}$ and $p27^{KIP1}$ did not induce as many 'quiescence programme' genes as the quiescence generating methods described above. This suggests ectopic $p21^{CIP1}$ and $p27^{KIP1}$ overexpression induces G1 arrest rather than true G0, and further supports G0 being a distinct state (Coller et al., 2006).

Importantly, the use of two quiescence triggers caused the 'quiescence programme' to be induced quicker. Thus, the method used in this project (a combination of contact inhibition and serum deprivation) promotes a state of quiescence that would appear to be representative of a general quiescent state.

1.1.6 Re-entry to the cell cycle from quiescence

Cells are released from quiescence in the method used here, by splitting 1:4 to remove contact inhibition and replacement of serum depleted medium with fresh medium with 10 % serum. Cells released in this way pass through $G1_Q$, as a synchronous wave with defined timing. For the 3T3 cells used for synchronisation in this thesis, the restriction point occurs at approximately 15 hours, and entry to S-phase at approximately 18 hours (Coverley et al., 2002).

The major difference that exists between $G1_M$ and $G1_Q$ is that $G1_Q$ is significantly longer (reviewed in Coller, 2007). Many cell cycle regulators, including cyclins and pre-RC components are degraded during quiescence. Therefore, extension of G1 may be due to the need to re-synthesise these components, and facilitate their re-binding to chromatin. The differences between $G1_Q$ and $G1_M$ are likely the

requirement for additional G1Q steps. This suggests that information about steps that are common to both G1s is likely to be broadly transferable.

1.1.7 Origins of replication

During G1 the cell prepares for DNA replication. Unlike in bacterial cells, where DNA replication begins from only one origin on the circular bacterial chromosome, DNA replication in mammalian cells begins at thousands of origins. In human cells, between 30,000 and 50,000 replication origins are thought to be activated per cell cycle in a spatially and temporally ordered fashion (reviewed in Mechali, 2010). *Saccharomyces cerevisiae* origins of replication are defined by DNA sequence, the autonomous replication sequence (ARS). However, similar short sequences do not specify origins in higher eukaryotes. Instead, structural information and epigenetic marks that can be stably inherited by daughter cells play a role in specification. These include promoter status, CpG methylation, nucleosome positioning, DNase I sensitive sites, DNA topology and chromatin loop architecture (reviewed in Mechali, 2010). For example, there is a higher probability of initiation occurring just before or after transcription start sites, with and without CpG-rich regions (Cayrou et al., 2011). Even in *S. cerevisiae* the ARS is not sufficient to specify origin use as contextual features are known to play a role (Nieduszynski et al., 2006). The apparently weak dependence on primary sequence has made it difficult to predict higher eukaryote origins.

1.1.8 Pre-replication complex

During initiation of DNA replication, a multi protein complex assembles at origins, the replication complex (RC). However, this is built up in stages (fig 1.2). Firstly, members of the pre-RC bind to origins. CDC45, MCM10 and the GINS complex are then recruited. These, as well as the activity of CDK complexes and Dbf4-dependent kinase (DDK) complexes, are required to convert the pre-RC to the pre-initiation complex (pre-IC), which recruits the DNA replication machinery itself to form the RC (reviewed in Bell and Dutta, 2002; Boos et al., 2012; Diffley and Labib, 2002; Remus and Diffley, 2009; Sclafani and Holzen, 2007). I have used members of the pre-RC as markers of early stages of initiation (reviewed in more detail in Bell and Dutta, 2002; Sclafani and Holzen, 2007; Takisawa et al., 2000).

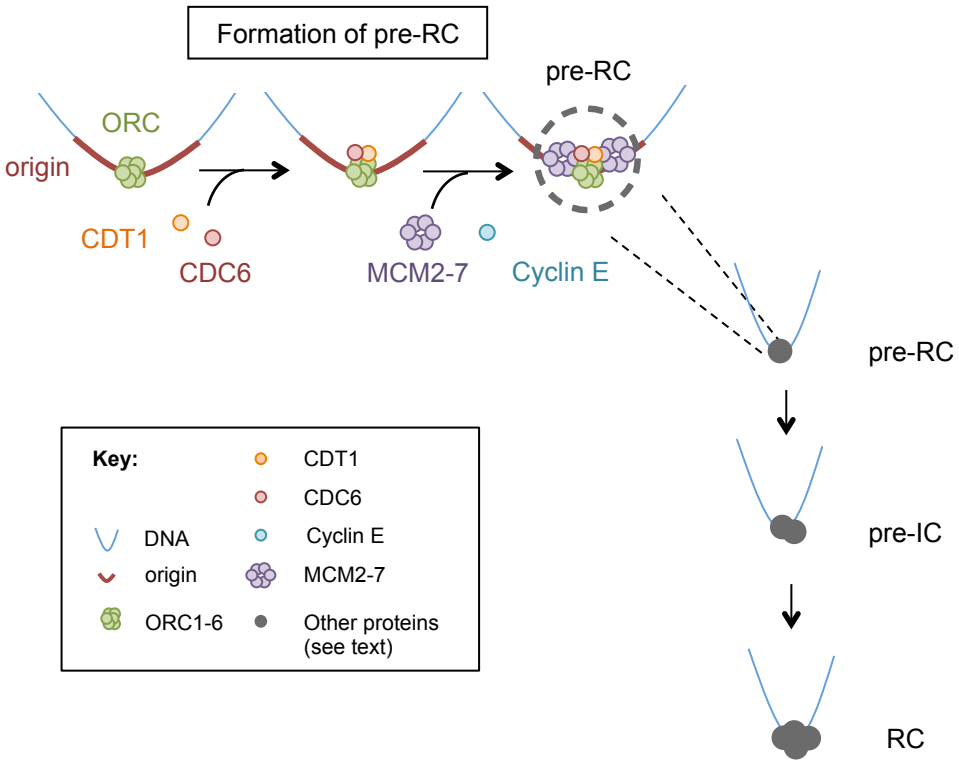

Figure 1.2: Schematic showing formation of the pre-Replication complex (pre-RC) and subsequent conversion to pre-initiation complex (pre-IC) and replication complex (RC).

Potential DNA replication origins are first marked by the heterohexameric origin recognition complex (ORC1-6). Following ORC binding cell division cycle 6 (CDC6) and chromatin licensing and DNA replication factor 1 (CDT1) are recruited independently, although both depend on ORC. The activities of all three protein (complexes) are necessary to enable loading of the mini-chromosome maintenance (MCM2-7) complex (Cook et al., 2004). At this point the pre-RC is complete and the origin is said to be licensed. The heterohexameric MCM2-7 complex is believed to be the helicase responsible for unwinding DNA during replication (reviewed in Takisawa et al., 2000), and there can be many molecules loaded at each origin (Edwards et al., 2002). Although many of these key players have been known for many years there are still outstanding questions about requirement and the mechanism of each step. For example, there have been many models proposed for the function of the MCM complex as the helicase responsible for unwinding DNA, that are yet to be confirmed (models reviewed in Sclafani and Holzen, 2007).

Importantly, pre-RC assembly has never been thoroughly investigated in relation to the NM (section 1.4.5-1.4.9).

A key feature of the cell cycle is that all DNA must be replicated once but only once. Therefore, there exist several mechanisms to prevent re-replication. One key mechanism is that once a region of DNA has been replicated it cannot be re-replicated without assembly of new pre-RCs, and once a cell has entered S-phase, pre-RC binding is prevented until the cell has passed through the next mitosis. This is achieved by several mechanisms. Firstly, ORC is regulated by subunit availability. In mammalian cells ORC2-6 remain chromatin bound throughout the cell cycle (Fujita et al., 2002; Madine et al., 2000; McNairn et al., 2005; Ohta et al., 2003; Tatsumi et al., 2003 and reviewed in DePamphilis, 2003) but ORC1 is released in S-phase and degraded (Li and DePamphilis, 2002; Mendez et al., 2002; Tatsumi et al., 2003). (Please note, this is the case for human cells, in others it is released and ubiquitinated or phosphorylated but not degraded.)

Second is the sequential activities of cyclin E and cyclin A. During G1 cyclin E, along with CDC6 and CDT1, facilitates MCM2-7 loading, described as 'opening the window of opportunity' for pre-RC assembly (Coverley et al., 2002). However, cyclin A, in complex with CDK2, then phosphorylates various proteins including CDC6, preventing further pre-RC assembly, thereby 'closing the window of opportunity' (Coverley et al., 2002). This helps to prevent reloading of the pre-RC after cyclin A levels rise. There is some debate about the fate of phosphorylated CDC6, whether it remains bound to chromatin or not. Nevertheless, surplus, soluble CDC6 does appear to be exported from the nucleus so it is not available for fresh loading of MCM2-7 (Coverley et al., 2000; Mendez and Stillman, 2000; Petersen et al., 2000; Saha et al., 1998).

High levels of CDK activity also appear to negatively regulate pre-RC function through phosphorylation of other components (reviewed in Bell and Dutta, 2002). MCM appears to be phosphorylated leading to reduced binding to chromatin during S-phase (reviewed in Lei and Tye, 2001). In contrast, CDT1 is both negatively regulated by CDK-dependent proteolysis through Cul4-DDB1 and SCF-Skp2 pathways (Li et al., 2003b; Liu et al., 2004; Nishitani et al., 2006) but also inhibited by Geminin, which is synthesised only during S and G2-phase (Tada et al., 2001;

Wohlschlegel et al., 2000). By all of these mechanisms and others not discussed (see Diffley, 2011 for a recent review), the cell prevents pre-RC loading and activation in phases other than G1, helping to prevent re-binding of the pre-RC on already replicated DNA, and therefore prevent the possibility of re-replication. The redundancy highlights just how important this control step is.

1.1.9 Cyclin E interaction with the pre-RC and the NM

A key point to stress is that cyclin E, unlike other cyclins, is involved with pre-RC assembly. In contrast, cyclin A is involved with pre-RC activation. Data from a cyclin E1-/- E2-/- knock-out mouse showed that during G1$_Q$, although ORC2 and CDC6 were loaded onto chromatin normally, in the absence of cyclin E, MCM2 was not loaded onto chromatin (Geng et al., 2003). However, it should be noted that it has since been shown that cyclin E null cells can re-enter the cell cycle from quiescence in the presence of dominant negative p53 (DNp53), albeit slower and at lower efficiency (Hanashiro et al., 2008). Therefore, in a functional p53 context (only), cyclin E is required for G1$_Q$. Nevertheless, these data agree with previous data from *in vitro* studies that addition of cyclin E to mid-G1$_Q$ nuclei increased the number that could respond to and be activated by cyclin A-complexes to enter S-phase, and that cyclin E facilitated MCM2 loading (Coverley et al., 2002). Other studies showed that cyclin E is NM-bound in differentiated, non-cancer cells (Munkley et al., 2011), and that overexpression of cyclin E caused deregulated pre-RC loading (Ekholm-Reed et al., 2004a). Therefore, cyclin E is a candidate protein involved with recruitment of pre-RC proteins to the NM (see section 1.4.5-1.4.10), and as such is of interest for this project.

There is also a well established association of deregulated cyclin E expression with many cancers (Bito et al., 1997; Bortner and Rosenberg, 1997; Dou et al., 1996; Dutta et al., 1995; Ekholm-Reed et al., 2004b; Erlandsson et al., 2003; Erlanson et al., 1998; Nielsen et al., 1998; Porter et al., 1997; Sakaguchi et al., 1998; Schraml et al., 2003 and reviewed in Hwang and Clurham, 2005; Keyomarsi and Herliczek, 1997) and overexpression of cyclin E (but not cyclin A or D) causes chromosomal instability (CIN) (Spruck et al., 1999). It has been suggested that the link between cyclin E and cancer may be partly due to failure to recruit the pre-RC to the NM in cancer cells, facilitating a degree of plasticity (Munkley et al., 2011). Also of interest

is CIZ1, which interacts with cyclins E and A, promotes DNA replication and is NM bound, so is therefore another candidate for the recruitment of pre-RC and other replication proteins to the NM.

1.1.10 CIZ1 and its function

The p21$^{CIP1/WAF1/CDKN1A}$-interacting zinc finger protein 1 known as CIZ1 (also nuclear protein NP94 and LSFR1), has at least one documented role during G1, but this is not yet fully characterised. CIZ1 was independently identified through interaction with p21^{CIP1}-cyclin E (Mitsui et al., 1999) and functional interaction with cyclin A during initiation (Coverley et al., 2005). CIZ1 is a complex protein that has several documented splice variants, multiple motifs, interacts with a range of other proteins and appears to have involvement in a variety of processes. However, in terms of the best understood functions, CIZ1 can be thought of as consisting of two domains, dividing the protein roughly in half (fig 1.3).

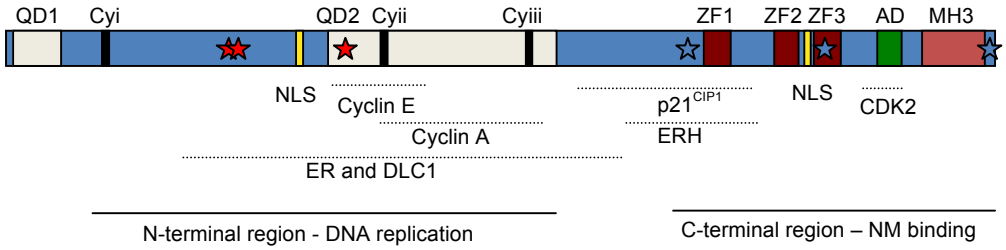

Figure 1.3: Map of the CIZ1 protein showing motifs and location of interaction sites. Gluatamin-rich domains (QD, white), zinc fingers (ZF, dark red), acidic domain (AD, green), matrin 3 domain (MH3, pink) taken from Mitsui et al., 1999. Nuclear localisation sequences (NLS, yellow) from D. Coverley, personal communication. Cyclin binding motif (Cy, black) taken from Copeland et al., 2012. CDK phosphorylation sites, where phosphorylation causes negative regulation taken from Coverley et al., 2002 (red stars), other putative CDK phosphorylation sites taken from Mitsui et al., 1999 (blue stars). Interacting proteins are outlined in the text.

The N-terminal domain of CIZ1 has been shown to promote DNA replication both in intact cells and cell free systems (Coverley et al., 2005). Addition of CIZ1 to asynchronous cells and late G1 nuclei *in vitro* increased the number that undergo replication (Coverley et al., 2005). Whereas depletion of newly synthesised CIZ1 by RNA interference (RNAi) in asynchronous cells, caused a reduction in cell proliferation and the percentage in S-phase (Coverley et al., 2005), and reduced S-

phase re-entry after release from quiescence (Copeland et al., 2010; Coverley et al., 2005). CIZ1 foci colocalise with 5-bromo-2'-deoxyuridine (BrdU) labelling in early S-phase and a proportion colocalise with proliferating cell nuclear antigen (PCNA) suggesting that CIZ1 is present at replication factories and may mark these sites (Ainscough et al., 2007; Coverley et al., 2005).

Cyclin E and A are known to have sequential roles during $G1^{Q}$ (Coverley et al., 2002) and one way in which CIZ1 may promote replication could be through co-ordination of this step since CIZ1 can interact with both cyclin E and A, in this same order, through cyclin binding motifs (Cy) (Copeland et al., 2010). This would both push the cell cycle forward, but also help prevent re-replication. Depletion of CIZ1 leads to an increase in MCM3 and PCNA positive cells suggesting that CIZ1 function is post-pre-RC formation (Coverley et al., 2005). CIZ1 may also promote DNA replication through the release of CDK2 from inhibition by the $p21^{CIP1}$ since CIZ1 has been suggested to regulate the location of $p21^{CIP1}$ by increasing export from the nucleus (Mitsui et al., 1999). However, this is not the sole explanation for the promotion of DNA replication as exogenous CIZ1 promotes DNA replication in $p21^{CIP1}$ null cells as in wild type cells (Coverley et al., 2005).

The C-terminal region of CIZ1 (and potentially other regions) mediates binding to the NM, likely via the matrin 3 (MH3) domain (Ainscough et al., 2007). CIZ1 is therefore a candidate protein to mediate recruitment of other replication proteins to the NM. Indeed, it has been proposed that CIZ1 acts as a link between the spatial and temporal control of DNA replication, by anchoring initiation factors to the NM (Ainscough et al., 2007; Copeland et al., 2010).

Increasingly, cell cycle proteins are being ascribed additional non-replicative roles. Recently a post-replicative role for CIZ1 has been suggested in DNA double-strand break repair during meiosis in non-proliferative spermatocytes, due to the expression profile and interaction with cyclin A1 (Greaves et al., 2012). CIZ1 also has the potential for other roles due to a number of interactions, which have largely not been functionally investigated (table 1.1).

Table 1.1: Published interaction partners of CIZ1 and identified motifs.

Interacting partner/motif	Data	Location	Reference
N-terminal domain			
'Replication domain'	Promotes DNA replication	75-471 (murine)	Copeland et al., 2010; Coverley et al., 2005
Cyclin binding motifs (Cyi, cyii, cyiii)	Cyclin E binds cyii cyclin A binds cyii, cyiii	i 87-89 ii 321-323 iii 447-449 (murine)	Copeland et al., 2010
Cyclin E		321-391 (+) (murine)	Copeland et al., 2010
Cyclin A		391-471 (+) (murine)	Copeland et al., 2010
CDK-phosphorylation sites	Phosphorylation negatively regulates DNA replication	191, 192, 293 (murine)	Coverley et al., 2005
SQ/TQ DNA damage response (DDR) phosphorylation sites	CIZ1 phosphorylated after ionising radiation.	(human)	Matsuoka et al., 2007
	18-21 predicted sites.	(murine/human)	Roper, 2011
Oestrogen receptor (ER)	ER co-activator, also oestrogen and glucocorticoid responsive	145-528, ERE sites in intron 1 and 2 (human)	den Hollander et al., 2006; Hakim et al., 2009
Dynein light chain 1 (DLC1)		145-528 (human)	den Hollander and Kumar, 2006

Table 1.1 (cont.): Published interaction partners of CIZ1 and identified motifs.

Interacting partner/motif	Data	Location	Reference
2 glutamine rich domains QD_1, QD_2		4-45, 276-471 (human)	Mitsui et al., 1999
Nuclear localisation sequence (NLS)	Monopartite	258-263 (human)	D. Coverley, personal communication
NM binding region (possible)		379-406 (human)	Dahmcke et al., 2008
C-terminal domain			
NM binding		708-830 (murine)	Ainscough et al., 2007
Matrin 3 (MH3) domain		783-837 (human)	Mitsui et al., 1999
NLS	Bipartite	697-699, 710, 712 (human)	D. Coverley, personal communication
putative CDK-phosphorylation sites		585, 696, 876 (human)	Mitsui et al., 1999
$p21^{CIP1}$		494-640 (human)	Mitsui et al., 1999
CDK2	Competes away $p21^{CIP1}$	733-760 (human)	den Hollander and Kumar, 2006; Mitsui et al., 1999
3 zinc fingers (ZF)	Weak consensus binding sequence, perhaps sequence independent	595-618, 656-677, 687-710 (human)	Mitsui et al., 1999; Warder and Keherly, 2003
acidic domain (AD)		741-762 (human)	Mitsui et al., 1999

Table 1.1 (cont.): Published interaction partners of CIZ1 and identified motifs

Interacting partner/motif	Data	Location	Reference
enhancer of rudimentary homologue (ERH)		531-644 (human)	Lukasik et al., 2008

Motif amino acid numbers were determined in previous publications based on sequence, as indicated. Regions interacting with other proteins were determined in indicated publications based on fragments of CIZ1. Therefore, most regions (given by amino acid number of full length CIZ1) are large and infer the interaction with a particular protein is found within that range, + refers to the potential for additional amino acids involved in the interaction. Murine and human CIZ1 have approximately 70 % overall homology in amino acid sequences (Coverley et al., 2005) and all domains appear to be conserved.

1.1.11 Location of CIZ1

In mammalian systems CIZ1 is expressed in a fairly ubiquitous manner, but at higher levels in testes and kidney (Mitsui 1999) and lower levels in skin and muscle (Greaves et al., 2012). Expression of CIZ1 appears to be developmentally-regulated with expression in the embryo and adult tissue but at lower levels around birth in all tissues tested (Greaves et al., 2012). CIZ1 is only found in higher eukaryotes, for example, human, mouse, rat and fugu (Coverley et al., 2005), which suggests a vertebrate specific function (Coverley et al., 2005). Endogenous CIZ1 is predominantly located in the nucleus in punctuate foci which resist salt and nuclease extraction and colocalise with some components of replication foci (Ainscough et al., 2007; Coverley et al., 2005). The location of CIZ1 is developmentally-regulated with CIZ1 being recruited to the NM during development and generally absent from the NM in cancer cells (appendix D). In addition, recruitment appears to be cell cycle-regulated as although existing endogenous CIZ1 is NM bound throughout the cell cycle, newly synthesised protein is recruited to the NM in late G1/S (Ainscough et al., 2007). Although the C-terminal region is

necessary and sufficient to localise to the NM, regions in the N-terminal half appear to be important for correct spatial positioning and foci formation, which are lost in some cancers and other pathologies (Dahmcke et al., 2008; Rahman et al., 2007).

1.1.12 CIZ1 splice variants and pathology

CIZ1 is upregulated in various cancer cell lines although it is unclear as yet if this is wild-type CIZ1 or a variant form (appendix D). CIZ1 has the possibility to be highly alternatively spliced and several different forms of CIZ1 have been reported in non-cancer cells, including ~100 kDa and ~125 kDa forms in differentiated cells, and an embryonic specific form (Mitsui 1999 and Coverley 2005). However, other splice variants have been identified in cancer cell lines and tumours, including medulloblastoma, lung cancer and Ewing's sarcoma (Higgins et al., 2012; Rahman et al., 2007; Rahman et al., 2010; Warder and Keherly, 2003). Due to the role of CIZ1 in cell cycle progression it seems likely that altered CIZ1 is part of the process of tumour formation rather than just a consequence. It has been shown that alterations in CIZ1 can occur very early in tumour formation, for example, B-variant CIZ1 can be detected in the blood of individuals with very early stage lung cancer (Higgins et al., 2012). In addition, when mice with xenograph tumours, formed by cells from a small cell lung cancer derived cell line which expressed the CIZ1 B-variant, were treated to cause induction of small hairpin RNA (shRNA) against CIZ1 B-variant, tumour growth was reduced (Higgins et al., 2012). This suggests the altered form of CIZ1 has a biologically relevant and adventitious role in tumour cell proliferation.

Uncoupling of the two ends of CIZ1 has also been observed in cancer cells (section 1.4.10), suggesting a change in the spatial restriction of CIZ1 function. Specifically, promotion of DNA replication may no longer be constrained by attachment to the NM (appendix D). However, it is as yet unclear if CIZ1 is an oncogene or tumour suppressor. Overexpression of CIZ1 in breast cancer cell lines caused increased tumorigenic properties, which may suggest an oncogenic role, however, this was dependent on oestrogen, making the conclusions less than straightforward (den Hollander et al., 2006). Data presented in this thesis, and by personal communication, from work undertaken with a CIZ1 knock-out mouse indicate a tumour suppressor role for CIZ1, also suggested from another knock-out mouse model (Nishibe et al., 2013).

Altered CIZ1 has also been reported for other conditions including Alzheimer disease, rheumatoid arthritis and cervical dystonia (Dahmcke et al., 2008; Judex et al., 2003; Xiao et al., 2012). Most reports show altered subnuclear localisation of pathology associated forms of CIZ1 (Dahmcke et al., 2008; Higgins et al., 2012; Rahman et al., 2007).

1.2 The nuclear matrix

Descriptions of an insoluble proteinaceous nuclear substructure, in some ways analogous to the cytoskeleton, have existed for at least 40 years. This substructure is visualised in electron micrographs (EM) as a fibrogranular network of non-chromatin, protein rich components and RNA. Regions have been identified as interchromatin granule clusters, perichromatin fibrils, perichromatin granules and coiled bodies (Monneron and Bernhard, 1969). Largely from EM work, a model was proposed that the nuclear internal substructure consists of 10 nm fibers (revealed with the most harsh extraction methods) with associated additional substructure components and attached RNA, components of DNA metabolising machinery and DNA itself (He et al., 1990; Jackson and Cook, 1988; Nickerson et al., 1997 and reviewed in Nickerson, 2001). The internal network is connected to the nuclear lamina, which has attracted much less controversy, consisting of intermediate filaments and associated proteins, surrounding the nucleus and interacting with the internal side of the nuclear envelope (Capco et al., 1982; Nickerson et al., 1997). Connections have also been observed between the nuclear internal network and cytoskeletal components (Capco et al., 1982). Here, the nuclear lamina and internal substructure will be considered as one. Extraction methods were developed to study the internal nuclear substructure, however, difficulties associated with techniques and some residual controversy about its very existence mean that there are still many unanswered questions about structure and function. Nevertheless, there is now a large and growing body of evidence in favour of such a nuclear substructure and what its function may be.

This nuclear substructure has been termed the nuclear matrix (NM), the nuclear scaffold or the nuclear skeleton (or nucleoskeleton) depending on the technique used to reveal it. These are, respectively, extraction with high salt (2.0 M NaCl) (Berezney and Coffey, 1974), lithium 3,5-diiodosalicylate (LIS) (Mirkovitch et al.,

1984) or after encapsulation in agarose under physiologically relevant salt concentrations and electrophoresis (Jackson and Cook, 1988). A protein is termed part of the nuclear substructure if it resists extraction. However, there are also many variations of these techniques including stabilisation steps (reviewed in Martelli et al. 2002), and this means that interpretation is not always straightforward. Here the term NM is used as an overarching term, aiming to consolidate the reported observations to outline some general phenomena. Depending on extraction technique, the residual protein fraction varies slightly in composition but the core components revealed by several large-scale screens are similar (Albrethsen et al. 2009; Varma and Mishra 2011, and references therein). These include lamins, matrins, heterogeneous nuclear ribonucleoproteins (hnRNPs), other 'structural' proteins and various proteins involved in DNA metabolism, many of which are listed and categorised in a database of Nuclear Matrix Proteins, NMPdb (Mika and Rost, 2005).

1.2.1 The NM – simple interpretation?

Evidence for and against the NM has been extensively evaluated elsewhere with differing conclusions derived from the same data or subsets of the data (reviewed by Hancock, 2000; Martelli et al., 2002; Nickerson, 2001; Pederson, 1998). The controversy associated with NM research appears to be attributable to two key reasons. Firstly, it has proved difficult to show such a framework as that seen by EM using immunofluorescence methods in unextracted cells. Instead, immunofluorescence against candidate NM proteins usually reveals a pattern of punctate spots (reviewed in Martelli et al. 2002). This led to some concern that the structures observed were due to the process of extraction. In particular, the use of non-physiological conditions, especially high salt extraction, has been criticised as potentially causing aggregation of such protein assemblies (Pederson, 1998). However, to address this, the LIS and physiologically relevant buffer techniques were developed, and these give very similar results. In addition, one highly supportive study used electron spectroscopic imaging (ESI) to view unextracted nuclei by electron microscopy with the aim of identifying areas as protein and/or nucleic acid rich. Using paraformaldehyde fixed sections, this showed inter chromosomal areas to be composed of protein rich but nucleic acid poor structures, consistent with the description of a NM (Hendzel et al., 1999). Also worth

consideration when thinking about the NM is the idea that there may exist multiple local NMs (Martelli et al., 2002) that are dynamic, and capable of altering characteristics and composition based on the nuclear processes occurring at that point in time and space (reviewed in Nelson et al., 1986). Therefore, we might not expect to see filamentous structures composed of a small number of specific proteins, but instead transient associations between functional proteins and a 'core'.

The second major reason that appears to have added complexity and contributed to the controversy in the NM field is the widespread use of systems that now appear to lack or possess a different kind of NM, such as *Xenopus* eggs, cancer cell lines and progenitor cells. Recent research suggests that the NM changes as cells differentiate or become transformed (reviewed in Zink et al., 2004; Munkley et al., 2011, and discussed in more detail below).

The NM has been proposed as an anchor for chromatin, the site of transcription (Jackson and Cook, 1985), DNA repair (Qiao et al., 2001), splicing (Zeitlin et al., 1987), chromatin remodelling (Reyes et al., 1997) and DNA replication (Jackson and Cook, 1986b). Here, interactions between DNA and the NM are first introduced followed by evidence for DNA replication at the NM.

1.3 DNA and the NM

1.3.1 Structural organisation of DNA

In order to fit approximately 2 metres of DNA within a mammalian nucleus of the order of 10 μm in diameter, it is clear there must be multiple levels of organisation. The extremes of packing of DNA, from wrapping the double helix around histone octamers to form nucleosomes, to compartmentalisation into chromosome territories (reviewed in Cremer et al. 2006) are now as accepted as the helix itself. However, intermediate levels of organisation incur more debate (reviewed in Bian and Belmont 2012).

One model is that nucleosomes are organised into a 30 nm fibre. However, existence of this structure *in vivo* is still hotly contested as the evidence is largely from *in vitro* work (reviewed in Bian and Belmont, 2012). An alternative model is that of fractal

globules (reviewed in Fudenberg and Mirny 2012), in which short regions of DNA are proposed to 'crumple' (condense) together to form a series of globules (or domains). These then further crumple together to form larger globules, repeating until they achieve the size of chromosome territories. Some key points of this model are that DNA is not knotted as it would be in an equilibrium globule model (random compaction of DNA), and that it includes all the required levels of compaction. In this model spatially segregated domains would suggest flexible access to each region of DNA. There are supportive data for the idea of domains within domains, from Fluorescence *In Situ* Hybridisation (FISH) and Chromosome Conformation Capture (3C) techniques (Lieberman-Aiden et al., 2009). Consistent with both of the above, chromatin loops are thought to periodically attach to the NM. It is likely that the true state of chromatin is a combination of these proposed higher order structures and is likely to be highly dynamic. Here, the focus is primarily on the organisation inherent in attachment to the NM.

1.3.2 Attachment of DNA to the Nuclear Matrix

Attachment of DNA to a proteinaceous structure was first observed by electron microscopy in the 1970s (Paulson and Laemmli, 1977). Various methods have been used to study the DNA:NM attachment points (Mirkovitch et al., 1984) including imaging by FISH and Maximum Fluorescence Halo Radius (MFHR) (fig 1.4) and biochemical techniques (digestion of loop DNA with restriction enzymes, DNase I or topoisomerase II). Early studies showing attachment of DNA to the NM led to the idea of periodic attachments and the concept of intervening chromatin loops (Benyajati and Worcel, 1976; Marsden and Laemmli, 1979) (fig 1.5). Subsequent work has led to a modification to include loops of different sizes (fig 1.5) and with likely different functions (described in more detail below).

Attachments are termed MARs (matrix attached region), SARs (scaffold attached region) or skeleton-attached sequences depending on extraction method. These are respectively, resistant to extraction with high salt, LIS or physiological buffers after encapsulation in agarose, coupled with enzymatic digestion of DNA. The attachment points revealed by different extraction methods have significant overlap but some are method specific. For example, only approximately half of sequences revealed as MARs (resistant to 2.0 M NaCl) on chromosomes 14-18 were also identified as SARs

(resistant to 25 mM LIS) (Linnemann et al., 2009). It is likely that the total attachment points in a cell comprise a combination of those revealed by all techniques and those specific to one or two of these extraction methods. Discussed first are general features of attachment regions, for which the overarching term S/MAR is used, before highlighting some differences between MARs, SARs and skeleton-attached sequences.

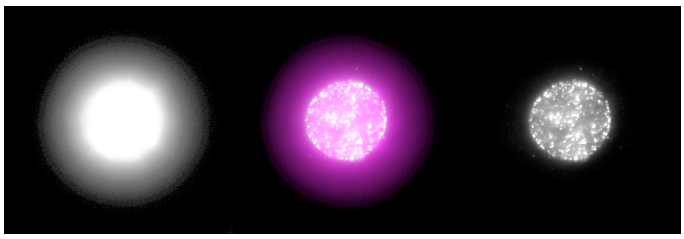

Figure 1.4: Newly synthesised DNA is located at the NM A) Left: Example of Maximum Fluorescence Halo Radius image from NIH3T3 cell showing DNA loops stained with DAPI emanating out from attachment points in the residual nucleus (RN) (MFHR method described in Buongiorno-Nardelli et al., 1982; Guillou et al., 2010). Right: Newly synthesised DNA is observed at the NM but not visible in loop DNA. Cells were pulsed for 30 minutes with BrdU and visualised with α-BrdU. Centre: Merged image showing BrdU (newly synthesised DNA) in white and DNA in magenta.

Previously published in Wilson and Coverley, 2013.

The length of DNA that is associated with the NM at each attachment point is variously reported as between 100-1000 base-pairs (bp) with individual loops ranging from 4-200 kilobase-pairs (kbp) (Buongiorno-Nardelli et al., 1982; Singh et al., 1997; Vogelstein et al., 1980 and reviewed in Bode et al., 2003). Previous estimates of average loop size are in the 60-86 kbp range (Jackson et al., 1990; Vogelstein et al., 1980). With a human haploid genome of ~ 3 billion bp, this would suggest that ~ 86,000 attachment points exist at any one time per diploid, G1 cell. As different S/MARs exist in different cell types, and most likely in different phases of the cell cycle and transcriptional programmes, the total number of potential S/MARs is likely to be much more than this (fig 1.5). Boulikas (1995) predicted around 100,000 potential S/MARs based on a) a loop size of 60 kbp, b) an estimated genome size of 3.6 billion bp, and c) the fact that some S/MARs are facultative (Boulikas, 1995). As will be discussed, predictive tools for S/MARs have their limitations, but it is interesting to note that all tools appear to over-predict S/MARs (Platts et al.,

2006). While we cannot currently differentiate between false positives and facultative S/MARs, a surplus of potential S/MAR regions would allow for flexibility in usage and imply some form of selection. Consistent with these ideas, it has been shown that a sequence that has the potential to be a functional S/MAR is not always recruited to the NM (Heng et al., 2004).

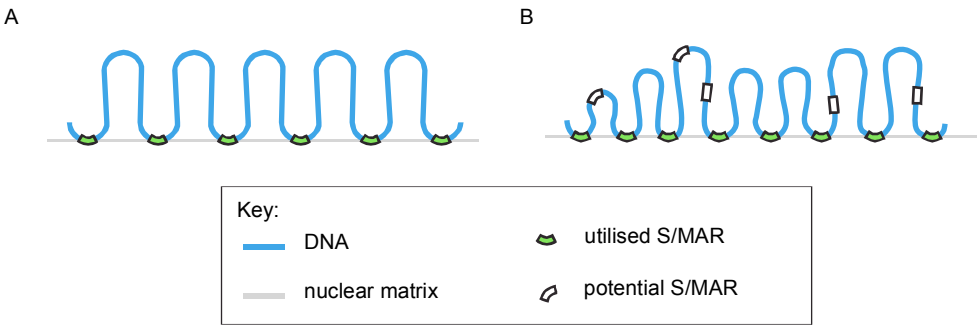

Figure 1.5: Arrangement of DNA by attachment to the NM with intervening loops. A) DNA is thought to be periodically attached to the NM at S/MARs forming intervening chromatin loops. B) Refined model illustrating variable loop sizes, and complex S/MAR usage including utilised S/MARs and function-related alternative potential S/MARs.
Previously published in Wilson et al., 2013. Designed by R. Wilson, drawn by P. Roberts.

1.3.3 Features of S/MARs

Many of the S/MARs that have been identified arise from studies at a particular gene or locus, and there have been few chromosome or genome wide investigations. The collation of S/MARs identified by individual groups into the S/MAR database (Liebich et al., 2002a) has allowed comparison of potential S/MAR motifs (Liebich et al., 2002b). However, other than an over-representation of adenine (A) and thymidine (T), the authors found little sequence similarity. Instead, structural motifs are thought to play a greater role in determining the potential for NM attachment. One predictive tool, 'MAR finder' uses combinations of the following structural motifs to predict S/MARs; origins of replication, thymidine-guanine (TG)-rich sequences (commonly in 3' untranslated regions - UTRs), curved DNA, kinked DNA, Topoisomerase II sites and AT-rich sequences (Singh et al., 1997). Other suggested characteristics include transcription factor binding sites and other regulatory sequences linked with promoter function (Singh et al., 1997). However, some reports are contradictory and motif enrichment may depend on the method used to remove loop DNA. Moreover, the predictive power of tools that use a combination of

structural motifs and AT-rich DNA is little better than prediction based on AT-content alone (Evans et al., 2007). One of the reasons for the lack of a good predictive model is that only a few S/MARs have been identified, and these by different methods, which appear to identify different populations. So while a particular motif may appear common to one set of identified S/MARs, it may not be hugely predictive of S/MARs in general. It may also be that many motifs can increase the probability of a region forming NM attachment with each increasing the probability only slightly. Therefore, the identification of more S/MARs and a better understanding of their function will be necessary in order to develop better predictive tools.

1.3.4 Functions of S/MARs

In spite of difficulties identifying and predicting S/MARs, several different functions have been suggested for these NM attachments. Constitutive attachments, which do not vary by cell type, are suggested to have a structural role in anchoring the DNA and maintaining nuclear architecture. Consistent with this organisational function, territories have been shown to remain after extraction to reveal the NM but be lost when the NM is disrupted with RNase (Ma et al., 1999). In contrast, other S/MARs appear to be transient and facultative in their attachment to the NM. Some vary by cell type and are thought to be involved in maintaining the transcriptional programme, others vary with external signals and the subsequent change in transcriptional programme. These include S/MARs associated with transcription units, enhancers and transcription factor binding sites. Further S/MARs vary by cell cycle stage and include regions at potential origins of replication. There is evidence that both transcription and replication occur at the NM. The facultative S/MARs that are implicated in these processes are likely to be involved in the recruitment of specific regions to the NM. Consistent with the idea of constitutive and facultative S/MARs, some proteins which bind S/MARs (MARBPs) are core components of the NM, such as matrins and lamins, topoisomerase II and high-mobility group proteins, while others are cell type or signal specific, such as Scaffold Attachment Factors A (SAF-A) and B (SAF-B) and special AT-rich sequence-binding protein-1 (SATB1) (reviewed in Wang et al. 2010).

Attachment regions could be grouped by characteristics, namely motif composition, extraction method or function. It is possible that classification by motif or extraction method reveals the same groups. For example, matrix attachment regions (MARs) may contain specific motifs, and be related to a specific function. Alternatively one of these characteristics or another currently not described, may predominate in the determination of function. Reports from two groups have started to correlate function with extraction method (reviewed in more detail in Wilson and Coverley, 2013).

One study compared MARs, SARs and skeleton-attached sequences microscopically in human lymphoblasts (Craig et al., 1997). Cells were extracted with the three methods and loop and attached DNA fragments separated. These were differentially labelled and used as chromosome paints. MARs were slightly enriched in gene poor regions and relatively absent from transcriptional promoters but varied between mitosis and interphase. SARs were also enriched in gene poor regions, but were not different in interphase. In contrast, skeleton-attached sequences were associated with gene rich regions and CpG islands, and varied between mitosis and interphase. Other studies compared MARs and SARs of HeLa and primary aortic adventitial fibroblasts (AoAF) using a microarray approach with much finer resolution than imaging approaches (Linnemann and Krawetz, 2009b; Linnemann et al., 2009). For both types of cell, MARs were generally found in intergenic and gene poor regions and were strongly associated with silenced genes, whereas SARs density did not depend on gene density but tended to overlap genes and be associated with expressed genes.

The lack of more genome wide studies makes definitive statements about subgroups of S/MARs and their function difficult. However, general conclusions from these studies suggest MARs to include structural, silencing attachment points and perhaps cell cycle phase dependent attachments, SARs to perhaps be important for cell type determination and maintenance, and SARs and/or skeleton-attached sequences to be important for gene expression. As described in more detail below, origins of replication are recruited to the NM, but as yet there is little indication which subgroup they are likely to fall into.

1.4 DNA replication and the nuclear matrix

Various lines of evidence suggest that DNA replication occurs in association with the NM. Both newly synthesised DNA and termination structures exist within NM fractions, DNA replication origins may also attach directly with the NM, and a number of key proteins involved in replication are themselves associated with the NM. No published investigations of pre-IC components in relation to the NM could be found, but several report findings for pre-RC and RC components. Covered below is evidence for elongation, termination and initiation of DNA replication.

1.4.1 Elongation of DNA replication

Biochemical fractionation of nuclei to localise nascent DNA, or visualisation after labelling with short pulses of nucleotide analogues, has shown newly synthesised DNA and replication intermediates to be located at the NM and crucially not in the loops (fig 1.4). Furthermore, pulse-chase experiments show that when newly synthesised DNA is observed at later timepoints, it has migrated from the NM fraction into loop regions (Gerdes et al., 1994; Jackson and Cook, 1986b; Nakayasu and Berezney, 1989; Pardoll et al., 1980; Vogelstein et al., 1980). This collection of studies indicates that the DNA synthesis step and presumably therefore also replication forks, are located at the NM. Consistent with this, S-phase cells possess both PCNA and DNA polymerase α in the nuclear skeleton fraction (Hozak et al., 1993; Hozak et al., 1994). Moreover, this population of polymerase α showed *in vitro* activity that was comparable to that *in vivo*, and nascent DNA remained associated with the skeleton (Jackson and Cook, 1986a, b). Similar conclusions were drawn from analysis of NM preparations (Nakayasu and Berezney, 1989).

1.4.2 Termination of DNA replication

Relatively little is known about the termination of DNA replication, however there are data that suggest an association with the NM. Firstly, topoisomerase II is located at the NM (Berrios et al., 1985), and appears to be required for resolving replication intermediates. More direct evidence comes from analysis of NM attached DNA, by 2D agarose gel electrophoresis, which revealed termination structures in addition to replication intermediates. Patterns were consistent with both termination at specific points and as a consequence of the convergence of forks (Little et al., 1993).

1.4.3 Initiation of DNA replication

The most direct evidence that initiation of DNA replication is located at the NM makes use of synchronised late G1-phase cells treated with DNase to remove chromatin loops (Radichev et al., 2005). When incubated in soluble extract from S-phase cells (which contains regulatory protein kinases that induce initiation) more DNA synthesis occurred on the residual NM-associated chromatin than in control incubations that only support elongation. This indicates that NM-attached chromatin from late G1 cells can undergo initiation. Because this was found to be both located within characteristic foci, and dependent on protein kinase activity, these data support the idea that the initiation step of DNA replication occurs in chromatin that is protected by association with a nuclease-resistant structure.

Interestingly, under the same conditions, chromatin-depleted early G1 nuclei did not undergo kinase dependent initiation. This may be due to incomplete assembly of all required factors of the pre-IC or because origins are not located at the NM during early G1. Data described below does indeed suggest that origins are recruited to the NM only during late G1. However, we cannot assume that all origins are recruited to the NM together, as this may occur in conjunction with their activation.

1.4.4 Origins of replication

S/MARs have been identified in the vicinity of origins of replication for a handful of exemplar genes (reviewed in Cayrou et al. 2010) and early experiments suggested that mammalian cell origins were permanently associated with the NM (Lagarkova et al. 1998, and references therein). Furthermore, the similarity in size between replication units and chromatin loops reported in the 1980s (Buongiorno-Nardelli et al., 1982), suggested that they might be one and the same, with all attachment points being origins. In apparent support of this conclusion, regions of DNA labelled in early S-phase by incorporation of nucleotide analogues are observed at the NM fraction.

More recent evidence, however, suggests that recruitment of origins of replication to the NM occurs only transiently in late G1 and S-phase. Attachment to the NM and nucleoskeleton has been investigated for the well-studied origin of replication, *oriB*, at the *dihydrofolate reductase* (DFHR) locus in Chinese Hamster Ovary (CHO) cells

(Djeliova et al., 2001a, b; Ortega and DePamphilis, 1998). In one study, DNA from CHO cells was separated into loop and NM attached fractions (Djeliova et al., 2001a) and then probed with the *oriB* sequence or with nascent DNA from early S-phase (the collective origin fraction). No enrichment of origins, either *oriB* or the collective origin fraction was observed in the NM attached DNA from asynchronous cells (Djeliova et al., 2001a). However, *oriB* was enriched in the NM attached DNA (Djeliova et al., 2001b) and nucleoskeleton attached DNA (Ortega and DePamphilis, 1998) from late G1 phase cells (but not early G1), and lost from this fraction as cells progressed through S-phase (Djeliova et al., 2001b). In contrast to this early replicating origin, the late replicating origin from the *β-globin* gene was investigated in HeLa cells, where the NM association was maintained through S-phase (Djeliova et al., 2001b). Origins from other exemplar genes have also been described to temporally associate with the NM (reviewed in Ottaviani et al. 2008). Collectively, these studies show that origins have the potential to reside close to the NM, but that their association is not constitutive, being recruited during late G1 and lost during S-phase.

1.4.5 Pre-replication complex components (pre-RC)

Consistent with their role in the regulation of temporally restricted events, pre-RC proteins have tightly controlled temporal expression and degradation, as well as restricted subnuclear localisation. Unfortunately, many researchers limit their analysis by failing to include a nuclease digestion step in cellular extraction protocols, allowing only generalised conclusions about association with chromatin and/or NM. Furthermore, the cell cycle context of potential NM recruitment means that the fraction detected may be small and their recruitment to the NM may in fact be cell-type specific making the overall picture difficult to interpret. An important consideration to highlight here is that pre-RCs are laid down at potential origins (origin licensing) during late telophase in the mitotic cell cycle (Dimitrova et al., 2002; Mendez and Stillman, 2000), but lost if cells become quiescent (Cook et al., 2004; Madine et al., 2000; Tatsumi et al., 2003) necessitating their re-synthesis and recruitment upon cell cycle re-entry. Thus, the timing of both pre-RC formation and their NM recruitment is likely to be different for $G1^{Q}$ compared to $G1^{M}$. However, the accumulation of increasingly sophisticated reports on NM attachment of pre-RC components is beginning to support the idea that some core components become

attached to the NM, possibly in particular combinations and only around the time of initiation of DNA replication.

1.4.6 Origin recognition complex (ORC)

Several studies have looked at the relationship between ORC subunits and the NM. ORC1 has been detected in the NM fraction of asynchronous populations of HeLa, BJAB and BC3 cells (Fujita et al., 2002; Kreitz et al., 2001; Ohsaki et al., 2009; Ohta et al., 2003; Tatsumi et al., 2003) and in *Drosophila melanogaster* cells (Varma and Mishra, 2011). Several investigators have temporally resolved this NM association by cell cycle phase, which revealed ORC1 to be enriched in the NM fraction in G1 in BJAB and BC3 cells and in G1 or from late G1 in HeLa cells (Fujita et al., 2002; Kreitz et al., 2001; Ohsaki et al., 2009; Ohta et al., 2003; Tatsumi et al., 2003). This suggests that when ORC1 is expressed it becomes NM bound. However, it should be borne in mind that NM attachment of ORC1 might be cell type dependent as one report shows ORC1 as DNase I sensitive in proliferating NIH3T3 cells (Madine et al., 2000).

Other ORC subunits have also been detected in NM fractions, specifically ORC2-5 in asynchronous HeLa cells (Fujita et al., 2002; Kreitz et al., 2001; Ohta et al., 2003) and ORCs 2, 4, 5 and 6 in *Drosophila melanogaster* cells (Varma and Mishra, 2011), although again this may be cell type specific as little ORC2 was NM bound in Raji cells (Mendez and Stillman, 2000).

Where temporal resolution was attempted ORC2-5 were enriched in the NM fraction in G1 (Kreitz et al., 2001) or from late G1, in HeLa cells (Ohta et al., 2003). In both cases, this was at the same time as ORC1 was expressed and NM bound. Further investigation in HeLa cells showed that when ORC1 was depleted by RNAi, ORC2 was no longer enriched in the NM fraction (Ohta et al., 2003). Thus, NM binding of ORC2-5 may well be dependent on ORC1.

1.4.7 Cell division cycle 6 (CDC6)

The majority of investigations into the subnuclear localisation of the CDC6 protein have revealed a proportion that is attached to the NM. This has been noted in asynchronous HeLa cells, BJAB, BC3 and HEK293 cells, and is somewhat depleted in the absence of ORC1 in FT210 cells (Fujita, 1999; Fujita et al., 2002; Ohsaki et al.,

2009; Ohta et al., 2003). However, little CDC6 was found to be NM bound in NIH3T3 cells (Madine et al., 2000) or Raji cells (Mendez and Stillman, 2000). Where cell cycle phases were investigated, CDC6 was present in the NM fraction during G1 or early S-phase but not in G2/M cells (Fujita et al., 1999; Ohsaki et al., 2009). Therefore, it is clear that independent groups, using different methods and cell lines, have shown ORC and CDC6 to be at least transiently attached to the NM.

1.4.8 Chromatin licensing and DNA replication factor 1 (CDT1)

Few investigators have looked at NM attachment for CDT1 but one report described recovery of CDT1 in the NM fraction for BJAB, BC3 and HEK293 cells, and this occurred specifically in G1 phase but not S or G2/M phases (Ohsaki et al., 2009). This suggests that CDT1 may be recruited to the NM but there is not enough information available to draw generalised conclusions.

1.4.9 Mini Chromosome Maintenance (MCM) complex

The relationship between MCM and the NM is not as clear as for other pre-RC components. The majority of MCM3 and MCM2 is not NM bound in asynchronous HeLa cells (Fujita et al., 1997; Todorov et al., 1995) with similar results for MCM2, MCM3 and MCM5/7 in REF52 cells (Cook et al., 2002), MCM3 in Raji cells (Mendez and Stillman, 2000) and MCM5 in NIH3T3 cells (Stoeber et al., 1998). However, Burkhart *et al.* (1995) report a small but significant fraction of MCM3 in HeLa cells, which is not released by nuclease or high salt extraction. There are also several reports identifying MCM4, MCM2, MCM3 and MCM7 in NM proteomic screens in human or *Drosophila melanogaster* cell lines (Gerner et al., 2002; Mitulovic et al., 2004; Varma and Mishra, 2011). Although the majority of the MCM complex does not appear to be NM bound it is possible that the small amount of MCM protein in NM preparations reflects a weak, transient association, which is easily missed in bulk preparations from asynchronous cells. Some circumstantial support for the idea that attachment to the NM may be important for MCM function comes from ORC1 or CDC6 depletion studies, in which immobilisation of MCM (on chromatin or NM) is prevented (Ohta et al., 2003). Similarly, immobilisation of ORC2-5 complexes on chromatin is not sufficient for MCM2 loading in the absence of ORC1 (Ohta et al., 2003). As ORC1 appears to recruit the rest of the ORC complex to the NM, this begins to suggest that loading of MCM2 occurs in that fraction.

1.4.10 Co-ordinators and regulators

A few proteins involved in the regulation of initiation of DNA replication and cell cycle progression have also been studied in the context of the NM, including cyclin E (Munkley et al., 2011), RB (Mancini et al., 1994) and CIZ1 (Ainscough et al. 2007; appendix D).

One study of cyclin E has been particularly revealing, because it compared NM recruitment at different developmental stages (Munkley et al., 2011). In fact the NM attachment of cyclin E, a key regulator of initiation of DNA replication, may serve as a case study that goes some way to explain the differing reports of NM attachment of other replication proteins. A proportion of cyclin E is NM bound in differentiated, non-cancer primary and established cell lines. However, in all but one of eight cancer cell lines investigated, no cyclin E was observed in the NM fraction (Munkley et al., 2011). A similar distinction was seen between differentiated cells and undifferentiated cells in mouse, human and *Xenopus* model systems, so that in all cases cyclin E was easily extracted from progenitor cells but resistant to extraction in differentiated derivatives. This suggests that cyclin E is recruited to the NM as cells differentiate, and that cancer cells either originate from cells that have not recruited cyclin E, or that cyclin E is released from the NM as a consequence of one of the events that lead to transformation. In fact, failure to recruit cyclin E (and by implication, initiation) to the NM in undifferentiated and cancer cells may be one of the factors that promote plasticity in response to extrinsic or intrinsic signals. Initially, one of the aims for this PhD was to investigate the timing of recruitment of cyclin E to the NM during the cell cycle. However, due to problems with the specificity of antibodies (Santa Cruz, E4) I moved away from this part of the PhD and focussed my efforts elsewhere. At present it is not clear what protein the data that I collected refers to, so they are included here as an appendix only. This contains important information about the antibody and also demonstrates a protein transitioning between chromatin bound and NM bound fractions during the cell cycle (appendix C).

A follow on study from this lab found a similar trend for the DNA replication promoting and NM bound protein CIZ1, and the pre-RC components CDC6, ORC4 and MCM2 (appendix D). CIZ1 was found to be recruited to the NM as embryonic

stem cells (ESC) differentiated, while a proportion of pre-RC components were attached to the NM in differentiated non-cancer cells but not in a panel of cancer cell lines. The work on the pre-RC was jointly undertaken between L. Klakus, a summer student, and myself.

Although following the same trend, the behaviour of CIZ1 in cancer is more complex than that of cyclin E. In a panel of cancer cell lines, the N-terminal replication domain of CIZ1 was found to be overexpressed but not attached to the NM. At the same time, the C-terminal NM anchor domain was also somewhat overexpressed, but it maintained attachment to the NM. This suggests that the two domains of CIZ1 can be uncoupled in cancer cells. Overexpression of the replication domain would lead to the function of CIZ1 no longer being constrained to the NM. Similarly, overexpression of the anchor domain could out-compete full length CIZ1 from the likely, limiting number of attachment sites at the NM, again resulting in unattached and unconstrained replication function of CIZ1. This model is consistent with the suggestion that NM recruitment during differentiation helps to fix cell specific programs and that avoidance of this mechanism is beneficial for plasticity.

Overall, the work outlined here suggests that all three phases of DNA replication can occur in association with the NM. However, this may not be true for all cell types, making choice of experimental system crucial when planning further work. For various practical reasons, much of the analysis of DNA replication is undertaken with *Xenopus* eggs, or cancer cell lines such as HeLa, sometimes leading to the conclusion that NM immobilisation may not be important for DNA replication. I would argue that the reported differences in nuclear organisation in terms of proteins and loop attachments between embryonic systems and cancer cell lines on the one hand, and non-cancer, differentiated cells on the other, offers a clear path forward.

1.5 Nuclear changes in cancer and disease

As a common feature of cancer cells, changes in nuclear architecture and morphology have long been the basis for cancer diagnoses (reviewed in Zink et al. 2004). However, without a complete understanding of nuclear architecture in normal cells it is difficult to consider whether such changes are cause or

consequence of the dysregulation of cancer cells. In addition to genetic and epigenetic changes, there are many other recorded changes in the organisation of genes, subnuclear domains, non-linear DNA associations and regulatory and macromolecular complexes in cancer cells (reviewed extensively elsewhere, for example, in Zaidi et al. 2007). This is also true for several other diseases (reviewed in Bode et al. 2000; Linnemann and Krawetz 2009a), including the thalassaemias where deletions often correspond with S/MAR sites suggesting that a change in chromatin loop attachment is a contributory factor (reviewed in Bode et al., 2000). Changes in NM composition have been described for cancer cells compared to non-cancer cells, with some exploited as the basis of diagnostic tests (Albrethsen et al., 2009; Munkley et al., 2011, reviewed in He et al., 2008; Lever and Sheer, 2010; Zink et al., 2004, see also references therein). For example, splice variants of the NM protein CIZ1 have been reported to be associated with cancers and other disorders (section 1.1.10-12), many of which report alteration in subnuclear localisation. The MARBP SATB1 is linked to aggressive breast cancers, (reviewed in Lever and Sheer 2010) while SAF-B is inversely correlated with the proliferative rate of tumours (reviewed in Lever and Sheer 2010). A number of NM proteins (for example, RUNX, CIZ1 and cyclin E) have been reported to have an altered localisation in cancer cells, sometimes due to failure to be recruited to the NM (Higgins et al., 2012; Munkley et al., 2011; appendix D and reviewed in Zaidi et al., 2007).

This suggests that some of the dysregulation of cancer cells may be a direct result of events such as these, with DNA replication and transcription no longer spatially constrained by attachment to the NM. NM composition and loop attachments have been observed to change during differentiation and development (Munkley et al., 2011; Varma and Mishra, 2011 and reviewed in Getzenberg, 1994), leading to the idea that this may serve to 'fix' the developmental programme (Munkley et al., 2011; Vassetzky et al., 2000). This fixing of cell type specific characteristics such as transcriptional programme and replication timing may be defective in cancer cells, resulting in a partial reversal to a less specified, embryonic-like organisation of chromatin.

1.6 Project aims

Review of the aforementioned data reveals many outstanding questions relating to the interaction between DNA replication and the NM. On the basis of this, the aims of my PhD were the following;

- Develop and validate computational analysis of MFHR output in order to allow non-subjective and higher throughput analysis of MFHR data, and facilitate the investigation of NM-attached chromatin loops and how they change during the cell cycle. (Chapter 3)

- Develop and validate variations of the MFHR method to investigate the stability of chromatin loops. (Chapter 3)

- Understand how NM-attached chromatin loops change during preparation for initiation of DNA replication in order to develop our understanding of the interaction between DNA replication and the NM and the roles of the NM in this process. (Chapter 4)

- Understand the characteristics of NM-attached chromatin loops and how they change following oncogene transformation, in order to further our understanding of the role of higher order chromatin structure in cancer. (Chapter 4)

- Develop our understanding of the role of CIZ1 in relation to control of the cell cycle and cancer formation through analysis of CIZ1 knockout mouse derived cells. (Chapter 5)

2 Materials and methods

2 Materials and methods

2.1 Cell culture

2.1.1 Cell lines

CIZ1 wild type (CIZ1+/+) and knock-out (CIZ1-/-) tail tip fibroblasts (TTFs) from 3 week old mice and primary mouse embryonic fibroblasts (PEFs) were a kind gift from J. Ainscough, University of Leeds (table 2.1, appendix B). Transformed human Mesenchymal Stem Cells (MSC) were a kind gift from J. Funes and C. Boshoff, University College London, via D. Lagos, University of York (Funes et al., 2007) (table 2.2). Dominant negative p53 transformed (DNp53) Cyclin E1/E2 WT and knock-out (KO) mouse embryonic fibroblasts (MEFs) were a kind gift from Y. Geng and P. Sicinski, Dana-Farber Cancer Institute, Harvard (Geng et al., 2003) (table 2.3). MCF10A cells were a kind gift from I. Wood, University of Leeds. ARPE19 cells were a kind gift from J. Milner, University of York. MDA-MB-231 cells were a kind gift from W. Brackenbury, University of York. BJ-hTERT cells were a kind gift from R. Laskey, Hutchinson/MRC Research Centre, Cambridge. Normal Human Urothelial (NHU) cells were established and maintained as described (Southgate et al., 1994), and were kindly provided for use by J. Southgate and grown by E. Bowen. All other cell lines were obtained from American Tissue Culture Collection (ATCC) or Japanese Collection of Research Biosciences Cell Bank (JCRB).

2.1.2 Maintenance

Primary cells and cell lines were cultured at 37 degrees centigrade (°C) in a humidified atmosphere in air with 5 % CO_2 on Nunclon™ Δ Surface tissue culture coated plastic (168381, Nunc). Cells were maintained at approximately 70 % confluent density and passaged as recommended (table 2.4). To split cells, medium was removed, cells washed with warm Dulbecco's phosphate buffered saline (D-PBS) and cells lifted with 0.1 % weight per volume (w/v) trypsin-Ethylenediaminetetraacetic acid (EDTA) in D-PBS, at 37 °C in a humidified atmosphere with 5 % CO_2. Trypsin was quenched with serum in fresh medium and cells split onto new plates as appropriate. Unless otherwise stated, penicillin,

streptomycin and glutamine (PSG) was added to all media (10 U/ml, 10 µg/ml, 2.92 mg/ml final concentration respectively). Unless otherwise stated all media were obtained from Gibco® (Invitrogen) and other chemicals obtained from Sigma-Aldrich. RPMI and EMEM were obtained from Sigma-Aldrich. Fetal bovine serum (FBS) was obtained from Biosera. Cell stocks were frozen in appropriate medium with 5 % dimethyl sulphoxide (DMSO) and stored in liquid N_2.

Table 2.1: CIZ1+/+ and -/- cells used

CIZ1 status	Cell type	Sex	Number
+/+	Tail Tip Fibroblast	Female	97
+/+	Tail Tip Fibroblast	Male	101
+/+	Tail Tip Fibroblast	Female	126
+/+	Tail Tip Fibroblast	Female	133
-/-	Tail Tip Fibroblast	Female	1016
-/-	Tail Tip Fibroblast	Female	1017
-/-	Tail Tip Fibroblast	Female	1018
+/+	MEF e12		2
-/-	MEF e12		2

See appendix B for generation. Cells were supplied at passage 2 as frozen aliquots.

Table 2.2: MSC cell oncogenic transformations

Cell name	Oncogene transformations (Funes et al., 2007)			
MSC 1	pBabe(puro)-hTERT	pLXSN(neo)		
MSC 2*	pBabe(puro)-hTERT	pLXSN(neo)-E6		
MSC 3	pBabe(puro)-hTERT	pLXSN(neo)-E6E7		
MSC 4	pBabe(puro)-hTERT	pLXSN(neo)-E6E7	pBabe(zeo)-small-t	
MSC 5	pBabe(puro)-hTERT	pLXSN(neo)-E6E7	pBabe(zeo)-small-t	pWZL(hygro)-H-RASV12

MSC cell lines were supplied as frozen aliquots and did not require maintenance with antibiotic selection as advised by D. Lagos.

Table 2.3: Cyclin E KO and WT control cells used

Cell name	Details (Geng et al., 2003)
MEF WT	DNp53 transformed
MEF cyclin E1-/- cyclin E2-/- (KO)	DNp53 transformed, code G45-3/4

Table 2.4: Details of cell culture media for cell lines used

Cell line	Media	Supplements	Reference
3T3	DMEM	10 % FBS	Coverley et al., 2001
ARPE19	1:1 DMEM:F12	10 % FBS	Dunn et al., 1996
BJ-hTERT	EMEM	10 % FBS	From R. A. Laskey
CIZ1 WT and KO TTFs	DMEM	10 % FBS	From J. A. Ainscough, unpublished
CIZ1 WT and KO MEFs	DMEM	10 % FBS	From J. A. Ainscough, unpublished
Cyclin E DNp53 WT and KO MEFs	DMEM	10 % FBS	Geng et al., 2003
EJ/T24	RPMI	10 % FBS	Marshall et al., 1977, Southgate et al., 1995
HeLa (flat)	DMEM	10 % FBS	Jones et al., 1971
MCF7	MEM	10 % FBS	Brookes et al., 1973
MCF10A	1:1 DMEM:F12	5 % Horse serum, epidermal growth factor (EGF) 20 ng/ml, cholera toxin 100 ng/ml, insulin 10 µg/ml, hydrocortisone 500 ng/ml	Tail et al., 1990
MDA-MB-231	DMEM	5 % FBS	Cailleau et al., 1978

Table 2.4 (cont.): Details of cell culture media for cell lines used

Cell line	Media	Supplements	Reference
MRC5	EMEM	10 % FBS	Jacobs et al., 1970
NHU*	KSFM	0.05 mg/ml bovine pituitary extract, 0.005 µg/ml EGF, 30 ng/ml cholera toxin	Southgate et al., 1994
NIH3T3 and D3T3	DMEM	10 % FBS	Jainchill et al., 1969
RT112	RPMI	10 % FBS	Marshall et al., 1977
RT4	RPMI	10 % FBS	Rigby and Franks, 1970
Transformed Mesenchymal Stem Cells (MSCs)	MesenCult® MSC Basal Medium (Human) (05401, Stemcell Technologies)	Mesenchymal Stem Cell Stimulatory Supplements (Human) (05402, Stemcell Technologies)	Funes et al., 2007
Wi38	EMEM	10 % FBS, 1x NEAA	Hayflick and Moorhead, 1961

* Grown by E. Bowen, and without the addition of PSG.

DMEM – Dulbecco's modified Eagle's medium
EMEM – Eagle's minimum essential medium (Sigma)
KSFM – keratinocyte serum free medium
MEM – minimum essential medium
RPMI – Roswell Park Memorial Institute medium 1640 (Sigma)
NEAA – non-essential amino acids

2.1.3 Cell synchrony

Cells were synchronised in quiescence (G0) by a combination of contact inhibition and serum depletion as described (Coverley et al., 2002). Briefly, cells were plated at 70-80 % confluency and grown to 100 % confluency with no visible mitotic cells. This typically occurred 3 days after plating. Medium was changed at this point (day 0) and cells left for 4 days to reach quiescence. Quiescence was confirmed by flow cytometry, described below, or retrospectively by synchronous re-entry to S-phase.

To release quiescent cells back into the cell cycle as a synchronous wave, cells were split 1:4 into fresh medium. To monitor synchronous release, the proportion of cells in S-phase was estimated by incorporation of nucleotide analogues. At specified timepoints after release, cells on coverslips were pulsed with 100 µM of 5-bromo-2'-deoxyuridine (BrdU) or 5-ethynyl-2'-deoxyuridine (EdU) in conditioned medium (taken from the same plate as the appropriate coverslips) for 30 minutes (min).

2.1.4 Detection of BrdU

Incorporated BrdU was detected using anti-BrdU (RPN202, GE Healthcare). Cells on coverslips were washed twice with D-PBS and fixed in 4 % neutral buffered paraformaldehyde (PFA) for 25 min. Coverslips were incubated in antibody buffer (AB) (1 x PBS, 10 mg/ml bovine serum albumin - BSA, 0.02 % sodium dodecyl sulphate - SDS, 0.1 % volume per volume - v/v Triton X-100 – Tx-100) for 30 min then incubated with 20 µl anti-BrdU/DNase in a wetbox (sealed and humidified) for 60 min at 37 °C. Coverslips were washed three times in AB, 5 min per wash and then incubated with 20 µl of 1:2000 secondary antibody (table 2.6) and 0.1 µg/ml Hoechst 33258 (1:10,000 from 1 mg/ml stock) in AB in the dark in a wetbox. Coverslips were washed as previously, dipped in distilled H_2O (dH_2O) and mounted on slides with Vectashield® (H-1000, Vector Laboratories).

2.1.5 Detection of EdU

Cells pulsed with EdU were processed using the Click-iT® EdU Alexa Fluor® 555 nm Imaging Kit (C10338, Invitrogen) as per manufacturer's instructions with the following modifications: EdU was used at 100 µM, PFA was used at 4 % and

coverslips were processed in 24-well plates. Washes were 0.5 ml and 20 µl Click-iT® reaction cocktail was used per coverslip in a wetbox with Hoechst 33258 used at 1 µg/ml.

2.1.6 Classification of EdU and BrdU patterns

Patterns of nuclear DNA replication were classified as described previously (Nakayasu and Berezney, 1989), into initiating, early (both type I – excluded from nucleoli), mid (type II – including perinuclear and/or perinucleolar regions) or late (type III – heterochromatic regions). Initiating cells were classed as early pattern cells that required a high imaging exposure (minimal incorporation of nucleotide into small evenly distributed foci).

2.1.7 Imaging

Slides processed for immunofluorescence, including EdU and BrdU detection, were imaged using a Zeiss Axiovert 200M inverted light microscope, and viewed at 40 x or 64 x magnification using the filter sets shown in table 2.5. Images (file size 1388 x 1040 pixels) were taken using an AxioCam HRm digital camera and Openlab software (Perkin Elmer). Typical exposures used were 100-500 milliseconds (ms) for Alexa dyes, fluorescine isothiocyanate (FITC), tetramethylrhodamine isothiocyanate (TRITC), EdU and BrdU detection, and 5-20 ms for Hoechst 33258, 4',6-diamidino-2-phenylindole (DAPI) and ethidium bromide (EtBr) detection. Within experiments exposure times were kept constant and all images were processed equally using Photoshop CS4 (Adobe).

2.1.8 Flow cytometry

For flow cytometric analysis, adherent cells were lifted as described above, trypsin was quenched with fresh medium and cells pelleted at 10,000 revolutions per minute (rpm) for 5 min. The cell pellet was resuspended and fixed in 70 % cold ethanol and stored at -20°C. Cells were counted using a hemocytometer, then washed in D-PBS and DNA stained with 0.1 % v/v Tx-100, 0.1 mg/ml propidium iodide, at 1 mg propidium iodide per $1x10^6$ cells, in D-PBS at ambient room temperature (RT) for 1 hour (hr) then held at 4 °C overnight (O/N). Data were

collected using a CyAn™ ADP Analyser (Beckman Coulter) using Summit 4.3 software and analysed with FlowJo software. Data were gated for cells using forward and side scatter, and singlets based on linear and area of propidium iodide staining. The percentages within each cell cycle phase were determined using the vertical gates as indicated.

Table 2.5 Axiovert filter sets used

Colour	Usage	Filter set	Excitation filter	Emission filter	Emission Filter
Blue	Hoechst 33258, DAPI	2	G 365 nm	beam splitter farb teiler 395 nm	emission long pass 420 nm
Green	FITC, Alexa 488	10	Band pass 450-490 nm	beam splitter farb teiler 510 nm	emission band pass 515-565
Red	EtBr, TRITC, Alexa 555, Alexa 568	15	Band pass 546/12 nm	beam splitter farb teiler 580 nm	emission long pass 590 nm

2.2 RNAi

2.2.1 Transfection

3T3 cells were transfected with 0.3 μM small interfering RNA (siRNA) by electroporation (Nucleofector®, Lonza), using Amaxa® Cell Line Nucleofector® Kit R and programme U-030 as per manufacturer's instructions. The siRNA used were anti-*CIZ1* siRNA 4 and 8 (Coverley et al., 2002) or scrambled anti-*CIZ1* siRNA (unpublished), or anti-*cyclin E* siRNA or scrambled anti-*cyclin E* siRNA generated during this project (appendix C). Mock transfections were electroporation with no siRNA. RNA and protein samples were collected 24 hr after treatment (or as indicated) and used to confirm knock down by western blot or quantitative real time PCR (qRT-PCR).

2.3 Cell growth assays

2.3.1 Foci formation

Cells were plated in triplicate at $1.5x10^5$ cells per 6 centimetre (cm) plate and left to proliferate for 21 days, with a medium change twice-weekly. After 21 days, cells were washed twice in D-PBS at RT. Cells were fixed with 4 % PFA for 10 min. Foci were stained with 0.05 % w/v filtered crystal violet, 30 min then plates washed with dH_2O until water ran clear. Plates were air dried, scanned and foci counted.

2.3.2 Cell proliferation

Rate of cell proliferation was measured by cell counts. Equal numbers of cells were plated onto 3.5 cm dishes containing four coverslips. At day 1, 3, 4, 5 and 6 one coverslip from each cell lines was taken for counting. Coverslips were fixed with 4 % PFA for 10 min then stained with 0.1 µg/ml Hoechst 33258 in D-PBS for 30 min and mounted on slides. Nuclei were counted using a Zeiss Axiovert microscope using 64x magnification and filter set 2 (table 2.5). For each coverslip 5 whole fields were counted, averaged and expressed relative to the cell count at day 1 cell.

2.3.3 Apoptosis assay

Apoptotic cells were detected using the Click-iT® Tunel Alexa Fluor® 594 nm kit (C10246, Invitrogen), which incorporates a nucleotide analogue at nicks in DNA which are an early marker of apoptosis. Coverslips were processed as per manufacturer's instructions except for the following modifications: washes were 500 µl and incubations were 20 µl and performed in a wetbox. A positive control was prepared as recommended, one coverslip was incubated with 2 U DNase I (Epicentre) in 20 µl DNase buffer for 30 min at 37 °C.

2.4 Protein analysis

2.4.1 Total protein lysates from cells

For total protein cell lysates, cells grown on tissue culture plates were washed twice with ice cold D-PBS, drained for 2 min and scraped into cold microcentrifuge tubes with a typical volume of ≤ 100 µl per 9 cm dish. The appropriate volume of loading buffer was added from a 4 x stock to give 2 % w/v SDS, 10 % w/v glycerol, 250 mM β-mercaptoethanol, 0.004 % w/v bromophenol blue, 62.5 mM Tris-HCl pH 6.8 final concentration. Samples were vortexed and heated at 95°C for 5 min, then stored at -20 °C.

2.4.2 Nuclear fractionation lysates

For subnuclear fractionation, samples were prepared as described (Wilson et al., Submitted by request to Cold Spring Harbour Laboratory Protocols). Specifically, cells grown on 15 cm plates were washed once with ice cold D-PBS, twice with ice cold cytoskeletal buffer (CSK) (10 mM Pipes pH 6.8, 0.1 M NaCl, 1 mM ethylene glycol tetraacetic acid - EGTA, 300 mM sucrose, 1 mM $MgCl_2$, 1 mM dithiothreitol - DTT, 0.1 % v/v Tx-100, protease inhibitor - PI EDTA-free tablet – 05 056 489 001, Roche) and drained for 2 min on ice. Cells were scraped into an ice cold microcentrifuge tubes and phenylmethanesulfonylfluoride (PMSF) added to a final concentration of 1.25 mM. Samples were divided into four equal parts (1 x vol). 4 x loading buffer was added to one part (total) and heated as above (section 2.4.1). Other parts were diluted 1:1 with CSK 0.2 % v/v Tx-100, mixed and pelleted at 10,000 rpm for 2 min. All centrifugations were using a benchtop microfuge of radius 5 cm and at 4 °C. 4 x loading buffer was added to one pellet, which was resuspended in 1 x vol CSK (detergent pellet) and to one supernatant (detergent supernatant) to form soluble and insoluble cell fractions. Other parts were resuspended in 1 x vol CSK 0.1 % v/v Tx-100, 0.5 M NaCl, mixed and pelleted at 10,000 rpm for 3 min. 4 x loading buffer was added to one supernatant (salt wash) to form the 'loosely bound to chromatin' fraction. Other parts were washed in 100 µl DNase buffer (10 mM Tris pH 7.5, 10mM $MgCl_2$, 5 mM $CaCl_2$ - Epicentre) then resuspended in 1 x vol DNase buffer with or without 1:30 DNase I (D9902K, Epicenter) (DNase or Mock) and

incubated at 37 °C for 60 min with mixing. NaCl was added to 0.5 M and samples were incubated at 37 °C for a further 5 min, then pelleted at 13,000 rpm for 5 min. Supernatants were transferred to fresh microcentrifuge tubes and DNase pellet and Mock pellet were resuspended in 1x vol DNase buffer. 4 x loading buffer was added to pellet and supernatant fractions. DNase supernatant represents the 'tightly bound to chromatin' fraction and DNase pellet represents the NM bound fraction. Samples were stored at -20 °C. For western blot analysis, α-histone H3 (Abcam) was used to confirm fractionation, with presence expected in total, detergent pellet, DNase supernatant and mock pellet lanes only.

2.4.3 SDS –PAGE gels and transfer

Total protein lysates or fractionated lysates were separated using 5 % stacking and 8 % separating SDS-PAGE. Stacking gel was 5 % w/v acrylamide (ProtoGel®, National Diagnostics), 0.13 M Tris-HCl pH 6.8, 1.0 mg/ml ammonium persulphate (APS), 0.2 % w/v SDS, 0.2 % v/v tetramethylethylenediamine (TEMED). Separating gel was 8 % acrylamide, 0.37 M Tris-HCl pH 8.8, 0.8 mg/ml APS, 0.1 % w/v SDS, 0.13 % v/v TEMED. 30 µl of sample was loaded into each well or 15 µl of marker. Lanes had equivalent cell number apart from 'detergent supernatant' which had half the equivalent cell number. Gels were run in Tris Glycine SDS running buffer (0.025 M Tris, 0.192 M glycine, 0.1 % w/v SDS, B9-0032, Geneflow). Precision Plus Protein™ All Blue (161-0373, Biorad) was used as a size marker.

Separated proteins were transferred onto Protran® Nitocellulose Transfer Membrane (10402096, Watman®) using Sigma semi-dry blotter (Sigma) at 0.8 mA/cm^2 for 2 hr. Specifically, SDS-PAGE gel, membrane and blotting paper were soaked in transfer buffer (0.3 M Tris, 10mM N-cyclohexyl-3-aminopropanesulfonic acid - CAPS, 0.02 % w/v SDS, 10 % v/v methanol) and layered up as follows, four pieces blotting paper, membrane, gel, four pieces blotting paper. Alternatively, proteins were transferred onto iBlot™ Gel transfer Stack (IB3010-01, Invitrogen) using iBlot™ (Invitrogen) programme P3, 7 min. Membranes were stored at -20 °C.

2.4.4 Western blotting

For western blotting analysis, membranes were blocked with milk or BSA blocking buffer depending on antibodies (table 2.6), for 30 min, then incubated with primary antibody in blocking buffer for 2 hr at RT or O/N at 4 °C. Membranes were washed three times, each for 10 min in blocking buffer then incubated with the appropriate secondary antibody (horse radish peroxidase (HRP) conjugated anti-mouse, anti-rabbit or anti-rat) in blocking buffer for 1 hr at RT. Membranes were then washed three times in wash buffer (as blocking buffer without milk or BSA). Blots were imaged using 1:1 mix of EZ-ECL A and B detection reagent (20-500-500A and B, Biological Industries), Amersham Hyperfilm™ ECL (GE Healthcare) and a Compact X4 Automatic X-ray Film Processor (Xograph Imaging Systems).

2.4.5 Nuclear fractionation for immunofluorescence

Cells on coverslips underwent sequential extractions to reveal detergent resistant and DNase resistant fractions as described (Wilson et al., Submitted by request to Cold Spring Harbour Laboratory Protocols). Specifically, for total protein samples, coverslips were washed in D-PBS, then fixed in 4 % PFA for 15 min at RT. Detergent extracted samples were washed in D-PBS, then CSK buffer with 0.1 % v/v Tx-100 and again in D-PBS and fixed as for total. High salt and DNase I or High salt only extracted samples were washed in D-PBS, then CSK 0.1 % v/v Tx-100, followed by CSK 0.1 % v/v Tx-100, 0.5 M NaCl, and twice in DNase I buffer (Epicentre). Coverslips were incubated with 20 µl DNase I buffer (Epicentre) with or without 1:10 DNase I (D9902K, Epicentre) at 37 °C for 60 min in a wetbox. Coverslips were washed in CSK 0.1 % v/v Tx-100, 0.5 M NaCl then fixed as for total. Coverslips were processed for immunofluorescence as described for BrdU staining except primary antibody (table 2.6) incubations were 2 hr. In all cases Hoechst 33258 was used to counterstain cells except for samples in which the protein of interest was extracted making visualisation after DNase treatment difficult. In this case Propidium iodide was also used to counterstain cells. Absence of Hoescht 33258 staining was used to confirm DNase digestion.

2.4.6 Antibodies

Unless otherwise stated all mouse antibodies were monoclonals, and all rabbit and goat antibodies were polyclonals.

Table 2.6: Details of antibodies used, buffers and timings

		Western blot		IF
Antibody	**Dilution**	**Blocking buffer**	**Time**	**Conc.**
mouse α-actin (A-4700, Sigma)	1:1000	milk TBS	2 hr RT	-
mouse α-BrdU (RPN202, GE Healthcare)	-	-	-	1:100
mouse α-CDC6 (180.2, sc9964, Santa Cruz)	1:250	milk TBS or BSA TBS	4 °C O/N	1:50
rabbit α-CDK2 (ab7954, Abcam)	-	-	-	1:200
rabbit α-CIZ1 (1793, Coverley et al., 2005)	1:1000	milk PBS	2 hr RT	1:200
rabbit α-CIZ1 (NB100-74623, Novus Biologicals)	1:1000	5 % milk PBS	2 hr RT	-
mouse α-cyclin A (C4710, Sigma)	1:1000	milk TBS	2 hr RT	1:500
rabbit α-cyclin D2 (M20, sc593, Santa Cruz)	-	-	-	1:100
rabbit α-cyclin E (07-687, Upstate)	1:500	milk TBS	2 hr RT or 4 °C O/N	1:500
rabbit α-cyclin E (ab7959, Abcam)	1:500	milk TBS	4 °C O/N	1:500
mouse α-cyclin E (E4, sc25303, Santa Cruz)	1:200	BSA TBS	2 hr RT	1:100

Table 2.6 (cont.): Details of antibodies used, buffers and timings

	Western blot			IF
Antibody	**Dilution**	**Blocking buffer**	**Time**	**Dilution**
mouse α-γH2AX (05-636, Upstate)	-	-	-	1:2000
rabbit α-histone H3 (ab1791, Abcam)	1:10,000	milk TBS	2 hr RT	-
mouse α-lamin B2 (E-3, 33-2100, Invitrogen)	1:200	milk TBS	2 hr RT	1:200
mouse α-MCM2 (BM28, 610700, BD Transduction Laboratories)	1:1000	milk TBS	2 hr RT or 4 °C O/N	1:100
rat α-ORC1 (7A7, 05-935, Upstate)	1:500	BSA TBS	4 °C O/N	1:50
rabbit α-pATM (S1981) (ab2888, Abcam)	-	-	-	1:400
rabbit α-pCHK1 (S345) (2348S Cell Signalling Technology)	-	-	-	1:100
mouse α-$p21^{CIP1}$ (556430, BD Pharmingen™)	-	-	-	1:500
rabbit α-$p21^{CIP1}$ (PC55, Calbiochem)	-	-	-	1:100
mouse α-$p27^{KIP1}$ (P2092, Sigma)	-	-	-	1:100
rabbit α-$p27^{KIP1}$ (ab7961, Abcam)	-	-	-	1:50
mouse α-p53 (Pab246, Santa Cruz)	-	-	-	1:100
rabbit α-substrate for ATM/ATR (2851S, Cell Signalling Technology)	-	-	-	1:200

Table 2.6 (cont.): Details of antibodies used, buffers and timings

	Western blot			IF
Antibody	**Dilution**	**Blocking buffer**	**Time**	**Conc.**
goat α-mouse Alexa fluor® 488 (A11001, Invitrogen) 568 (A11031, Invitrogen)	-	-	-	1:1000 except for E4, 1:200
goat α-rat Alexa fluor® 488 (A11006, Invitrogen)	-	-	-	1:1000
goat α-rabbit TRITC (T6778, Sigma)	-	-	-	1:100 – 1:200
goat α-mouse HRP (ab6789, Abcam)	1:10,000	As primary	1 hr RT	-
goat α-rabbit HRP (ab6721, Abcam)	1:10,000	As primary	1 hr RT	-
goat α-rat HRP (A9037, Sigma)	1:10,000	As primary	1 hr RT	-

Milk PBS - 10 % w/v non-fat dried milk (Marvel), 1 x phosphate buffered saline (PBS), 0.1 % tween-20
Milk TBS - 10 % w/v non-fat dried milk (Marvel), 1 x tris buffered saline (TBS), 0.1 % tween-20
BSA TBS – 1 % w/v BSA, 1 x TBS, 0.1 % tween-20

Suggested dilutions are given to aid future students in the Coverley lab, however, they should be optimised before use.

2.5 Transcript analysis

2.5.1 Total mRNA extraction and cDNA synthesis

RNA was extracted using Trizol® (Ambion). Plates were washed with D-PBS, scraped into 800 µl Trizol® and stored at -80 °C. Samples were thawed, mixed

vigorously with 200 µl chloroform and left to stand for 5 min at RT. Aqueous and organic phases were separated at 12,000 rpm (benchtop microfuge, radius 5 cm) for 15 min at 4 °C and 700 µl isopropanol added to top aqueous phase. RNA was precipitated at -20 °C O/N then pelleted at 12,000 rpm for 20 min at 4 °C. The pellet was washed with 500 µl 70 % ethanol, air dried, resuspended in diethylpyrocarbonate treated (DEPC) H_2O and stored at -80 °C. cDNA was synthesised from 2 µl RNA with 0.5 µl 500µg/ml random primers (C118A, Promega), 0.5 µl 500ng/µl oligo dT (RT, Thermo scientific) and 1 µl 10 mM deoxyribonucleotide tiphosphate (dNTP) mix in 13 µl. Samples were heated at 65 °C for 10 min then left on ice for 5 min before addition of 4 µl 5 x first strand buffer, 1 µl DTT, 1 µl DEPC H_2O and 200U SuperScript III (18080-093, Invitrogen). Samples were heated at 25 °C for 5 min then at 50 °C for 50 min followed by 70 °C for 15 min, and then diluted to 80 µl.

2.5.2 Quantitative real-time polymerase chain reaction (qRT-PCR)

QRT-PCR was performed by the standard protocol. cDNA was assayed in triplicate at 5 µl per well with addition of 12.5 µl Power SYBR® Green PCR mix (4367659, Applied Biosystems), 0.5 µl of each primer and 6.5 µl H_2O for cyclin E primers (table 2.7), or 12.5 µl TaqMan® 2x PCR Master Mix (R03224, Applied Biosystems), 0.625 µl primer and 6.875 µl H_2O for GEX primers (β-actin, table 2.7), both prepared as a mastermix. QRT-PCR was performed on the 7000 system (ABI) with the following protocol; 50 °C for 2 min, 95 °C for 10 min, 40 cycles of 95 °C for 15 seconds (s) and 60 °C for 1 min, followed by 95 °C for 15 s, 60 °C for 20 s and 95 °C for 15 s. Primer sequences are shown below (table 2.7), mouse cyclin E1 and E2 primers were described previously (Parisi et al., 2003). Relative transcript expression was calculated using the Livak method (Livak and Schmittgen, 2001) with the following formulae.

ΔC_T = C_T gene of interest – C_T normalising gene (actin)
$\Delta\Delta C_T$ = ΔC_T for condition x – ΔC_T for calibrating condition (mock)
RQ = Average of triplicate ($2^{-\Delta\Delta CT}$)

Table 2.7: RT-PCR primers

Primer	Forward	Reverse
MmCcne 1 (Mouse cyclin E1)	TGTTTTTGCAAGACCCAGATGA	GGCTGACTGCTATCCTCGCT
MmCcne 2 (Mouse cyclin E2)	GGAACCACAGATGAGGTC	CGTAAGCAAACTCTTGGAG
Mouse β-actin	Mm00607939_sl (Applied Biosystems)	

2.6 Maximum Fluorescence Halo Radius (MFHR)

Methods for MFHR using EtBr and DAPI are described in the following method development chapter (section 3.3). Also described are analysis methods including the development of an ImageJ macro to semi-automatically and non-subjectively measure halos from MFHR analysis. The developed method for MAR analysis is also including in the method development chapter.

2.7 Chemical inhibitors

The protein synthesis inhibitor cycloheximide was used at 0.1 μg/ml in cell culture and activity was confirmed by failure to enter S-phase. The topoisomerase II inhibitor etoposide was used at 10 μM and activity was confirmed by γH2AX staining. The CDK inhibitors Roscovitin and Olomucin were used at 20 μM and 100 μM respectively. Activity was confirmed by failure to enter S-phase. The proteasome inhibitor MG132 was used at 100 μM and activity was confirmed by failure to enter S-phase. DMSO controls contained the appropriate amount of DMSO, at no more than 1:1000.

3 Maximum Fluorescence Halo Radius (MFHR) method development

3 Maximum Fluorescence Halo Radius (MFHR) method development

3.1 Introduction

This chapter concerns the technical development, calibration and validation of the MFHR method. It is written so that naïve users in the future will find all the practical information necessary. The chapter also describes the development of MFHR to allow accurate measurement of nuclear stability and the isolation of nuclear matrix associated DNA fragments (MARs).

The MFHR technique was first developed in 1980 to observe chromatin loops under a light microscope (Vogelstein et al., 1980), to complement evidence from electron micrographs (Paulson and Laemmli, 1977). The advantages of the fluorescence-based methods are that they are easier to perform than electron microscopy and allow many more conditions to be tested. Briefly, cells are treated with detergent to removed membranes, then NaCl or other salts to remove histones and other chromatin bound proteins, and finally DNA is stained with ethidium bromide (EtBr) or another intercalating dye. Cells are also usually treated with ultraviolet (UV) light to cause nicking of DNA and aid chromatin loop expansion. These extracted cells are then visualised under a microscope revealing a central bright region corresponding to the original nuclear area (hereafter referred to as residual nucleus, RN), with an outer halo corresponding to chromatin loops that have extended out from the RN (fig 3.1). The halo radius can be measured giving the average chromatin loop size as twice the radius. Several variations of this technique exist and include combining MFHR with FISH or immuno-labelling, and a method for isolated metaphase chromosomes (Aranda-Anzaldo and Dent, 1997; Bickmore and Oghene, 1996; Cai and Kohwi-Shigematsu, 1999; Gerdes et al., 1994; Heng et al., 2004; Iarovaia et al., 2004; Paulson and Laemmli, 1977; Roti Roti and Wright, 1987; Thomas and Thomas, 1989). However, the most common methods are the original Vogelstein method, described here as Ethidium Bromide MFHR (EtBr MFHR), and the DAPI MFHR method, described by Guillou et al. (2010), which includes a chemical fixation step.

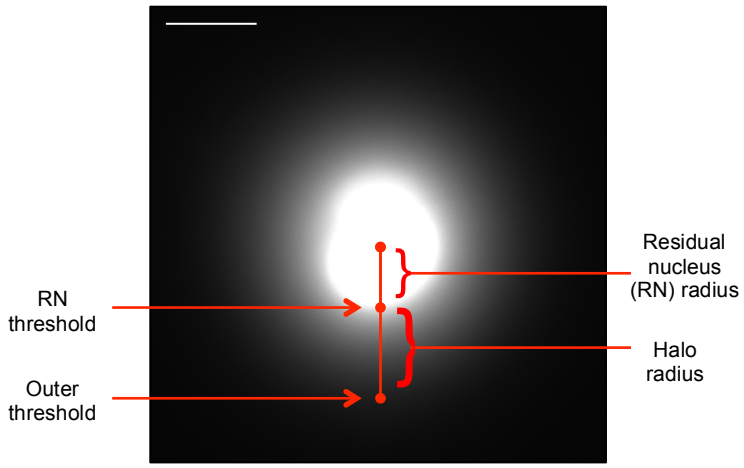

Figure 3.1: Definition of MFHR terms. Example MFHR image showing RN and halo, indicating RN and outer thresholds. Note that automatic measurement of thresholds (derived from area measurements) compensate for non-spherical nuclei (see later).

Please note: The outer threshold in particular, reproduces better on screen than in print. I have chosen not to contrast enhance these images for print copies as this would visually change the RN threshold. Please see the accompanying DVD to view MFHR images on screen.

MFHR has been used to interrogate individual genes (Gerdes et al., 1994; Heng et al., 2004), to compare chromatin loop sizes from different organisms and different developmental stages (Buongiorno-Nardelli et al., 1982; Flickinger et al., 1986; Taylor et al., 1991), and determine the effect of knockdown of specific proteins (Guillou et al., 2010; Yamazaki et al., 2012), or different replication conditions (Courbet et al., 2008; Lemaitre et al., 2005; Vogelstein et al., 1980). As a result of MFHR analysis we now know, for example, that newly replicated DNA is found at the base of loops and then moves into the loop itself, suggesting DNA replication occurs at the nuclear matrix (Gerdes et al., 1994; Vogelstein et al., 1980) and that transcriptionally active genes tend to be tightly bound to the nuclear matrix rather than on long chromatin loops as for transcriptionally inactive genes (Gerdes et al., 1994). It has also been shown that cohesin and Rif1 regulate the size of chromatin loops (Guillou et al., 2010; Yamazaki et al., 2012) and that larger chromatin loops are observed in cells with faster replication fork speed (Courbet et al., 2008). Other methods have been used to interrogate chromatin loop sizes including digestion by nucleases or topoisomerase (Jackson et al., 1990; and reviewed in Wilson and Coverley, 2013).

MFHR related methods have been developed to study MARs, that is, the bases of chromatin loops. Briefly, cells are processed in a similar way to MFHR, DNA loops are digested and the fraction remaining attached to the NM is recovered. Depending on the extraction method employed, DNA fragments are referred to as MARs, SARs or skeleton-attached regions (section 1.3.2-4). To my knowledge, only one genome wide investigation of MARs, comparing them to SARs and skeleton-attached sequences, has been published (Linnemann et al., 2009). Other evidence about MARs comes from the collation of MAR data revealed from individual gene studies (reviewed in Wilson and Coverley 2013).

3.2 Aims

The aim of this piece of work was to further develop the use of the MFHR technique allowing more detailed analysis of loop size and stability. Initial work to set up basic MFHR had been undertaken by a summer student, Laura Knight. Continuing from her work my aims were as follows:

- determine appropriate microscope settings for standard image capture
- develop an automatic and non-subjective method to measure halo radius from microscope images
- develop other methods, based on MFHR, to compare the stability of chromatin loops between cell lines
- develop a method to fractionate and sequence MARs

3.3 Experimental procedures

Development of image analysis techniques to determine chromatin loop size were undertaken using samples from mouse 3T3 cells processed by EtBr MFHR. An ImageJ macro, entitled Halo Intensity Macro (HIM) was written for automated processing of MFHR images (fig 3.2). New analysis methods were developed during this work to interrogate response of cells to MFHR and stability of loop attachments over time. In addition, a method was developed to isolate and sequence MARs.

A

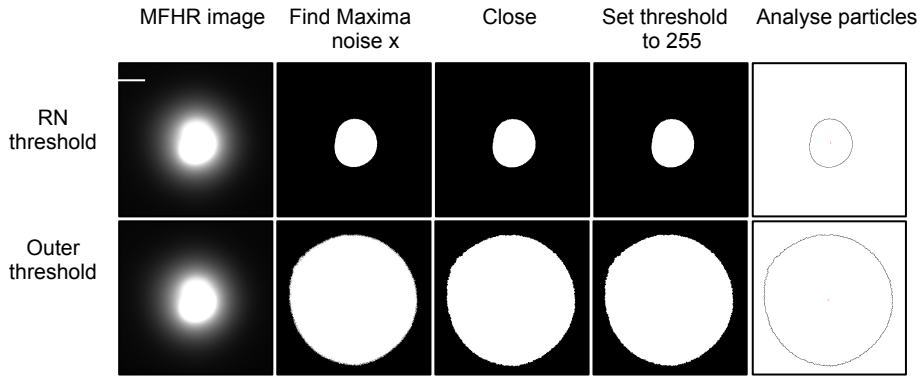

B

```
// Ask user for source and destination directories
dir = getDirectory("Roses Source Directory");
dest1 = getDirectory("Roses Destination Directory");
dest2 = getDirectory("Roses Destination2 Directory");

list = getFileList(dir);
setBatchMode(true);

for (i=0; i<list.length; i++) {
        name = list[i];
        path = dir + name;

      // Open image
      open(path);
            // Macro
            run("Find Maxima...", "noise=55 output=[Maxima Within Tolerance]");
            run("Close-");
            //run("Threshold...");
            setThreshold(255, 255);
            run("Convert to Mask");
            run("Analyze Particles...", "size=3000-Infinity pixel circularity=0.00-1.00 show=Outlines display
exclude");
            //
            saveAs("Tiff", dest1+name);
            close();
            close();

            run("Find Maxima...", "noise=240 output=[Maxima Within Tolerance]");
            run("Close-");
            //run("Threshold...");
            setThreshold(255, 255);
            run("Convert to Mask");
            run("Analyze Particles...", "size=3000-Infinity circularity=0.00-1.00 show=Outlines display exclude");
            saveAs("Tiff", dest2+name);
            close();
            close();


      // Clean up
      selectWindow(name);
      close();
}
```

Figure 3.2: Explanation of HIM for ImageJ. A) Images show visual representation of the steps within the macro. B) ImageJ HIM macro script. File name: Halo 55 240, archived in Coverley lab R drive, methods.

3.3.1 Cell culture

Cells for MFHR analysis were grown on coverslips in asynchronous cultures or taken at desired timepoints after synchronisation. For asynchronous analysis cells at 50-70 % confluence were used. For each data point (excluding some development data) the minimum number of replicates used was four. Cells were taken for MFHR on two separate days, the second being after at least one passage to include a biological replicate. On each day, two coverslips were taken forming technical replicates.

3.3.2 EtBr MFHR

The EtBr MFHR method has been described previously (Buongiorno-Nardelli et al., 1982; Lemaitre et al., 2005). For analysis performed here, the following changes were made: 0.25 % Igepal (NP40 substitute) was used instead of 0.5 % NP40, and a development incubation of 5 mins was included. Briefly, cells on coverslips were washed in D-PBS followed by 1 min incubation in NP40 extraction buffer (0.25 % Igepal, NP40 substitute, 10 mM $MgCl_2$, 0.5 mM $CaCl_2$, 50 mM Tris-Cl pH 7.5). Coverslips were incubated 30 s in each of 0.5 M NaCl, 1.0 M NaCl and 1.5 M NaCl extraction buffers (0.2 mM $MgCl_2$, 10 mM Tris-Cl pH 7.5). All incubations were performed in ice cold buffers, on ice. Coverslips were incubated in ice cold 2.0 M NaCl, 100 µg/ml EtBr for 2 min at RT including 1 min 240 nm UV treatment. Coverslips were mounted on slides and incubated in the dark for 5 min. Halos were imaged at 5 ms, on a Zeiss Axiovert 200M fluorescent microscope using Zeiss filter set 15 (table 2.5). Images (file size 1388 x 1040 pixels) were taken using an AxioCam HRm digital camera and Openlab software. Images were taken for a maximum of 10 min with typically 50-80 images taken per coverslip.

3.3.3 DAPI MFHR

Cells were extracted to reveal chromatin loops and proteins or nucleotide incorporation visualised by immunofluorescence based on the method previously described (Guillou et al., 2010) with some differences. Cells on coverslips were pulsed with BrdU if required (section 2.1.3-4). All incubations were using ice-cold buffers and performed on ice. Coverslips were washed in D-PBS, incubated in nuclei buffer (10 mM Tris-HCl pH 8.0, 3 mM $MgCl_2$, 0.1 M NaCl, 0.3 M sucrose, PI) with 0.25

% Igepal for 10 min, and in nuclei buffer without Igepal for 30 s. All further steps were performed in the dark. Coverslips were incubated in 2 μg/ml DAPI in D-PBS, 10 min, in 0.5 M NaCl buffer (25 mM Tris pH 8.0, 0.5 M NaCl, 0.2 mM $MgCl_2$, 1 mM PMSF, PI), 1 min, and in HaLo buffer (10 mM Tris-HCl pH 8.0, 2.0 M NaCl, 10mM EDTA, 1mM DTT, PI), 4 min including 1 min 240 nm UV. Coverslips were washed in wash 1 (25 mM Tris-HCl pH 8.0, 0.2 M NaCl, 0.2 mM $MgCl_2$) for 30 s, in wash 2 (25 mM Tris-HCl pH 8.0, 0.2 mM $MgCl_2$) for 30 s and fixed in 2 % PFA for 10 min. Coverslips were then processed for immunofluorescence as described (section 2.1.4) with the alterations that the cells were incubated with primary antibody instead of BrdU and DNase, and for 2 hrs, and the secondary antibody concentration used was 1:1000. DAPI MFHR images were taken as for EtBr MFHR with the alteration that images were taken at 14 ms, using filter set 2 (table 2.5).

3.3.4 File types

MFHR images were saved as Openlab LIFF files and also using the 'save as multiple' function, as 'TIFF For Publication' files. Openlab LIFF files were stored on DVDs, archived by experimental date, to allow cross-reference with lab books. TIFF For Publication files were used to determine halo radius, using ImageJ 1.46 for Mac OS X (NIH).

3.3.5 Analysis by eye

For analysis by eye, TIFF For Publication files were opened in ImageJ. Areas were calculated using the 'polygon' function to draw around the required area and quantified using the 'measure' function to derive an area value. Halo radius measurements were calculated using the 'line' function to draw from the outer edge of the RN to the outer edge of the halo, followed by the 'measure' function. Where possible, all measurements were taken at the lower edge of each halo.

3.3.6 Analysis by HIM

Use of HIM (fig 3.2) is described in more detail below. Briefly, HIM opens each TIFF For Publication file within the data folder, selects a region of interest (ROI) within each individual image based on the 'RN threshold', measures the area and saves a

copy of the new file, with the ROI shown, in the Threshold RN folder. This is repeated for the 'outer threshold', saving the new file in the Threshold outer folder. The output for each file is a RN threshold analysis picture, an outer threshold analysis picture and area measurements for each within the Results dialogue box. ROIs and area measurements are numbered to allow cross checking.

3.3.7 Operational instructions for HIM

The following folder structure was created, Desktop: ImageJ analysis: Data, Threshold RN, Threshold outer. Macro files were saved in the folder ImageJ analysis. To use ImageJ macro HIM, ImageJ was opened and desired HIM loaded using the command, Plugins: Macros: Install. Appropriate TIFF For Publication files were copied into the Data folder and Threshold folders were emptied. The HIM was run by the following command, Plugins: Macro: and the installed HIM selected.

Dialogue boxes are first opened to ask for source and destination directories. These refer respectively to the folder containing source data, and folders where output files will be stored. Data folder should be selected as Roses Source Directory and Threshold RN and Threshold outer should be chosen as Roses Destination Directory and Roses Destination2 Directory. The HIM then runs without further prompting. The 'setBatchMode' command stops the visual opening and processing of each file. This command may be removed to visualise the steps or to troubleshoot.

To manually perform the same steps as HIM the following instructions should be followed (direct instructions in italics):

Open file in ImageJ
Select ImageJ: Process: Binary: Find maxima
Dialogue box opens, *select Noise tolerance 55, Maxima within tolerance, nothing ticked*. This results in a new picture, and selects the pixels based on the threshold of pixel intensity 55. The area in white will be measured.
ImageJ: Process: Binary: Close
The individual pixels selected will then be closed as an ROI.
ImageJ: Image: Adjust: Threshold
In dialogue box, *Set thresholds at 255, default, red, box not ticked, Apply, close box*

ImageJ: Analyze: Analyse Particles

In dialogue box, *Size 3000-Infinity, Pixel units ticked, Circularity 0.00-1.00, Show Outlines, Only Display results and Exclude on Edges ticked*.

This results in area measurements taken for white areas bigger than 3000 pixels.

Save new picture in Threshold RN, Close all open files.

These steps are then repeated using Noise tolerance as 240 to generate the total area, using the outer threshold, and the analysis picture is saved in Threshold outer.

3.3.8 Manual checking of measurement output and final output

Area measurements generated by the HIM were copied to an Excel document for further analysis (table 3.1). Firstly all files with an area measurement equalling 1.4387E+10 were selected, deleted and recorded as 'Failed whole pic'. For these, ROIs correspond to the whole picture and occur when the threshold selected the whole area due to an abnormally bright picture, or if the whole image was extremely pale. Very occasionally a single measurement is recorded, these were also excluded from analysis.

Images within the 'Threshold outer' folder were then manually checked for joined cells, cells cut by the edge of the picture and occasional extraneous particles. For each file name there may then be two, four or six area measurements, corresponding to images with one, two or three cells, respectively. Lists of areas were manually checked to ensure this was the case. For file names with, for example, three measurements, images were checked to identify and remove the inappropriate measurement. The relevant formulae were applied (table 3.1), ensuring these were correct for filenames with more than two measurements, and mean, count and standard error outputs generated for each data set.

3.3.9 Classification method

For 'halo classification', halos were visually scored from images based on the following criteria; class I (bright) – defined RN that is bright, almost 100 % white (pixel intensity ≥ 250), class II (pale) – defined RN which is pale and does not meet criteria for class I (pixel intensity < 250), and class III – no defined RN and appear disintegrated.

Table 3.1: Excel formulae for MFHR analysis.

	A	B	C	D	E	F	G
1	5ms	macro 55, 240					
2	3T3	Image	Area	Area/10000	Radius	Halo radius (pixels)	Halo radius (µm)
3	1	3T3 Maxima	X	=C3/10000	=SQRT (D3/3.141)	=E4-E3	=E3/9.5238
4	2	3T3 Maxima	Y	=C4/10000	=SQRT (D4/3.141)		

Template archived in Coverley lab R drive: methods.

3.3.10 Stability data sets

Collection of a series of images over time can be used to quantify stability and rate of decay of halos. For stability data sets the above manual checks were undertaken with the exclusion of the removal of 1.4387E+10 areas, and an additional check to ensure 7 images were collected for each MFHR treated cell. After relevant formulae were applied, halo radius measurements of > 60 µm were identified (derived from files with areas of 1.4387E+10). These represent timepoints at which halo radius measurements were no longer possible because the halo failed to survive the method. For each sample, for each timepoint, the number of cells with a measurable halo radius was then determined.

3.3.11 MAR sample preparation

Samples from stated timepoints were prepared to closely follow the above MFHR method. Cells on 15 cm plates were washed twice in ice cold D-PBS and scraped into ice cold microcentrifuge tubes (volume approximately 1.5 ml). Cells were pelleted at 10,000 rpm (benchtop microfuge), 2 min, 4 °C. Cells were resuspended in 900 µl NP40 buffer (as section 3.3.2 with addition of one PI-EDTA free tablet per 50 ml) and incubated on ice 1 min. Cells were pelleted as above. Cells were resuspended in 900 µl 0.5 M NaCl extraction buffer (as section 3.3.2 with addition of one PI-EDTA

free tablet per 50 ml) and incubated on ice. NaCl was increased by 0.5 M every 30 s up to 2.0 M and cells incubated 30 s. Nucleoids were pelleted at 14,000 rpm, 10 min, 4 °C. Supernatant was removed to leave approximately 100 µl volume. To this was added 600 µl high-performance liquid chromatography (HPLC)-H_2O, 120 µl 10 x Roche DNase buffer (04 716 728 001, Roche), 120 U DNase I (04 716 728 001, Roche) and volume made up to 1.2 ml with HPLC-H_2O. Nucleoids were incubated 4 hr, 37 °C. DNase digestion was ended with addition of 179 µl Stop buffer (0.2 M EDTA, 10 mM Tris pH 7.5) (Maya-Mendoza et al., 2005).

Sample washing and protein digestion

Nuclear matrix preparations were washed as described (Maya-Mendoza et al., 2005). Specifically, preparations were vortexed 15 s and centrifuged 12,500 rpm, 10 min, 4 °C. Preparations were resuspended in 1 ml D-PBS, vortexed and centrifuged as above and this step repeated. Preparations were resuspended in 1 ml HPLC-H_2O, vortexed and centrifuged as above and this step repeated. Preparations were resuspended in 100 or 300 µl (digested or genomic samples) Tail Lysis Buffer (10 mM Tris-HCl pH 8.0, 50 mM EDTA, 1 % SDS). Preparations were incubated with proteinase K (V302B, Promega) at 1 mg/ml, 56 °C, 3 days, then reaction stopped with 5 mM PMSF. Volume made up to 300 µl with D-PBS.

Phenol:chloroform extraction of DNA and RNA digestion

Equal volume of phenol:chloroform:isoamyl alcohol (125:24:1, AM9720, Ambion®) was added and samples vigorously shaken for 30 min, then aqueous and organic layers separated by centrifugation, 10,000 rpm, 10 min, RT. Equal volume of chloroform:isoamyl alcohol (24:1) was added to top aqueous layer and shaken as above, then aqueous and organic layers separated by centrifugation, 10,000 rpm, 1 min, RT. NaOAc (3 M) was added at 1:10 vol to top aqueous layer and vortexed, followed by equal volume of cold isopropanol. DNA was precipitated O/N at -20 °C. DNA was pelleted at 13,000 rpm, 60 min, RT then washed in 95 % ethanol and pelleted at 13,000 rpm, 20 min, RT. Pellet was air dried and resuspended in nuclease free H_2O. 10U RNase I (EN0601, Fermentas) per µg sample was added and incubated 37 °C, 30 min. DNA fragments were separated on 1.2 % agarose gel, 50 v, 2 hr. Samples were loaded using 6 x Blue/Orange loading dye (G190A, Promega). 100 bp

(N3231S, NEB) and 1 kbp (N3232S, NEB) DNA ladders were used to determine size of DNA fragments. Fragments ≤ 5 kbp were cut from gel and extracted with either Gene Clean® Turbo gel extraction kit (1102-200, MP Biomedicals) or Elutrap Electroelution System (Whatman, as per manufacturer's instructions). Briefly, gel slices are inserted into a chamber bordered by manufacturer's membranes, BT1 and 2. The system was run as for a standard DNA gel, 150 V, 2 hrs. DNA samples run out of the gel and are trapped by a BT1 membrane. Polarity is then reversed for 20 s, sample moves into a buffer chamber created by membrane placement and can be recovered. After Elutrap Electroelution, samples were concentrated to ~ 66 µl using Ambion Ultra 0.5 spin columns, centrifugation at 14,000 g, 5 mins followed by reversal of inner tube and centrifugation at 1000 g, 2 mins. Salt concentration was reduced using QIA quick PCR purification kit (Qiagen) and DNA eluted in 30 µl nuclease free H_2O.

Ion Torrent high throughput sequencing

DNA fragment samples were visualised on an agarose gel and by 2100 Bioanalyzer (Agilent) using the DNA High Sensitivity chip (performed by Celina Whalley, York Technology Facility). Samples were submitted for sequencing using the Ion Torrent PGM™ sequencing system (Life Technologies). Libraries were prepared using the Ion Xpress™ Plus gDNA Fragment Library Preparation kit, and individually barcoded using Ion Xpress™ Barcode Adapters 1-16 kit. Samples were pooled in eqimolar amounts and library size assessed on a DNA High Sensitivity chip on the 2100 Bioanalyser. The pooled library was diluted to 26 pM and templates prepared by Ion OneTouch™ 200 Template kit v2 DL, and samples processed using the Ion PGM™ 200 Sequencing Kit v2 on an Ion 318™ chip using the Ion Torrent PGM™ Sequencer (Celina Whalley, York Technology Facility).

3.4 Results and discussion

3.4.1 Microscope settings

Firstly the appropriate microscope image capture settings were determined (fig 3.3). To accurately visualise the boundaries of the RN, 3T3 cells were transfected

with EGFP-CIZ1 C-term274 (anchor domain, AD), which is known to localise to the nuclear matrix (Ainscough et al., 2007). Cells were processed for MFHR and multiple exposures taken (3, 4, 5, 6, 10 ms) along with a 100 ms GFP image, which is a typical exposure used to capture the full dynamic range of GFP. For all images, RN areas were measured by eye and radius measurements calculated, then compared to those generated from GFP images. A 5 ms exposure generated the closest radius (100.3 %) to that derived from the GFP image. Therefore, 5 ms exposures were used in all future MFHR analysis.

3.4.2 Threshold choices

For a fixed exposure, appropriate pixel intensities for RN and outer thresholds could then be determined. First, the HIM was run for RN areas only, using a range of pixel intensity thresholds between 15 and 105 (fig 3.4 A, B). Using a threshold of 15 returned areas of intensity 0-15 (with white as 0) and 105 returned a range intensity of 0-105. As expected, when a smaller range of intensities was used (0-15) smaller areas were recorded. HIM calculated radius measurements were then compared to radius measurements calculated by eye. Using an intensity threshold of 55 (0-55) returned the most comparable RN radius measurement, with an average of 101.38 % of the visual measurement. As the boundaries of the RN can quite clearly be determined by eye (unlike the outer boundary) this was considered appropriate. The data set used for threshold determination included images with a range of RN intensities, (pale and bright RNs) and was a representative sample of the population. Unless otherwise stated, an intensity of 55 was used for all further RN thresholds.

The outer threshold is much more difficult to determine by eye, so was set to return measurements in line with Vogelstein *et al*. (1980) who reported a MFHR halo radius for 3T3 cells of 15 μm, which they determined by visual determination of the outer halo edge. The HIM was run using a 55 RN threshold and a range of outer thresholds between 210 and 240 (fig 3.4 C, D). An outer threshold of 240 returned the closest at 104.7 % to the Vogelstein measurement. Unless otherwise stated, 240 was used for the outer threshold for all further experiments.

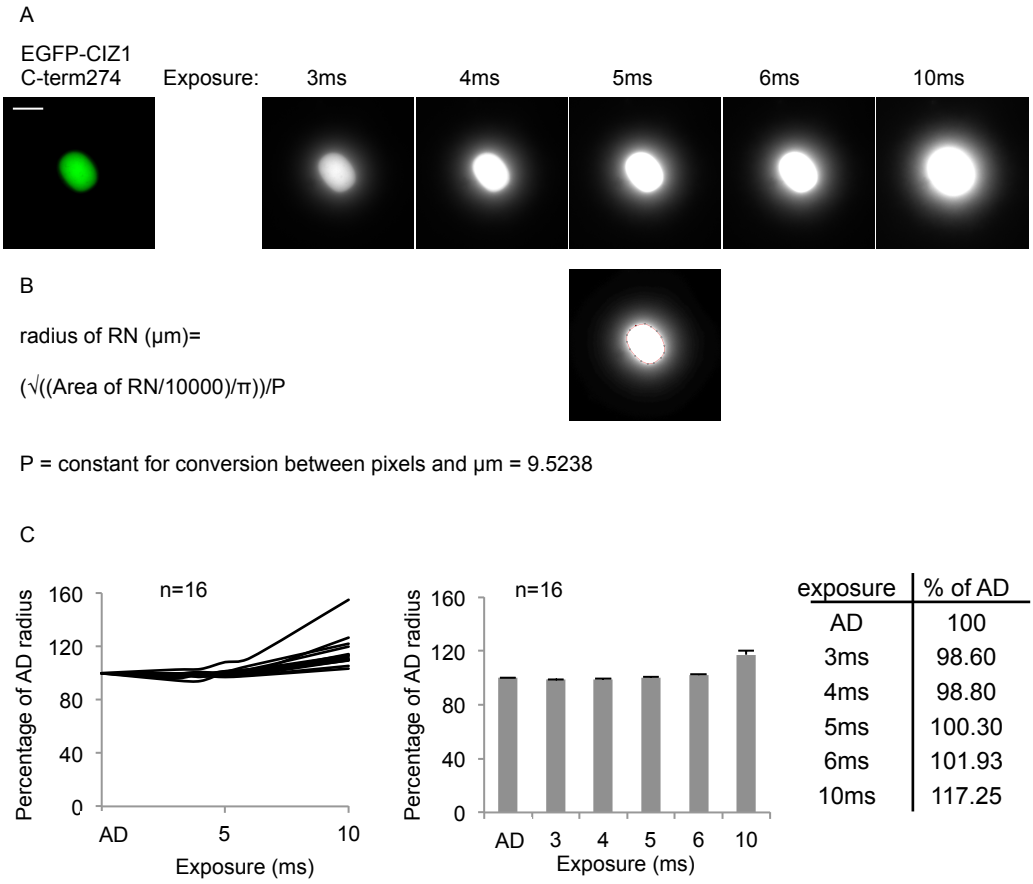

Figure 3.3: Exposure settings for MFHR images. A) Cells transfected with EGFP-CIZ1 C-term274 (green) were imaged for MFHR at multiple exposures. B) RN areas were calculated using the ImageJ polygon function as shown in the lower image and radius measurements calculated using the formula shown. C) Left: Graph shows calculated radius as a percentage of that from EGFP-CIZ1 C-term274 image for each of 16 cells as a function of exposure time. Right: Histogram shows averages from the same cells. Far right: Table shows values for average percentage of EGFP-CIZ1 C-term274 radius measurement.

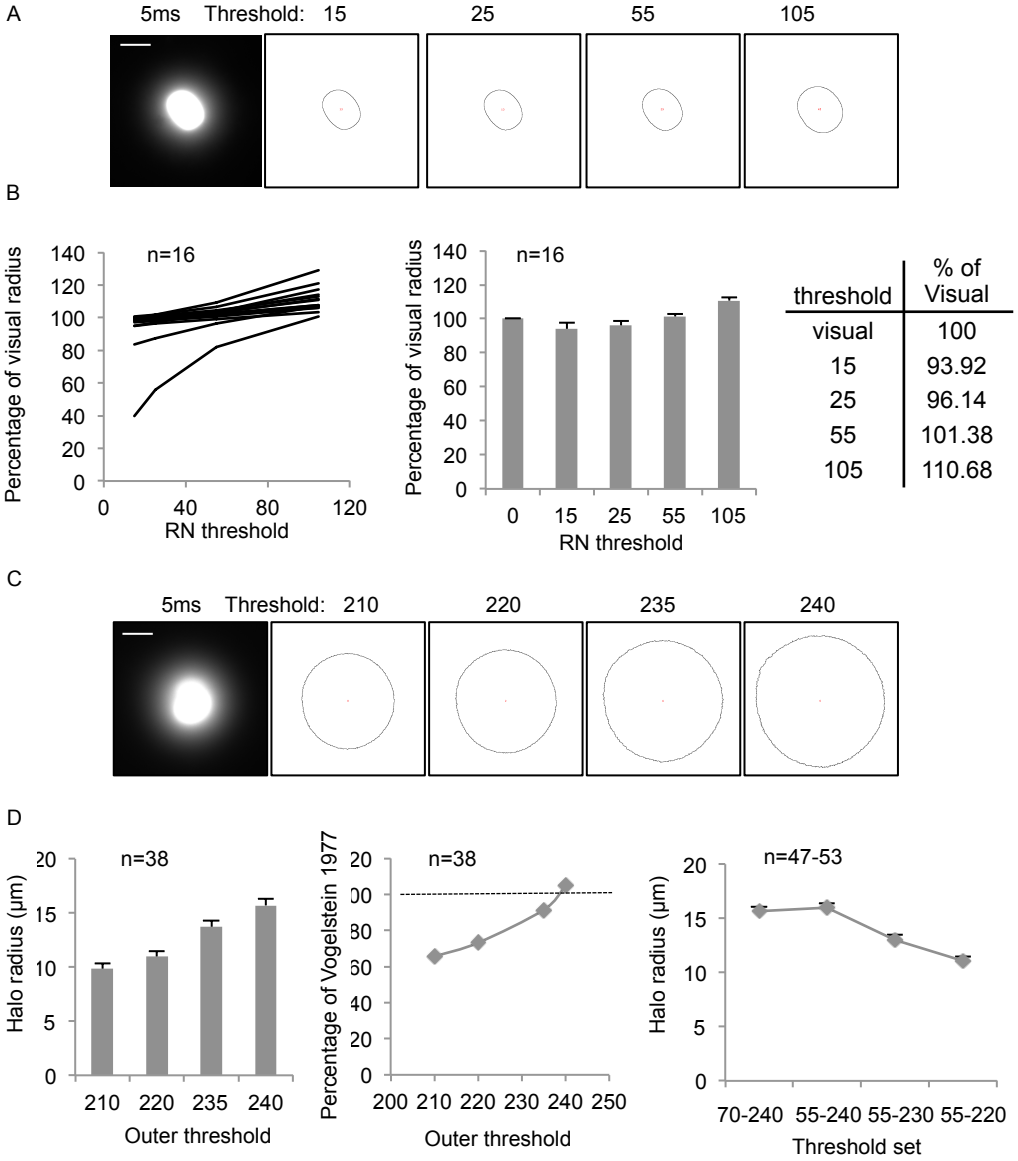

Figure 3.4: Determination of RN and outer thresholds. A) Left: Image shows a 5 ms MFHR image. Right: RN area analysis pictures from the HIM are shown for the indicated pixel intensity thresholds. B) Graph shows HIM calculated RN radius as a percentage of visual radius calculated from MFHR image for each of 16 cells. Histogram shows averages from the same cell set. Table shows values for average percentage of visual radius measurement. C) MFHR image and outer threshold analysis pictures from HIM for the indicated pixel intensity thresholds. D) Histogram shows average HIM calculated halo radius using the indicated outer thresholds from 38 cells expressed in µm. Centre: Graph shows HIM calculated halo radius measurements for the indicated outer thresholds as a percentage of those calculated for 3T3 cells by Vogelstein et al. (1980). Right: Graph shows the effect on halo radius when using different combinations of thresholds.

Unsurprisingly, when different pairs of thresholds were used, different radius measurements are returned (fig 3.4 D), therefore it is important to use the same thresholds when making comparisons between cell populations. The greatest effect was clearly seen when altering the outer threshold rather than the RN threshold. This has implications for cells with paler RNs, which are discussed later. The standard HIM settings used in this analysis are using the thresholds 55-240. These settings are such that MFHR images record accurately the RN and the outer halo (chromatin loops).

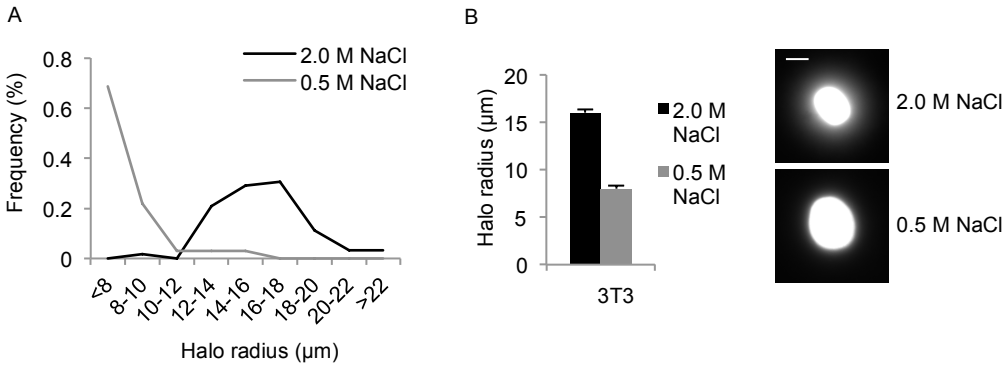

Figure 3.5 Halos are not due to flare. A) Frequency distribution of halo radii of cells treated with standard MFHR (2.0 M NaCl) or with only 0.5 M NaCl to produce a bright object to test for effect of flare. B) Average halo radius for cell sets described in A with representative MFHR images.

To rule out the possibility of flare from a bright object causing a perceived halo, MFHR was performed on cells without expanded halos. Cells were processed as for MFHR up to and including the 0.5 M NaCl step. Coverslips were then treated with EtBr, mounted and imaged. Without high salt or UV treatment chromatin loops largely remain within the nucleus. The frequency distribution of halo radius measurements from cells without extended chromatin loops (0.5 M NaCl), shows very little effect of flare within the system (fig 3.5). The calculated halo radius is clearly much smaller than the halos observed from cells treated with the full MFHR protocol and with clearly visible halos in representative images. Although it has been determined that flare does not account for halos, the small contribution of this effect should be bourn in mind when interpreting results. However, theoretically the effect of flare should be consistent for all cells and therefore differences between conditions should not be the result of flare.

3.4.3 Excel formulae

Raw data are recorded as area measurements. They were converted to halo radius measurements using the calculations shown in table 3.1. These fit the area measurements from the HIM to circles, and derive radii accordingly. Most MFHR images appear visually to be circular, but some are more elliptical. Halo radius measurements were calculated for 6 cells using formulae fitting areas to circles, ellipses or squares (fig 3.6). As expected fitting areas to squares gave dramatically different measurements, but there was little difference between measurements calculated using circular or elliptical formulae. For all further calculations circle formulae (table 3.1) were used as this allows the whole area to be taken into consideration rather than just the x- and y-axes.

Two important conversion factors are included in the calculations, both generated by imaging a slide with calibrating lines of known length. Firstly, a conversion factor between pixels (Openlab LIFF files) and μm was calculated using Openlab software, equalling 9.5238 pixels per μm (P, fig 3.6, table 3.1 box G2:G3) (Laura Knight, Nikki Copeland and Dawn Coverley). It subsequently became apparent that measurements made when files are viewed in ImageJ record pixel values that are two orders of magnitude greater than pixel values recorded in either Photoshop or Openlab. This necessitates a secondary conversion factor. Calibrating lines (described above) were measured in both Openlab and ImageJ software and measurements from ImageJ found to be 100 fold greater. Linear measurements from ImageJ were therefore, reduced by 100 fold (L, fig 3.6), and area measurements by 100^2 or 10000 fold (A, fig 3.6, table 3.1 box D2:D4). If original calibration between pixels and μm had been undertaken in ImageJ these two conversion factors could have been dealt with as one. To simplify halo analysis, formulae used in Excel for analysis of results could be altered to use this single conversion factor (halo pixels/(PxL). However, all results presented here were analysed by the method shown in table 3.1.

$$\frac{\text{Length (pixels Openlab LIFF)}}{P} = \text{Length (μm)}$$

$$\text{Length (Openlab)} \times L = \text{Length (ImageJ)}$$

$$\text{Area (Openlab)} \times A = \text{Area (ImageJ)}$$

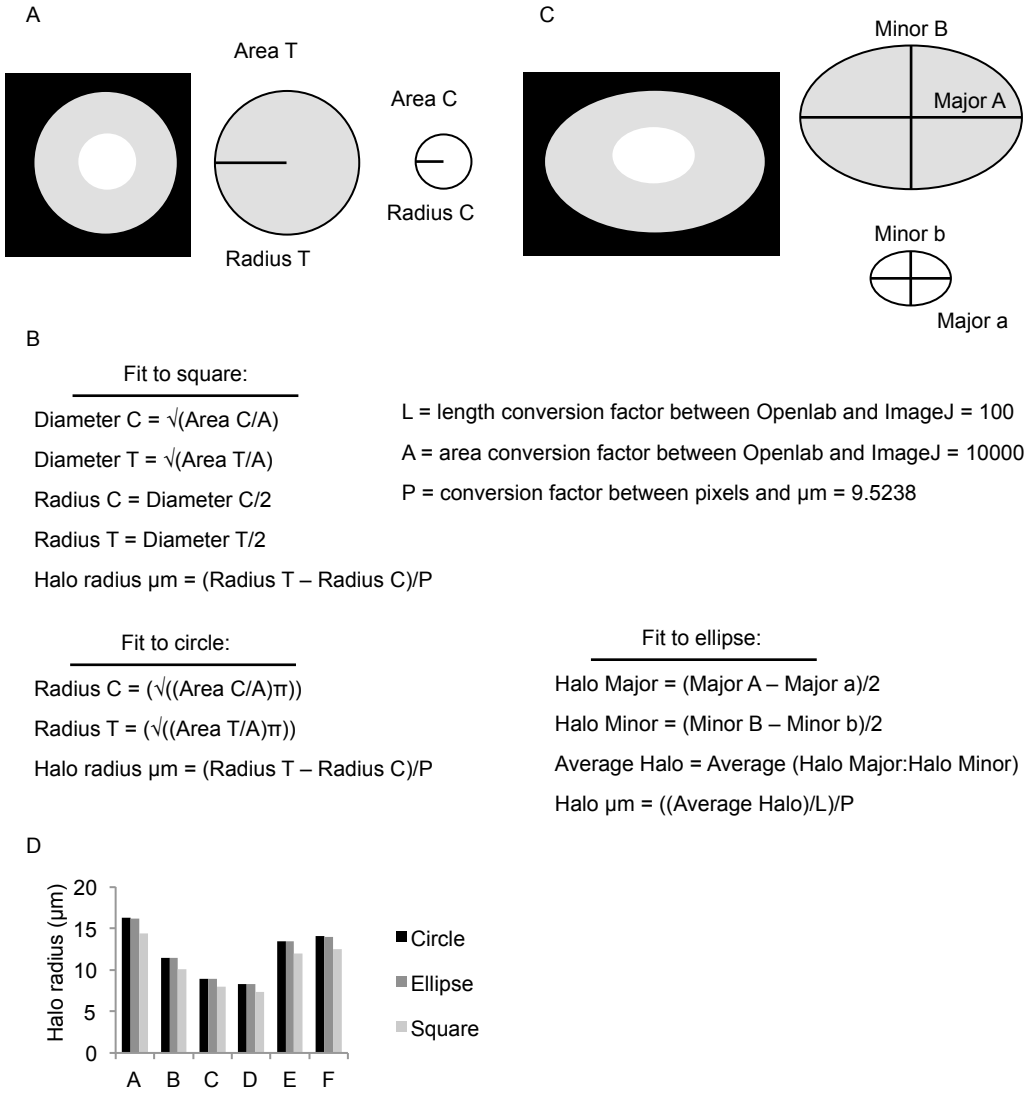

Figure 3.6: Options to calculate halo radius from ImageJ area measurements. A) Schematic of circular MFHR image showing total and RN radii. B) Formulae are shown to determine halo radius assuming the areas are squares, circles, or ellipses. C) Schematic of an elliptical MFHR image showing major and minor measurements. D) Histogram showing halo radius calculated using the three formulae described for 6 cells (A-F).

3.4.4 Comparison of alternative radius measurements

HIM allows several measurements to be made, both area and radius measurements for the RN and the total area, and also the derived halo radius (fig 3.7). From the data set shown, the halo radius was calculated to be just larger than the RN radius. From frequency distribution analysis, the spread of RN radius measurements is smaller than that of both halo and total radius (fig 3.7 C). Both halo radius and total radius measurements could be used to interrogate chromatin loops. However, the halo radius measurement is unaffected by the small variability in RN radius and has a higher number of consistent measurements, evidenced by a greater percentage of cells within one 2 µm wide bin. Halo radius is also a simpler measurement to use as it relates only to chromatin loops. Therefore, halo radius measurement was used in all further analysis.

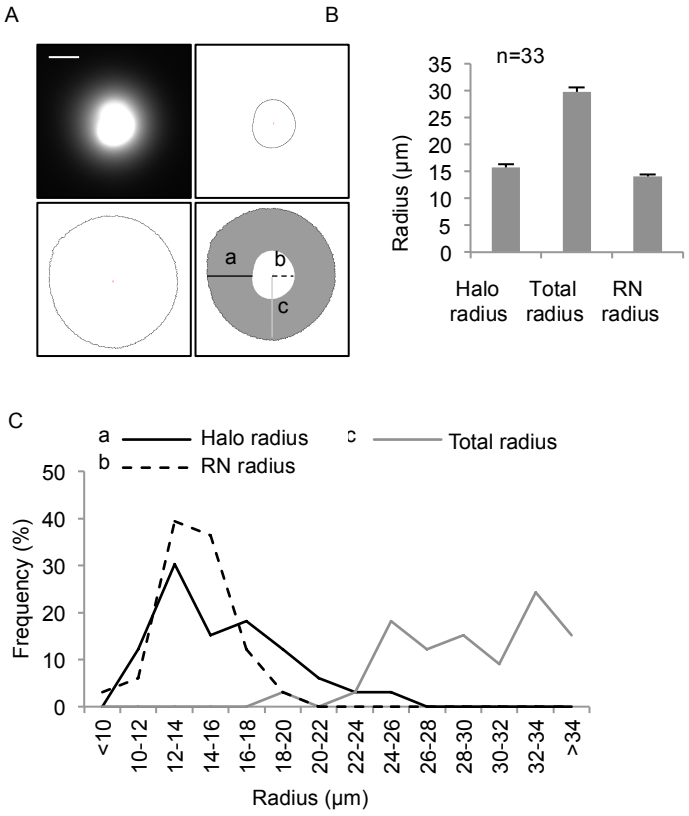

Figure 3.7: Comparison of RN, total and halo radii. A) Images showing MFHR, RN and outer threshold analysis pictures and combined image showing three radius measurements. B) Average radii measurements for a set of 33 cells. C) Frequency distribution of radius measurements after allocation to 2 µm bins.

.

3.4.5 Comparison of measurements by eye and HIM

Measurements were generated by the HIM as well as by eye for sample data sets A and B (fig 3.8). When MFHR images taken at 5 ms exposure were analysed in the same way, HIM measurements were larger than those made by eye for both sets of data (fig 3.8 A). This indicates that the chosen outer threshold is not possible to observe by eye. Before use, the HIM must be carefully calibrated, to choose appropriate pixel intensity thresholds. The outer threshold was chosen to return a halo radius measurement consistent with published chromatin loop measurement for 3T3 cells. This means that absolute values for halo radius measurements are less meaningful than differences between samples. Although the outer threshold was fixed to fit with previously published values I have confidence in these values since the edges of the halo as determined by HIM are clearly the point at which pixel intensity increases sharply above background (fig 3.8 B). This is important when comparing automated measurements and those by eye. Consistently the HIM returns halo radius values larger than those measured by eye. Unsurprisingly, therefore the automated results would appear to be more accurate because there is a pixel intensity increase at the edge of halos which is undetectable by eye. This suggests that measurements by eye are likely to underestimate halo radius. Increased exposure time might better reveal the complete halo to the eye, however this also increases the apparent size of the RN due to flare generated by the intense fluorescence of the RN (fig 3.5).

No difference was found between data sets A and B when average halo radius was calculated either by eye or HIM (fig 3.8 A). There was also a similar spread in values when measured by eye or HIM, for each cell line (fig 3.8 A). Images produced by Laura Knight were also analysed (fig 3.8 C). It is important to note that these were taken at 25 ms exposure, so HIM thresholds were not optimised for this image set.

As expected, HIM measurements were therefore smaller than those made by eye. Nevertheless, the same trend is observed as before, across data sets A-D when analysed by the two methods. Therefore, analysis methods by eye and HIM would lead to the same outcome.

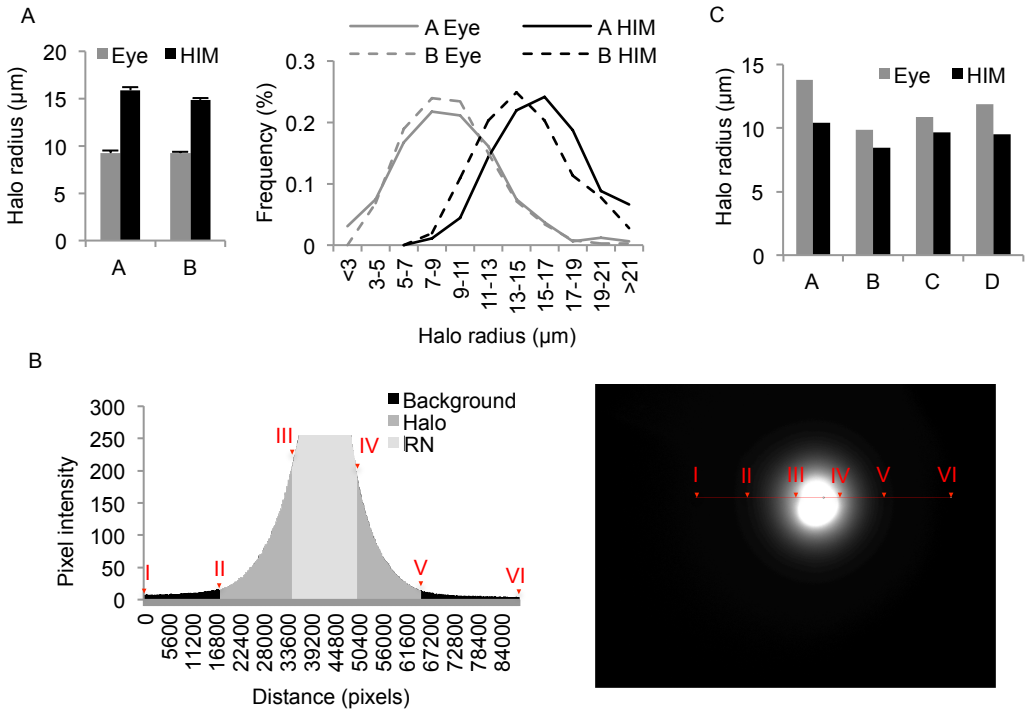

Figure 3.8: Comparison of measurements by eye and HIM. A) Left: Histogram shows average halo radius calculated for two sets of cells (A, B) collected at 5 ms exposure. Right: Frequency distribution of halo radius data of A and B by eye and by HIM. B) Left: Histogram showing pixel intensities across a traverse of a representative MFHR image (right). Arrow heads indicate extents of the line (I, VI) and boundaries determined by HIM using the 55-240 threshold combination. The RN threshold is at III and IV and outer threshold at II and V. C) Histogram shows average halo radius calculated for four sets of cells (A-D) either by eye using polygon ImageJ function or HIM. (Images collected by Laura Knight at 25 ms).

However, there are three major benefits to the automated non-subjective analysis method for MFHR images presented here when compared to measurement by eye. Firstly, the radius measurement for each image reflects an average of the whole of the halo, rather than one side. This means that anomalous parts of an image have less effect on analysis, and results should be both more representative and less variable. Secondly, the method is non-subjective, removing one source of human error. Thirdly, the method offers a dramatic time saving. In early MFHR papers all analysis was done by a method analogous to the by eye method used here (Vogelstein et al., 1980). More recent papers describe analysis using computer software to calculate the halo radius (Guillou et al., 2010). This, like the HIM method, has the advantage of recording an average radius measurement, however, it still relies on outer edge determination by eye, and must therefore be subjective. I have

found no other descriptions of a non-subjective automated analysis method for MFHR halo radii. In contrast, there already exists similar macros for ImageJ for the similar method of comet assay, again with non-subjective analysis (Bagnell, 2011).

3.4.6 Halo radius conversion to chromatin loop length

An average chromatin loop size in kbp can be calculated using the derived radius measurement and a conversion factor. Firstly, the radius is doubled, as a chromatin loop is attached to the RN at either end and therefore consists of two radius measurements. Previous papers have applied different conversion factors; Vogelstein et al (1980) and Buongiorno-Nardelli et al (1982) use 1 μm = 3 kbp, whereas Lemaitre et al (2005) use 1 μm = 2.3 kbp. To resolve this discrepancy I returned to direct DNA measurements. There exist 10.4 bp per helical turn in B-form DNA (Wang, 1979) with a helical turn measuring 3.4 nm (Watson and Crick, 1953). Therefore, 10.4 bp measures 3.4 nm, which converts to 3 kbp per 1 μm. Using this conversion factor, the 3T3 results presented here convert to an average chromatin loop size of 94.2 kbp, which is in line with previously published values, which range between 2–200 kbp with several previous estimates of 60-86 kbp (reviewed in Wilson and Coverley, 2013). Please note, the Lemaitre conversion factor was previously used for data presented here and previously (Wilson and Coverley, 2013), however, I now believe 94.2 kbp to be more accurate. However, both measurements fall within previously published values and are arbitrarily derived based on selection of threshold parameters.

Halo radius (μm) x c = Chromatin loop (kbp)

c = (2 x radius per loop) x (3 kbp per μm) = 6

3.4.7 Settings for different cell types

The microscope settings and analysis settings for all cell types are shown in table 3.2.

Populations of 'pale' cells

Cell types respond to MFHR differently making analysis by standard procedures impossible in some cases. Mesenchymal Stem Cells (MSCs) were observed to produce particularly pale MFHR images that often fail the HIM at 55-240. The percentage of measurable images from MSCh1 and MSCh3 cell lines (Funes et al., 2007) were determined for various outer thresholds (fig 3.9 A). Using 240, over 50 % of MSCh1 images were measurable, but less than 10 % of MSCh3 images (biological implications discussed in chapter 4). It was thought inappropriate to base measurements on such a small proportion of the population, therefore an outer threshold of 180 was chosen as this allowed measurement of over 30 % of MSCh3, but does result in a smaller halo size. A range of RN thresholds were then compared for measurement of MSCh1 and MSCh3 cell lines (fig 3.9 B). The standard threshold of 55 gave a smaller than visual measurement for both cell lines due to RNs being pale. A RN threshold of 75 was chosen as this gave a percentage of visual measurement of 100.75 % for MSCh3. It is important to note that MSCh1 RN measurements were slightly smaller than visual measurements at the 75 threshold which will cause MSCh1 halo radius measurements to be slightly overestimated by HIM. Finally, halo measurements were made for different pairs of thresholds for MSCh1 and MSCh3 cell lines (fig 3.9 C). The average MSCh3 halo radius was larger than MSCh1 for standard thresholds (55-240), despite being based on a very low percentage of MSCh3 cells, and also for the MSC threshold set (75-180), which incorporates a greater proportion of the total population. It can again be seen that the RN threshold has minimal impact on the halo radius as shown for MSCh1, analysed at 55-240 and at 75-240. This data set also clearly shows that using 75-180 gives significantly smaller halo radius measurements for both cell types. Therefore, data collected using these thresholds cannot be directly compared to data collected using the standard thresholds.

To allow analysis of MSCs by HIM, thresholds were recalibrated due to images being pale. However, another solution would have been to increase the image capture time above 5 ms, which would have raised the image intensity above the background threshold making quantification easier and might have allowed use of standard settings. However, neither method allows MSC and 3T3 data to be directly compared, and the downside of increased exposure would likely be an increased

rate of decay. The preferred method was therefore, to maintain the same exposure time.

Table 3.2: Microscope settings and analysis settings used for MFHR data for specific cell lines and types.

Data set	Exposure	Measurement technique	RN threshold	Outer threshold	Calculation
Laura Knight data	25 ms	Vertical halo radius by eye, in ImageJ	--	--	--
Rosemary Wilson data unless otherwise stated	5 ms	HIM 55, 240	55	240	Fit to circle
DAPI halo	14 ms	HIM class I class II	60 110	200 200	Fit to circle
Mesenchymal Stem Cell Lines	5 ms	HIM 75, 180	75	180	Fit to circle

Quiescent Mouse Embryonic Fibroblasts (MEFs)

Quiescent cells are more difficult to process by MFHR due to their close packing, since HIM requires individual cells. For some cell lines, such as mouse 3T3 cells, enough of the confluent sheet of cells detaches during the MFHR process to enable sufficient individual cells to be measured. However, for some cell types, exemplified by WT and cyclin E null MEFs (Geng et al., 2003), all quiescent images failed due to the high density of cells and quiescent measurements could not be made using HIM. To resolve this difficulty halo radius measurements were calculated by eye. As previously shown, measurements by eye are smaller than those made by HIM (fig 3.8 A), necessitating estimation of a conversion factor. The conversion factor was calculated by using cycling MEF WT and E null as test cases (fig 3.9 D). Cycling WT and cyclin E null MEFs responded to MFHR in a similar way to 3T3 cell line allowing standard settings of 55-240 to be used. Comparison of visual and HIM generated a

very similar conversion factor for each cell line, which were then averaged (fig 3.9 D). In subsequent experiments, this has been applied to each visual measurement individually before averaging. An alternative way of measuring halo radius in these cells could be to process them in solution (section 3.4.13).

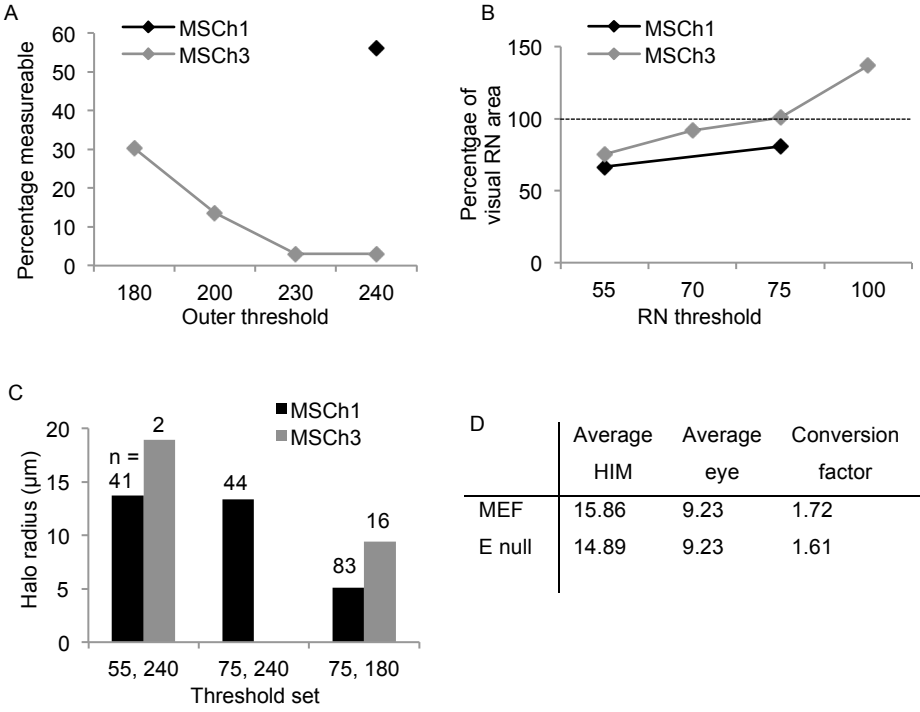

D

	Average HIM	Average eye	Conversion factor	Conversion factor
MEF	15.86	9.23	1.72	1.67
E null	14.89	9.23	1.61	

Figure 3.9: HIM adjustments for Mesenchymal Stem Cells (Funes et al., 2007) and cyclin E null cells (Geng et al., 2003). A) Graph shows percentage of cells which have a measurable halo using different outer thresholds for MSCh1 and MSCh3 lines. B) Graph shows HIM RN area calculations using different RN thresholds as percentage of visual calculation, for MSCh1 and MSCh3 cell lines. C) Histogram shows halo radii calculated using different pairs of HIM thresholds. D) Table shows average halo radius for control MEF and cyclin E null MEF cell lines calculated by HIM and by eye, with derived conversion factor.

DAPI MFHR

The DAPI MFHR method includes a fixation step and is useful because it is compatible with immunofluorescence and FISH. Fixation also makes experimentation more convenient and less time sensitive. Image analysis using HIM was calibrated using 3T3 cells. To set the image capture parameters, multiple exposures were taken for both a bright (class I) and a pale (class II) cell (fig 3.10 A). A full description of classification is given in section 3.4.8.

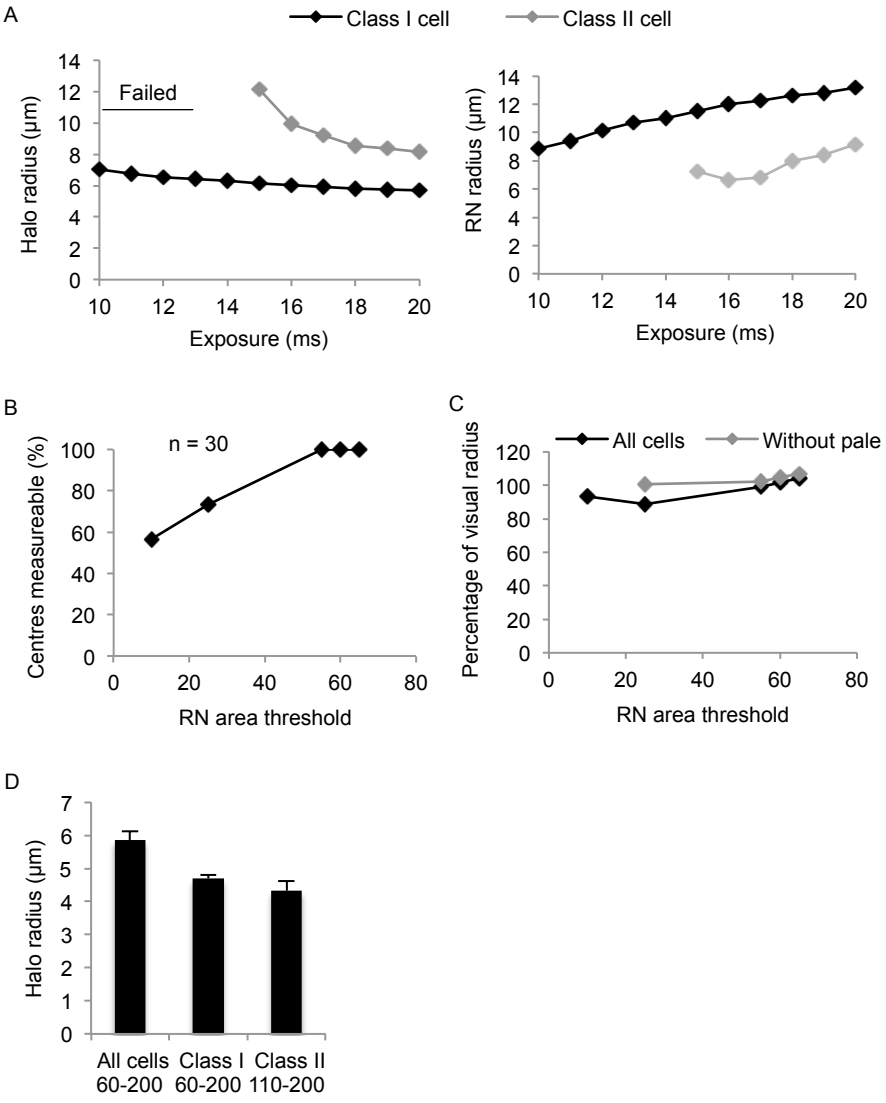

Figure 3.10: HIM adjustments for DAPI MFHR (fixed cells). A) Left: Graph shows halo radius for a bright (class I) and pale (class II) cell from DAPI fixed MFHR images. Class definitions are given in section 3.4.6. The class II cell was unable to be measured at less than 14ms, at 14 ms a measurement was generated but two cells were joined. Right: Graph shows RN radius for the same cells. B) Graph shows percentage of RNs measurable at different RN thresholds. C) Graph shows RN radius as percentage of visual radius at different RN thresholds for a set of cells including or excluding pale cells (class II). D) Histogram shows average halo radius for a set of cells using threshold pairs as shown.

The class II cell failed to be measured by HIM 55-240 below 14 ms. Exposure times greater than 14 ms caused the RN radius to increase which impacted on calculated halo radius, leading to a reduction in halo radius values (fig 3.10 A). Therefore, a 14 ms exposure was chosen as it enables the largest proportion of the population to be measured and minimises the impact of the RN measurement.

In order to choose the RN threshold, the percentage of RNs that were measurable was then interrogated using a range of RN thresholds (fig 3.10 B). Thresholds above 60 resulted in near 100 % of RNs being measurable. For the same data set, HIM and visual radius measurements were then compared, again for a range of RN thresholds. Using all cells, a threshold of 60 resulted in values near 100 % of the visual measurement (fig 3.10 C). However, a significant proportion of class II cells were excluded from this analysis due to inappropriate RN measurements. A threshold set of 110-200 appeared to be more appropriate for class II cells (fig 3.10 D). Unable to find a suitable threshold set to reliably measure the halo radius for all cells, further development of this method was not undertaken. It was however, used with immunofluorescence for qualitative images.

3.4.8 Class I, II and III residual nuclei

As previously alluded to, cells respond differently to MFHR. The different responses were classified into three types (fig 3.11 A). Class I images have a defined RN that is bright, and resemble the typical halos represented in the literature (Guillou et al., 2010; Lemaitre et al., 2005; Yamazaki et al., 2012). Class II images have a defined RN, which is pale and does not meet the criteria of class I. Class III images have no defined RN and appear disintegrated. Proportions of class I, II and III cells are presented for two example cell lines (fig 3.11 B). It is of note that the 3T3 cell line consists of 76 % class I images. Unsurprisingly, when MFHR is applied to individual classes, different radius measurements are recorded. Class III cells are unable to be measured, leaving class I and (the majority of) class II cells available for sampling. For all cell lines investigated, class I cells generated smaller derived halo values than class II cells (fig 3.11 C, D). This shows that the proportion of class I and class II cells within a population will have an effect on the average halo radius and should be considered. The halo radius measurement for an aggressive cancer line, which has a greater proportion of class II cells is therefore likely to be slightly overestimated.

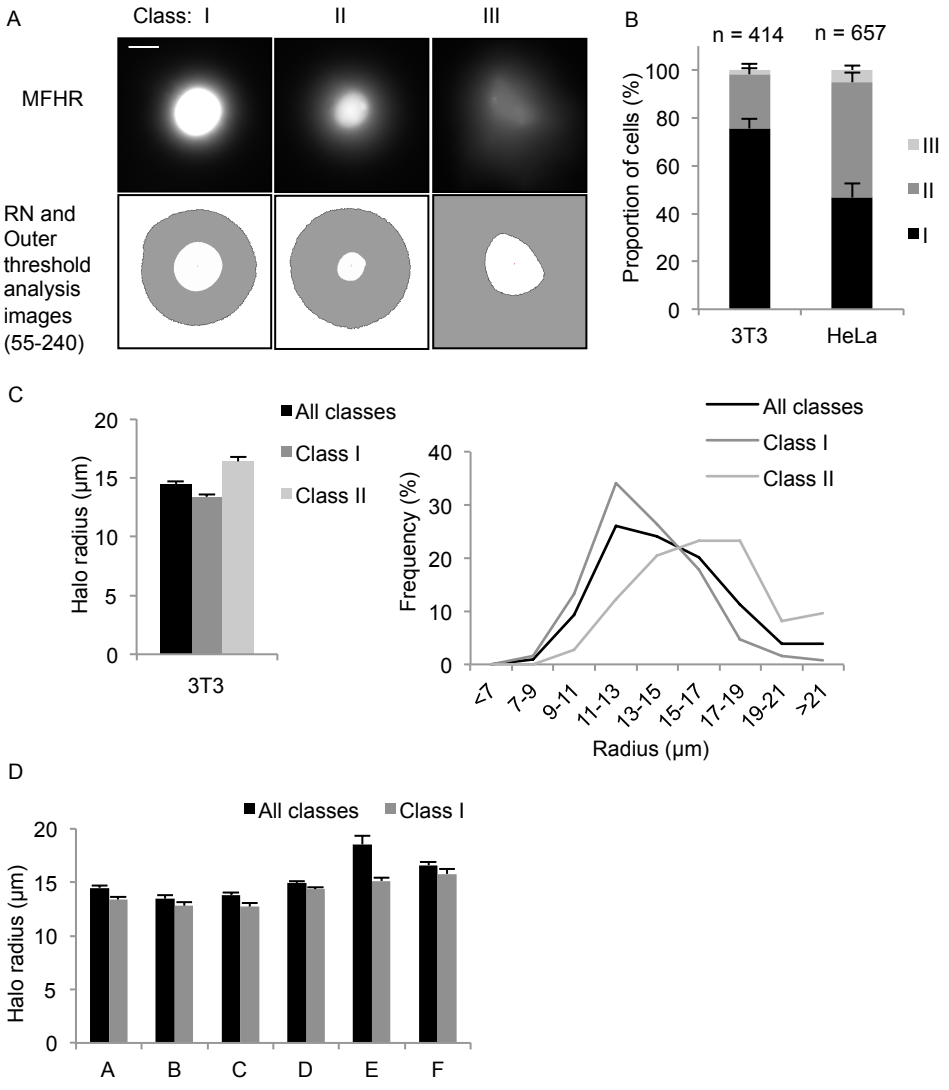

Figure 3.11: Cells respond to MFHR in different ways. A) MFHR images show representative images from each of the three classes of response to MFHR. Class I images have a bright RN. Class II images have a pale RN. Class III images do not have a clearly defined RN and appear disintegrated. B) Histogram shows example of proportion of MFHR images in each class for 3T3 and HeLa cell lines. C) Left: Histogram shows average halo radius for 3T3 cell line when using all cells or just class I or class II. Right: Frequency distribution of halo radius measurements. D) Histogram shows average halo radius measurements from 6 cell lines (A-F) using either all cells or just class I cells showing the impact that class II cells can have on the average. For cell line E 63.6 % of the total population was class II.

This should be borne in mind when interpreting results. Ideally HIM would assess the two thresholds for each individual image, perhaps by recognising a jump in intensity at the outer edge of the halo combined with a lack of change in intensity across the RN. This is one area in which HIM might be further refined in the future.

I hypothesise that class II cells began as class I cells but have degraded to some extent. MFHR halos are fundamentally unstable, and must be imaged within 10 minutes of preparation. When slides are observed at later times (2 hrs later), the majority of cells appear as class III. This suggests that cells pass through class I, class II to class III as they degrade. This is somewhat supported by my stability analysis (section 3.4.9) where some class I cells become class II images by the end of the timecourse. Thus, cell lines with a greater proportion of class II and III RN after MFHR appear to be fundamentally weaker. This may reflect the integrity of chromatin loop attachments to the nuclear matrix, and suggests that not all cells are the same in this respect.

3.4.9 Stability after MFHR

To directly measure stability of chromatin loops, individual cells were observed over a one minute timecourse, with exposure to > 590 nm light and 5 ms images taken every 10 seconds. As exemplified by the cell presented (fig 3.12 A) cells transition from class I to class II. For some cells, images become so pale that they fail to be measurable under standard HIM settings (55-240). In the example, this occurred at 50 seconds. This defines an objective definition of a decayed halo. The halo radius measurements for the cell presented are shown alone (fig 3.12 B) and within the complete data set for that cell line (3T3 – black lines) compared to a second cell line (HeLa – grey lines) (fig 3.12 C). Data was plotted as 'percentage halos surviving', which refers to the percentage of cells for which a HIM halo radius measurement could be generated at each time point (fig 3.12 D). Data was plotted as the mean percentage (± SEM) from four coverslips (biological and technical replicates, section 3.3.1) for which eight cells were measured. Notably, halos from 3T3 cells are better able to survive the timecourse than halos from HeLa cells. Only class I cells were used, allowing the cell lines to be directly compared. However, it should be highlighted that this compares the stability of subpopulations of cells from each population, which may represent different proportions of the population at

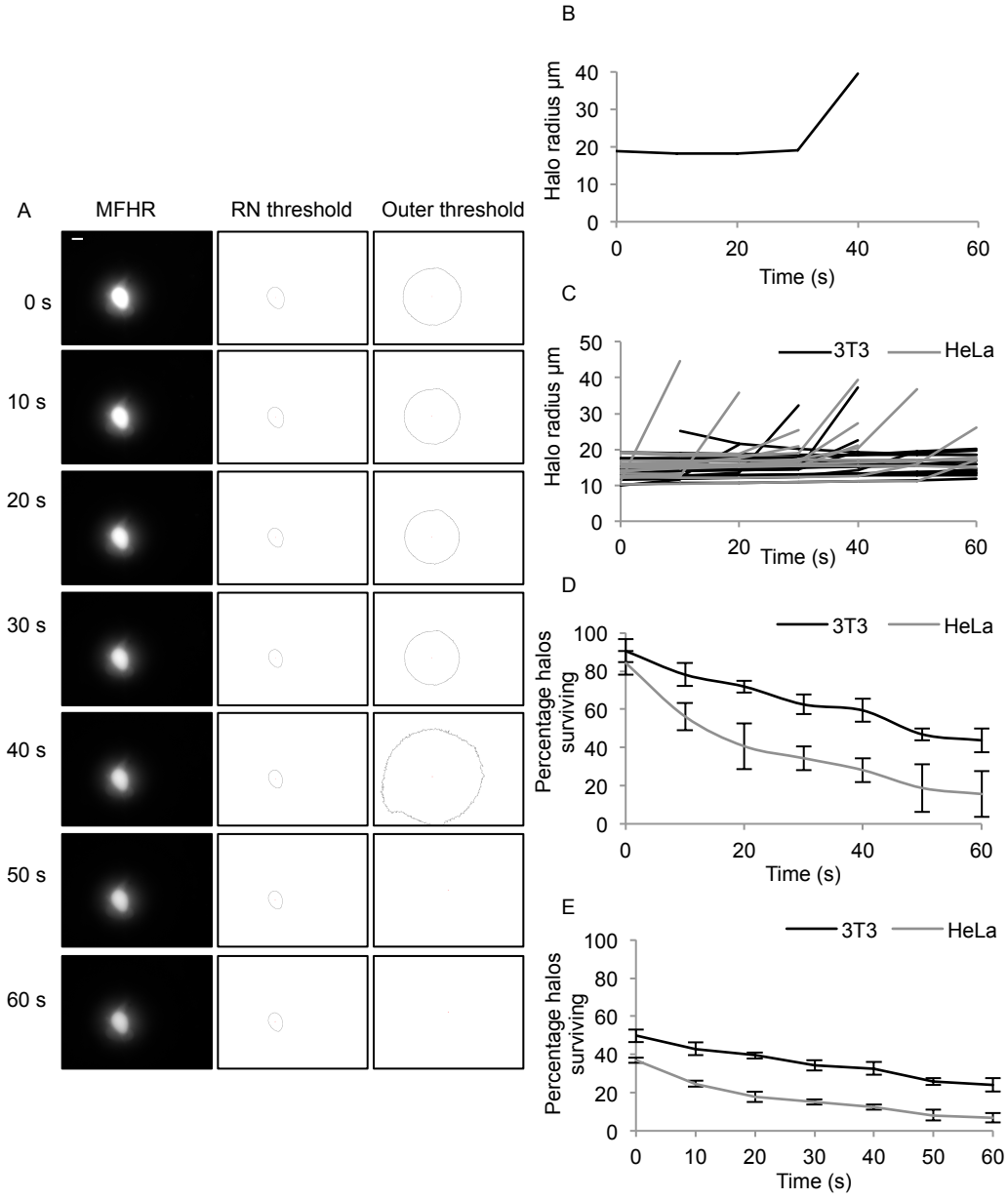

Figure 3.12: Stability measurements for MFHR halos. A) Images show MFHR images taken over a 1 min timecourse of exposure to > 590 nm light, showing RN and outer threshold analysis images. B) Graph shows halo radius calculated from the cell shown in A. After 40 s no measurement can be taken and the image is said to have failed the HIM. C) Example stability of halo radius measurements from individual cells of two cell lines. D) Average of the stability data from C, presented as percentage of cells which have a measurable halo at each timepoint with SEM. Only class I cells were used for this analysis. E) Alternative presentation of data in D), a conversion factor was applied to the data derived from the percentage of cells that are class I at time zero for each cell line.

time zero. To take this into account, an alternative way of presenting the data can be used, which applies a conversion factor derived from the percentage of cells that are class I at time zero (fig 3.12 E). In the example, fewer HeLa cells were class I (44 %) at time zero than 3T3 cells (55 %). When using this method, the separation between the cell lines is highly influenced by the proportion of the cells that are measurable at time zero, with only the gradients of the line directly measuring stability. Therefore the output is very similar to the stacked graphs showing response to MFHR (section 3.4.8).

3.4.10 Measures of stability

Described here are two versions of MFHR to record the response of cells to the process of MFHR. Although the classification of responses is potentially subjective, the differences between classes are gross ones and can be consistently scored. There are however, some difficulties with the stability estimation. Clearly the class of the image at time zero is an important determining factor, hence the decision to focus analysis on images from one class at a time. However, this does not completely abrogate the problem, particularly when working with class II cells since there is a wide range of intensity even within this class. This is highlighted by the fact that a proportion of class II cells will be unable to be measured by HIM even at time zero. An additional complication is the small window in which analysis is possible. Only eight cells can be imaged per coverslip within the valid collection window (10 min), which impacts on the statistical significance of the data set. However, stability analysis is largely supportive of the classification data and as such is a valid and useful addition. A further consideration is the presentation of such data, given that it may reflect only a subpopulation of the cells.

It has also been briefly mentioned but not characterised by another group, that different proportions of cell types have halos showing, “partial or complete release of loop DNA from the NM” (Trevilla-Garcia and Aranda-Anzaldo, 2011) and how well halos withstood 30 seconds exposure to microscope light varied with cells derived from different age animals (Alva-Medina et al., 2011; Maya-Mendoza et al., 2005). However, I have found no systematic analysis and quantification of these features between multiple cell lines in the literature making the analysis described in chapter 4 the first of its kind.

3.4.11 Effect of growth conditions

One of the intended applications of the assays described here was to compare halo size, class and stability between different types of cells. However, they are not all grown under the same conditions making it necessary to assess the effect of conditions. To determine whether different cell culture media would have any effect on cell response to MFHR treatment, 3T3 cells were plated in DMEM, EMEM, MEM or RPMI and halo radius and class measurements were taken (fig 3.13 A-C). There was no statistical difference between size data from 3T3 cells grown in DMEM, EMEM or MEM, or between any of the class data. 3T3 cells grown in RPMI produced a slightly smaller halo, which was significantly different from the size generated from other media ($p<0.05$), therefore caution should be taken when comparing halo data from cells grown in RPMI to a different media. Cells were also tested after plating at different densities (fig 3.13 D-F). Size of halo radius changed very little with density, with a range of less than 1 μm between average halo size. There was a slight increase in the proportion of class III cells and decrease in the proportion of class I cells observed as density decreased, although this was not significant. Nevertheless, to any prevent impact of plating density, all subsequent analysis was performed on cells at 50 - 70 % of confluence density.

3.4.12 Variability within results

Within each sample tested by MFHR, a range of halo radius values are recorded, one from each of 50-80 cells (fig 3.7 C). These are averaged to get a halo radius value for that sample. There is therefore, variability in halo radius size within a sample and this will affect variation between technical replicates. When measuring halo radius, and comparing between two conditions (for example, cell type) ANOVA (Analysis Of Variance) was used to determine if the difference between conditions was greater than the difference between replicates within each condition. ANOVA records the F-statistic, defined as 'variance between conditions' divided by 'variance within conditions'. A p value is also recorded, for how confident we can be in the F-statistic. A null hypothesis, that there is no difference between conditions, returns an F-statistic of 1. Values for F greater than 1 suggest there is a difference between conditions, with the amount of difference increasing with F. ANOVA results (Kirkman, 1996) are presented for data from MSC cell lines as an example (fig 3.14).

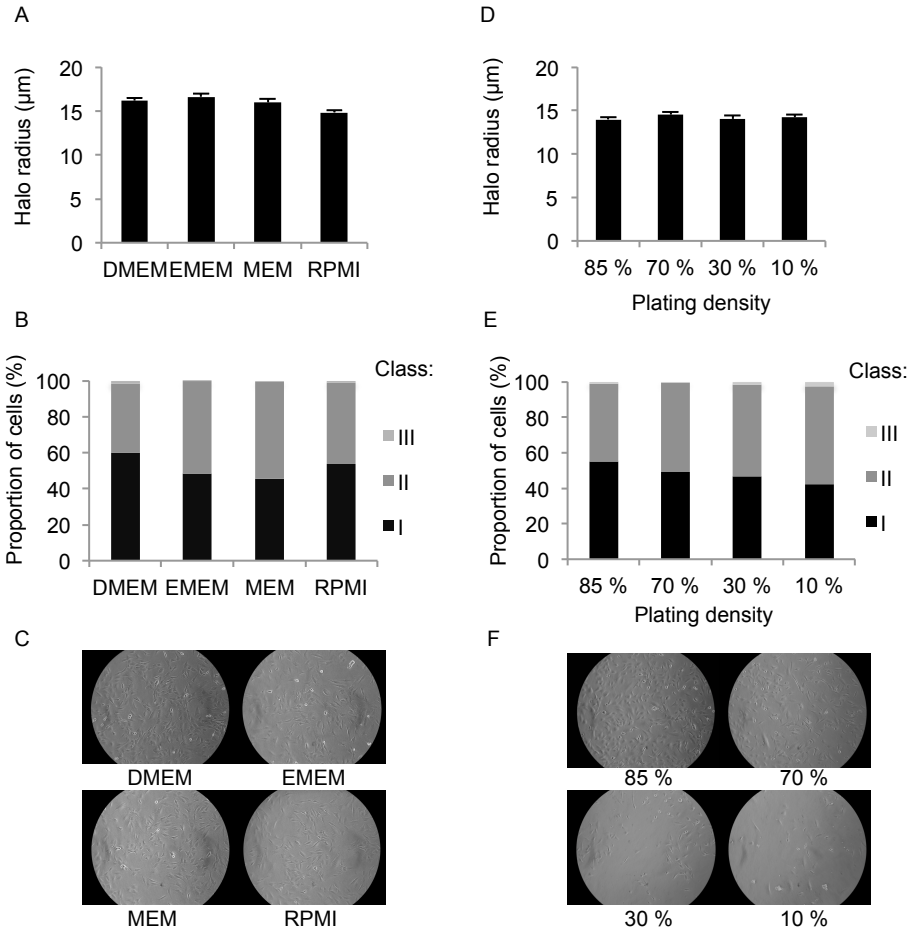

Figure 3.13: MFHR results do not vary significantly by cell culture media or density. A) Average halo radius for 3T3 cells grown in various cell culture media as indicated. B) Class distribution of 3T3 MFHR images from cells in A. C) Representative bright field images of cells in A and B. D) Average halo radius for 3T3 cells plated at various density as given by percentage of confluence. E) Class distribution of 3T3 MFHR images from cells in D. F) Representative bright field images of cells in D and E. For all conditions measurements were calculated from two coverslips (n=2), except RPMI for which data was collected from two coverslips on two separate occasions (n=4). From each coverslip 22-63 halos were measured.

A

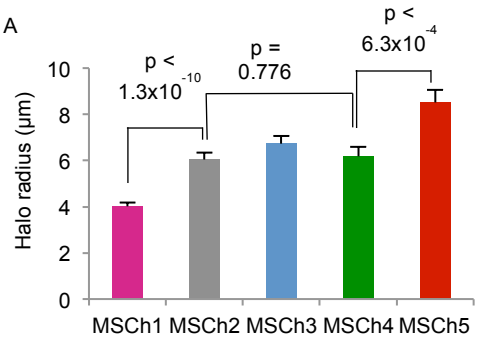

B

	One-Way ANOVA
MSCh1	$F_{(3, 331)} = 17.84$, $p < 0.0001$
MSCh2	$F_{(3, 154)} = 1.684$, $p = 0.17$
MSCh3	$F_{(3, 153)} = 2.586$, $p = 0.055$
MSCh4	$F_{(3, 126)} = 3.410$, $p = 0.020$
MSCh5	$F_{(3, 74)} = 0.7584$, $p = 0.52$

	One-Way ANOVA
MSCh1-5	$F_{(4, 853)} = 30.35$, $p < 0.0001$
MSCh1, 3, 5	$F_{(2, 567)} = 62.34$, $p = 0.17$
MSCh2-4	$F_{(2, 442)} = 1.148$, $p = 0.32$

Figure 3.14 ANOVA results for example data set (MSC, chapter 4). A) Histogram showing average halo radius for 5 different MSC lines with indicated p values from Student's t-test. B) One-Way ANOVA results presented from replicates of each cell line indicating the level of variability within each cell line (top) and between indicated cell lines (bottom).

The histogram suggests a difference in halo radius size between MSCh1 and MSCh2, and between MSCh4 and MSCh5, with no difference between MSCh2-4. The F-statistic is large (30.35 or 62.34) when comparing either the whole set of five conditions, or MSCh1, 3 and 5 suggesting that these differences are indeed due to their biology rather than random variation and giving confidence to these values. The F-statistic is close to 1 (1.148) for MSCh2-4 suggesting there is little difference between them. This confirms what is visually suggested from the histogram. When comparing the four technical/biological replicates of each of the cell lines the F values are very small (< 3.5) from all lines except MSCh1, where the F value is 17.84. This is likely due to biological variability as replicates were not as close in this cell line. However, in all cases the F statistic is smaller within cell lines than between cell lines (those with a difference). It should be noted that although ANOVA and Student's t-test assume a normal distribution of data, both are robust and can also usually be used for non-normal distributions of data, especially for large data sets as used here. Using the Kolmogorov-Smirnov test, it is unlikely that MFHR data is normally distributed, with closer approximation to log-normal distribution. However, the Kolmogorov-Smirnov test generated the same overall results as ANOVA, namely that the difference between conditions is greater than between replicates within conditions. For example, the maximum difference between the cumulative distributions of MSCh4 and MSCh5 data sets was D=0.3538, P<0.001,

considerably larger and with greater confidence than for biological replicates of MSCh4 (D=0.1358, P=0.565) or MSCh5 (D=0.1784, P=0.549). Therefore, ANOVA and t-test appear to be appropriate for this data. For simplicity Student's t-test is used in further analysis (Student's t-test results from this data shown in fig 3.14 A).

However, the range in halo radius measurements means that many cells must be imaged to produce a representative average measurement, and secondly that the settings should be optimised for the whole of a population (as previously mentioned, section 3.4.8) rather than for individual cells.

3.4.13 MAR isolation and sequencing

Described later is the use of MFHR to reveal a chromatin loop remodelling event associated with quiescence (chapter 4). In order to expand on these observations, a MFHR-derived protocol was developed to recover NM-associated DNA fragments (MARs) and applied to cells from before and after the observed remodelling event. The theory for this protocol drew from some existing MAR identification methods (Linnemann et al., 2009; Mirkovitch et al., 1988) and incorporated washing steps described by Maya-Mendoza (2003). However, the protocol described here was specifically designed to closely resemble the EtBr MFHR method used in loop size determination, in order to relate as closely as possible to other MFHR data shown here. The protocol (fig 3.15 A) for MAR isolation and sequencing is described in technical detail earlier (section 3.3.11). Presented here are controls and method development steps that are integral to the success of the approach.

Loop expansion and digestion

Cells were scraped and resuspended in the same series of buffers as the MFHR protocol. To confirm that this elicited the same effect as cells on coverslips, samples were stained with EtBr after the 2.0 M NaCl treatment, spotted onto a slide and imaged, revealing remarkably similar structures to MFHR halos (fig 3.15 B). This control indicates that membranes were successfully dissolved and histones removed so that chromatin loops were free to extend out from the nucleus, but that the NM attachments remain intact. With detailed calibration, this method could be used to measure halos in cells that grow in suspension or adapted so cells that form a dense

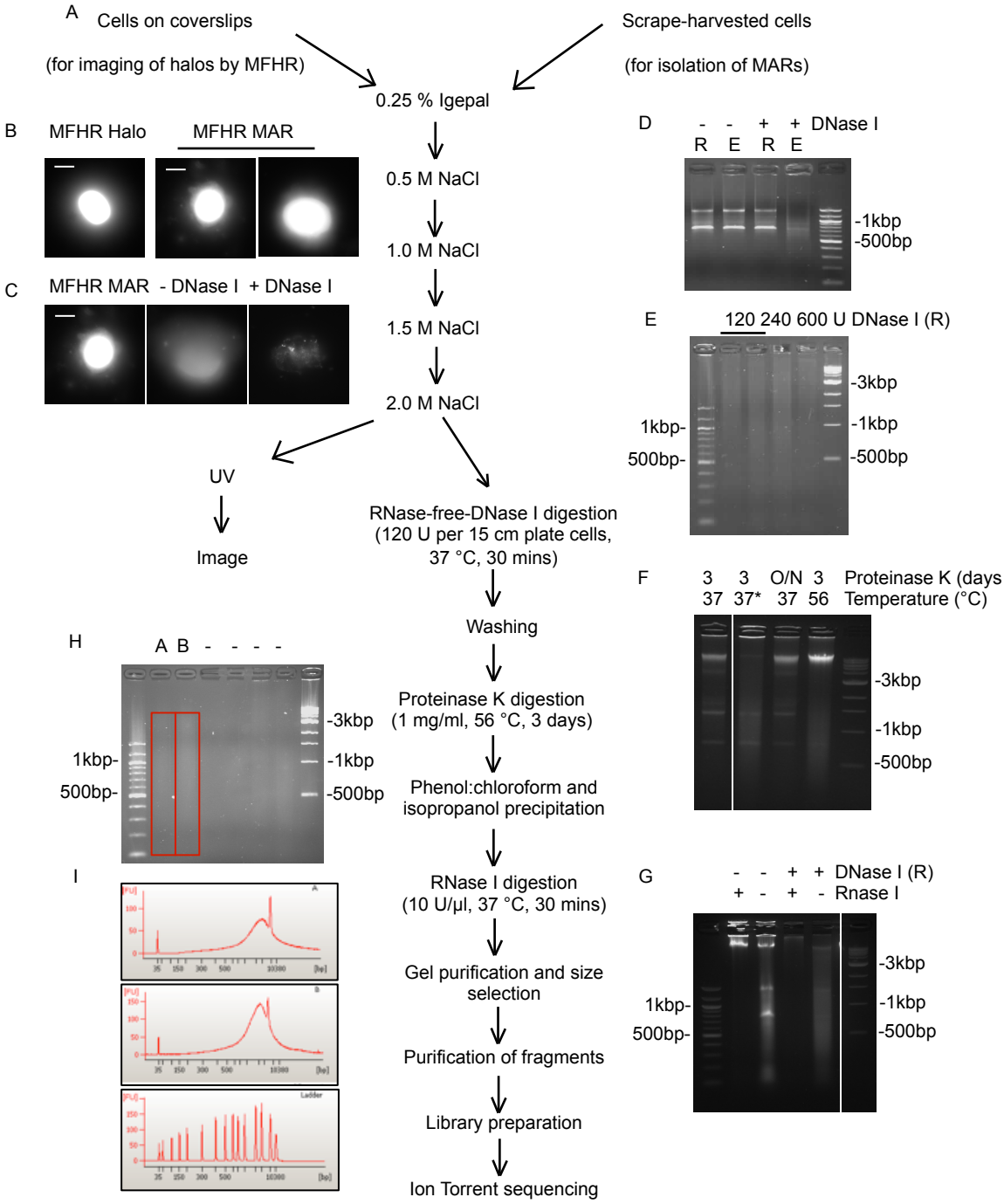

Figure 3.15: Method for MFHR Matrix Attachment Regions of DNA (MARs). A) Schematic showing steps of MFHR halo and MFHR derived MAR protocols. B) MFHR images from standard MFHR protocol (MFHR halo) and performed in solution using scraped cells. C) Images from MFHR MAR protocol as B +/- DNase I treatment in DNase buffer (37°C, 30 mins). D) Agarose gel showing impact of DNase I from Roche (R) or Epicentre (E) on RNA samples prepared by Trizol extraction. E) Agarose gel showing MFHR MAR samples (+ DNase I at the indicated concentrations) processed until gel purification. F) As E except changing proteinase K treatment and omitting RNase I treatment. * indicates 15 min, 95 °C pretreatment. G) Agarose gel showing MFHR MAR samples processed until gel purification using the conditions shown. H) MFHR MAR samples A and B showing gel slice cut from 100 bp to 5 kbp (red boxes). I) MFHR MAR DNA fragments from H visualised using 2100 Bioanalyzer (Agilent). Graphs show fluorescence units x base pairs.

layer and are unable to be measured by the standard protocol, can be lifted and also tested in suspension (section 3.4.7).

In order to isolate MAR DNA, DNase I was applied to the cells, following 2.0 M NaCl treatment, to digest loop DNA. MARs are protected from digestion and should remain associated with the NM (Berezney and Buchholtz, 1981). To confirm a loss of loop DNA, RNs were imaged (fig 3.15 C). In cells in DNase I buffer only (no DNase I) halos were of class III type. This was expected due to the time dependent degradation of halos. However, it is clear that DNA remains attached to the NM and that loops extend out from the RN. In contrast, the DNase I treated sample showed DNA present as discrete spots within an area, presumed to be the NM. This indicates that loop DNA was successfully digested and that a proportion of DNA remains protected.

Since RNA is thought to be an integral component of the NM, it was necessary to ensure minimal digestion of RNA during DNase I digestion, to ensure integrity of the NM and prevent potential loss of MAR protection. To test the DNase I preparations for contamination with RNase they were incubated with RNA and the products run on a gel (fig 3.15 D). As can be seen, there was significantly less RNase digestion with Roche DNase I (04 716 728 001) when compared to Epicentre DNase I (D9902K). Roche DNase I was used for all further experiments.

In order to ensure no contamination of loop DNA, samples were extensively washed, as recommended by Maya-Mendoza et al., (2005). Following this, the NM and any other remaining protein was then digested with proteinase K, followed by phenol chloroform separation, isopropanol precipitation, RNase I treatment to remove protein and RNA. Samples were then run on an agarose gel to visualise products. DNase I treatment conditions were calibrated by this method. It is clear that the recommended concentration of 1:100 (120 U per 15 cm plate of cells) is sufficient to digest DNA to produce a smear of fragments below 5 kbp (fig 3.15 E). There was no advantage of using higher concentrations of DNase I. A digestion time of 3 hours at 37 °C was chosen as this caused loss of the genomic sized band and a smear of DNA fragments in the desired range.

Sample processing

Proteinase K (Promega, V3021) treatment was optimised to 56 °C for 3 days to give good recovery of DNA (fig 3.15 F). Please note, samples shown were not treated under fully optimised DNase conditions and were not RNase I treated. During protocol development, RNA contamination of precipitated DNA was noted. This indicated the requirement for RNase I treatment of the sample before sequencing. Precipitated DNA samples from the indicated conditions were treated with RNase I (Thermo Scientific, EN0601) as shown (fig 3.15 G). At the exposure used, the DNA smear cannot be observed, however, the contribution of RNA to the smear can clearly be seen highlighting the importance of RNase I treatment.

MAR fragment samples were run out on an agarose gel to enable size selection (section 3.3.11). However, one of the most difficult parts of this protocol to optimise was the subsequent gel extraction method. QIAquick Gel Extraction kit (Qiagen, 28706), Gene Clean® Turbo gel extraction kit (1102-200, MP Biomedicals) and trapping DNA on DE81 chromatography paper within the gel and subsequent elution (method from Justin Ainscough) produced very poor yields. Some samples were able to be produced using Gene Clean® Turbo gel extraction kit, however yields were not consistent. For all later samples, Elutrap Electroelution System (Whatman, as per manufacturer's instructions) was used. Yields were higher and more consistent.

After careful optimisation, a smear of DNA was visualised on an agarose gel and by 2100 Bioanalyzer (Agilent) using the High Sensitivity DNA kit (performed by Celina Whalley, York Technology Facility) (fig 3.15 H, I). Analysis by Bioanalyser shows the final sample after size selection 100 bp and 5 kbp. This is in line with fragments used by Linnemann et al (2009), with an average length of 4.5 kbp (calculated from their supplementary raw data files). These should encompass previously published estimates suggesting MARs to be 100 bp to 1 kbp (reviewed in Wilson and Coverley, 2013). Samples were submitted for ion torrent sequencing (Life Technologies) (Section 3.3.11).

Analysis of MAR data is still ongoing with further optimisation of the amount of sample to be sequenced and how best to analyse the data. Initial sequencing

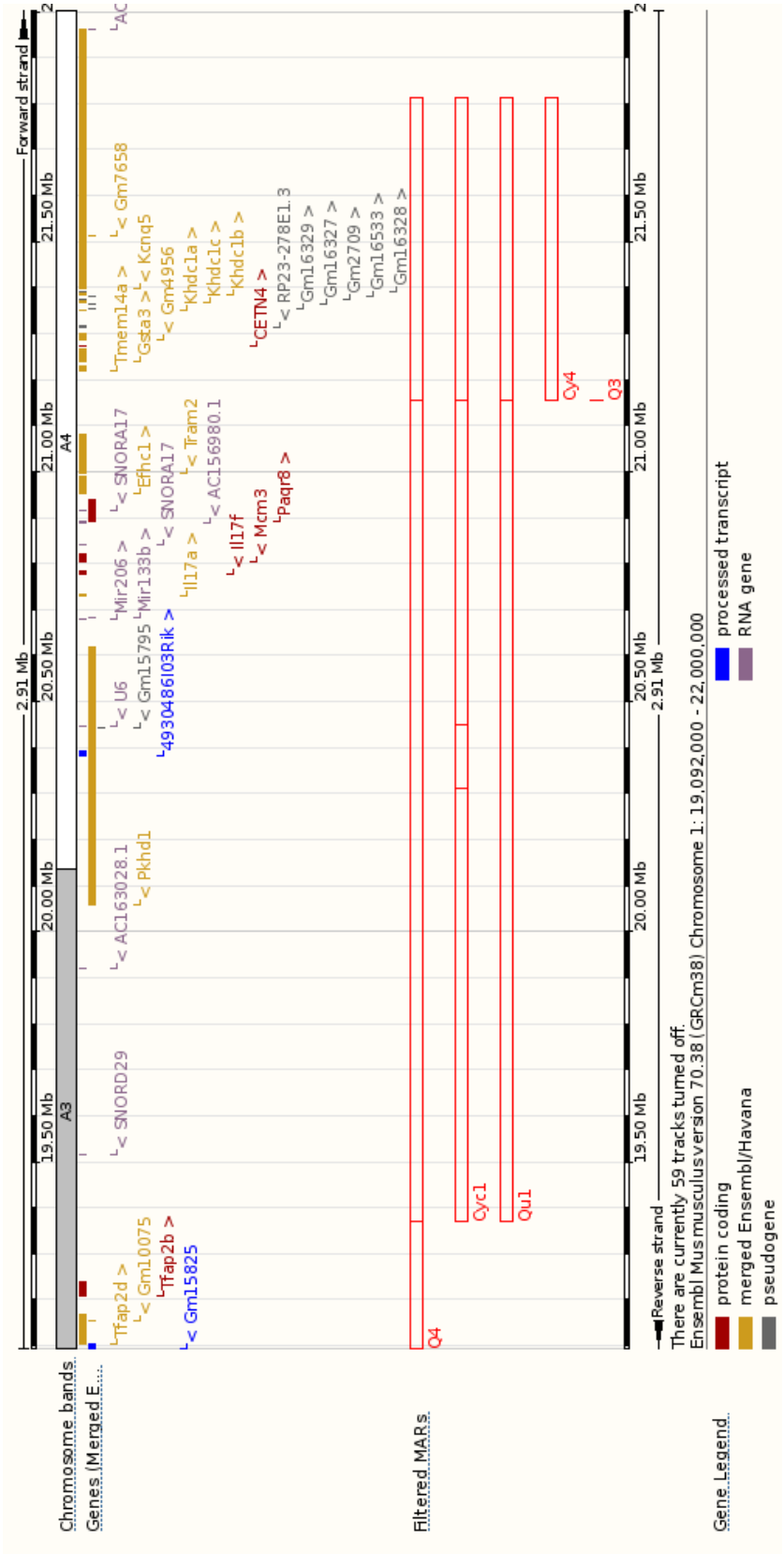

Figure 3.16: Example alignment of MARs to a small region of mouse chromosome 1. MARs are shown as vertical red bars. Only MARs with a mean coverage of reads of >5 are shown. Cy refer to cyclin samples. Q and Qu refer to quiescent samples.

Alignment and figure generated in collaboration with P. Ashton.

generated ~1x10^6 reads per sample. A second round of sequencing is ongoing to increase the number of reads. These technical replicates will either be combined or used separately such that a sequence occurring in both sequencing rounds generates increased confidence. A threshold of a chosen number of reads will be applied to the data. This is currently likely to be between 2-5 based on one round of sequencing. An example of the data that is being generated by this method is shown in fig 3.16. MARs from each of five samples (two cycling, three quiescent) have been aligned to a short section of the mouse genome, 19-22 Megabases (Mb) on chromosome 1. Some MARs are found in all or 4/5 samples (the two MARs at sites > 21 Mb). However, some MARs are present only in one sample (between 20 and 20.5 Mb). Once the additional sequencing is complete and confidence gating has been decided upon, the position of MARs in cycling and quiescent samples can be compared globally for the mouse genome.

3.5 Conclusions

MFHR is a conceptually simple but technically challenging method, largely because of the potential to introduce variability in this time sensitive method. However, it has the potential to return valuable and informative data about an under-investigated area of cell biology. Through this work significant progress has been made to establish appropriate parameters and improve analysis of MFHR data. The development of stability measurements has extended the reach of this technique and produced interesting results. If further time was available I believe it would be beneficial to try to develop a macro that automatically calculates appropriate thresholds, and to calibrate analysis for MFHR performed in solution. Additionally, perhaps this method can be developed to interrogate further the stability characteristics of MFHR halos. Further understanding of the inherent variability within the system would also be potentially beneficial, both in discovering potentially important biological reasons for the variability as well as the possibility to reduce its impact.

These methods have been used to address the following questions (chapter 4):

- Are chromatin loops different between cycling and quiescent populations?
- Do chromatin loops increase in size as cells exit quiescence?
- What does recovery depend on?
- Does the identity of MARs change during these transitions? (ongoing)
- How does transformation affect chromatin loops in terms of size, class and stability?

There are many more biological questions which can be answered using the powerful techniques described and calibrated in this chapter, in particular the novel assessment of stability.

4 Cell cycle dependent remodelling of chromatin loops, and loop stability in cancer cells

4 Cell cycle-dependent remodelling of chromatin loops, and loop stability in cancer cells

4.1 Introduction

DNA is periodically attached to the nuclear matrix forming loops from the intervening sequences (described in more detail, section 1.3.2). The attachment points (S/MARs) can be revealed by methods of extraction that leave the NM intact (section 1.2). If nucleases are used, only the attachment points (i.e. the base of loops) themselves remain protected and these can then be sequenced. Alternatively, in the absence of nucleases, chromatin loops remain intact and can be induced to extend out in a halo emanating from the original nuclear area, using Maximum Fluorescence Halo Radius (MFHR) methods (section 3.1). The MFHR method used here utilises 2.0 M NaCl to reveal chromatin loops, identifying them as NM attached loops as opposed to scaffold or skeleton attached loops (section 1.2).

There are thought to be many more potential S/MARs than are utilised at any one time, giving rise to the possibility of genome regulation through attachment region usage and chromatin loop choice (reviewed in Wilson and Coverley, 2013). Differences in attachment have been suggested to exist between cell types, cell cycle phases and in disease states. For example, origins of replication are thought to be recruited to the nuclear matrix during late G1/S-phase only (Djeliova et al., 2001b) implying that a subset of loop attachments change based on cell cycle stage.

The aim of this part of my PhD was to investigate changes in the higher order structure of the nucleus, specifically that of chromatin loops, as cells enter quiescence, as cells re-enter the cell cycle and as cells become transformed and acquire the deregulated proliferation control associated with cancer.

4.1.1 Existing Coverley lab data

The EtBr MFHR technique had been established within the lab (by summer student L. Knight) and used to generate some preliminary data, collected by visual

estimation of halo thresholds. The preliminary data generated suggested that chromatin loop sizes were smaller in quiescent cells, that loop size increased again as cells were stimulated to re-enter the cell cycle, and that this was dependent on CIZ1 (appendix A). As described in chapter 3, part of my project aims were to optimise the MFHR method and develop a less subjective and higher throughput method to analyse MFHR data. I developed and validated the ImageJ macro HIM and used it to build on these preliminary observations.

4.2 Aims

Using improved analysis methods for MFHR data (chapter 3) my aims were to:

- Confirm preliminary data suggesting a decrease in chromatin loop size in quiescent cells and subsequent increase upon cell cycle re-entry
- Determine the time at which recovery occurs
- Investigate the requirements for this event to help to establish the mechanism
- Investigate the characteristics of chromatin loops within a cancer transformation series

4.3 Experimental Design

Cells were grown on coverslips and taken for MFHR analysis from asynchronous cultures or at stated timepoints after synchronisation. MFHR analysis methods and their validation are described in chapter 3. Synchronisation was confirmed by EdU or BrdU incorporation and flow cytometry (section 2.1).

4.4 Results

4.4.1 Chromatin loop sizes are smaller in quiescence

In order to investigate the suggestion that chromatin loop size is reduced in quiescent cells, chromatin loop measurements were taken for both cycling asynchronous and quiescent populations of 3T3 cells and analysed by the ImageJ

macro HIM. Quiescent populations repeatedly showed smaller chromatin loops (fig 4.1 A, B), with a drop of 21.5 %, from 16.02 μm halo radius in asynchronous populations to 12.58 μm in quiescent populations. This converts to a reduction of 20.64 kbp, from 96.12 kbp average loop size in cycling cells to 75.48 kbp in quiescent populations. Despite this difference in average size, the range of halo sizes within quiescent and cycling populations was very similar, with the frequency distribution showing a single peak. However, the peak position is shifted left (fig 4.1 C). These data show that a global remodelling event of chromatin loop architecture occurs as cells enter a quiescent state and agrees with both initial data from this lab (appendix A) and other inconclusive data, using cells of stationary and log phase (Flickinger et al., 1986; Taylor et al., 1991).

4.4.2 Chromatin loop size increases during cell cycle re-entry, early in G1$_Q$

Cells were stimulated to re-enter the cell cycle from quiescence as described (section 2.1.3) and MFHR analysis undertaken at a range of timepoints. As previously mentioned the G1 occurring during release from quiescence is subtly different to that following mitosis, these are differentiated here by G1$_Q$ and G1$_M$. Entrance to S-phase was confirmed by nucleotide analogue incorporation (section 2.1.4-5). An example release is shown, indicating high efficiency of re-entry between 15 and 20 hours after release and clear synchronisation of cells (fig 4.2 A). Chromatin loop size increased during release with full recovery to cycling size by approximately 12 hours (fig 4.2 B). This confirmed the preliminary data on recovery (appendix A) and provides new information on the timing of this event.

The gradual nature of the recovery implies that this process occurs from 2 (or earlier) hours after release and is complete by 12 hours rather than as discrete, stepwise events. However, data are generated from a population of cells, which although synchronised may pass through G1$_Q$ in a heterogeneous way. Therefore, we cannot draw conclusions about the nature of the transition for individual cells.

Nevertheless it is clear that chromatin loop remodelling occurs earlier than other events that we can monitor and may be one of the first compulsory steps for cells to progress to S-phase. Loop size recovery occurred long before S-phase (20 hours)

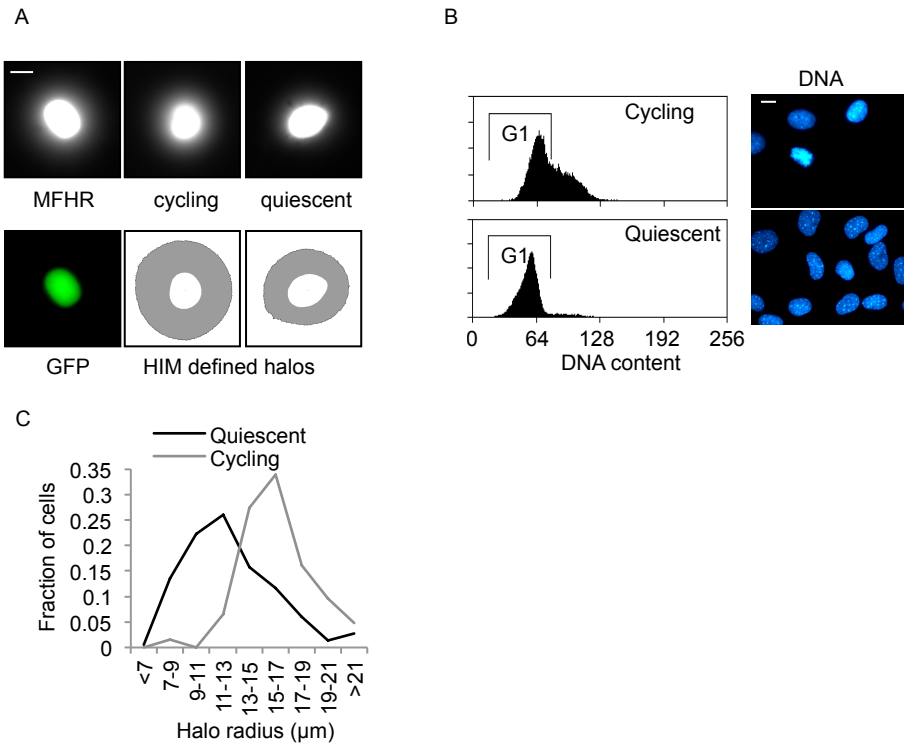

Figure 4.1: Chromatin loops are remodelled during entry to quiescence. A) Representative cycling and quiescent MFHR images with threshold analysis images from HIM (below). DNA is stained with ethidium bromide (white), and the area occupied by the nuclear matrix is visualised with EGFP-CIZ1 C-term274 (green) (Ainscough et al. 2007). Scale bar is 10 μm throughout. B) Confirmation of quiescence by propidium iodide incorporation and Flow cytometry analysis. Example images (right) show cycling and quiescent populations of cells, counterstained with Hoechst 33258 (blue). C) Frequency distribution of 3T3 halo radius shows quiescent cells have smaller chromatin loop size. Data are derived from cells whose halo boundaries fall within the range quantifiable with HIM (typically 80 % of the total population for 3T3 cells.

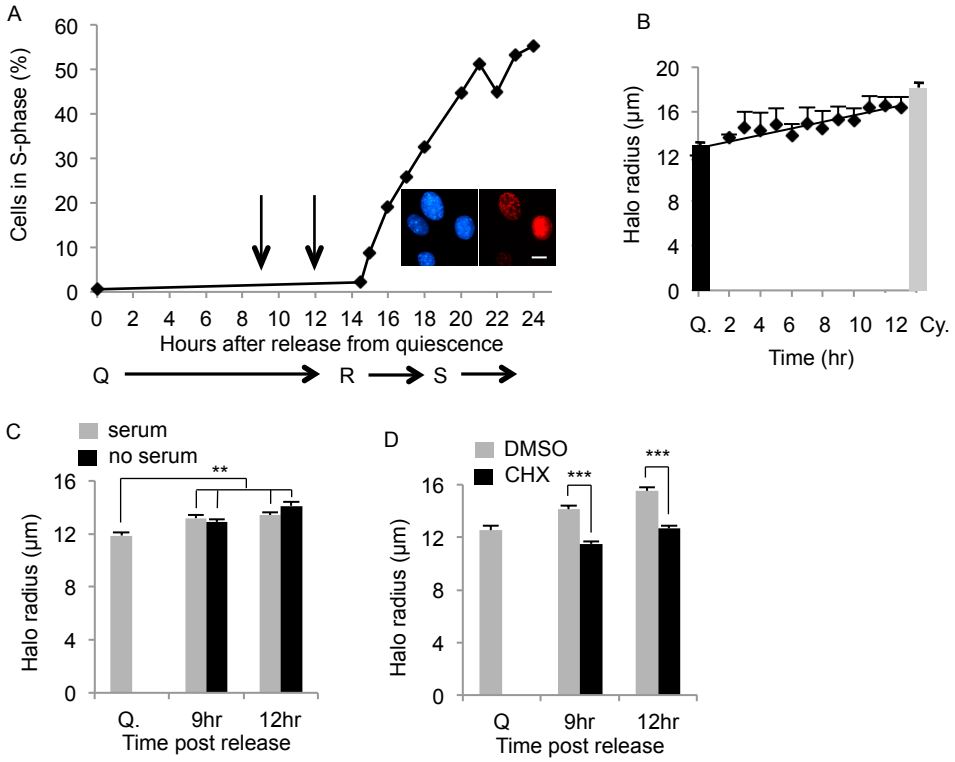

Figure 4.2: Chromatin loops size recovers during exit from quiescence. A) The timing of re-entry to cell cycle for 3T3 cells is confirmed by BrdU incorporation (red in inset image). DNA counterstained with Hoescht 33258 (blue). Scale bar is 10 µm. The timepoints for the majority of MFHR analysis are illustrated by arrows. B) Detailed investigation of recovery shows halo size returns to cycling size by 12 hours. Results are expressed as rolling average of 3 timepoints, error bars are SEM. C) Recovery of halo size for cells released into fresh media with or without serum Data presented here, and all further size measurements, are derived from > 100 halos per condition from > 4 coverslips, error bars are SEM. p values from Student's T-test. * ≤ 0.05, ** ≤ 0.005, *** ≤ 0.0005. D) Recovery of halo size for cells released into medium containing the protein synthesis inhibitor cycloheximide or DMSO control.

when global chromatin remodelling could be achieved by the passage of the replication fork, and also before the restriction point which happens at approximately 15 hours in this system (Coverley et al., 2002). The following experiments use the timepoints of 9 hours, with partial recovery, and 12 hours, with near complete recovery, to investigate this event.

Passage through the restriction point is dependent on growth factor signalling, supplied by serum in cell culture. To investigate whether loop remodelling is also driven by growth factors, cells were released from quiescence in the absence of serum. Without serum, cells completely failed to enter S-phase (monitored by BrdU incorporation, 0 % of cells released into serum free medium at 24 hrs). However, chromatin loop size recovery was unaffected (fig 4.2 C). The size recovery for these experiments was slightly smaller than previously shown, therefore this data would benefit from being repeated. However, loop size at all timepoints showed statistically significant increase compared to quiescent loop size, with no difference between cells with and without serum. This implies that the signals that initiate loop remodelling are cell autonomous, and may arise from loss of contact inhibition.

4.4.3 Chromatin loop size increase requires a newly synthesised factor/s but not cyclin E

To try to understand the trigger remodelling during cell cycle re-entry, the requirement for newly synthesised proteins was investigated by releasing cells into medium containing the translation inhibitor cycloheximide. Under these conditions, chromatin loop size completely failed to recover (fig 4.2 D), indicating that at least one newly synthesised factor is required for loop remodelling. Likely candidates should be transcribed or have a known function during $G1^{Q}$, and ideally interact with chromatin and/or the NM. Cyclin E fulfils all these criteria due to its role in pre-RC assembly (section 1.1.9) and essential function in release from quiescence (Geng et al., 2003). Furthermore, cyclin E interacts with CIZ1 (Copeland et al., 2010), which preliminary data suggested is required for loop remodelling (appendix A). I investigated requirement for cyclin E using cyclin E1-/-E2-/- and wild type MEFs, both immortalised by introduction of DNp53 (Geng et al., 2003), kindly made available by Yan Geng and Peter Sicinski, Dana-Farber Cancer Institute, Harvard. However, as can be seen (fig 4.3 A), cyclin E1-/-E2-/- MEFs were not significantly

different from control cells either in the cycling state, or during entry to or release from quiescence. It should be noted that DNp53 transformed cyclin E1-/-E2-/- MEFs show partial re-entry to the cell cycle unlike untransformed cyclin E1-/-E2-/- MEFs (fig 4.3 D and previously described, Hanashiro et al., 2008). This suggests that the role of cyclin E in re-entry is regulated by a p53-dependent checkpoint.

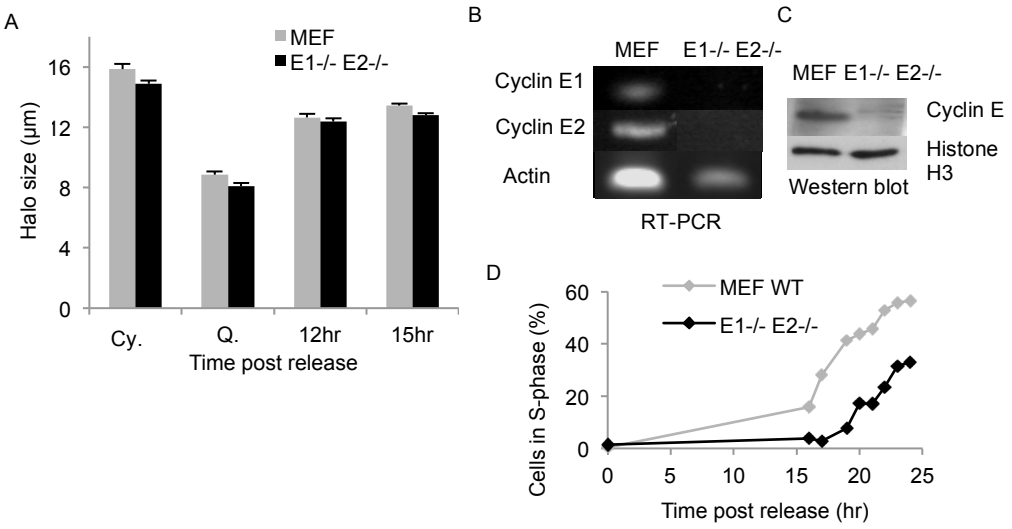

Figure 4.3: Chromatin loop size recovery does not depend on cyclin E. A) Average halo size measurements for cyclin E1-/- E2-/- MEFs are similar to control MEFs, in cycling, quiescent and G1 cells. Data collected as 4.2 C. B) Confirmation of absence of cyclin E1-/- E2-/- cells by RT-PCR (primers specified in chapter 2). C) Confirmation of absence of cyclin E at protein level by western blot (antibodies specified in chapter 2, ab7959). D) Representative re-entry to the cell cycle, monitored by BrdU incorporation.

4.4.4 Differences in chromatin loops for different non-cancer cell types

Having shown a remodeling of chromatin loops as cells enter and exit the cell cycle the next aim was to investigate chromatin loop characteristics in cancer cells. However, limited information suggests that chromatin loop size is impacted by cell type (Alva-Medina et al., 2010). Therefore, the characteristics of chromatin loops were investigated in a panel of non-cancer lines to establish if this is the case. The cell lines used were (see table 2.4 for references):

- 3T3, a mouse embryonic fibroblast line, which is used as a differentiated normal, spontaneously immortalised example
- BJ-hTERT, a human foreskin fibroblast line from a new-born, immortalised by hTERT expression
- MCF10A, a human breast epithelial line from an adult female with fibrocystic disease (non-cancerous fibrotic lumps), spontaneously immortalised
- NHU, normal human urothelial cells derived from tissues obtained from donors with no history of urothelial dysplasia or neoplasia, not immortalised (passage < 3)
- MSCh1, human mesenchymal stem cells (see 4.4.5) from bone marrow of a healthy donor, immortalised by hTERT expression
- ARPE19, a human retinal pigmented epithelial line established from a healthy adult male, which has been reported as spontaneously immortalised (passage < 20)
- MEF, mouse embryonic fibroblasts, immortalised with DNp53 (see 4.4.3)

3T3, NHU and MEF cells had a similar average halo size of ~ 16 μm, whereas the rest had a halo size of ~ 13.5 μm (fig 4.4 A). 3T3 and NHU cells also had high proportions of class I (see 3.4.9 or 4.4.7 for description) cells, of ~ 80 % (not determined for MEF). However, MCF10A also had ~ 80 % class I so this size difference does not appear to be the result of different class distributions. Consistent with this, despite having similar sized halos, BJ, MCF10A, MSCh1 and ARPE19 cells have very different class distribution, with class I at 25 %, 80 %, 45 % and 57 % respectively. Because multiple factors differ between cell lines (cell type, differentiation status and immortalisation status) it is not possible to draw strong conclusions about the meaning of class distribution. However, these results show no correlation with stem like state as NHU and MSCh1 cells had different characteristics, or immortalisation. One feature of interest however, is that 2/3 epithelial or epithelial progenitor like cells (NHU and MCF10A) had high proportion of class I cells. Nevertheless, having shown that differences in chromatin loops exist between cell types it was imperative to compare cells of the same origin as much as possible when investigating the impact of transformation.

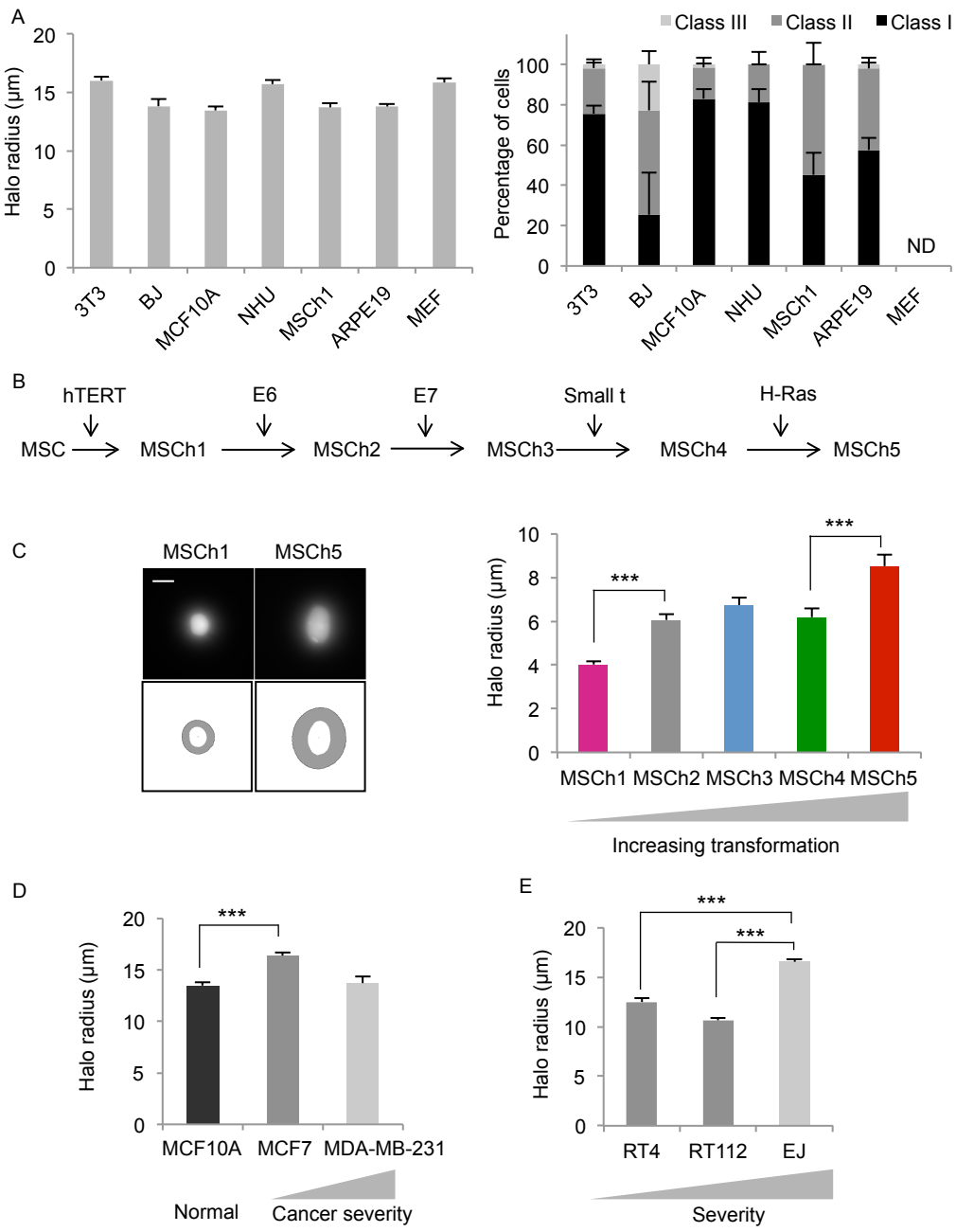

Figure 4.4: Transformation and increased severity of cancer correlates with increased halo size. A) Halo size (left) and class distribution (right) measurements for a panel of non-cancer cell lines. BJ and MSCh1 immortilised by hTERT, MEF by DNp53, MCF10A and 3T3 spontaneously, ARPE19 and NHU not immortilised. Size data collected as 4.2 C and 4.5 B except BJ, 2 coverslips. ND, not determined. B) Schematic of the relationship between MSCs with increasing number of oncogenic hits (adapted from Funes et al. 2007). C) Left: Example MFHR and threshold analysis pictures for MSCh1 and MSCh5. Average halo size measurements for MSC lines with 1-5 transforming hits as indicated. Colours correspond to those used previously (Funes et al 2007). Data collected as 4.2 C. D) Mean halo radius determined for breast epithelial cell lines, derived from normal tissue (MCF10A) or tumours (MCF7 and MDA-MB-231). Data collected as 4.2 C except for MDA-MB-231, 2 coverslips. E) Mean halo radius for bladder epithelial cancer lines (RT112, RT4 and EJ). Data collected as 4.2 C.

Amanda Collier (summer student) helped with MFHR of RT4, RT112, EJ and MCF7.

4.4.5 Chromatin loops are larger following oncogenic transformation *in vitro*

The characteristics of chromatin loops were investigated during step-wise transformation to a cancer phenotype. Several sets of cell lines that have been transformed with a series of oncogenes are available (Funes et al., 2007; Hahn et al., 1999; Hahn et al., 2002; Rangarajan et al., 2004). These include a set of mesenchymal stem cell lines (MSCs) that were kindly made available for use by J. Funes and C. Boshoff, University College London, via D. Lagos, University of York. These are particularly useful for two reasons, firstly, the cells all originated from the same starting population allowing direct comparisons to be made, and secondly, data is not complicated by the multitude of changes that occur during natural transformation and carcinogenesis. Using these cells allows comparison after each oncogenic hit, and interpretation in the light of previously characterised processes (Funes et al., 2007). The transforming oncogenes, telomerase (hTERT), E6, E7, small-t antigen and H-Ras, are shown in figure 4.4 B.

Chromatin loop size was investigated in asynchronous cycling cultures. It should be noted here that MSCs produced paler halos, which may reflect their stem cell state. A HIM protocol with settings specific to this cell type was first established and used throughout to enable data collection across the full range exhibited by the series (section 3.4.7). Therefore, size estimates cannot be directly compared to others shown in this chapter but within the series are internally consistent.

A dramatic and reproducible increase in loop size of 50.4 % between MSCh1 and MSCh2 was observed (fig 4.4 C), indicating that expression of Human papilloma virus (HPV) E6, which causes degradation of p53, impacts on the interaction between chromatin loops and the NM. This was highly significant and reproducible. No further change in loop size occurred between MSCh2 and MSCh4, despite the addition of E7, which inhibits RB, and small-t antigen, which promotes stability of c-Myc and reduces dependence on mitogens. However, a second dramatic increase in loop size was observed between MSCh4 and MSCh5. This increase was a further 37.8 % increase (from MSCh4), making the overall increase from MSCh1 to MSCh5 greater than 2 fold. Therefore, H-Ras, which like c-Myc reduces dependence on mitogen stimulation for growth, also impacts directly or indirectly on the interaction between chromatin loops and the NM.

4.4.6 Chromatin loops are larger in cell lines from tumours of higher severity

To begin to ask whether similar changes in chromatin loop organization are observed during transformation *in vivo*, analyses were performed on two sets of stable cell lines derived from tumours of similar origin. Firstly breast epithelial cell lines derived from i) normal breast tissue – MCF10A (spontaneously immortalised) (Tait et al., 1990), ii) a metastatic tumour that gave rise to cells that retain dependence on oestrogen for tumour formation in mice (which are described as poorly metastatic) – MCF7 (Brooks et al., 1973; Osborne et al., 1985) and iii) cells derived from a metastatic 'poor prognosis', poorly differentiated tumour that is oestrogen receptor negative - MDA-MB-231 (Cailleau et al., 1978; Minn et al., 2005). Metastatic tumours show worse prognosis and oestrogen receptor negative tumours (or basal subgroup) also show worse prognosis supporting this order of severity (Sorlie et al., 2001). In addition a set of bladder cancer cell lines were used, all derived from transitional bladder cell carcinomas. These are i) RT4 from a differentiated tumour (Rigby and Franks, 1970) and does not form tumours in nude mice, ii) RT112 (Marshall et al., 1977) and iii) EJ (Marshall et al., 1977). EJ cells have clearly acquired the most characteristics of transformation within these three lines, they can grow under anchorage independent conditions (in soft agar), are the least differentiated, and the most invasive (Booth et al., 1997; Marshall et al., 1977). However, RT4 and RT112 are difficult to order in terms of severity. They have previously been published with the order of severity increasing between RT4 and RT112 due to increased invasion and grade of originating tumour (Booth et al., 1997). However, RT112 retain the ability to differentiate (J. Southgate personal communication), retain NM bound cyclin E (Munkley et al., 2011) and do not show dramatic differences from RT4 in terms of expression of urothelial markers (Booth et al., 1997). Therefore, the differences between EJ cells and either RT4 or RT112 are more interpretable than differences between RT4 and RT112.

Within the breast epithelial cell lines, MCF7 had a significantly larger average halo size than the normal control, MCF10A, however MDA-MB-231 showed little difference in size (fig 4.4 D). For the bladder cancer lines EJ cells had significantly larger halo size than RT4 or RT112 (fig 4.4 E). These data broadly support conclusions from the MSC series though results are harder to interpret.

4.4.7 Chromatin loops are more unstable following oncogenic transformation *in vitro* and *in vivo*

The stability of chromatin loops can also be quantified using MFHR-derived methodology (section 3.4.8). Briefly, the response of a population of cells to MFHR is not homogeneous and can be separated into three categories. Class I is defined as halos that retain a bright residual nucleus (RN), class II retain a pale RN, and class III are those with no clear RN, having a disintegrated appearance (fig 4.5 A). Halos transition from class I to class II and III as they degrade. Therefore cell lines with greater number of class II and III halos are likely to have more unstable chromatin loop attachments than cell lines with a greater proportion of class I halos. Analysis of the class distribution again showed two dramatic shifts across the MSC series, and again these were in response to transfection with E6 and H-Ras (fig 4.5 B). The proportion of class I halos decreased from > 45% in MSCh1 to < 11% in MSCh2, with a corresponding increase of both class II and class III. Little change in proportions occurred between MSCh2 and 4, but the proportion of class III increased from < 15 % in MSCh4 to > 38 % in MSCh5, with a decrease in class I and II. These data suggest that the stability, as well as frequency, of loop base attachments decreases as cells receive increasing numbers of oncogenic transformations.

The rate of degradation of individual halos can also be determined by taking a set of readings over time (section 3.4.9). Briefly, MFHR images show the RN and the halo becoming paler over time so that at a certain timepoint they fail to fall within the parameters measurable by HIM (fig 4.5 C). This offers a non-subjective measure of the disintegration of an individual halo. Data are presented as the percentage of cells with a measurable halo at each timepoint. As for size and class distribution, halo stability decreased with transformation so that a smaller percentage of cells were measurable at each timepoint (fig 4.5 D, E). For example, when following class I and class II cells from MSCh1 and MSCh5, a halo measurement can be made from most MSCh1 cells, whereas most MSCh5 cells fail to be measured during the same time period (fig 4.5 D). For those that can, a reduction in stability of halos can again be observed when cells are transformed with E6 and, to a lesser extent, H-Ras (fig 4.5 E). This does not purely reflect different proportions of halo classes, as when just class II cells are plotted, stability decreases across the series (fig 4.5 E right). Taken together these data suggest that as cells receive increasing oncogenic

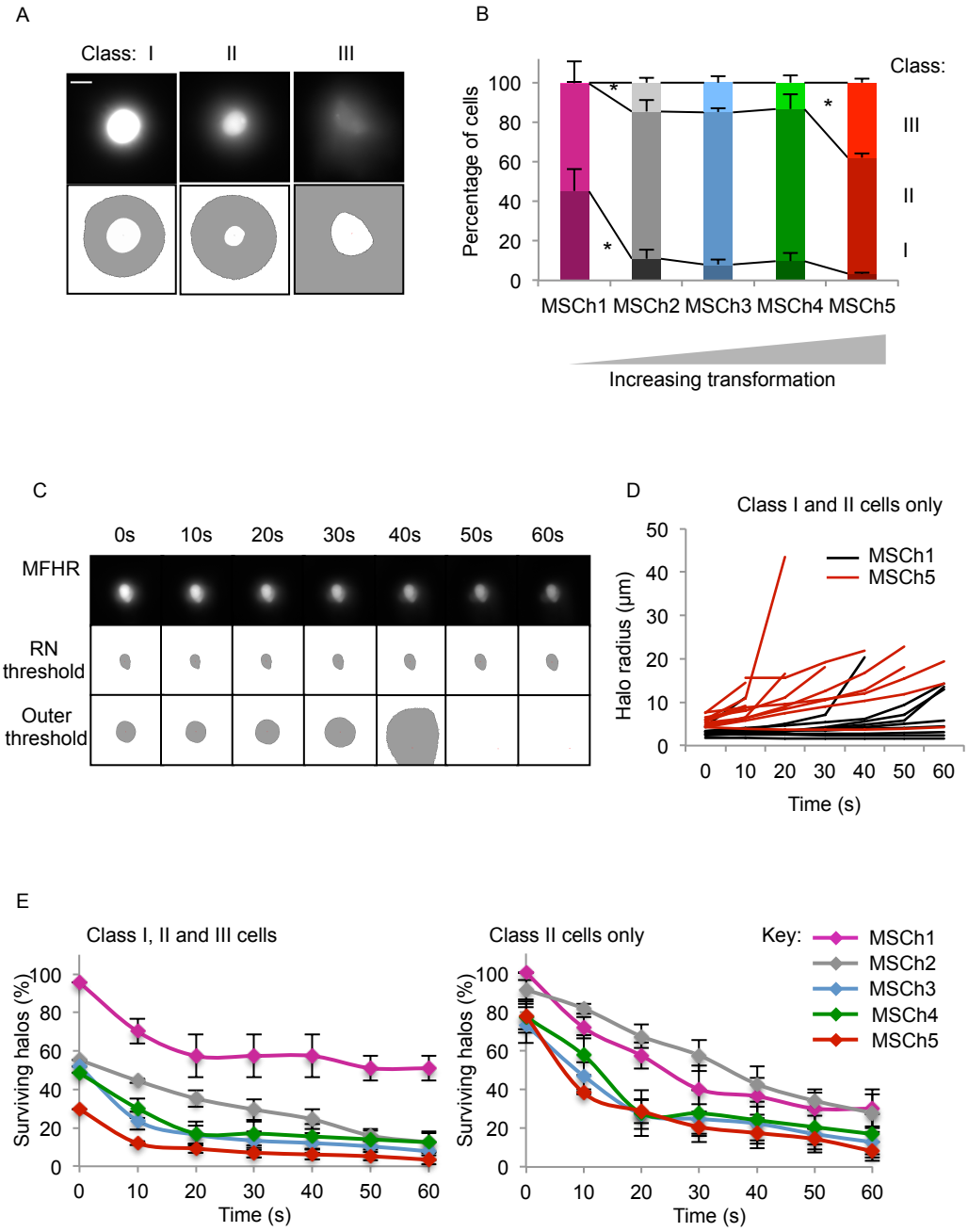

Figure 4.5 Transformation destabilises chromatin loops. A) Example halo images for different class response to MFHR with threshold analysis images. Class I have a bright RN, class II a pale RN and class III have an indistinct/disintegrated RN. B) Class distribution shown for MSC lines. Data presented here, and all further class distributions, are derived from > 100 halos per condition from > 4 coverslips, error bars are SEM. p values from Student's T-test. * ≤ 0.05, ** ≤ 0.005, *** ≤ 0.0005. Shading reflects the proportion of cells in classes I-III as indicated. C) Images show decay of a halo over time, with corresponding HIM threshold analysis images. D) Stability measurements over time of class II MSCh1 (n=15) and MSCh5 (n=30) cells. Note that 4 MSCh1 cells failed by 10s, compared to 18 MSCh5 cells. E) Results show proportion of all cells (left) or class II cells only (right) whose halos fall within threshold parameter of HIM at the indicated timepoint, with SEM. Data presented, and for all further stability measurements, are derived from 32 halos per condition from 4 coverslips. Error bars are SEM.

transformations, and become more 'cancer-like', changes in chromatin loop organization occur, with attachments becoming weaker.

From the three types of MFHR analysis, it is clear that expression of E6 and H-Ras both have significant effects on chromatin loop attachment and stability. It is notable that although both c-Myc and H-Ras reduce dependence on mitogenic signals, of these only H-Ras has a dramatic effect on chromatin loops. Published analysis of other characteristics of these cells revealed a number of transitions (Funes et al., 2007). For example, proliferation rate and bioenergetics parameters changed after 4 hits, suggesting no relationship with loop size or stability. However, a shift towards anchorage independent growth and tumour formation in mice was observed after H-Ras transfection, correlating with the observed change in chromatin loops.

Stability of chromatin loops were also investigated for the breast cancer and bladder cancer series. Unlike halo size measurements, MCF7 showed little difference in class distribution compared to MCF10A however, MDA-MB-231 showed a dramatically smaller proportion of class I halos (27 % compared to 83 % in MCF10A) with corresponding increase in both class II and III (fig 4.6 A). Therefore, both MCF7 and MDA-MB-231 exhibit perturbed loop attachments compared to the normal control, although likely by differing mechanisms. Within the bladder cancer series, the most anaplastic cancer cell line EJ exhibited increased proportions of unstable halos with a decrease in class I proportion from 81-95 % in RT4 and RT112 cells to only 19 % in EJ cells (fig 4.6 B). EJ cells were also the least stable over time (fig 4.6 C). Therefore, these data are again supportive of the conclusion from the MSC series that decreased stability of chromatin loop attachments correlates with transformation.

4.4.8 CIZ1 protein levels increase in response to E6 expression

Newly synthesised CIZ1 (section 1.1.10-12 for background on CIZ1) is required for chromatin loop remodelling (appendix A). CIZ1 is a NM protein and can bind to some pre-RC proteins, and regulatory cyclin:CDK complexes (Ainscough et al., 2007; Copeland et al., 2010; Coverley et al., 2005; Copeland and Coverley personal communication). Because accumulating evidence suggests that (in normal cells) initiation of DNA replication occurs in association with the NM

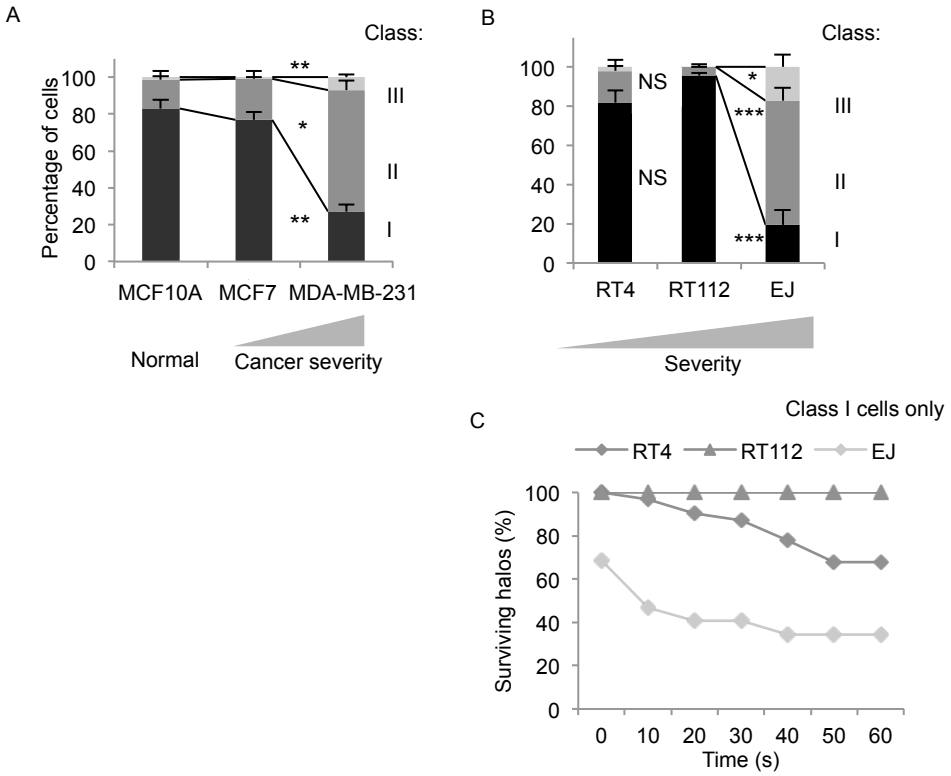

Figure 4.6: Increased severity of cancer cells correlates with destabilisation of chromatin loops. A) Class distribution of halos from breast epithelial cell lines. Data collected as 4.5 B, except MDA-MB-231, 2 coverslips . Shading reflects the proportion of cells in classes I-III as indicated. B) Class distribution of halos from bladder epithelial cancer cell lines. Data collected as 4.5 B. Shading reflects the proportion of cells in classes I-III as indicated. NS, not significant. C) Stability measurements for bladder epithelial cancer cell lines. Data collected as 4.5 E.

Amanda Collier (summer student) helped with MFHR of RT4, RT112, EJ and MCF7.

(reviewed in Wilson and Coverley, 2013), this suggests that CIZ1 functions at the NM, possibly at the base of chromatin loops. Immuno-staining of MFHR treated cells revealed that CIZ1 remains in the RN as foci in 3T3 cells, as would be expected for a NM protein present at loop bases (fig 4.7A). CIZ1 status was therefore investigated in the MSC transformation series used in this analysis. The α-CIZ1 polyclonal antibody 1793 recognises several species by western blot (Coverley et al., 2005), including a doublet of relative molecular weight ~125 kDa (see chapter 5) which binds to the NM (Ainscough et al., 2007), also recognised by α-CIZ1 NB100-74623. Analysis of total protein from the MSC lines showed an increase of p125 relative to actin, upon the transformation with E6 (fig 4.7 B). This correlates with dramatic changes in chromatin loop size and stability. This alteration in CIZ1 expression is consistent with the hypothesis that CIZ1 may play a role in the observed changes by an as yet unknown mechanism that is dependent on E6 expression. Increased CIZ1 has also been observed in the three bladder lines investigated here (appendix D). The data in this chapter suggest that chromatin loop destabilisation, potentially related to changes in CIZ1, may be an integral part of the transformation process.

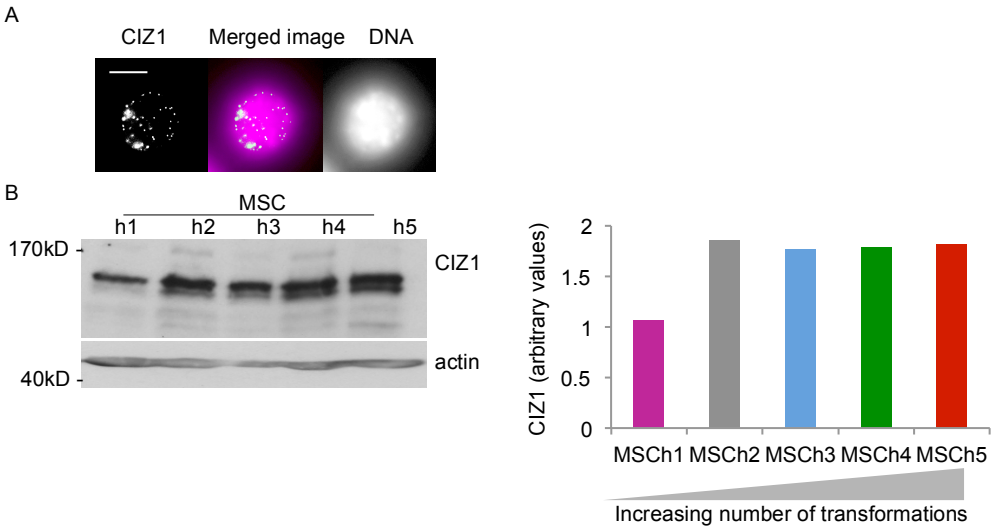

Figure 4.7: Transformation with E6 correlates with increased CIZ1. A) CIZ1 is retained as discrete NM-associated foci after MFHR (fixation protocol, see materials and methods). Left: CIZ1 protein detected with 1793 (white). Right: DNA stained with DAPI (white). Centre: Merged image, CIZ1 in white, DNA in magenta. B) CIZ1 protein (detected with NB100-74623) in whole cell extracts from MSCh1 to MSCh5. Actin is used as loading control. Histogram (right) shows quantification of CIZ1 doublet relative to actin.

4.5 Discussion

Described here are two remodelling events for nuclear higher order structure, which occur on entry to and exit from quiescence. Upon exit, remodelling occurs very early in G1Q, is independent of serum derived growth factors but requires newly synthesised factor(s) including CIZ1 (appendix A). These results are discussed in light of the wider literature, before consideration of differences observed between chromatin loops in non-cancer and cancer cells.

4.5.1 Chromatin loop remodelling on entry to quiescence

Data presented here show that as cells enter quiescence, halo size decreases. There are several options for how this may occur (fig 4.8 A). Firstly and the most obvious explanation, is that chromatin loop size decreases (fig 4.8 A i). This would mean smaller intervals between S/MARs and therefore, more of them. Hopefully, use of MAR analysis will help to determine if this is the case. Alternatively, the number of S/MARs may stay the same but more DNA may be attached to the NM with less being able to extend out from the loops. This could either be due to an expanded NM (fig 4.8 A ii) or just increased attachment length (shown as a condensed domain at the NM) to the existing NM (fig 4.8 A iii). In both cases, MAR analysis should reveal an equal number of MARs but of longer length. A further possibility is that smaller halos arise from a combination of these options. Two additional points to note are that MARs may well not be the same in cycling and quiescent populations and it is the intervals and length, which are more important to determine the reason for small halo size. Also that packaging of DNA may also be altered in quiescent cells but this should not impact MFHR analysis as all non-NM, chromatin bound proteins should be removed. Options i and iii appear to be most likely as a significant increase in RN was not observed in quiescent cells.

It is likely that the increase in halo size upon cell cycle re-entry is the direct reversal of the mechanism causing a smaller halo on entry to quiescence. However, it should be bourn in mind that this could also be achieved by the opposite of the possibilities mentioned above, whether or not that was the reason for smaller halo in quiescence.

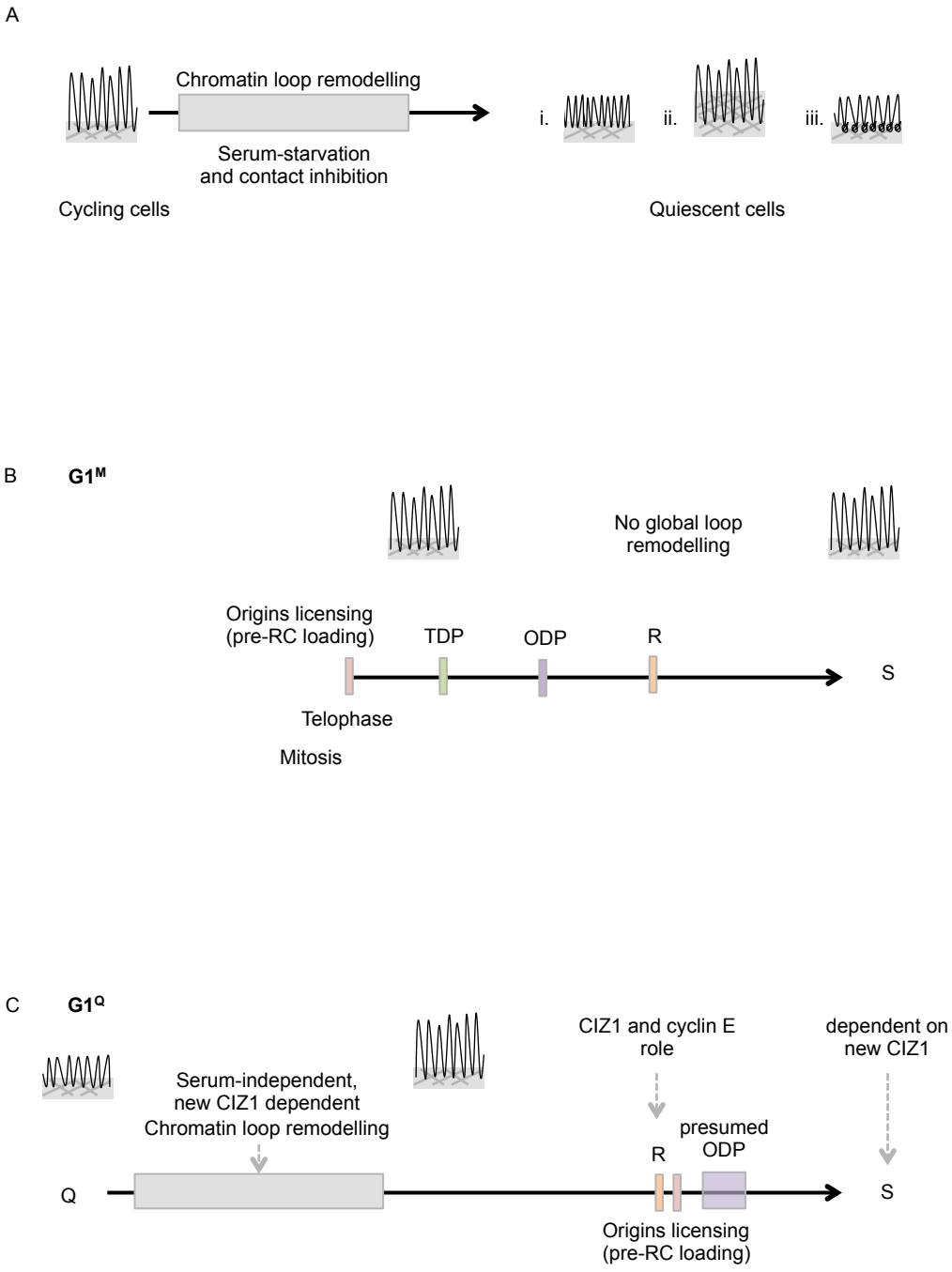

Figure 4.8: Schematics showing chromatin remodelling events. A) Schematic shows options for chromatin loop remodelling event as cells enter quiescence. Grey box indicates loop remodelling event. B) Schematic shows events during $G1^{M}$. ODP origin decision point, R, restriction point, S, S-phase, TDP, timing decision point. C) Schematic shows events during $G1^{Q}$. Grey dashed arrows indicate roles for CIZ1. Not shown to scale.

Below is discussed how loop remodelling upon re-entry fits into the timescale of other events.

4.5.2 Global chromatin loop organisation and the cell cycle

Previous studies have investigated chromatin loop size during different phases of the mitotic cell cycle but reported little difference. For example, Jackson et al. (1990) found no difference in loop size using a method that measured enzymically detached loops, when looking at unsynchronised populations of HeLa cells, compared to those synchronised in mitosis, G1 or S-phase. Conversely, Roti Roti and Wright (1987) showed a very slight increase in overall nucleoid diameter (diameter across the RN and halo) as cells progressed through the cell cycle, however, this may be due to a slight increase in RN caused by increased DNA content during S-phase (Taylor et al., 1991). Therefore, there is no convincing evidence in the literature of a global chromatin loop restructuring between phases of the mitotic cell cycle. This contrasts with the findings presented here and suggest that the phenomena we have uncovered here do not relate to progression through the mitotic cell cycle.

4.5.3 What is its purpose?

The lack of DNA replication and suppression of transcription in quiescence may be related to the chromatin loop characteristics. In the absence of a requirement to maintain a specific arrangement of chromatin loops to support efficient replication and transcription, an alternative chromatin loop arrangement might be employed which is more suited to genome maintenance and protection during long periods of quiescence. Considering the situation in an alternate way, it may be that smaller intervals and more numerous chromatin attachments are the preferred state but ongoing replication and transcription, and the repeated opening of DNA and displacement of attachments, prevent this. When these processes occur at a reduced level (or not an all) default arrangement of chromatin loops would be permitted.

4.5.4 Local chromatin loop arrangement and the cell cycle

Although not supported at the global level, available evidence does suggest that locally, loops may differ by cell cycle stage. As previously discussed (section 1.4.4)

S/MARs have been identified in the vicinity of a number of exemplar replication origins (reviewed in Cayrou et al., 2010; Johnson et al., 2011). The available information suggests that origins are recruited to the NM during G1 although one reports this as very early in G1 (Courbet et al., 2008) and another as late G1/S phase (Djeliova et al., 2001a, b). It fact, it may be that different origins (i.e. early or late replicating) are recruited at different times. Despite this complication the data suggest a local shuffling of attachment points or increase in attachment points in preparation for S-phase. In addition, the location of some exemplar genes at the base of loops compared to within the loop itself, was shown to alter during S phase and mitosis compared to interphase cells (Gerdes et al., 1994). The loop remodelling event that we observe during quiescence and $G1^{Q}$ may therefore be a more extreme version of the 'attachment shuffling' which appears to occur in $G1^{M}$.

4.5.5 Chromatin loop remodelling as part of reorganisation of the higher order organisation of the nucleus

The changes in chromatin loops size shown here are in some ways reminiscent of another change in the higher order structure of chromatin. It has been reported that chromosome territories shift both on entry to and exit from quiescence (Bridger et al., 2000; Mehta et al., 2010). However, for this phenomenon the shift back to a cycling conformation occurred in the second G1-phase after release from quiescence suggesting that, unlike loop remodelling it requires passage through mitosis and/or DNA replication. Therefore, the two observations are unlikely to reflect the same event. For entry to quiescence it remains possible that the two processes are co-regulated. One interesting point to note in this respect, is that shifts in territories on entry to quiescence were found to require molecular motors (Mehta et al., 2010; and reviewed in Mehta et al., 2008). Chromatin loop remodelling requires CIZ1 (appendix A), which can interact with the motor dynein light chain 1 (DLC1) (den Hollander and Kumar, 2006).

4.5.6 Chromatin loop remodelling and origin specification

Two events which may relate to changes in higher order organisation of DNA are that of origin specification and replication timing determination. In preparation for DNA replication, origins must first be licenced by the loading of the pre-RC. Two

other transitions occur, at the timing decision point (TDP) when replication timing is determined, and at the origin decision point (ODP) when origin usage is specified (characterised in CHO cells (Wu and Gilbert, 1996)). All of these events have the potential to be part of the same event as loop remodelling. In the mitotic cell cycle pre-RC loading occurs during late telophase (Dimitrova et al., 2002), followed by the TDP after 1-2 hours (Lu et al., 2010) and the ODP, also early in $G1^{M}$ and before the restriction point (Li et al., 2003a; Wu and Gilbert, 1996, 1997). Timings shown in schematic figure 4.8 B.

The ODP in particular was characterised for $G1^{M}$ only and $G1^{Q}$ has subtle differences, but we can order these events for $G1^{Q}$ based on some deductions. Firstly, replication timing determination remains through quiescence, despite nuclear reorganisation (Lu et al., 2010) implying no TDP during $G1^{Q}$. Secondly, origin licensing and specification are lost as cells become quiescent because pre-RC components are degraded (Wu and Gilbert, 1997). The pre-RC are not transcribed and loaded until around R during the transcription and translation cascade that is initiated at this point, shortly before S-phase re-entry (Geng et al., 2003). Therefore, as the ODP occurs after licensing it is likely that during $G1^{Q}$, the ODP does not occur till R or later. With no TDP, and licensing and the ODP not occurring until around 15 hours, that leaves none of these events occurring at the same point as loop remodelling which has taken place by 12 hours (fig 4.8 C). Further analysis could be undertaken to confirm their independence. It is notable that like $G1^{Q}$ remodelling, $G1^{M}$ ODP does not require serum but unlike $G1^{Q}$ remodelling, the inhibition of protein synthesis by cycloheximide does not prevent the $G1^{M}$ ODP. The ODP does, however, require proteasome dependent proteolysis, and transcription to supress origins in transcribed regions (Keezer and Gilbert, 2002; Sasaki et al., 2006). Determining the effect of these factors on chromatin loop remodelling may help confirm independence, or aid further mechanistic analysis.

Nevertheless, this leaves us with the tentative conclusion that loop remodelling during $G1^{Q}$, described in detail here, is a novel and previously undescribed organisational event. Two major features of cell cycle re-entry is the need for cells to a) transcribe many genes required for cell cycle progression whose expression is reduced or lost in quiescence and b) preparation of DNA for undergoing replication. Both of these may involve alteration of chromatin loop attachment regions. It could,

for example, bring origins, or their closest MAR, to the NM. Origin recruitment is discussed further in chapter 6.

4.5.7 CIZ1 during cell cycle re-entry

CIZ1 is required for timely re-entry to S-phase (Copeland et al., 2010). However, it appears to have several roles during G1Q (fig 4.8 C), including sequential interaction with cyclins A and E (Copeland et al., 2010) and a role in loop remodelling (appendix A), and it is not certain which are required for S-phase entry. Data presented here, show that cyclin E is not involved in loop remodelling and this suggests that, although cyclin E and CIZ1 interact later in G1Q, they might not interact at this timepoint. It is possible that involvement in chromatin loop remodelling is part of a previously unidentified role of CIZ1, and that loop remodelling is required for S-phase entry. Further experiments are needed to establish the method of action, possibly starting with determination of the required motifs within CIZ1. Nevertheless, I have shown here that this event occurs early in G1, is independent of serum yet requires the synthesis of new factors during release.

4.5.8 Changes in chromatin loop size in cancer

Presented here are data that chromatin loops become larger and less stable as cells become transformed and gain cancer phenotypes. This is also supported by some data from 1991, that showed lymphoblast lines to have a larger nucleoid diameter than lymphocytes (Taylor et al., 1991). As nucleoid diameter consists of RN and the halo this cannot be solely attributed to chromatin loops, however, it is consistent with the data presented here. Similar results for nucleoid area were recorded in a study which compared retinal endothelial cells (REC) before and after transfection with Myc and/or Ras (Malyapa et al., 1996). Interestingly, in the MSC series used here, stabilisation of c-Myc did not cause a change in chromatin loops. This may mean that Myc can replicate the change we observe following p53 degradation, or that Myc had an impact on RN rather than halo size. Finally, mutations of cohesin have been identified in cancers (reviewed in Remeseiro and Losada, 2013) and knockdown of cohesin components have previously shown to cause large chromatin loops by MFHR (Guillou et al., 2010).

Larger chromatin loops implies that cancer cells have fewer attached S/MARs or that the length of S/MARs is decreased and less DNA is held within the NM at each attachment point. These could be the result of mutations in S/MARs themselves, alterations in the S/MAR recruitment mechanism or altered or fewer MARBPs to act as NM receptors. As previously discussed (section 1.5), changes in the NM have been recorded for cancer cells supporting this later possibility. Data showing cyclin E and CIZ1 to be lost from the NM in cancer (Munkley et al., 2011; appendix D) suggest that MARBPs or other associated proteins may also be lost from the NM. The lack of recruitment of both protein and DNA to the NM may be adventitious in cancer by aiding plasticity.

4.5.9 CIZ1 and chromatin loops

The NM protein and DNA replication promoting factor CIZ1 (section 1.1.10-12) has previously been suggested to help regulate the spatial and temporal control of DNA replication (Ainscough et al., 2007; Copeland et al., 2010). This could be through the recruitment of other proteins to 'the right place at the right time' but it is also possible that this involves recruitment of chromatin loops to the NM. The following data are the foundation for this hypothesis. 1) CIZ1 can interact with members of the pre-RC, and its regulators through domains in its N-terminus (Copeland et al., 2010; Coverley et al., 2005; Copeland and Coverley, in preparation). 2) CIZ interacts with the NM through domains in its C-terminus (Ainscough et al., 2007). 3) Preliminary data suggest CIZ1 to be required for chromatin loop remodelling (appendix A). 4) Moreover, CIZ1 expression is disrupted in a range of different cancers (den Hollander et al., 2006; Higgins et al., 2012; Rahman et al., 2007) and the two domains appear to be commonly uncoupled in cancers (appendix D). In fact the C-terminal anchor domain has been shown to have a dominant negative effect causing removal from the NM of wild-type CIZ1 and also the pre-RC. This therefore, leads to the hypothesis that alterations in CIZ1 may be a (partial) cause of the genetic instability of cancer by affecting chromatin loop arrangement.

There are several options as to how CIZ1 interacts with chromatin loops. Firstly, CIZ1 could be a MARBP, present at the NM, to facilitate loop attachments (fig 4.9 A i). This could be investigated by removing CIZ1. In this hypothesis, as there are multiple MARBPs, it is likely that in the absence of CIZ1, a subset of loop

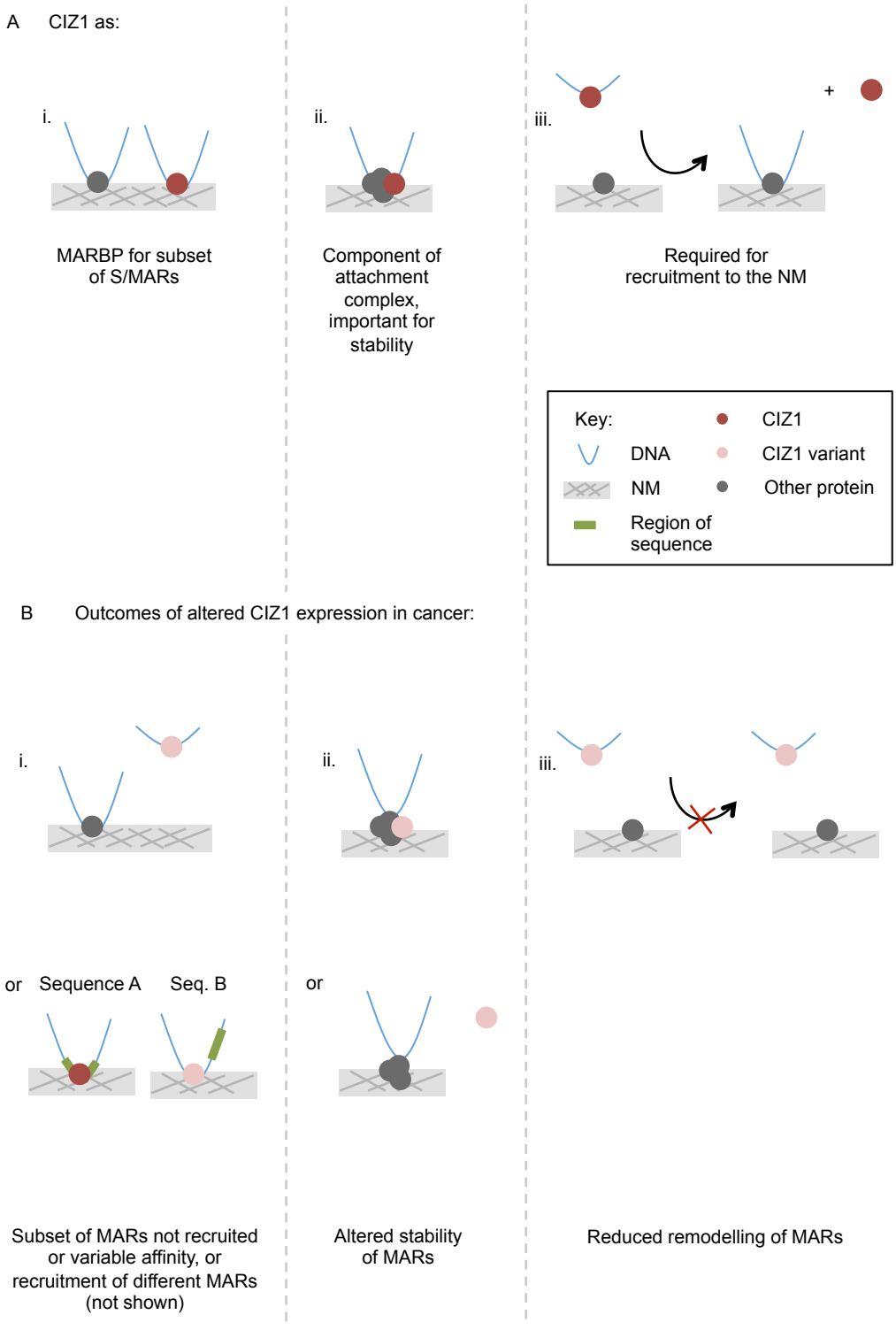

Figure 4.9: Model of how CIZ1 may interact with chromatin loops. A) Options shown for the role of normal CIZ1 and B) how altered CIZ1 expression in cancer cells may affect chromatin loop maintenance, choice or stability.

attachments are not made resulting in larger loops. Alternatively, CIZ1 may exist at the base of loops but as part of a larger complex and be involved with loop maintenance and stability (fig 4.9 A ii). In the absence of CIZ1 loops would be likely to be more unstable. Another possibility is that CIZ1 does not locate to the base of loops permanently but is important for the mechanisms of their recruitment to the NM, that is, taking a previously unused MAR to the NM to become a new loop base, but not remaining there (fig 4.9 A iii). In this case an absence of CIZ1 might be expected to cause reduced remodelling of loop attachments. From the data presented here, the latter two hypotheses appear the most likely. CIZ1 -/- cells (chapter 5) could be used to investigate these hypotheses, and this work is ongoing, however, preliminary data are inconclusive.

Alterations of CIZ1 observed in cancer cells include inappropriate expression of variants (Higgins et al., 2012; Rahman et al., 2007; Warder and Keherly, 2003), but also increased levels and an unbalancing of the two ends of the protein causing a dominant negative effect (appendix D). If, as suggested above, CIZ1 has a role in the maintenance and choice of chromatin loop attachments there are several possibilities for the effect of alterations in CIZ1. If CIZ1 is a MARBP, altered expression of CIZ1 could cause loss of attachments, reduced stability of attachments, or change the subset of S/MARs with which CIZ1 is able to interact (fig 4.9 B i). This could be due to altered affinity for S/MARs or other proteins. If CIZ1 is important for stability of attachments, altered expression of CIZ1 could reduce stability of attachments (fig 4.9 B ii). Alternatively if CIZ1 is required for movement of attachments but does not remain at those sites, altered CIZ1 may be unable to perform this role, either due to reduced affinity for NM sites or inability to either interact with or release S/MARs (4.9 B iii). Data presented here correlate increased CIZ1 with reduced loop stability, suggesting CIZ1 to be present at loop bases (options i or ii). Future work to determine the precise role of CIZ1 in relation to chromatin loops, by the use of CIZ1 -/- cells, CIZ1 overexpressing cells and expression of CIZ1 mutants, could resolve these possibilities.

Chromatin loop attachments and their stability appear to be significantly affected in cancer cells and suggests that chromatin organisation is less firmly fixed in space. This could cause genetic instability due to lack of fidelity of chromatin loop attachments, both in terms of choice and stability. This may increase the plasticity of

cancer cells, and reverse the fixing of a cell type specific programme. Although sometimes detrimental, this might also allow beneficial mutations, features that might also make the cancer cell able to respond to and take advantage of changes in its environment.

5 CIZ1 modulates cyclin and CDKi expression and protects against activation of the DNA damage response

5 CIZ1 modulates cyclin and CDKi expression and protects against activation of the DNA damage response

5.1 Introduction

This chapter concerns the *in vitro* analysis of CIZ1 knock-out (CIZ1-/-) cells derived from a CIZ1-/- mouse. The mice and cells were generated in University of Leeds by Justin Ainscough, with help from Sumia Bageghni and Ghadeer Albadrani, who kindly made the cells available for me to investigate cell cycle characteristics in the absence of CIZ1 (Wilson, R. H. C., Roulson, J-A., Bageghni, S., Albadrani, G., Coverley, D. and Ainscough, J. F. X., in preparation).

5.1.1 CIZ1 Summary

The known roles of CIZ1 (UniGeneID 64561 Hs. 212395, UniGeneID 297753 Mm. 170508) and its implication in disease are reviewed in section 1.1.10-12. The available literature about CIZ1 reveals this protein to be highly complex, in terms of expression, location and function. The function which is best understood to date, although not completely, is the promotion of DNA replication, which involves functional interaction with cyclins E and A (Copeland et al., 2010). The likely importance of this role is highlighted by the many instances of altered CIZ1 found in cancer. For several other proteins, knock-out animals have revealed previously unknown functions despite detailed, previous work using inhibitory antibodies or transient knockdown by RNAi. For example, generation of the cyclin E1-/- E2-/- mouse identified a hitherto unknown role for cyclin E in endoreduplication (Geng et al., 2003), while at the same time clarifying that many of its roles are redundant and can be fulfilled by cyclin A. In the case of CIZ1, some previous work has been undertaken by transient knockdown using RNAi, leading to restraint of entry to S-phase during release from quiescence (Coverley et al., 2005).

5.1.2 DNA damage response and cancer

In this chapter I will describe data that indicate activation of the DNA damage response (DDR) in cells lacking CIZ1, under specific circumstances. The following is a brief overview of the salient features of this field. There are many characteristics that a cell must acquire to escape normal control mechanisms and potentially give rise to cancer (reviewed in Hanahan and Weinberg, 2000; Hanahan and Weinberg, 2011). Cells may do this through progressive acquisition of mutations due to DNA damage. Damage can be caused by external factors such as radiation, internal factors such as reactive oxygen species, or the stalling of replication forks. Cells respond to damage by activation of the DDR (reviewed in Bartek and Lucas, 2003; Harper and Elledge, 2007; Kastan and Bartek, 2004; Zhou and Elledge, 2000), leading to cell cycle arrest through activation of cell cycle checkpoints. This is accompanied by either resolution of damaged structures, sometimes with the introduction of sequence errors, or if unresolved, induction of senescence or apoptosis.

Two key sensors and transducers of the DDR are ataxia telangiectasia mutated protein (ATM), which is generally activated by double strand breaks (DSB) caused by ionizing radiation, and ataxia telangiectasia and Rad3-related protein (ATR), activated by single strand breaks (SSB) caused by UV or replicative stress. Replicative stress includes the inefficient replication of DNA, which occurs in response to limiting dNTPs or secondary structural blocks, and results in stalled replication forks and regions of single stranded DNA (reviewed in Burhans and Weinberger, 2007). ATM and ATR primarily phosphorylate the checkpoint kinases Chk2 and Chk1, respectively. However, there is also significant overlap between the two pathways, with both leading to phosphorylation and recruitment of the histone variant H2AX (γH2AX) to sites of damage. The DDR and cancer are exquisitely inter-related since DDR activity resolves or prevents the impact of potential cancer inducing mutations. Crucially, the DDR (both the response to DSBs and SSBs) is activated in tumours and in bladder, breast, lung and colon early precursor lesions (Bartkova et al., 2005) and was identified as an anti-cancer barrier in early stages of transformation. However, chronic activation of the DDR also provides a selective pressure for mutations within components of the DDR. Consistent with this, later stage tumours show reduced activation of the DDR often through loss of function of

one or more signalling molecules (Bartkova et al., 2005). The mechanisms that cause activation of the DDR in early stage tumours remain to be established in detail.

5.2 Aims

The aims of this project were to better understand the roles of CIZ1, with particular attention to promotion of the cell cycle and DNA replication, and how CIZ1 is connected with cancer. As such the specific aims were:

- Understand the impact of absence of CIZ1 on the proliferation of cycling cells.

- Understand the impact of absence of CIZ1 on the expression, sub-nuclear localisation and patterning of its interaction partners, namely cyclins, CDK2 and CDKis.

- Understand the effect of absence of CIZ1 on the ability of cells to transition between the proliferating state and quiescence.

- Understand the effect of absence of CIZ1 on the incidence of cancer formation in the mouse and transformation in mouse-derived cells.

5.3 Experimental design

CIZ1-/- mice were generated at University of Leeds from CIZ1-/- embryonic stem cells (ESCs), clone IST13830B6, purchased from Texas A&M Institute for Genomic Medicine (TIGM). CIZ1-/- ESCs were generated by gene trap gene inactivation using insertion of a gene trap vector containing the neomycin resistance gene into intron 1 causing a novel splicing event such that the downstream exons are not expressed (Zambrowicz et al., 2003) (appendix B). Justin Ainscough generated primary embryonic fibroblasts (PEF) (at e12/13) and tail tip fibroblasts (TTF) (at 3 weeks) cells from wild type control (CIZ1+/+) and CIZ1-/- animals. This enabled analysis in both differentiated (TTF) and undifferentiated (PEF) cells, as CIZ1, like its interacting partner cyclin E (Munkley et al 2011), exhibits changes in sub-nuclear

localisation and immobilisation during differentiation (appendix D). All *in vitro* analysis of CIZ1+/+ and CIZ1-/- cells was undertaken by myself, using low passage and therefore low volume experiments. Results from a variety of assays concerning cell cycle, cell proliferation and growth characteristics are presented. *In vivo* analyses performed at Leeds are also outlined here, with appropriate accreditation, in order to complete the story.

5.4 Results

5.4.1 Mouse generation and *in vivo* results

Successful ablation of CIZ1 expression was confirmed by genotyping of mice using insertion differentiating primers, and qRT-PCR of *CIZ1* mRNA expression in embryos, PEFs and TTFs (appendix B and personal communication from J. Ainscough). Immunohistochemistry in differentiating male germ cells, which normally express CIZ1 at very high levels (Greaves et al., 2012) was also carried out in the Ainscough lab. I confirmed loss of CIZ1 protein expression by western blot and immunofluorescence in TTFs using the α-CIZ1 antibody 1793 (Coverley et al., 2005) (fig 5.1 A, B).

CIZ1-/- mice were viable, generated at the expected Mendelian ratio and fertile. No difference in growth rate or adult or kidney weight was detected in CIZ1-/- females compared to CIZ1+/+ controls. However, secondary lymphoid tissues (lymph node, lung, spleen and to a lesser extent livers) were enlarged in all CIZ1-/- mice examined. In addition, spleen and lymph node architecture were abnormal with infiltration of B and T lymphocytes, and all CIZ1-/- females developed spontaneous lymphoproliferative disorder (8/8) between 9-18 months (all personal communication, J. Ainscough, J. Roulson, S. Bageghni, G. Albadrani). Therefore, although CIZ1 is not essential for embryogenesis, early post-natal development or cell viability *ex vivo*, it does appear to protect against tumour formation and this is first evident in lymphoid lineages.

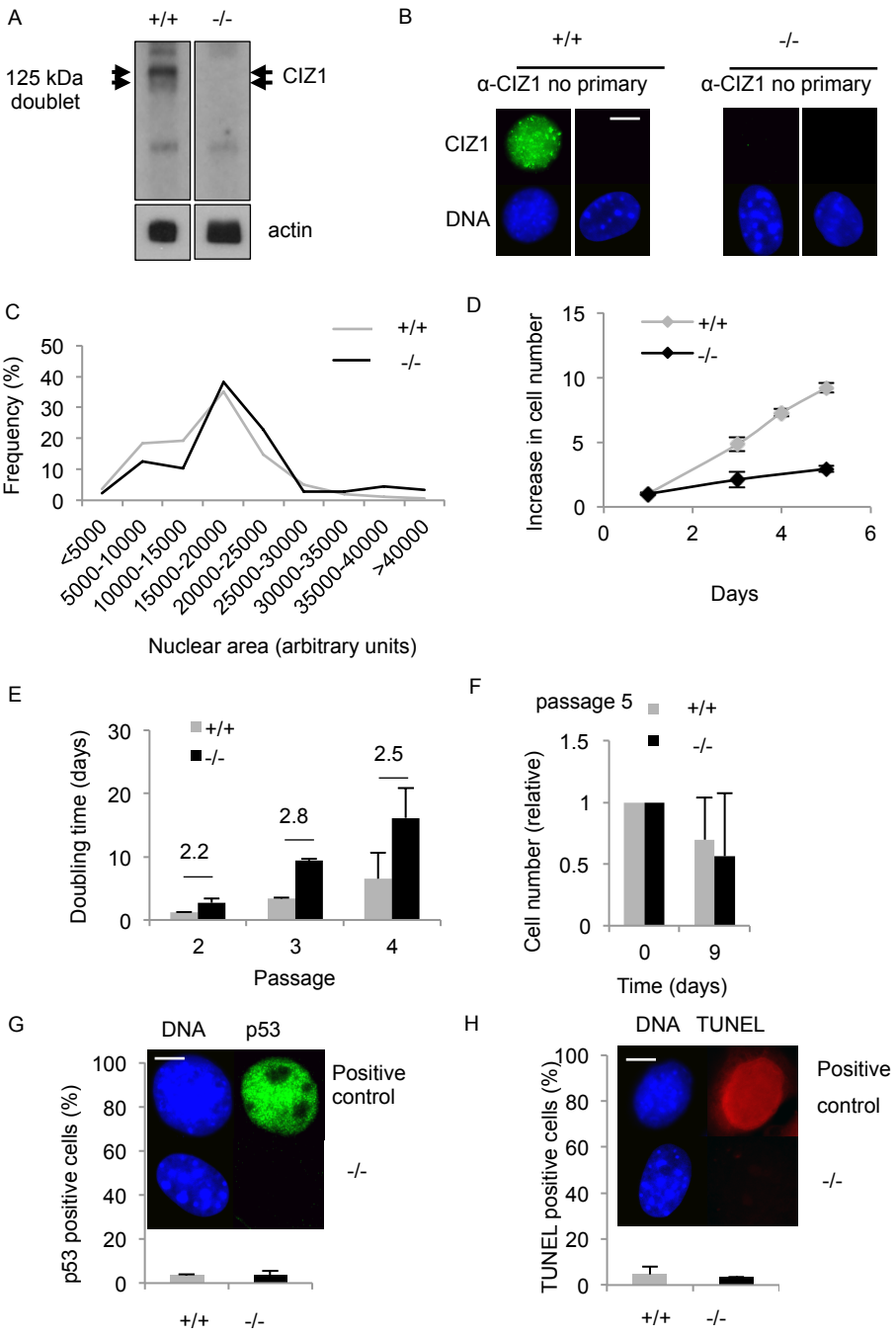

Figure 5.1: CIZ1-/- TTFs proliferate slower than wild type cells. A) Western blot of total cell lysate from TTFs (+/+ 101 and -/- 1017), detected with antibody 1793. Actin is shown as loading control. B) Representative immunofluorescence of total CIZ1 protein in CIZ1+/+ and CIZ1-/- TTFs detected with anti-CIZ1 antibody 1793. DNA is counterstained with Hoechst 33258, scale bar is 10 microns. C) Frequency distribution graph shows little difference in nuclear area between +/+ and -/- cells as determined by area of Hoescht 33258 staining. D) Proliferation of passage 2 TTFs +/+ (126, 133) and -/- (1017, 1018), over 6 days, expressed as fold increase in cell number relative to day 1. Data are average, ± SEM. E) Mean relative doubling time for TTFs +/+ (101, 126, 133) and -/- (1017, 1018) at passage 2, 3 and 4. F) By passage 5 proliferation is negligible. G) Histogram and representative image showing proportion of cells expressing p53. Data are average ± SEM. Positive control is a spontaneously immortilised cell line from CIZ1-/- foci. H) Histogram and representative images showing cells in apoptosis, determined by TUNEL assay. Positive control generated by treatment with DNase I to generate DSB.

5.4.2 CIZ1-/- cells proliferate slower

Isolated primary TTFs from CIZ1-/- mice did not show any gross morphological differences, for example, nuclear size was no different (fig 5.1 C) and they proliferated in culture. However, proliferation rate was much slower in CIZ1-/- cells, with more than twice the doubling time at passages 2-4 (fig 5.1 D, E). Beyond passage 4, growth rate characteristics were not reliable (fig 5.1 F), limiting analysis on these non-immortalised lineages to low volume experimentation. Reduced proliferation is consistent with that observed previously with CIZ1 siRNA knockdown (Coverley et al., 2005). No evidence for increased apoptosis or DNA damage in CIZ1-/- cells was found, as determined by p53, TUNEL (fig 5.1 G, H).

The proportion of the CIZ1-/- population that actively engaged in DNA replication (as determined by EdU incorporation) was reduced to approximately half that in CIZ1+/+ cells (fig 5.2 A, 13 % compared to 23 %). Consistent with this, flow cytometry of propidium iodide stained cells to profile DNA content, indicated a reduction in S-phase cells and a concomitant small increase in G1 cells (fig 5.2 B). This suggests CIZ1-/- cells spend slightly longer in G1-phase and is consistent with the $G1^{Q}$ restraint reported for siRNA knockdown of CIZ1 (Coverley et al., 2005).

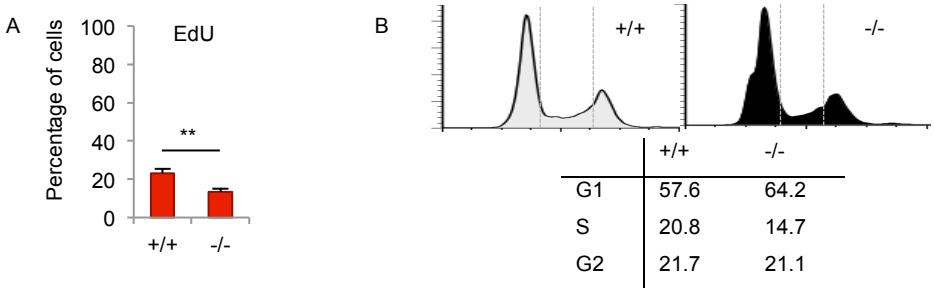

Figure 5.2: CIZ1-/- populations contain increased numbers of G1 cells and less S-phase cells. A) Histogram shows percentage of TTFs CIZ1+/+ (97, 101, 126) and CIZ1-/- (1016, 1017, 1018) cells (passage 3-4) that engaged in DNA synthesis during a 30 min pulse with EdU (S-phase). Data are average from multiple experiments ± SEM, ** p< 0.005. B) Representative flow cytometry profile for propidium iodide stained TTFs +/+ (133) and -/- (1018). The proportion of cells in G1, S and G2 were determined using the boundaries indicated by dotted lines.

Both a reduced doubling time and fewer CIZ1-/- cells in S-phase could be the result of altered S-phase progression. Absence of CIZ1 could affect the length of S-phase,

cause cells to stall within S-phase or affect replication timing. Therefore, to investigate progression through S-phase in more detail a 30 min EdU pulse (pulse 1) was performed, followed by a 4 hr chase period, followed by a 30 min BrdU pulse (pulse 2). EdU and BrdU staining was then classified into initiating, early, mid and late S-phase by a combination of pattern and intensity (section 2.1.6). EdU labelled CIZ1-/- cells in S-phase during pulse 1 progressed to the expected pattern in S-phase during pulse 2 (BrdU) suggesting timely progression (fig 5.3 A). Crucially there were no cells exhibiting only an early pulse 1 pattern (and no pulse 2 pattern), which would be consistent with a significant pause in S-phase. There also did not appear to be any cells that had re-entered S-phase after a long pause, as would be shown by absence of a pulse 1 pattern with a mid-late pulse 2 pattern. Furthermore, all cells that had entered S-phase after pulse 1 (therefore not labelled with EdU) showed an early or early-mid BrdU pattern (perinucleolar foci) rather than a clearly mid-pattern of nucleolar replication. Quantifications of EdU patterns also revealed the normal range of patterns and no significant difference in relative incidence (fig 5.3 B), as well as little difference in the intensity of staining within each classification (fig 5.3 C). Combined, these data suggest that although less CIZ1-/- cells are in S-phase at any one time, the length of S-phase and organisation of replication forks are unaffected, and cells do not stall in S-phase. Therefore, replication timing and patterning do not appear affected, at least at the gross level. It is not certain from these data whether the local sequences being replicated at any one time are affected by loss of CIZ1.

5.4.3 Cyclin D, E and A expression is prolonged or elevated in the absence of CIZ1

Cell cycle regulators, particularly those known to interact with CIZ1, were monitored by immunofluorescence. A far greater proportion of CIZ1-/- cells expressed cyclin D2 and cyclin E1, normally expressed in G1 and late G1 respectively, than in CIZ1+/+ cells (fig 5.4 A). However, the increase in numbers is greater than the increase in G1 observed by flow cytometry. Partially accounting for this, there was also a greater proportion of CIZ1-/- S-phase cells which expressed cyclin D2 and cyclin E1, indicating that both proteins persist beyond the point at which they would normally be degraded. CIZ1 may therefore be required for timely degradation or export. No difference in level of expression for either cyclin was

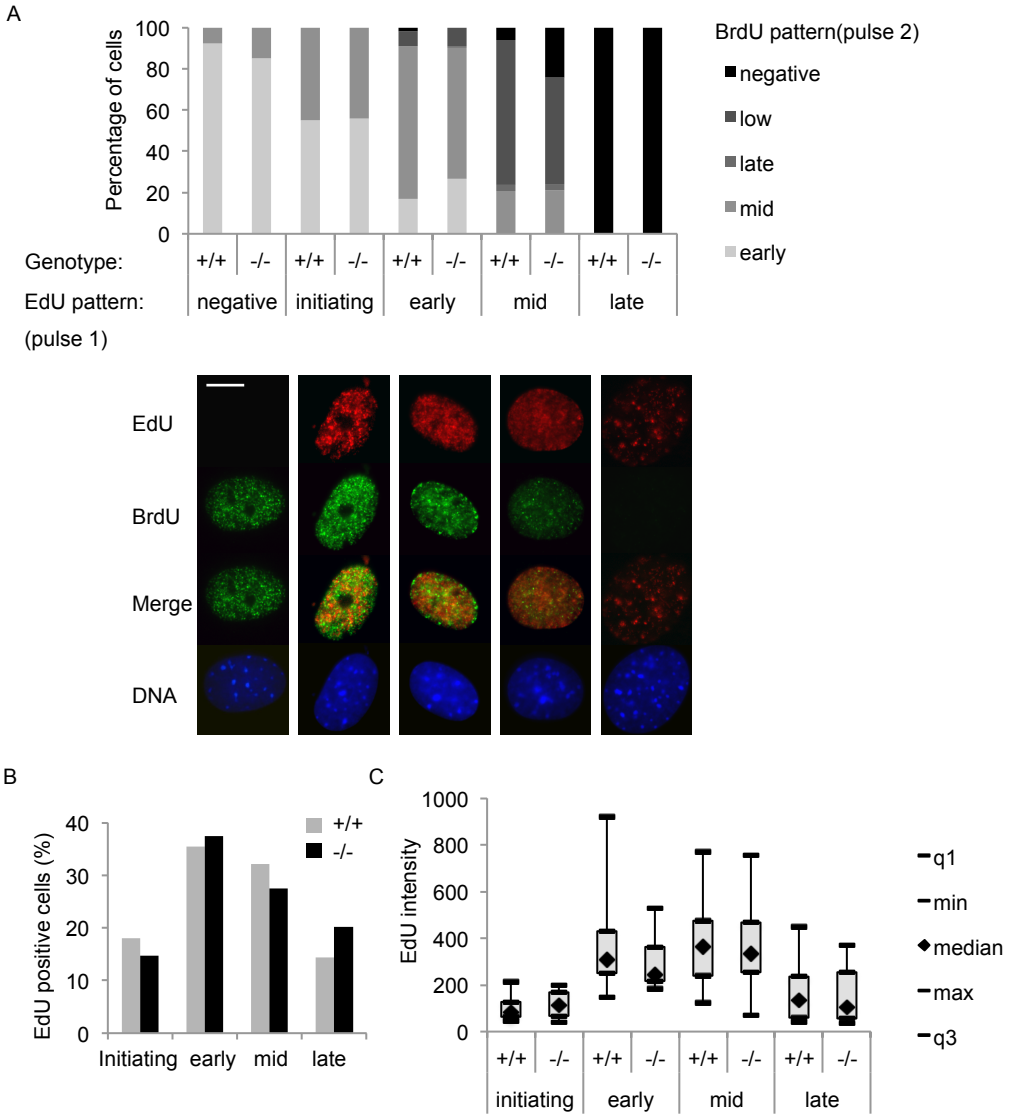

Figure 5.3: S-phase is unaffected in CIZ1-/- cells. A) Stacked histogram showing S-phase staining patterns in TTFs. Cells received an EdU pulse of 30 mins followed by a chase period of 4 hours prior to a BrdU pulse of 30 mins. EdU (pulse 1) pattern is depicted on the x-axis. BrdU (pulse 2) pattern is depicted in grey scale, see key. Representative images are shown of major BrdU (pulse 2) patterns for each EdU (pulse 1) pattern observed. EdU, red; BrdU, green; DNA, blue. Merged images show no co-staining indicating no incorporation in the same place. B) Histogram shows frequency of each S-phase pattern in TTF CIZ1+/+ (101, 126) and CIZ1-/- (1017, 1018) at passage 4. C) Box and whisker plot showing fluorescence intensity of EdU incorporation (30 min pulse) for each S-phase pattern for +/+ and -/- TTFs. n=12-66 cells per group.

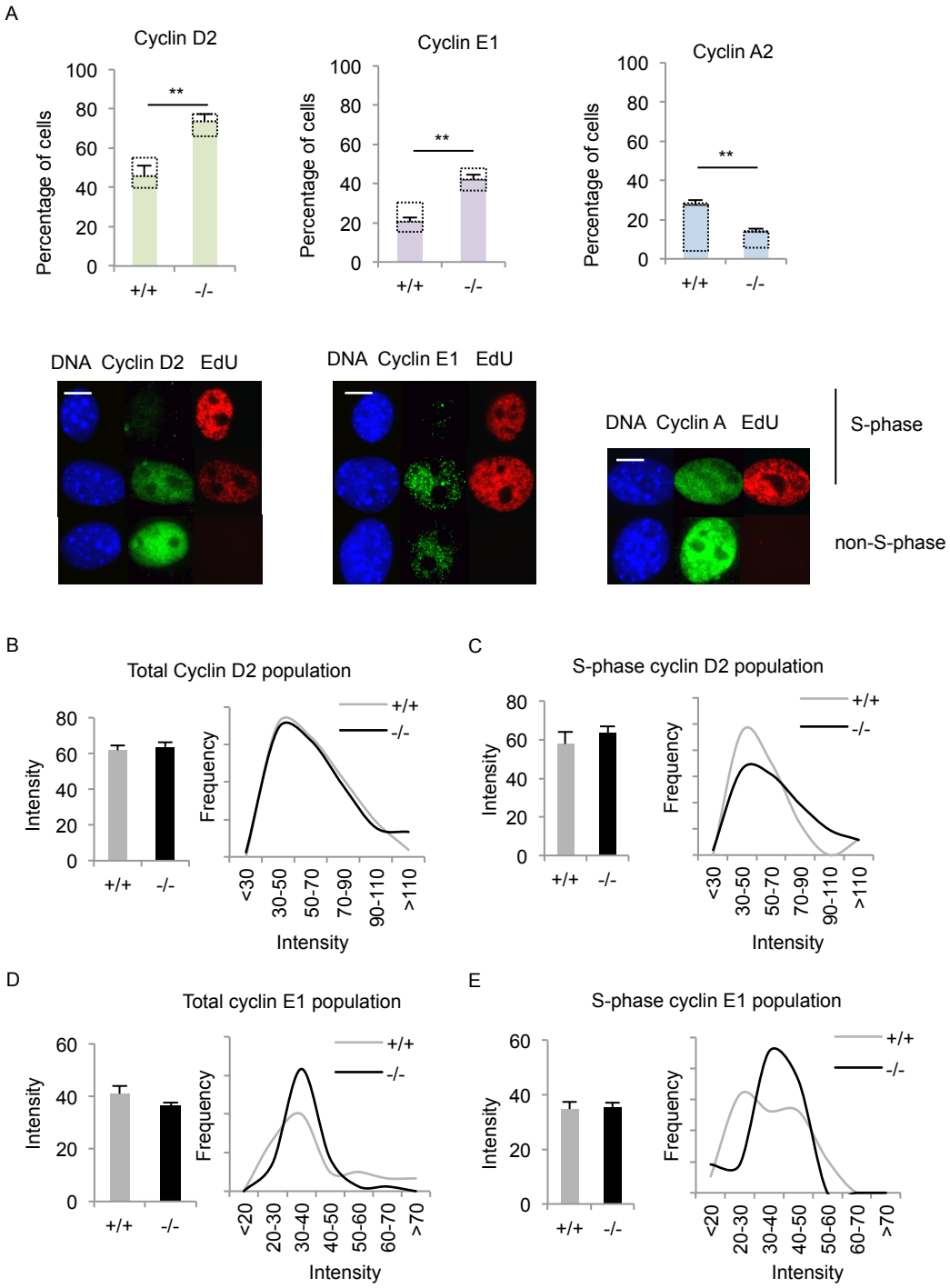

Figure 5.4: Cyclin D and E expression is prolonged and cyclin A expression reduced in the absence of CIZ1. A) Histograms with representative images (below) show percentage of CIZ1+/+ (97, 101, 126) and CIZ1-/- (1016, 1017, 1018) cells (passage 3-4) within a cycling population that express the indicated cyclins. Filled bar shows the indicated cyclin, open box shows the percentage that also incorporated EdU. EdU data for cyclin D2 and cyclin E1 are from the same experiment, cyclin A2 from a separate experiment. Cyclin data are average ± SEM. ** p< 0.005. B) Mean fluorescence intensity (left) and intensity distribution (right) for all TTFs within a cycling population stained for total cyclin D2, expressed in arbitrary units. C) As B except S-phase population is shown (determined by EdU incorporation after 30 min pulse). D) As B except for cyclin E1. E) As C except for cyclin E1.

observed either in positive cells from the total population or those in S-phase (fig 5.4 B-E). From these data I hypothesise that CIZ1 facilitates normal function of cyclin D and E. This may be in terms of recruitment to the right location at the right time, or interaction with the right proteins at the right time (discussed in section 6.4.2).

In contrast the proportion of cells expressing cyclin A2 (normally expressed during S-phase and G2) was decreased in the CIZ1-/- population, from 27.5 % to 13.9 % (fig 5.4 A), which is consistent with less cells in S-phase. Again unlike cyclins D2 and E1, the average level of cyclin A2 in the cells that express it, was abnormally high in CIZ1-/- cells (fig 5.5). This was true for each class of S-phase pattern (by EdU staining), with cyclin A levels higher in each class, with between 32 % and 73 % more (fig 5.5 A, B, E). This is supported by an increase in cyclin A detection by immunoblot of asynchronous whole cell lysates, despite the presence of a reduced fraction of cyclin A positive cells (fig 5.5 C). Even those cells with cyclin A but no EdU (very late G1 or early G2), express on average more cyclin A when CIZ1 is absent (fig 5.5 A, B, E), painting a very consistent picture of cell cycle progression in the presence of unusually high levels of cyclin A. Notably, when soluble cyclin A was removed the immobilised, detergent-resistant pool of cyclin A was much more similar in CIZ1+/+ and CIZ1-/- cells (fig 5.5 C-E). Therefore, it is the soluble cyclin A rather than the chromatin or NM bound cyclin A that is increased in CIZ1-/- cells.

These data suggest that, in the absence of CIZ1, cells require higher concentrations of cyclin A in order to initiate DNA replication throughout the S-phase program. Previous data indicated that CIZ1 is required for delivery of cyclin A to insoluble structures (Copeland et al., 2010), however, in CIZ1-/- cells the detergent-resistant cyclin A was not reduced. Therefore, this suggests that the total level of cyclin A is increased to facilitating binding of cyclin A to appropriate (and possibly inappropriate) sites in a stoichiometric manner in the absence of the recruiter CIZ1. It should be considered whether the detergent-resistant pool of cyclin A in CIZ1-/- cells is inactive, possibly due to $p21^{CIP1}$ inhibition. However, evidence suggesting that detergent-resistant $p21^{CIP1}$ mainly exists in G1 cells (section 5.4.6) argues against this explanation.

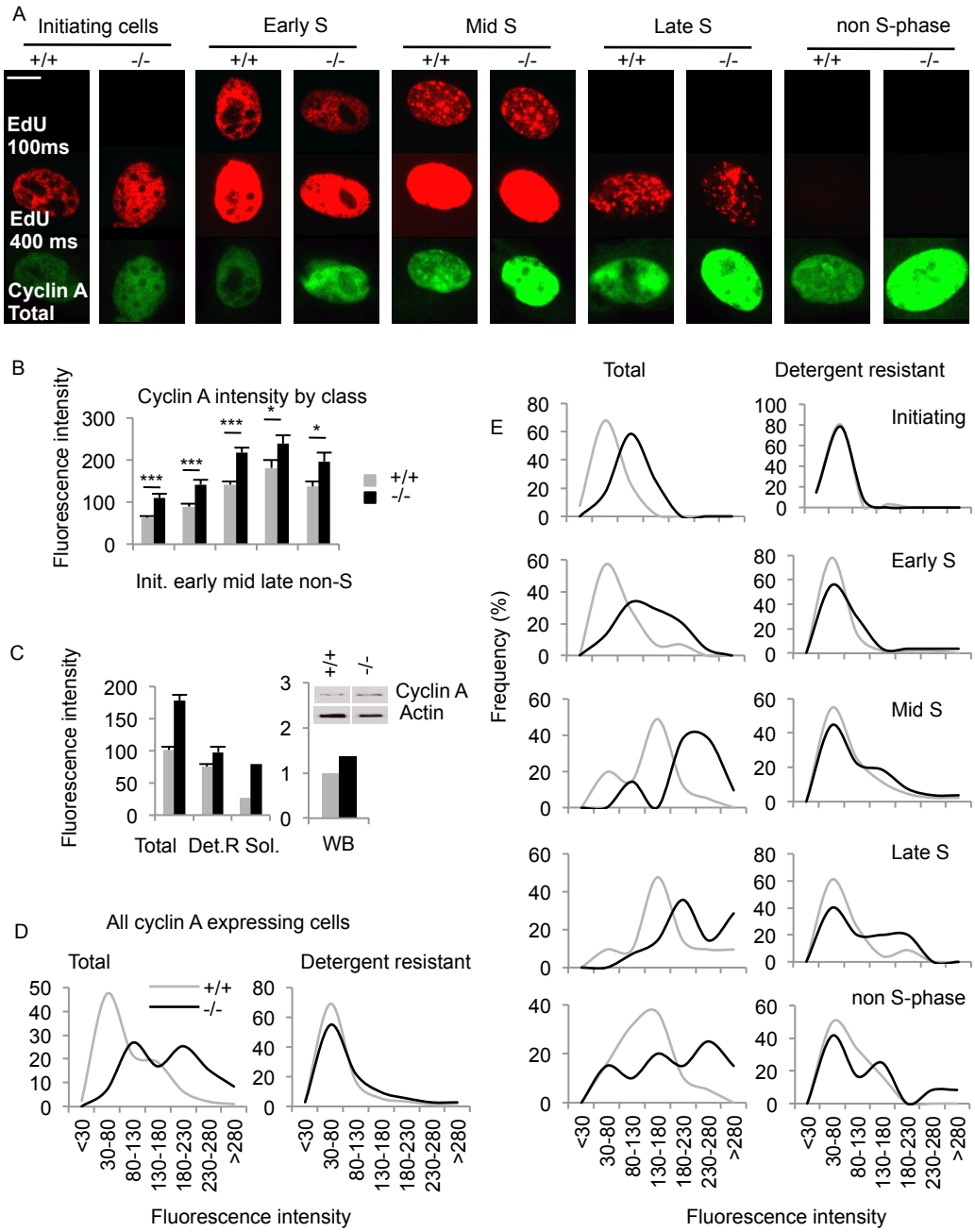

Figure 5.5: CIZ1-/- cells execute all stages of S-phase with elevated levels of cyclin A. A) Representative images for CIZ1+/+ and CIZ1-/- TTFs showing EdU (red) incorporated into newly synthesized DNA during a 30 minute pulse immediately prior to isolation. Cyclin A shown in green. EdU was imaged at low and high exposure time. A combination of intensity and pattern was used to classify cells as initiating, early, mid, and late S-phase. Scale bar is 10 microns. B) Average total cyclin A intensity was elevated at all stages of S-phase in CIZ1 -/- cells (black bars). n= 12-68 nuclei per class, data are average ± SEM, TTF used were +/+ 101, 126 and -/- 1017, 1018, at passage 4. C) Total cyclin A and detergent-resistant (Det.R) cyclin A in S-phase cells (all classes), with derived soluble pool (Sol.) intensity. Right: Total level of cyclin A determined by densitometry from Western blot. Actin was used as a loading control. D) Frequency distribution for cyclin A intensity, showing total cyclin A (left) and the detergent-resistant fraction (right) from the whole population. E) As D except categorised by S-phase stage, showing elevated total but not immobilised cyclin A in CIZ1-/- cells at all stages of S-phase.

5.4.4 Little difference in pre-RC proteins

In contrast to the differences observed for cyclins A, E and D, there were very few differences observed for three pre-RC components, ORC1, CDC6 or MCM2, either in terms of proportions of cells which expressed the component or the level of expression (fig 5.6). The only statistically significant change was a slight decrease in the number of cells that expressed ORC1 (fig 5.6 A). It is possible that this could relate to NM recruitment of the pre-RC since ORC1 recruits at least ORC-6 and CDC6 to the NM and it has been suggested that CIZ1 may be involved in this. No analysis of NM recruitment of pre-RC components was undertaken but it would be valuable to explore this avenue. As previously described, pre-RC components are loaded onto chromatin at telophase before $G1^{M}$ and lost from chromatin during S-phase (apart from ORC2-6 which are not investigated here), so should mark the majority of G1 and S-phase cells. The general observation of little change may reflect the fact that although the G1 proportion is increased and S-phase proportion is decreased, when counted together there is little change.

5.4.5 Model for the effect of absence of CIZ1 on cyclin expression

Integration of these analyses into a single model of cell cycle progression suggests the relationship proposed in figure 5.7. This takes into account 1) approximately 2.5-fold increased cycling time (fig 5.1 E), 2) reduced proportion in S-phase and increased proportion in G1-phase hence a longer G1 and G2 but the same S-phase length (fig 5.2-3), 3) the markedly increased number of cells expressing cyclins D and E (fig 5.4 A), 4) less cells expressing cyclin A (fig 5.4 A), and 5) an increased proportion of EdU positive cells that are also positive for cyclin D2 or E1 (fig 5.4 A). Immediately evident is that cyclin D2 expression extends through G1 into most of S-phase and beyond the demise of cyclin E, and also may begin earlier in G1. Thus these data appear to point to an unresolved functional interaction between CIZ1 and cyclin D. Similarly, cyclin E expression lasts longer also extending further into S-phase than in CIZ1+/+ cells. Thus absence of CIZ1 elongates the cell cycle and shifts the relationship between cyclins D, E and A, suggesting that it contributes to cell cycle homeostasis, having roles beyond its documented function in cyclin-A regulated initiation of DNA replication (Copeland et al., 2010).

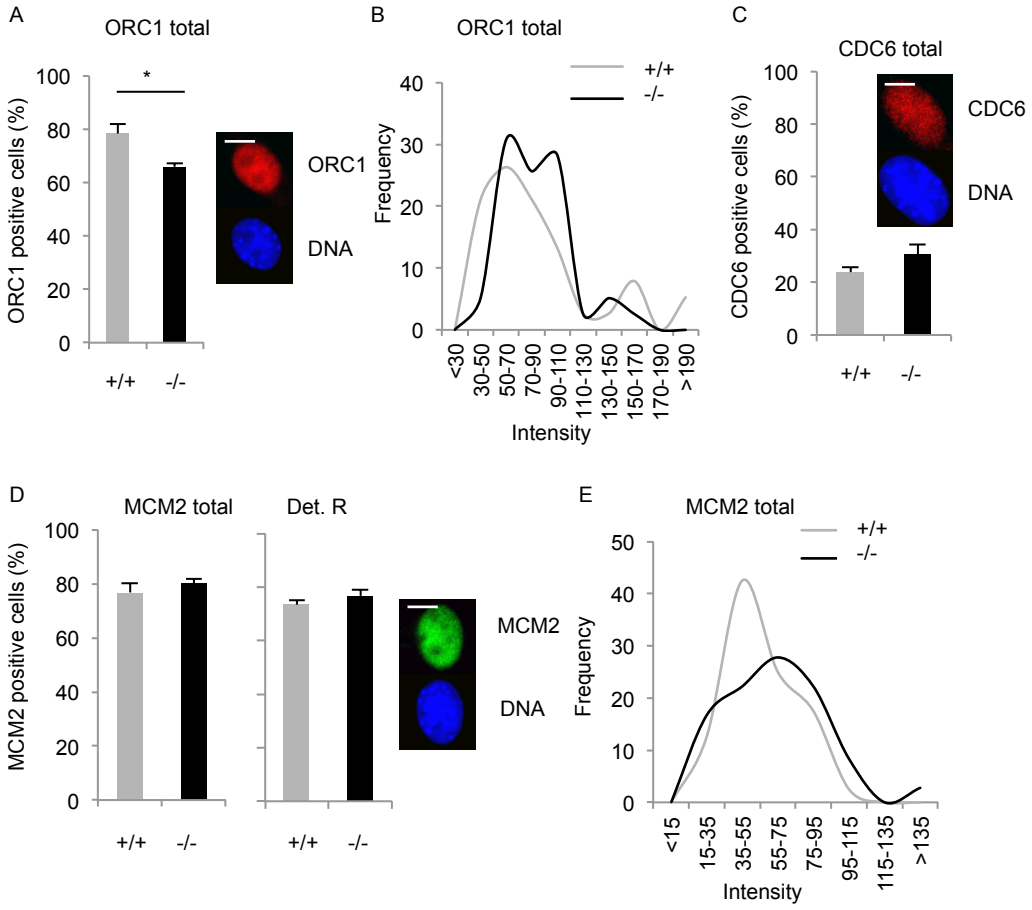

Figure 5.6: CIZ1-/- cells show little change in investigated pre-RC components. A) Histogram showing percentage of cycling TTFs (+/+ 101, -/- 1018) expressing ORC1 with representative image, DNA in blue, ORC1 in red, scale bar 10 μm. * = $p<0.05$. B) Frequency distribution showing fluorescence intensity of ORC1 in the positive population from A, expressed in arbitrary units. C) As A except for CDC6, shown in red. D) As A except for MCM2 total and detergent resistant protein. MCM2 shown in green. E) As B except for total MCM2.

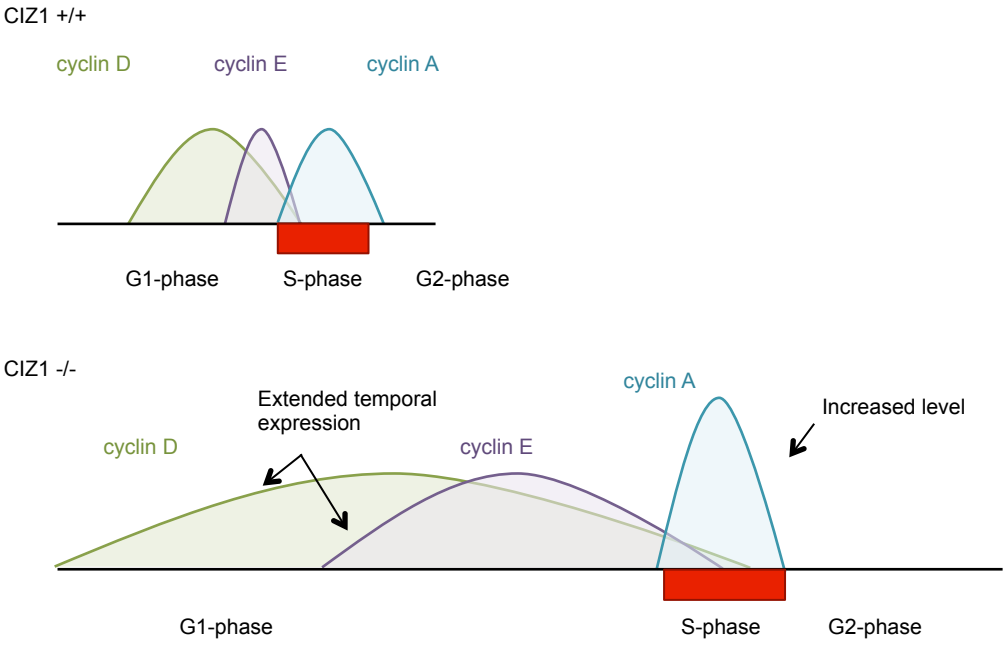

Figure 5.7: Schematic representation depicting dysregulation of cyclin D2, E1 and A2 expression in TTFs in the presence and absence of CIZ1. The proportion of CIZ1+/+ cells with cyclins D2, E1 or A2, and those that co-stain for EdU fits well with the established profile for cyclin expression and cell cycle progression in normal cells. However, the data for CIZ1-/- cells cannot be fit to the same model, even when 2.5-fold longer cycling time is taken into account. The model was constructed as follows; 1. Cell cycle length reflects the calculated 2.5 fold increase in doubling time. 2. G1 and G2 proportion determined from flow data. 3. S-phase proportion is determined by EdU incorporation. 4. Time of cyclin expression (width of peak) is determined from immunofluorescence staining data. 5. Overlap of cyclin expression with S-phase determined from immunofluorescence co-staining with EdU. 6. Height of cyclin A peak reflects increased expression level. This model assumes that all cells within the population are behaving similarly.

5.4.6 Altered expression of CDKis

A dramatic increase in the number of cells with detergent-resistant $p21^{CIP1}$ (CDKN1A) was also observed in CIZ1-/- cells (fig 5.8 A), though no differences were observed at the total level when looking at the proportion of positive cells or overall intensity (fig 5.8 A, B). Looking specifically at the S-phase fraction (EdU labelled) a small increase in the proportion with detergent-resistant $p21^{CIP1}$ was again noted (fig 5.8 C), with no change in total $p21^{CIP1}$ when looking at proportion of positive cells or intensity (fig 5.8 C, D). However, the increase was smaller than in the whole population suggesting that the majority of extra cells with detergent-resistant $p21^{CIP1}$ were likely to be in G1-phase. Indeed, almost the entire detergent-resistant $p21^{CIP1}$ positive population co-expressed cyclin D2, indicating that they are in G1- or early S-phase (fig 5.8 E). Thus $p21^{CIP1}$ appears to be immobilised on insoluble structures within the nucleus of G1-phase cells for a greater length of time in the absence of CIZ1.

A similar trend was observed for $p27^{KIP1}$ (CDKN1B), with the major difference between CIZ1-/- and +/+ cells being an increase in proportion of cells expressing $p27^{KIP1}$ both in the total population (fig 5.9 A) and the S-phase fraction (fig 5.9 B). None of the $p27^{KIP1}$ resisted extraction with detergent in either population (fig 5.9 A), and there was no increase in levels for the total population (fig 5.9 C). However a significant increase in levels was evident in mid/late S-phase cells (fig 5.9 D). Thus, for both CDKis there is a trend towards elevated, sustained or targeted expression in CIZ1-/- cells, which may be the result of extended cyclin expression or due to the proposed reduced cyclin function (section 6.4.2).

CIZ1 and $p21^{CIP1}$ interact directly via domains in the C-terminal end of CIZ1 and the N-terminal CDK-interaction domain of $p21^{CIP1}$ (Mitsui et al., 1999), and overexpression of CIZ1 results in cytoplasmic localisation of $p21^{CIP1}$ where it is degraded (Cayrol and Ducommun, 1998; Mitsui et al., 1999). Therefore, absence of CIZ1 might be expected to negate timely export of $p21^{CIP1}$. However, there was no evidence of nuclear accumulation of $p21^{CIP1}$. The increased detergent-resistant pool suggests a more subtle explanation, most likely impaired displacement from insoluble structures in G1-phase. Furthermore, failure to achieve turnover may contribute to inefficient entry to S-phase and the observed prolonged G1-phase.

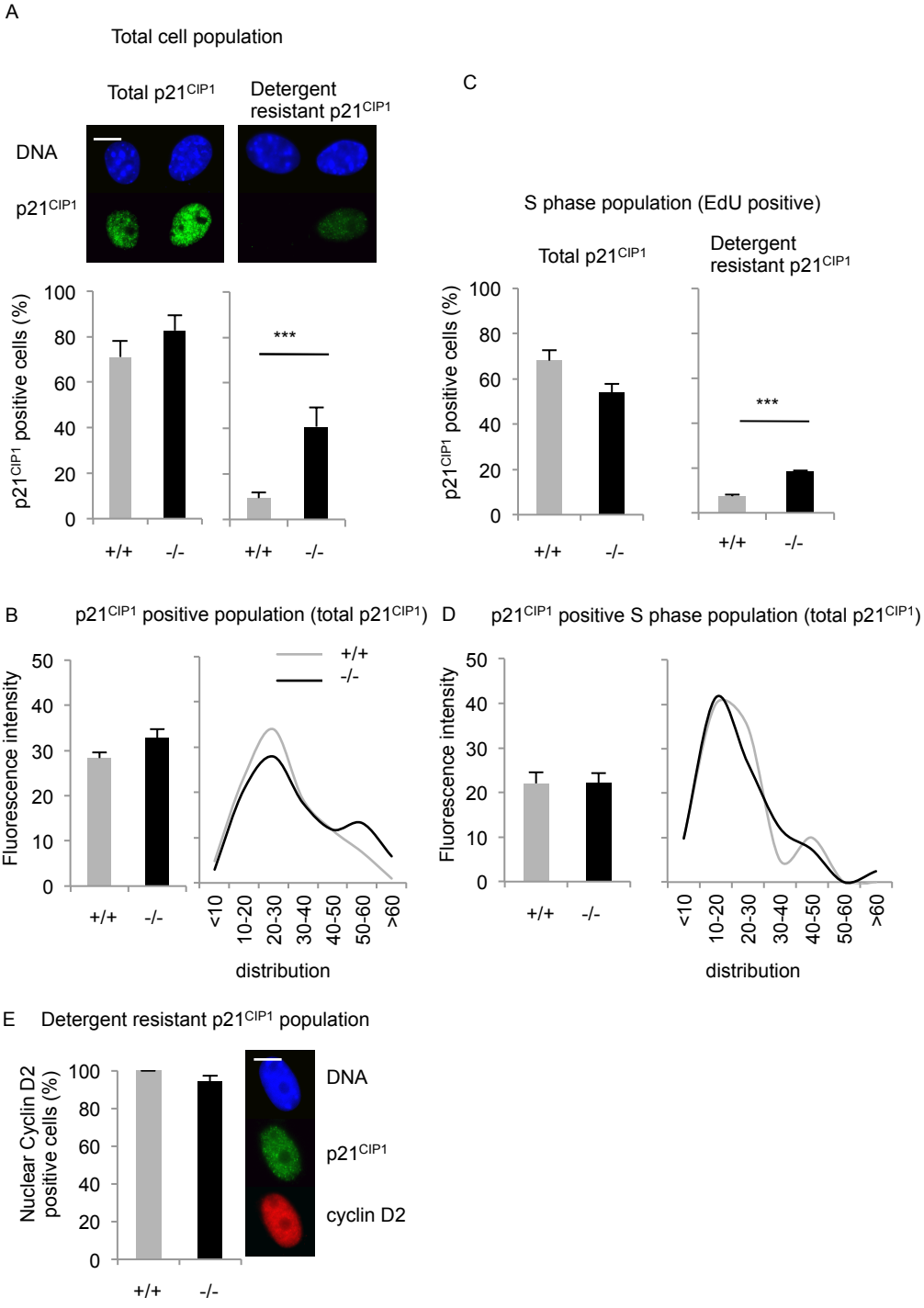

Figure 5.8: Absence of CIZ1 results in increased p21^{CIP1} immobilisation. A) Histograms and representative images show proportion of cells expressing total and detergent resistant p21^{CIP1} in passage 3-4 cycling populations of TTFs CIZ1+/+ (101, 126) and CIZ1-/- (1016, 1017, 1018). Data are average ± SEM.*** = p<0.0005. p21^{CIP1} shown in green, DNA shown in blue. Scale bar is 10 microns. B) As A, except S-phase population is shown (identified by EdU incorporation). C) Mean fluorescence intensity (left) and intensity distribution (right) for all TTFs within a cycling population stained for total p21^{CIP1}, expressed in arbitrary units. Cells as in A. D) As C except S-phase population is shown. E) Histogram shows percentage of cells with detergent resistant p21^{CIP1} which co-stain for cyclin D2. Representative images right: DNA shown in blue, p21^{CIP1} shown in green, cyclin D2 shown in red.

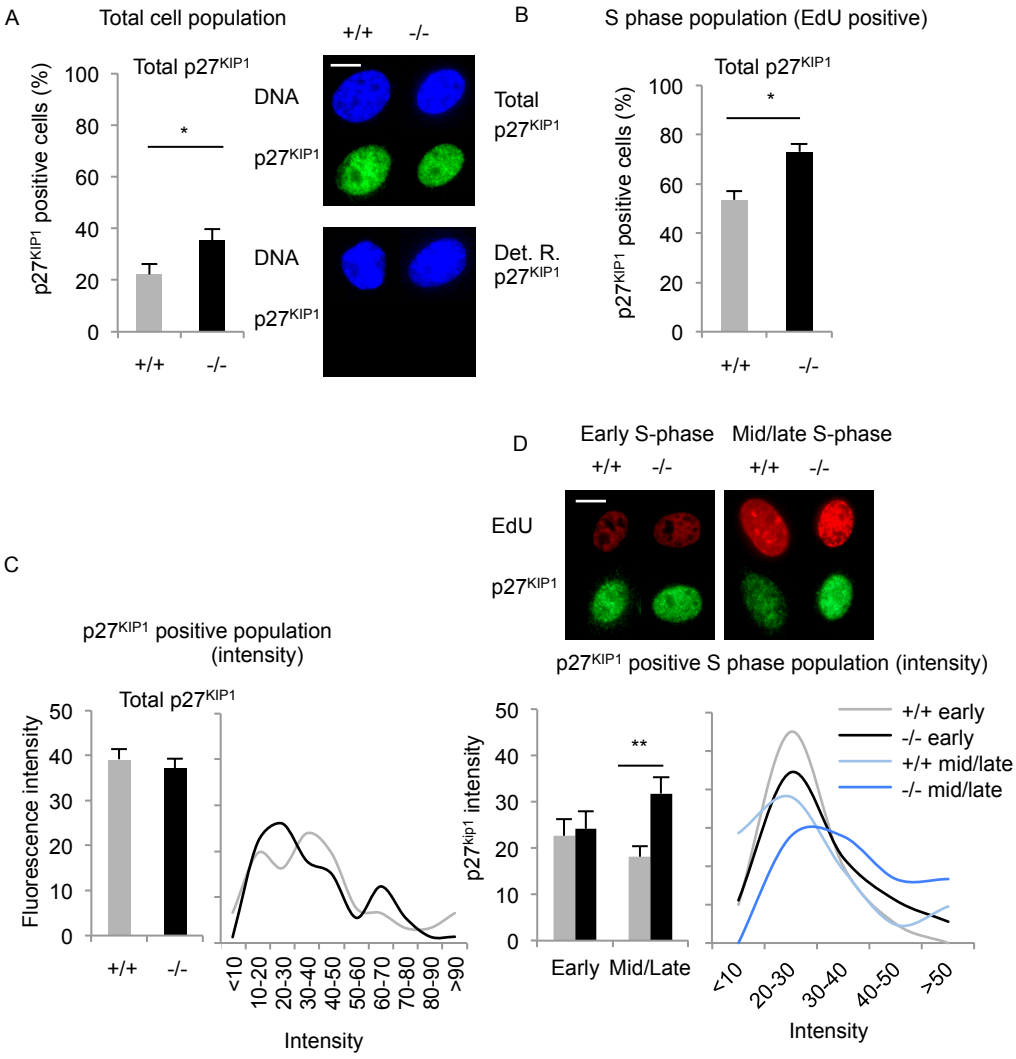

Figure 5.9: Absence of CIZ1 results in increased p27^{KIP1} expression. A) Histograms and representative images show proportion of cells expressing total p27^{KIP1} in passage 3-4 cycling populations of TTFs CIZ1+/+ (97, 101, 126) and CIZ1-/- (1016, 1017, 1018). Data are average ± SEM.*** = p<0.0005. p27^{KIP1} shown in green, DNA shown in blue. Scale bar is 10 microns. B) As A, except S-phase population is shown (identified by EdU incorporation). C) Histogram (left) and frequency distribution (right) show fluorescence intensity of p27^{KIP1} for total cell population (as A). Data are average ± SEM. D) As C except S-phase population is shown, separated by class (5-12 cells) ** = p<0.005. Representative images (above), EdU shown in red, p27^{KIP1} shown in green.

5.4.7 CIZ1-/- cells form foci at high density

Under conditions where CIZ1+/+ TTFs form a contact-inhibited monolayer, CIZ1-/- TTFs spontaneously form proliferating colonies at a rate of approximately one per 200 cells plated, evident as foci when stained with crystal violet (fig 5.10 A). Similar results were obtained with CIZ1-/- PEFs but with a slightly lower frequency (fig 5.10 B). These are in contrast to the reduced proliferation rate of CIZ1-/- lines but consistent with the proliferative disorders observed in the mice. Colonies arise from within the CIZ1-/- monolayer in the absence of external oncogenic or chemical stimulus, suggesting that absence of CIZ1 is sufficient to confer resistance to growth arrest signals. Foci cells are actively proliferating demonstrated by incorporation of EdU (fig 5.10 C) and expression of the pre-replication complex protein MCM2 (fig 5.10 D). They also appear to be somewhat invasive, growing into and over the surrounding pre-focus monolayer (fig 5.10 E). Failure to respond to restraining signals is a key characteristic of transformed cells, with focus formation a well-established indicator of cellular transformation. This suggests that CIZ1-/- cells have acquired at least one key step towards transformation, and therefore that CIZ1 normally possesses tumour suppressor activity.

Like wild-type cells, CIZ1-/- non- or pre-foci forming monolayer TTFs showed no evidence of DNA synthesis even after a long pulse with EdU (fig 5.10 C), and MCM2 was not detectable (fig 5.10 D), indicating that the population is no longer cycling and appear therefore to have responded appropriately to restraining signals. Thus the strikingly different behaviour of foci precursor cells may be the result of an acquired capability that is a secondary consequence of lack of CIZ1, rather than one that is directly conferred.

5.4.8 Activation of the DNA damage response

CIZ1 has previously been linked with the cellular response to DNA damage (Matsuoka et al., 2007; Roper, 2011), raising the possibility of a mutator phenotype leading to randomly acquired alterations. Analysis of cells of the pre-foci monolayer (fig 5.11) revealed no evidence for p53 activation and a negative outcome with TUNEL (fig 5.11 D). However, there was a striking change in localisation of γH2AX, towards a pattern of large foci that are indicative of activation of the DNA damage

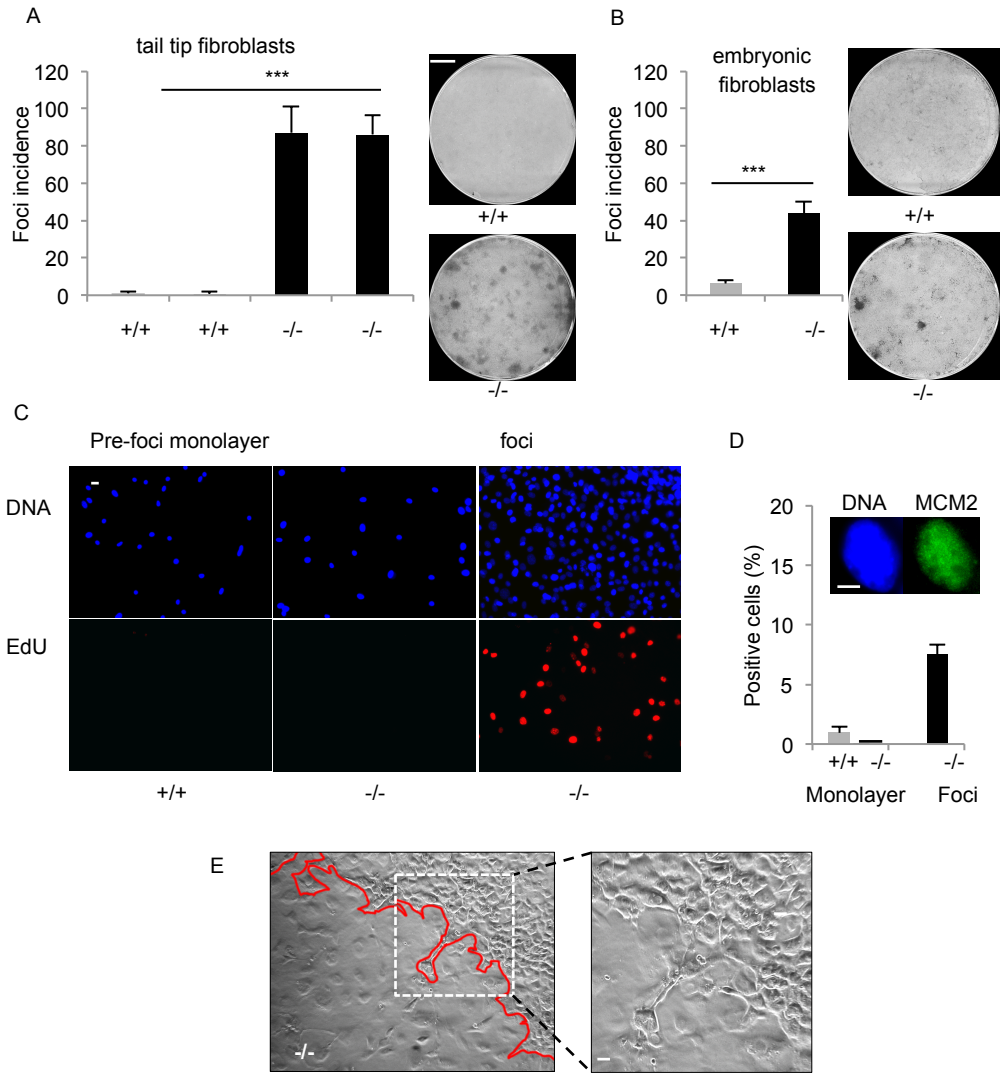

Figure 5.10: CIZ1-/- cells fail to form contact inhibited monolayers. A) Foci incidence per 4.5x10(5) cells for TTFs CIZ1+/+ (101 and 126) and CIZ1-/- (1017 and 1018) cells, plated at passage 4, and visualised by staining with crystal violet after 21 days. Data are average from triplicate ± SD. Images show representative plates, scale bar is 1cm. Similar results were obtained with all TTF cells. B) As in A, but for PEFs (passage 3-4). C) Representative images show replicative quiescence in monolayers cells in both CIZ1 +/+ and CIZ1 -/- cells after a 16 hour pulse with EdU. Right: 15% of -/- cells within focal outgrowths were in S-phase. TTFs used were +/+ (126, 133), -/- (1017, 1018). D) Histogram and representative image show expression of MCM2 in a proportion of foci cells. Cells as in C. E) Bright field image of the edge of a growing colony of -/- TTF cells showing invasion of the surrounding monolayer. Scale bar is 20 μm.

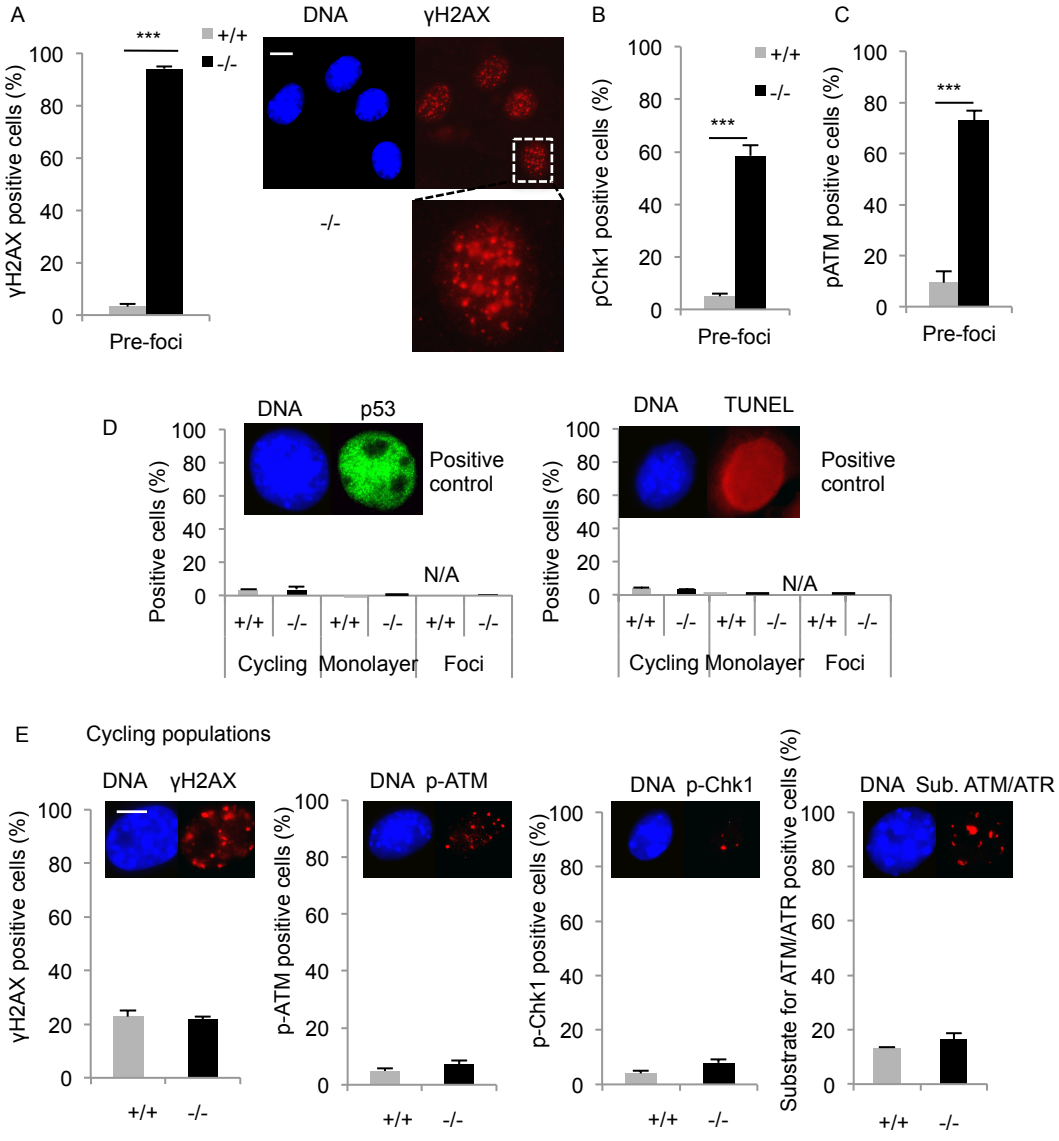

Figure 5.11: Contact inhibited but not cycling CIZ1-/- cells show activated DDR. A) Histogram and representative images show TTFs with γH2AX in large subnuclear foci. TTFs used were CIZ1+/+ (126, 133), CIZ1-/- (1017, 1018). B) Histogram shows proportion of TTFs (+/+ 101, -/- 1017) expressing detergent resistant pChk1. C) Histogram shows proportion of TTFs (as in B) expressing detergent resistant pATM. For all DDR markers, cells with ≥ 3 large foci were scored positive. Data are average ± SEM. *** = p<0.0005. D) Histograms shows percentage of cycling, monolayer and foci TTFs expressing p53 (left) or positive for TUNEL (right) Representative images fro positive controls shown. E) Histograms show percentage of cycling TTF populations expressing γH2AX, pATM, pChk1 and phospho-(Serine/ threonine) ATM/ATR substrate motif as indicated. Representative images are shown, scale bar is 10 microns. Cells with ≥ 3 large foci were scored positive.

response (fig 5.11 A). This was evident in the whole population of contact inhibited CIZ1-/- monolayer cells and also in the foci themselves (fig 5.11 A). Other markers of an activated DNA damage response, including phosphorylated-Chk1 foci (indicative of SSBs and replication stress, fig 5.11 B) and phosphorylated-ATM foci (indicative of DSBs, fig 5.11 C), were also evident in the monolayer cells of CIZ1-/- TTFs but absent in CIZ1+/+ cells. Thus a population-wide activated state exists in the CIZ1-/- genotype, out of which clonal populations of unrestrained cells emerge.

Significantly, none of the markers of an activated DNA damage response were elevated in CIZ1-/- cells when in the cycling state, despite the dysregulated cyclin expression described previously (fig 5.1 G, 5.11 E). However, it remains possible that instability occurs instead at the epigenetic level or chromatin organisation level, which may not induce activation of the markers studied. The clear observations lead to the hypothesis that the activated state is triggered by aberrant interaction between contact-induced signals of cell cycle restraint and cell cycle machinery in the absence of CIZ1.

In summary, the data presented here show that expression of cyclins is extended or elevated in the absence of CIZ1 and that the cell cycle progresses more slowly suggesting reduced function. This may also affect CDKis, the expression of which was elevated, extended or showed increased subnuclear immobilisation. However, when CIZ1-/- cells receive contact-induced growth restraining signals they fail to respond appropriately, leading to chronic, widespread activation of the DNA damage response. This suggests that this response may play a driving role in the tumorigenesis observed in the animal.

5.5 Discussion

5.5.1 CIZ1 – tumour suppressor and promoter

Data presented here show that CIZ1 possesses tumour suppressor properties. During this project, a study of another CIZ1 knock-out mouse was published also showing tumour suppressor properties, where absence of CIZ1 causes increased foci formation in response to oncogenic challenge (Nishibe et al., 2013). The work

presented here goes further by showing that absence of CIZ1 causes increased transformation even without challenge, and identifying a mechanism. A tumour suppressor role for CIZ1 was somewhat unexpected as previous work from the Coverley lab and others suggested a tumour promoting role for CIZ1 (den Hollander et al., 2006; Higgins et al., 2012; Rahman et al., 2007; Rahman et al., 2010; Warder and Keherly, 2003). In most of these papers altered variant expression of CIZ1 was linked with cancer, including altered level, location and splicing (section 1.1.12) (Higgins et al., 2012; Rahman et al., 2007; Rahman et al., 2010; Warder and Keherly, 2003). It is therefore possible that full-length CIZ1 (and possibly other isoforms) possess suppressor activity, while cancer-associated variants possess tumour promoting activity. There are at least 25 suggested transcript variants based on minimal assemblies of expressed sequence tags (ESTs) (Aceview, 2007 Update, Thierry-Mieg and Thierry Mieg, 2006). Variants may be expressed normally at a particular stage in development or in response to a specific stimulus, but appear to be inappropriately expressed in cancer. The overall effect of CIZ1 on a cell is likely to be the result of the balance between tumour suppressing and promoting forms. It is possible that too much 'normal' CIZ1 could also function in an oncogenic manner due to disruption of cyclin/CDKi homeostasis. This suggestion of different forms of a protein possessing tumour suppressor or promoter properties has been observed before, for the tumour suppressors FANCL (Zambrowicz et al., 2003), p53, Ras and possibly RB (Panneerselvam et al., 2012) whose variant forms are oncogenic. It would be beneficial to identify which splice variants of CIZ1 fall into each category, especially the tumour suppressing forms.

5.5.2 Tumorigenesis caused by absence of CIZ1

With such a marked formation of foci by all CIZ1-/- cell strains, it seems odd that animals only start to form tumours at a late age. However, contact inhibition is just one of the cell's regulatory mechanisms that must be bypassed before a tumour can form (reviewed in Hanahan and Weinberg, 2011). In addition, preliminary evidence from the culture of foci outgrowths from CIZ1-/- 1016 suggests foci cells are not immortal but instead undergo death after several more passages. It is therefore possible that foci may form and die in the animal unless other mutations are acquired, or in certain cell types such as B cells, which undergo rapid proliferation and may be particularly sensitive.

It is possible that families may exist with mutations in the CIZ1 gene or even an absence of the protein since there is little effect on development. Patients with mutations in the *CIZ1* gene have already been reported for cervical dystonia (Xiao et al., 2012). From findings discussed here in CIZ1-/- mice, these families would be expected to also have an increased risk of cancer, most likely leukaemias and lymphomas. Although far distant, it might be possible that further understanding of the effects of CIZ1 could guide treatment. It has already been shown that treatment using siRNA against the 14B splice variant of CIZ1 in mice with xenograph tumours containing the 14B variant reduces tumour size (Higgins et al., 2012).

5.5.3 CIZ1 and quiescence

Because of failure to enter a normal quiescence, the role of CIZ1 during release from quiescence could not be investigated making detailed analysis of $G1^{Q}$ impossible. Nevertheless, analysis of the mitotic cell cycle has suggested some new roles for CIZ1 during $G1^{M}$. My work has also thrown up some interesting new information about the role of CIZ1 during entry to quiescence. The foci that form when cells would normally become quiescent indicate a reduced ability to establish or maintain quiescence, possibly reflecting increased sensitivity to proliferation cues during this transition.

It is noteworthy that despite the fact that CIZ1-/- cells form foci, the animals do not exhibit general hyperplasia. This contrasts with the $p27^{KIP1}$-/- mouse in which hyperplasia of multiple tissues is observed due to the important role of $p27^{KIP1}$ in enabling quiescence (Fero et al., 1996; Kiyokawa et al., 1996; Nakayama et al., 1996). This therefore suggests that CIZ1 is not essential for this transition and its role here can be partially compensated by other factors, or that it is specific to certain cell types, including B-cells.

Failure to establish quiescence in the absence of CIZ1 could be a direct effect, due to the absence of the proposed cyclin/CDKi exchange function hypothesised for the mitotic cell cycle (discussed in more detail in section 6.4.2). This might prevent the timely degradation of cell cycle regulators leading to a conflict between promoting and inhibitory factors. It is possible that the transition between proliferation and quiescence (and back) may be particularly susceptible to altered cell cycle regulator

balance, as it involves an exit and 're-start' rather than ongoing cycling. It is interesting that in situations when CIZ1 is absent (this study), and when it is ectopically expressed in newly confluent cells (Coverley et al., 2005), there is an increased propensity for inappropriate S-phase entry. Tight control over the level of CIZ1, and as a result cyclins and CDKis, may be important for correct response to contact inhibition signals, so that too much or too little CIZ1 deregulates this transition. This is consistent with previous reports that the effect of CIZ1 on promotion of DNA replication is highly concentration dependent (Coverley et al., 2005). However, a direct effect such as this might be expected to result in inappropriate proliferation in many cell types, rather than just the lymphoid lineages as described above.

The second possibility is that CIZ1-/- cells have increased susceptibility to transformation when experiencing growth inhibitory signals as a consequence of a more indirect process. The DDR is activated in almost the entirety of the pre-foci monolayer (in addition to foci), which may suggest that these cells have experienced some form of stress or damage like those that are postulated to take place in early tumours (Bartkova et al., 2005), possibly triggered by inability to respond to growth inhibition signals. This further suggests the possibility that these cells are arrested at a cell cycle checkpoint, either instead of or in combination with quiescence proper. Transformation and resultant foci may occur either through mutation of one or more components of the DDR, or other factors involved in cell cycle arrest.

Features from both these possibilities may in fact be true, with unbalanced cell cycle regulators being the activating event for the DDR. The fact that foci form rather than the whole culture continuing to proliferate, suggests the cause of the breakout colonies to be stochastic, such as random mutation.

Perhaps supporting the idea that cells experiencing growth inhibitory signals are sensitive to transformation, the overproliferating B-cells observed in CIZ1-/- animals closely resemble centrocytes (J-A. Roulson and J. Ainscough, personal communication). During antigen stimulated B-cell activation, mature B-cells differentiate into centroblasts with high proliferative potential, then centrocytes with low proliferative potential, and finally antibody producing plasma cells or

memory cells (reviewed in Allen et al., 2007). Therefore, the lymphoma appears in cells that should be exiting the cell cycle.

5.5.4 Model for DDR activation

Data presented here show that CIZ1 protects against transformation. Some potential mechanisms are shown in schematic form in figure 5.12. My preferred model is that altered expression of cyclins and CDKis in cycling cells in the absence of CIZ1 leads to stress and activation of the DDR when cells receive signals to exit the cell cycle (fig 5.12, 1). Activation of the DDR has been shown to be an early event during tumorigenesis and to act as an anti-cancer barrier, but also a selection pressure in favour of cells with mutations in this pathway (Bartkova et al., 2005). Loss of CIZ1 tumour suppressor function, either through mutation to oncogenic isoform (Higgins et al., 2012; Rahman et al., 2007) or absence (this study), may be one such activator of this oncogenic pathway. Indeed, Bartkova et al. suggested two characteristics of candidate inducers to be overstimulation of growth factor pathways and over-expression of cyclin E, both of which are observed in cells from CIZ1-/- mice.

Alternatively, Nishibe et al. (2013) suggested that CIZ1 might directly influence fidelity of replication (fig 5.12, 2). However, there is no evidence to suggest involvement of CIZ1 directly in DNA synthesis, and the lack of DDR activation in cycling CIZ1-/- cells argues against this explanation.

Other potential mechanisms relate to the spatial constraint (fig 5.12, 3) of replication as CIZ1 has previously been suggested to have a role in this process (Ainscough et al., 2007), and in doing so may protect against illegitimate replication events that lead to genome instability. Spatial constraint of replication could be effected in at least five ways: (i) global patterning of replication foci, (ii) active formation of replication foci, (iii) defining local regions collected together in a factory, (iv) defining precise local regions of the genome to be replicated at one time (ie origin usage), and (v) recruitment of DNA replication factories to the nuclear matrix (reviewed in Wilson and Coverley, 2013). Data presented here show visually normal replication foci and patterning, thus arguing against options (i) and (ii). However, options (iii-v) remain open possibilities. This is consistent with the previous suggestion that pre-RC assembly is spatially restricted by attachment to

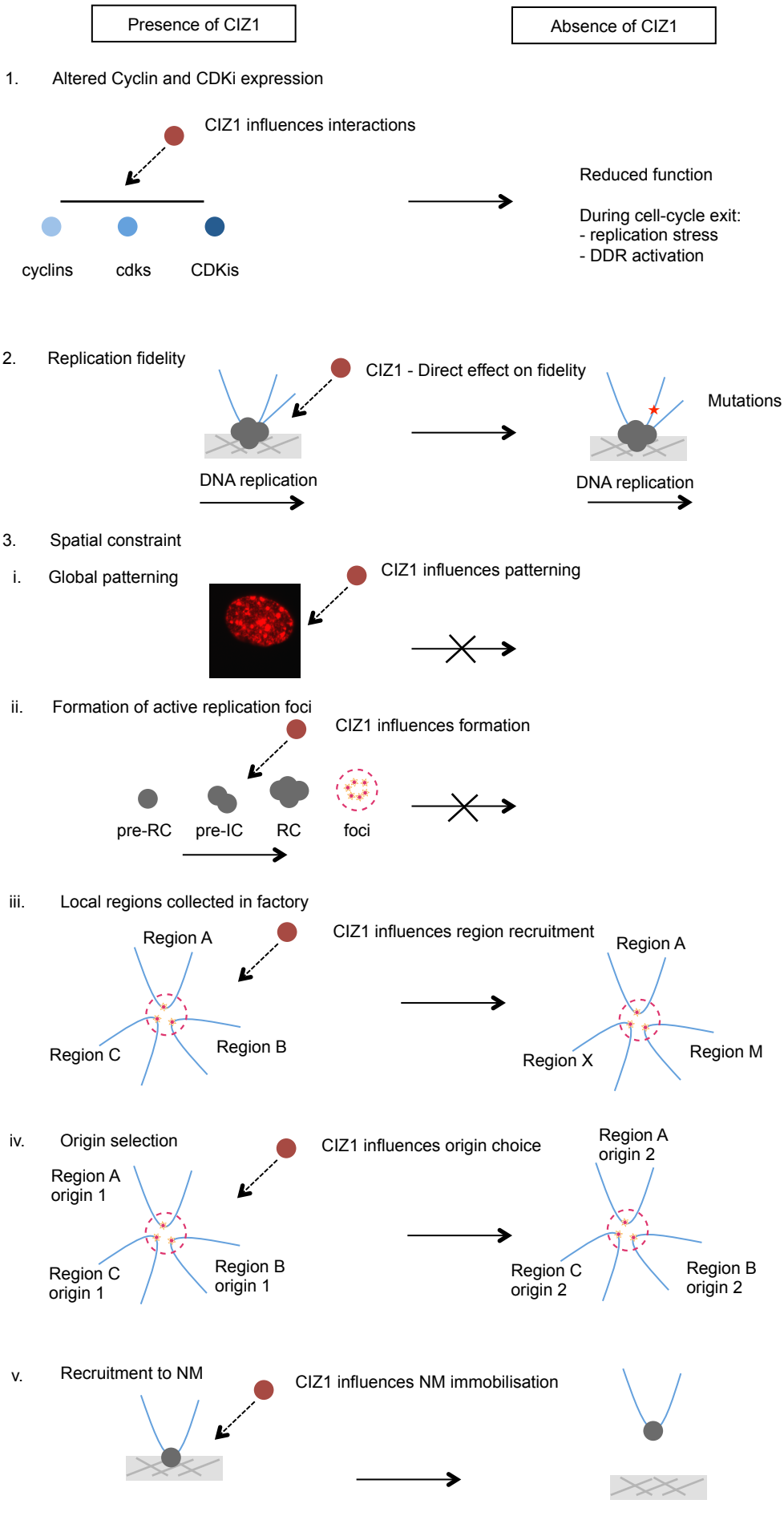
Presence of CIZ1
Absence of CIZ1
1. Altered Cyclin and CDKi expression
CIZ1 influences interactions
cyclins
cdks
CDKis
Reduced function
During cell-cycle exit:
- replication stress
- DDR activation
2. Replication fidelity
CIZ1 - Direct effect on fidelity
DNA replication
Mutations
DNA replication
3. Spatial constraint
i. Global patterning
CIZ1 influences patterning
ii. Formation of active replication foci
CIZ1 influences formation
pre-RC
pre-IC
RC
foci
iii. Local regions collected in factory
Region A
Region B
Region C
CIZ1 influences region recruitment
Region A
Region X
Region M
iv. Origin selection
Region A
origin 1
Region C
origin 1
Region B
origin 1
CIZ1 influences origin choice
Region A
origin 2
Region C
origin 2
Region B
origin 2
v. Recruitment to NM
CIZ1 influences NM immobilisation

the NM as template usage is defined, and that absence of appropriate spatial restriction in cancer cells may aid plasticity (Munkley et al., 2011).

It should be noted that activation of γH2AX, Chk1 and ATM could be in response to replicative stress and SSBs, DSBs, or some other trigger, so the underlying cause for their activation remains undetermined at present. Further investigation into the mechanism is likely to reveal added complexities and will elucidate the exact mechanism of how absence of CIZ1 causes transformation. Hypotheses are discussed in chapter 6.

Figure 5.12 (Previous page): Schematic showing possible mechanisms for why absence of CIZ1 causes activation of DDR. DNA shown in blue, NM as grey mesh, CIZ1 shown in red.

6 Discussion

6 Discussion

My PhD has focused on the process of entry to and exit from quiescence, with the aim of understanding the steps required for preparation for DNA replication during G1Q. This was approached with particular attention to the role of the NM during this period and the behaviour of cyclin E and CIZ1. The processes that take place during G1 are crucial for accurate replication of DNA, and the changes in cell cycle control found in cancer cells reveal how important this process is. Nevertheless, much of what takes place in G1 in terms of nuclear reorganisation, remains undescribed and the aim here was to increase our understanding of some of these events. Data presented here show that chromatin loops change as cells re-enter the cell cycle and that chromatin loops are less stable in cancer cells. Data also show that CIZ1 (which is involved in loop reorganisation) is involved with temporal expression of cyclins, with implication for activation of the DDR and tumorigenesis.

6.1 How and why is higher order nuclear structure different in quiescent cells?

6.1.1 Increased NM attachment of DNA in quiescent cells

Data presented here show that average chromatin loop size decreases in quiescence, and as cells are induced to re-enter the cell cycle, they pass through a newly identified step where chromatin loop size increases. With smaller and therefore likely more chromatin loop base attachments in quiescent cells, it is tempting to think of quiescent cells as deeply packaged or 'locked down' for a long period of stability. DNA in a quiescent cell does not have to undergo DNA replication and undergoes less transcription (Mauck and Green, 1973). During this time the cell must maintain its cell type and prevent senescence, apoptosis or further differentiation, while continuing to do the job for which it may be specialised. It has previously been suggested that reduced attachment to the NM may allow for plasticity in cancer and stem cells (Munkley et al., 2011). Therefore, since plasticity is an undesirable characteristic in quiescent cells, the stability of cell type may be maintained by increased attachment to the NM.

Data from other studies are supportive of these ideas. In one study, rat quiescent hepatocytes were compared to those stimulated to enter S-phase following partial hepatectomy. DNA was shown to be more protected from the action of DNase I, which was inferred to be due to increased association with the NM, and also the absence of single stranded DNA in the absence of S-phase (Maya-Mendoza et al., 2003).

Additional analysis compared cells derived from different age animals. These observations may be a feature of increased age or of cells being driven deeper into quiescence over time. It was reported that as hepatocytes age, there is increased NM attachment of DNA, larger nuclear and NM diameter and volume, greater expression of lamins, and smaller, more stable MFHR halos (Alva-Medina et al., 2011; Maya-Mendoza et al., 2005). An increase in nuclear diameter and volume with age has also been recorded for fibroblasts showing that increased ploidy is not the explanation (Pienta et al., 1992). This agrees with the idea of 'locked down' DNA, in terms of increased attachment to the NM and an increase also in the components of the NM itself. Interestingly, neurones did not show increased NM attachment with age, however, stability of DNA and halo size was comparable to 'old' hepatocytes even by post natal day 0 (Alva-Medina et al., 2010; Alva-Medina et al., 2011). Neurones have dramatically less proliferative potential than hepatocytes and therefore, even young neurones may have very 'locked down' nuclear structure. Therefore, this suggests 'locked down' characteristics are likely to represent the level of quiescence of a cell rather than age itself.

6.1.2 No general compaction of DNA in quiescent cells

From the available data it therefore appears that in quiescent cells, DNA is attached to the NM at more points leading to smaller loops that are stable. However, this cannot be extrapolated to all levels of higher order nuclear structure, such as chromosome territories, nucleosome density or the impact of histone modifications on compaction of DNA. In fact, the territories of chromosomes 13 and 15 were reported to be less condensed in G0 cells (Zink et al., 1999). Further studies are needed to establish the characteristics of other levels of nuclear higher order structure in quiescent cells. Nevertheless, together, the data suggest that although attachment to the NM is enhanced, the loops are not in a tightly packed

conformation and remain accessible. This fits with a requirement for on-going transcription and suggests that attachment to the NM may be more important for stabilising cell type and status, possibly as a protective feature.

6.2 How and why does nuclear higher order structure change during preparation for DNA replication?

As discussed in chapter 1, we have an increasing understanding of higher order structure of DNA within the nucleus, including chromatin loop attachments. These appear to include structural attachments as well as more transient attachments that are specific to cell type and cell cycle stage, including attachments in close proximity to origins of replication. There are now many pieces of evidence that DNA replication occurs at the NM, including attachment of pre-RC proteins and proteins involved in later stages of preparation for DNA replication including DNA polymerase itself, incorporation of nucleotide analogues at the base of loops and in extracted preparations, and evidence of termination structures at the NM (reviewed in Wilson and Coverley, 2013).

6.2.1 Models of replication

Template DNA and DNA replication enzymes must move relative to each other during DNA synthesis. The evidence concerning NM attachment therefore suggests that the DNA replication machinery is static and the DNA moves through these fixed sites (Pardoll et al., 1980). Nevertheless, it is still common to see depictions that show the DNA replication machinery as an entity that moves along the DNA strand. Depending on which direction researchers have approached this problem, models tend to appear in one of two forms, either a flower shaped factory of loops with little consideration of the NM (Frouin et al., 2003), or attachment to a NM at loop bases without representation of how these may come together into a factory (Cook, 1999; Ottaviani et al., 2008b) (fig 6.1). Below, factories are described in more detail followed by how chromatin loops and factories can be represented together.

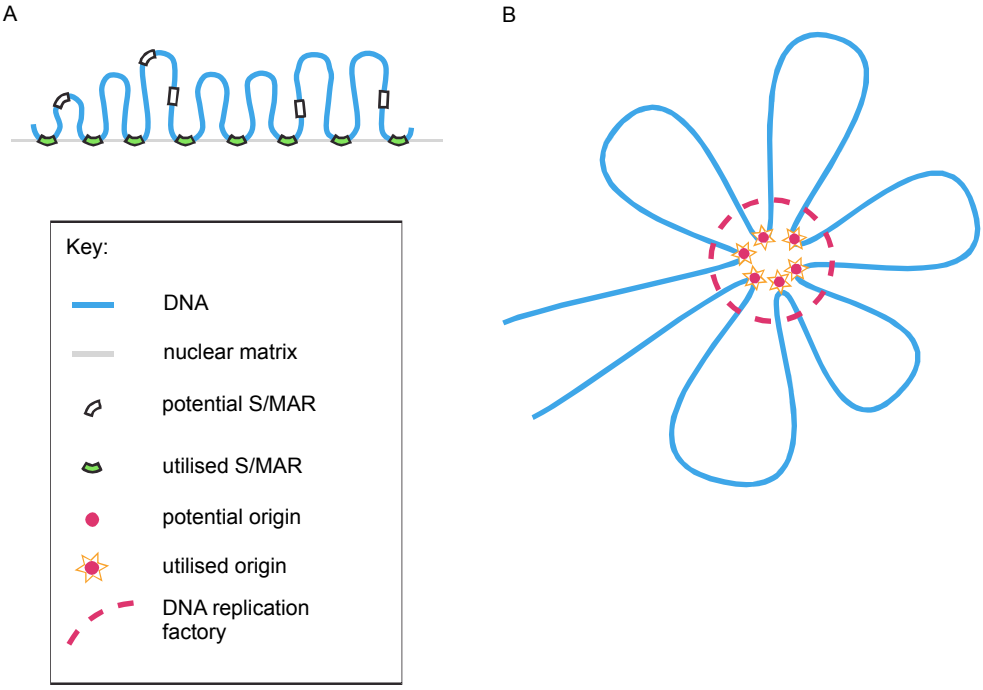

Figure 6.1: Common representations of chromatin loops. A) Refined model illustrating variable chromatin loop sizes, and complex S/MAR usage, including function-related alternative potential S/MARs. B) Alternative representation of chromatin loops showing replication origin clustering within a DNA replication factory, with no representation of NM attachments. Our preferred model combines NM attachment and factory formation.

Previously published in (Wilson and Coverley, 2013). Designed by R. Wilson, drawn by P. Roberts.

6.2.2 Replication factories

Replication foci or 'factories' can be visualised by immuno-detection of replication enzymes, or by following incorporation of nucleotide analogues into nascent DNA. They are macromolecular assemblies populated by the enzymes that replicate DNA, forming several hundred efficient factories representing clusters of origins, which are activated at the same time. The number of origins is thought to be highly heterogeneous but to be an average of 5-6 per factory (reviewed in Berezney et al. 2000; Frouin et al. 2003, see also references therein). There is some reason to think that clustering of origins may offer an energy saving, as activation in near space may enable more efficient processing due to locally higher concentrations of factors (reviewed in Frouin et al., 2003) (fig 6.1 B). However, not all origins are activated at the same time in S-phase. Some areas of the genome are replicated early in S-phase while others are replicated later. Replication foci from all temporal stages of S-phase have been shown to be NM associated (Nakayasu and Berezney, 1989) complete with nascent DNA which gradually moves out from each focus (Hozak et al., 1993; Hozak et al., 1994), consistent with the concept of emanating loops. Cohesin is thought to help hold loops together because it is present at origins, interacts with the pre-RC and its absence slows S-phase (Guillou et al., 2010). These data indicate that the replication machinery is located at NM attachment points at the base of chromatin loops.

6.2.3 Recruitment of origins in $G1^{M}$

It has been hypothesised that, recruitment of origins to the NM is part of the process of initiation (Cook, 1999; Ottaviani et al., 2008b; Rivera-Mulia et al., 2011; Wilson and Coverley, 2013) (fig 6.2), and that recruitment probably occurs after pre-RC formation, as much of this is laid down at telophase in the mitotic cell cycle, yet origins appear to be recruited later in G1-phase (Djeliova et al., 2001b). When incorporating origin recruitment into models, several show an origin located distally on a loop, being recruited to the NM in late G1/S-phase. As DNA is spooled through replication factories, newly synthesised DNA is extruded as two new loops, with their origins returning to their original location at the distal end of the daughter loops (Cook, 1999; Ottaviani et al., 2008b). This implies a transient shortening of loops as origin attachments are made and a further transient shortening as DNA is

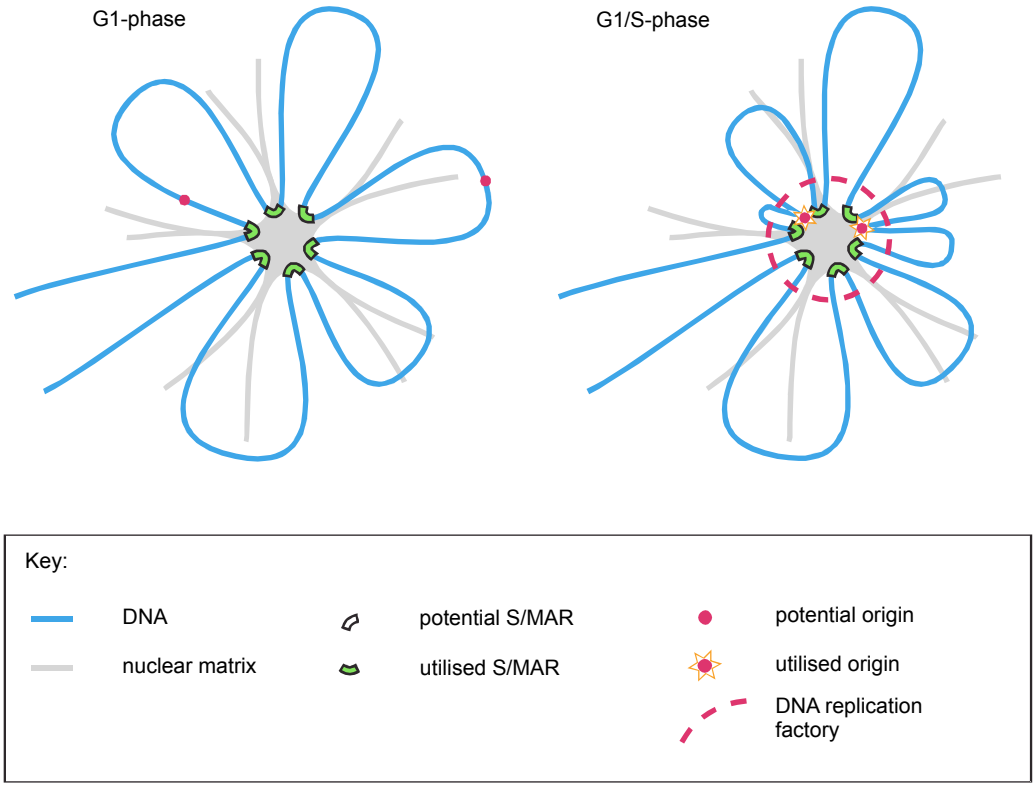

Figure 6.2: Possible relationships between DNA replication and the nuclear matrix. Our preferred model showing attachment to the NM via non-origin S/MARs, and recruitment of DNA replication origins at G1/S-phase with possible impact on loop size.

Previously published in (Wilson and Coverley, 2013). Designed by R. Wilson, drawn by P. Roberts.

reeled through replication machinery upon origin activation. To understand the impact this would have on average loop size, we must consider whether origins are all recruited at the same time because if this is not synchronous the effect on loop size could be minimal. Djeliova *et al.* (2001b) report that both an early and a late origin were recruited to the NM during late G1 (described in more detail in section 1.4.4), suggesting that recruitment to the NM is synchronous rather than temporally distributed as for replication factory activation. However, analysis of chromatin loop size by MFHR has revealed no global loop remodelling between different phases of the cell cycle (Jackson et al., 1990).

To reconcile these observations, the consequences of recruitment of origins that are more proximal to existing attachment points, as proposed elsewhere (Rivera-Mulia et al., 2011), were considered. Recruitment of origins at the 'top' of loops would cause a reduction in loop size by up to 50 % but this would be the maximum observed. Recruitment of origins closer to an existing S/MAR would have less of an effect on loop size. For example, recruitment of origins a quarter of the way 'up' a loop would initially cause only a maximum of 12.5 % drop in loop size (fig 6.2), and the closer the origin is to an existing S/MAR the less the effect would be. Recruitment of origins close to existing S/MARs may preferentially occur (Rivera-Mulia et al., 2011), in which case a small decrease in global loop size may be difficult to observe and may explain why no decrease is reported for late G1-phase.

Similarly, no decrease in loop size is reported during S-phase despite a theoretical decrease as the DNA is reeled in towards the replication machinery at the NM. This is perhaps not surprising given that origins are not all activated at the same time but as part of an organised temporal programme. Taken together, these arguments go some way to accounting for little global impact on average chromatin loop size in either late $G1^{M}$ or S-phase.

6.2.4 Recruitment of origins during $G1^{Q}$

Given that no global chromatin loop size change appears to occur during $G1^{M}$, it is striking that a significant change occurs during $G1^{Q}$. This may be attributed to one of three possibilities (or a combination of these); either 1) preparation for replication, involving the recruitment of origins, or 2) the preparation for transcription of genes

needed for cell cycle progression, or 3) the removal of the quiescence specific 'lock down' of DNA, which may underlie both of these processes. Further work must be undertaken to determine the cause but since this change was detected by analysing NaCl treated loops and transcription related loops appear to be LIS resistant rather than NaCl resistant (Linnemann et al., 2009), this may suggest that the $G1^{Q}$ size change is not related to transcription. In addition, as recruitment of origins to the NM during $G1^{M}$ does not appear to be associated with a global loop size change, this may suggest that reversal of a quiescence specific organisation is the cause of this observation. However, a possibility that should not be ignored is that although origins are not constitutively NM attached during the mitotic cell cycle, they might be 'primed' for re-attachment in late G1. In contrast, this may be lost during quiescence necessitating a widespread reoganisational event in G1 (see section 5.5.3).

6.3 How and why is higher order nuclear structure different between cell types?

6.3.1 Higher order nuclear structure in cancer cells

Differences in nuclear architecture, including the NM, have been found between cancer and non-cancer cells (section 1.5). However, it can be difficult to establish whether these are cause or consequence of transformation, and understanding of the functional importance is hampered by a lack of understanding of the 'normal' situation. One potentially significant impact of differences in NM composition is altered chromatin loop attachments, which could lead to transformation (Linnemann and Krawetz, 2009b and reviewed in He et al., 2008; Zink et al., 2004). However, few investigations of attachments have been undertaken in cancer cells (Linnemann and Krawetz, 2009b), likely because of the difficulty and complexity of the work involved, especially given that cell type specific attachments also exist (Chavali et al., 2011; de Belle et al., 1998; Montazer-Torbati et al., 2008; Ottaviani et al., 2008a; Trevilla-Garcia and Aranda-Anzaldo, 2011; and reviewed in Zink et al., 2004). The data presented here shows that NM attachment of chromatin loops is significantly altered in cancer (fig 6.3) and may prove to be an adventitious characteristic. Further investigation of the causes of altered NM attachment in

cancer may therefore reveal novel mechanisms of transformation and potential therapeutic targets.

6.3.2 Cell type specific higher order nuclear structure

Nuclear organisation appears to be cell type specific and to vary by differentiation status (below). This is important as pathological or cell cycle changes in chromatin loops should therefore not be considered alone (fig 6.3). For example, naïve B lymphocytes were recorded as being much more sensitive to DNase I digestion than G0 hepatocytes and to have a larger proportion which disintegrated following MFHR halo treatment (Rivera-Mulia and Aranda-Anzaldo, 2010; Trevilla-Garcia and Aranda-Anzaldo, 2011). Similarly, glial cells were much more sensitive to MFHR preparation than neurones (Alva-Medina et al., 2011). However, despite apparently having less DNA embedded within the NM, exemplar genes were recorded as being closer to the NM in naïve B lymphocytes compared to hepatocytes (Trevilla-Garcia and Aranda-Anzaldo, 2011). Therefore, when investigating characteristics of chromatin loops (or other levels of nuclear organisation) between cancer and non-cancer cells it is important to try to compare like with like in terms of cell type of origin as much as possible.

6.3.3 Chromatin loops size appears to increase during differentiation

As well as varying by cell type, higher order nuclear structure, including NM attachment appears to change during differentiation (fig 6.3). There is not a huge amount of data addressing this question but what there is suggests that average chromatin loop size increases during development. Buongiorno-Nardelli et al (1982) showed that chromatin loop size increases from *Xenopus* blastula (9.4 μm) to gastrula (10.3 μm), neurula (13.5 μm) and blood (14.5 μm). A similar trend was also seen with embryos of another Frog (*Rana pipiens*), with chromatin loop size increasing from blastulae (6.2 μm), yolk plug (7.5 μm), tail buds (9.4 μm), belly endoderm cells of tail bud (12.6 μm) to adult red blood cells (17.3 μm) (Flickinger et al., 1986). However, it should be noted that these samples would have contained multiple cell types. There do not appear to be any studies monitoring chromatin loop size during induced differentiation of a defined cell type. Nevertheless, the general conclusion from these studies is that more differentiated cells tend to show

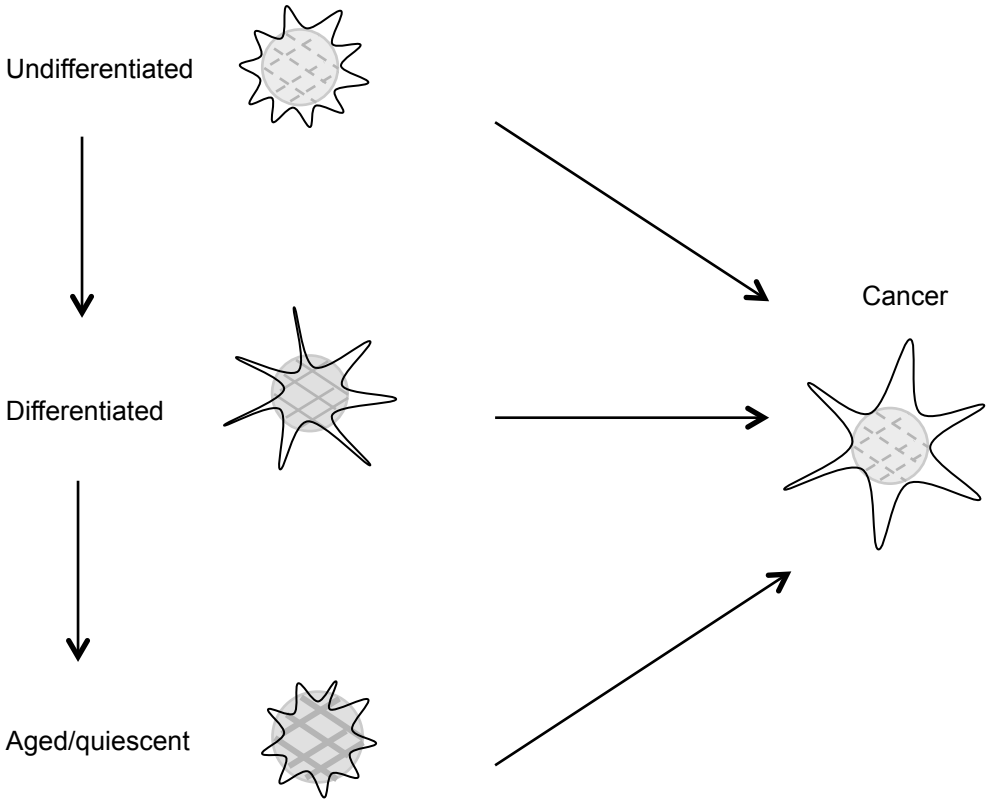

Figure 6.3: Schematic combining data on chromatin loops and the nuclear matrix for different cell types. DNA represented in black, nuclear periphery and NM in grey. Data presented here show increased chromatin loop size and reduced stability in cancer (section 4.4.5-7), altered NM is discussed in section 1.5. Increase in chromatin loop size during differentiation is discussed in section 7.3.3, altered NM discussed in section 1.4.10. Data presented here show reduced chromatin loop size in quiescent cells (section 4.4.1), also discussed, along with differences in NM attachment and aged cells, in section 7.1.1.

increased chromatin loop size. In support of this conclusion, analysis of the 5S rRNA gene cluster by MFHR-FISH showed maximal loop length to be larger in lung and brain tissue than in embryonic stem cells. Interestingly, during spermatogenesis loop size length decreases from meiotic (pachytene) spermatocytes and post-meiotic spermatids (Klaus et al., 2001; Nadel et al., 1995), which corresponds to the time of CIZ1 re-expression (Greaves et al., 2012) and suggests the possibility for CIZ1 involvement. The reduction in loop size of the 5S rRNA gene cluster occurs before protamine induced nucleus compaction and protamine extracted sperm halos are small (reviewed in Johnson et al., 2011), suggesting multiple levels of higher order structure compaction within sperm.

Cell type specific differences in NM proteins themselves and DNA attachment points S/MARs have previously been highlighted (see sections 1.3.4, 1.7) and are likely to impact global loop architecture. This interesting paradox that chromatin loops appear to increase in size during differentiation but decrease during ageing, spermatogenesis and as cells become more quiescent (fig 6.3), remains to be untangled.

6.3.4 Nuclear plasticity

A previous study from the Coverley lab showed that cyclin E becomes attached to the NM during *in vitro* and *in vivo* differentiation, but is not attached in a panel of cancer cell lines (Munkley et al., 2011). This trend has since been observed for CIZ1 and members of the pre-RC; MCM2, ORC4 and CDC6 (appendix D). These data suggest a model where replication takes place in association with the NM in differentiated cells in order to maintain cell type specific spatial programming, and to provide a protective framework that minimises drift or damage. In contrast the lack of recruitment in undifferentiated and cancer cells is suggested to provide adventitious plasticity to the cell by enabling reconfiguration (Munkley et al., 2011). Data presented here suggest that this may similarly be true for DNA itself, especially in relation to transformation. Further work would be needed to establish how this relates to differentiation.

6.4 The role of CIZ1 during preparation for DNA replication

6.4.1 CIZ1 during G1

The work presented in chapter 5 has significantly expanded our understanding of the role of CIZ1 in the cell cycle, although many outstanding questions remain. As a result of this work, CIZ1 has been identified as non-essential for the cell cycle, but in its absence, cells cycle slower, with altered expression of cyclins and CDKis and are more prone to transformation. Three points of action of CIZ1 during $G1^{Q}$ had been documented prior to this project; requirement for (timely) S-phase entry, requirement for loop remodelling, and involvement in recruitment of cyclin A to detergent-resistant structures (fig 6.4). It remains unknown whether its effect on loop remodelling early in G1 has downstream effects on recruitment of cyclin A and/or S-phase restraint. Work presented here suggests that CIZ1 may play a role as a more general cyclin/CDKi exchange factor (fig 6.4). The apparent paradox that depletion of new CIZ1 by RNAi inhibits S-phase while CIZ1-/- cells inappropriately re-enter cycle should also be highlighted. This suggests that CIZ1 levels may be crucial and that potentially the balance of different forms may be important. Despite not being essential for development, cells clearly do not cycle properly without CIZ1 with dramatic consequences for quiescence capabilities.

6.4.2 Does CIZ1 act as an exchange factor for cell cycle regulators?

Analysis of cyclins in cycling CIZ1-/- cells revealed that cyclin D2 and E1 are expressed in more cells and many more of these than expected are in S-phase (chapter 5). Combining these data with the observed increased doubling time and increased G1 population suggests that these cyclins are expressed for a longer period. This is only partly accounted for by the longer G1, and appears to include an increased temporal window of expression that extends significantly into S-phase. Overexpression of cyclins E and D are known to cause a shortening of G1-phase, both $G1^{M}$ and $G1^{Q}$ (Imoto et al., 1997; Ohtsubo and Roberts, 1993; Resnitzky et al., 1994; Wimmel et al., 1994). However, the total level of cyclin D and E expression was unchanged in CIZ1-/- cells, which leads to the hypothesis that cyclin D and E

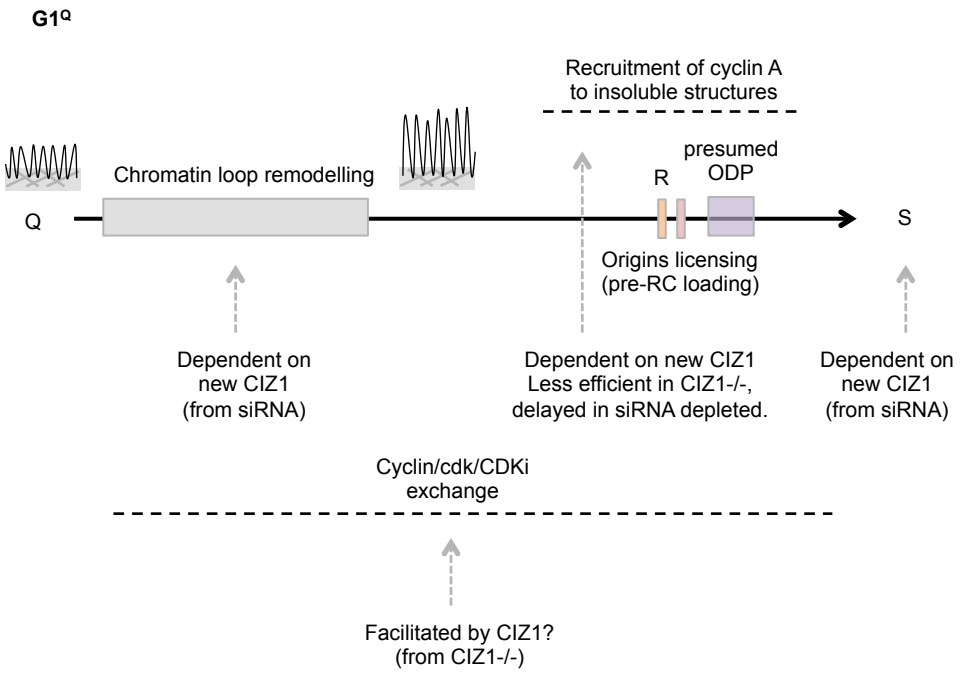

Figure 6.4: Events during cell cycle re-entry in which CIZ1 is believed to play a part. Data from (Copeland et al., 2010; Coverley et al., 2005; Knight, L., personal communication) and from CIZ1-/- cells investigated here. Events are depicted in relation to R, presumed ODP and S.

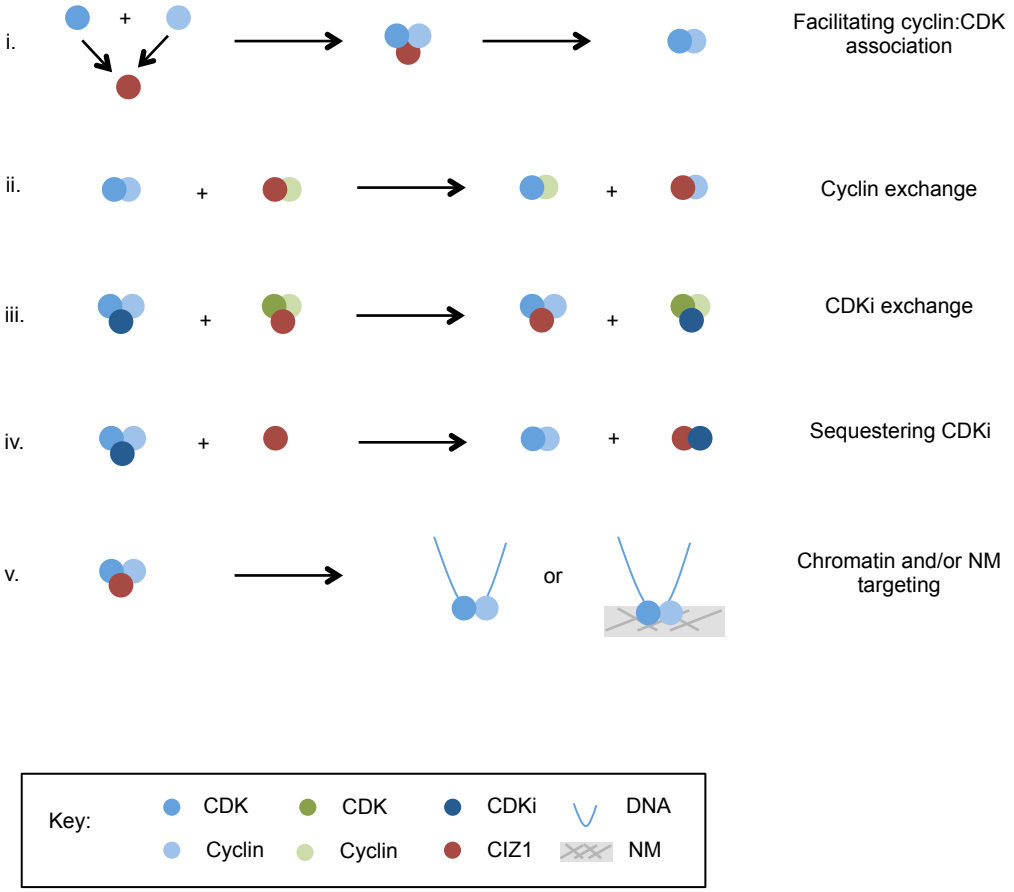

Figure 6.5: Schematic showing possible roles of CIZ1 as a cyclin/CDKi exchange factor.

have, at some level, reduced function in the absence of CIZ1, and that progression through G1 is restrained.

Reduced function of cyclins could be related to kinase activity, the formation of the active complex, inhibition or spatial targeting. These possibilities are illustrated in figure 6.5. It seems unlikely that CIZ1 affects the kinase activity, however, CIZ1 is known to interact with cyclin A, cyclin E, CDK2 and $p21^{CIP1}$ (Copeland et al., 2010; Greaves et al., 2012; Mitsui et al., 1999) and overexpression of CDK2 was shown to prevent the interaction between CIZ1 and $p21^{CIP1}$ (Mitsui et al., 1999). Therefore, CIZ1 could feasibly act to influence complex formation for all or some of these proteins. CIZ1 could act, like $p21^{CIP1}$, to facilitate cyclin:CDK complex formation (i) so in the absence of CIZ1 the formation of these complexes are less efficient. Alternatively, CIZ1 may act as an exchange factor for transferring cyclins between CDKs (ii), or CDKis between cyclin:CDK complexes (iii). For example, cyclin D:CDK4/6 complexes can relieve $p21^{CIP1}$ inhibition of cyclin A/E:CDK2 complexes by acting to sequester this inhibitor and this event could be facilitated by CIZ1. CIZ1 could itself also sequester $p21^{CIP1}$ (iv) as suggested by Mitsui et al., (1999). These options relate to 'the right proteins interacting at the right time' but it is also conceivable that CIZ1 targets these factors to specific sub-nuclear locations (v), affecting the ability of complexes to be in 'the right place at the right time'. For example, CIZ1 has already been shown to recruit cyclin A to insoluble structures (Copeland et al., 2010), and could similarly act to target cyclin D or E containing complexes.

6.5 Further work

If time were not limiting I would have liked to go on and ask the following questions that have arisen from my work:

- The identification and characterisation of MARs in quiescent, G1 and S–phase cells would enable a sequence based understanding of the global chromatin loop reorganisation observed during $G1^{Q}$, and how this relates to gene position or other sequence motifs. This would also potentially help to resolve the reason for quiescence specific chromatin loop reorganisation,

and whether the G1Q remodelling event relates to cell cycle specific transcription.

- Determination of origins and whether MAR remodelling corresponds to origin recruitment would significantly enhance our understanding of the preparation of DNA replication. In depth investigation of exemplar early and late-replicated origins and the S/MARs by which they are recruited would reveal detailed timing information and in combination with determination of the required proteins, would establish the mechanism of how origins are recruited during preparation for DNA replication.

- Further investigation of how CIZ1 plays a role in the remodelling of chromatin loops, during G1Q, and potentially during differentiation and spermatogenesis, would develop our understanding of how chromatin loops are remodelled and establish whether this is related to its role in cancer. We can hypothesise that variant expression observed in cancer could alter chromatin loop attachments and thereby facilitate plasticity.

- Further investigation of the role of CIZ1 and its interaction partners would establish the mechanism for altered cyclin and CDKi expression in CIZ1-/- cells, and whether CIZ1 acts as an exchange factor. More information about this role will enhance our understanding of how altered expression of CIZ1 relates to cancer.

- Investigation of CIZ1 splice variant expression in cancer and non-cancer samples would help to classify forms as tumour promoting or suppressing. Variant CIZ1 could also be expressed in CIZ1-/- mice or cells to establish the effect of various clinically observed changes. Once variant forms are classified as tumour promoting or suppressing, this could lead to further biomarker tests (Higgins et al., 2012) or even the possibility for therapeutic targets.

Appendices

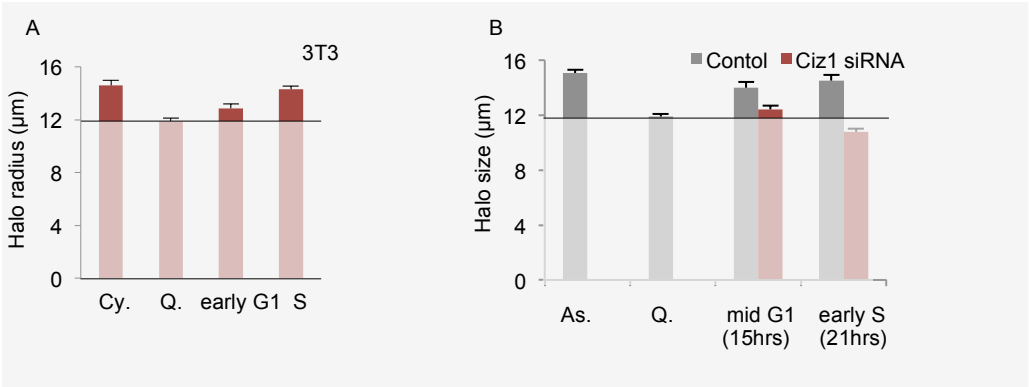

Appendix A: Chromatin loops are smaller in quiescent cells and increase as cells return to the cell cycle, in a mechanism dependent on CIZ1. A) Visual MFHR Halo radius measurements from asynchronous cycling populations (Cy.) or from synchronised populations at the stated cell cycle phase. Data are average from >8 nuclei from ≥2 technical replicates, error bars are SEM. B) Halo measurements as in A except taken after transfection of quiescent cells with Ciz1 siRNA. Controls are shown in Copeland et al 2010, figure 5.

Data generated in the Coverley lab group prior to this PhD project and presented with kind permission from L Knight.

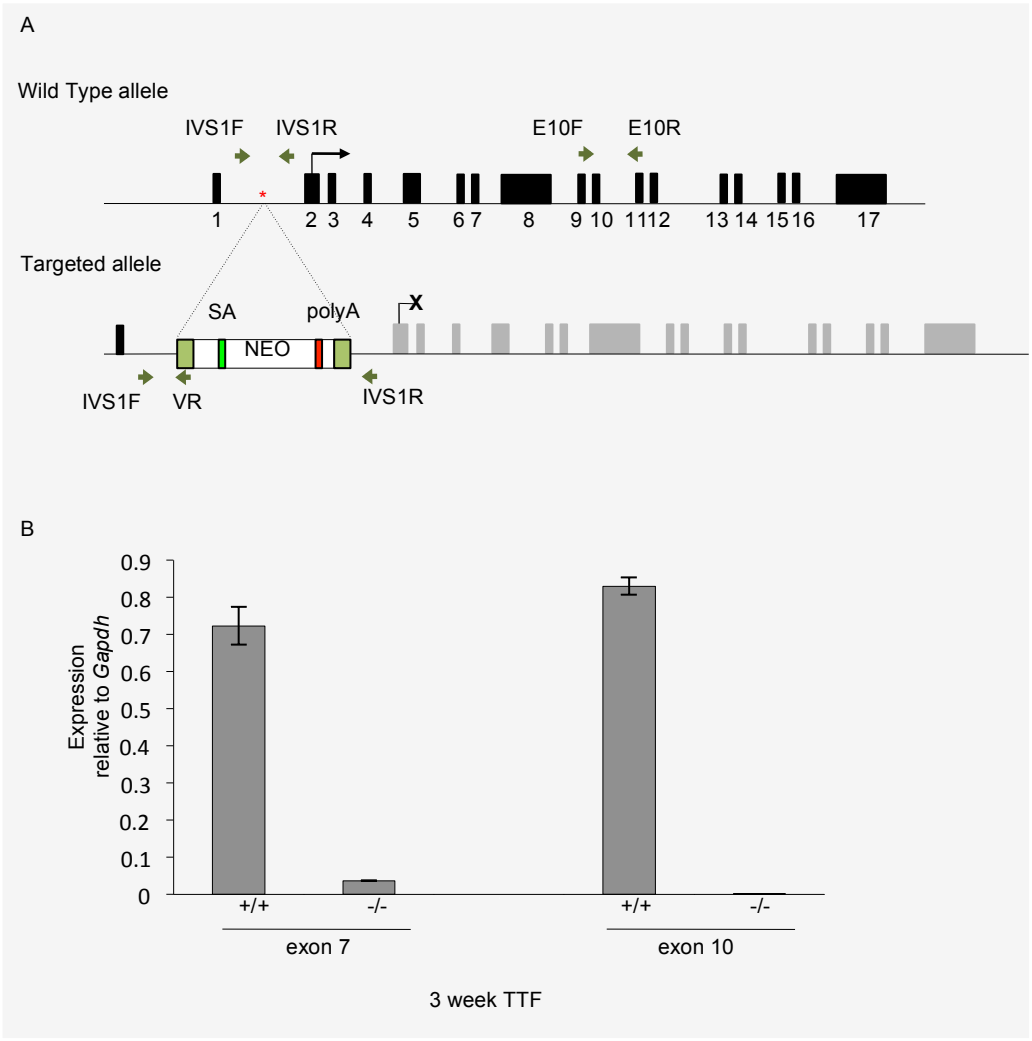

Appendix B: Generation and confirmation of CIZ1-/- mice. A) Map showing cassette which is inserted after exon 1. B) Q RT-PCR data showing ≥ 99 % reduction in *CIZ1* mRNA expression in CIZ1-/- TTFs.

Data kindly provided by and presented with permission from Justin Ainscough, University of Leeds.

Appendix C Subnuclear localisation of the E4 antibody epitope

This work was conducted in the first year of my PhD and was intended to discover more about the behaviour of cyclin E. However, the α-cyclin E antibody used for this work was found to identify E4 specific staining in cyclin E1-/- E2-/- MEFs and therefore this antibody cannot be used to reliably identify cyclin E. This work is included as an appendix because it is informative for others who may use the antibody, and the results using E4 are interesting and should be available if the E4 epitope can be identified.

Introduction

Previous work from the Coverley lab has shown that cyclin E is immobilised on the NM in mouse 3T3 cells (Munkley et al., 2011). This was the case in all differentiated cell lines tested. In contrast, in the majority of cancer cell lines tested and undifferentiated cells cyclin E was not immobilised on the NM. In fact, when cells were induced to differentiate using two *in vitro* models or monitored during Xenopus development, cyclin E was recruited to the NM during this differentiation process. This was recorded in human urothelial cells using the α-cyclin E antibody sc-247 HE12 (Santa Cruz), in mouse ES cells using the α-cyclin E antibody ab7959 (Abcam) and in *Xenopus* using an α-cyclin E antibody from Tim Hunt (Munkley et al., 2011). Association with the NM is consistent with the idea that cyclin E may be involved in recruitment of pre-RCs into NM-associated DNA replication factories. Changes during differentiation may reflect changes in genome organisation necessitated by changes in gene expression.

Aims

The original aim of this work was to describe in detail, the subnuclear localisation of cyclin E during cell cycle re-entry after release from quiescence, to ask specific questions about the functional significance of the association with the NM. Monoclonal anti-cyclin E (E4) (Santa Cruz sc-25303) was used to investigate the

subnuclear localisation of cyclin E in murine 3T3 cells. This antibody was raised against amino acids 1-145 of human cyclin E and is reported to detect mouse, rat and human cyclin E by western blot, immunofluorescence, immunoprecipitation and ELISA (http://www.scbt.com/datasheet-25303-cyclin-e-e-4-antibody.html). It has been used in a number of high profile published papers (Bustany et al., 2011; Chen and Li, 2010; Chiaradonna et al., 2006; Geng et al., 2007; Milsom et al., 2008; Munkley et al., 2011; Revuelta-Cervantes et al., 2011; Stolfi et al., 2010; Su et al., 2010; Tan et al., 2009; Tokuriki et al., 2009; Veiga-Fernandes and Rocha, 2004; Wang et al., 2009). However, after some detailed analysis using this antibody (described below) E4 specific nuclear staining was observed in cyclin E1-/- E2-/- MEFs, therefore E4 cannot be said to reliably recognise cyclin E. Data presented below describes the interesting behaviour of the E4 antigen but cannot be interpreted as cyclin E.

Experimental Design

Cells grown on coverslips were harvested at stated timepoints during G1Q or from asynchronous populations. Where indicated, cells were pre-treated with inhibitors or siRNA to facilitate mRNA knock-down. Cells underwent extraction procedures to produce the following fractions: total cellular protein, detergent resistant fraction, high salt resistant fraction and the insoluble fraction that is resistant to extraction with high salt and DNase (section 2.4.5). These were probed using the indicated antibodies as described (table 2.6). For western blots, cells underwent similar extraction procedures (section 2.4.2-4).

Generation of anti-*cyclin E* siRNA

Primers were designed (table C1) that were homologous to *cyclin E1* (mouse) and *cyclin E2* (human and mouse compatible). Scrambled *cyclin E* siRNA was generated from the Ccne1 # 3 sequence. Blast searches revealed no significant similarity with other genes. Anti-*cyclin E* siRNA were synthesised using Silencer® siRNA Construction Kit (Ambion) as per manufacturer's instructions, and the concentration determined by NanoDrop (Thermo scientific). Each siRNA was tested for effect on both the target *cyclin E* and the alternative form (fig C1). Depletion of

one *cyclin E* (E1 or E2) form caused some increase in the other form, therefore a cocktail of Mouse E1 # 2, Mouse E1 # 3, MouseHuman E2 # 2 and MouseHuman E2 # 4 was chosen as the best candidate combination to deplete both *cyclin E* forms. A small amount of work was undertaken using these siRNAs, shown in this appendix. However, the direction of the project moved away from cyclin E as previously described.

Table C1: *Cyclin E* siRNA primers

Name	Sense	Anti-sense
Mouse E1 # 1	AACATGAAAGAAGAA-GGTGGCCCTGTCTC	GCCACCTTCTTCTTT-CATGTTCCTGTCTC
Mouse E1 # 2	AAGACTGTGAAAAGC-GAGGATCCTGTCTC	ATCCTCGCTTTTCAC-AGTCTTCCTGTCTC
Mouse E1 # 3	AAGAGGACAATGAGC-TTGAATCCTGTCTC	ATTCAAGCTCATTGT-CCTCTTCCTGTCTC
Mouse E1 # 4	AATGAGCTTGAATAC-CCCAGGCCTGTCTC	CCTGGGGTATTCAAG-CTCATTCCTGTCTC
MouseHuman E2 # 1	AAAAACCACCAGGAA-AACACTCCTGTCTC	AGTGTTTTCCTGGTG-GTTTTTCCTGTCTC
MouseHuman E2 # 2	AATGGAGGCATTATG-ACACCACCTGTCTC	TGGTGTCATAATGCC-TCCATTCCTGTCTC
MouseHuman E2 # 3	AAGCTGAAGACTTTT-AAGAAGCCTGTCTC	CTTCTTAAAAGTCTT-CAGCTTCCTGTCTC
MouseHuman E2 # 4	AAGGCTTTAAAATGG-GAACTTCCTGTCTC	AAGTTCCCATTTTAA-AGCCTTCCTGTCTC
Mouse E Scrambled	AACAGTGGATCGATA-AGAGTACCTGTCTC	TACTCTTATCGATCCA-CTGTTCCTGTCTC

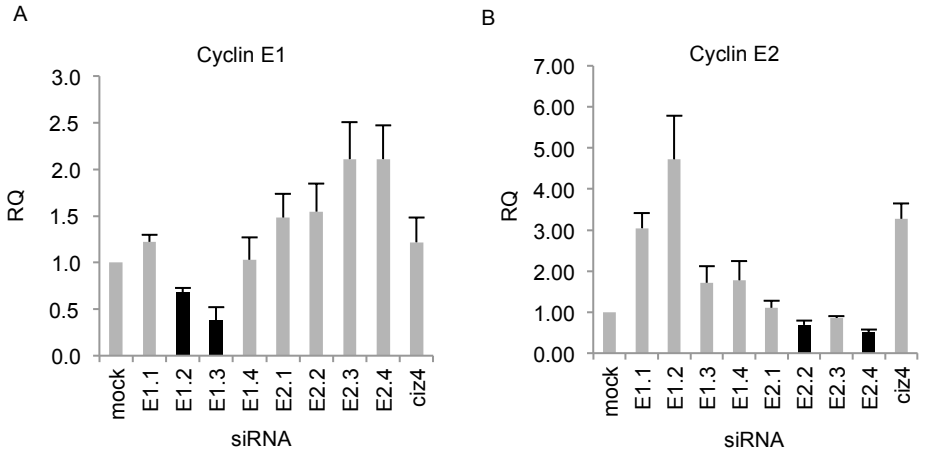

Figure C1: Validation of cyclin E siRNA. Cells were transfected with the indicated *cyclin E* siRNAs, *ciz4* (Coverley et al., 2005) or as a mock transfection. Transcript analysis shows effect on A) cyclin E1 or B) cyclin E2 expression. qRT-PCR data were normalised to actin and expressed relative to mock treated control. Data are average of triplicate wells, error bars are SEM. The siRNA used in later experiments are indicated in black.

Results

The E4 epitope is NM bound in the majority of cycling but not quiescent 3T3 cells

E4 specific foci resisted extraction by DNase in 82 % (± 7.8 SEM) of asynchronous 3T3 cells (fig C2 A), consistent with previous data (Munkley et al., 2011). This shows that the E4 epitope is NM bound in the vast majority, but not all cycling 3T3 cells, which suggested cell cycle variation and this was investigated further. In contrast, the E4 epitope is completely extracted by DNase in almost all quiescent 3T3 cells, only remaining after DNase treatment in 7 % (± 3.3 SEM) of cells (fig C2 B), indicating proliferation specific binding.

The E4 epitope rebinds to the NM by one hour after release back into the cell cycle independent on serum

Reasoning that at some point during cell cycle re-entry from quiescence the E4 epitope would have to re-bind to the NM, extractions were performed at various timepoints in G1Q. Surprisingly, the E4 epitope resisted DNase extraction in almost

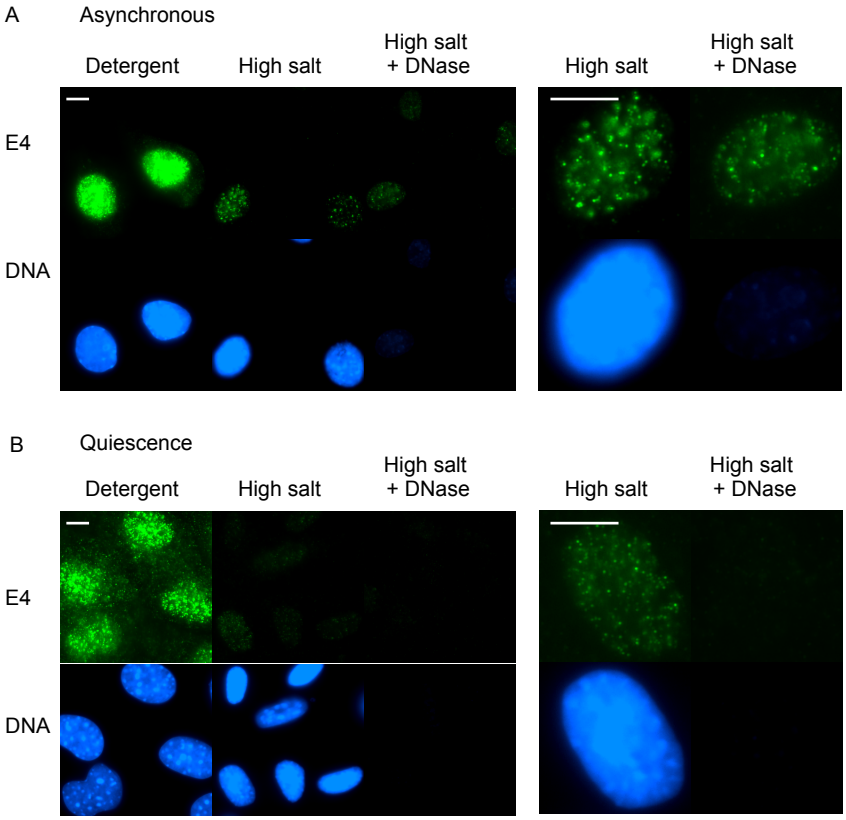

Figure C2: The E4 epitope is NM bound in cycling but not quiescent 3T3 cells. A) E4 foci remain in cycling cells treated with detergent, high salt or high salt and DNase. E4 epitope shown in green, DNA counterstained with Hoechst 33258 (blue). 82 % (± 7.8 SEM) of cycling 3T3 cells retain E4 foci after DNase treatment. B) E4 foci in quiescent populations resist detergent and high salt treatment but not DNase. Staining as above. 7 % (± 3.3 SEM) of quiescent 3T3 cells retain DNase resistant E4 foci. Scale bar is 10 µm.

all cells by as early as 1 hour post release suggesting an initial or at least very early step in cell cycle re-entry (fig C3 A, B). Releases were calibrated by monitoring incorporation of BrdU (example release fig C3 C), which is first evident around 17hrs. Interestingly, the percentage of cells that retained DNase resistant E4 epitope decreased at timepoints after 1 hour (fig C3). Further timepoints were not undertaken but it would be informative to determine if the E4 epitope becomes completely sensitive at a point after 4 hours, or if the E4 epitope becomes DNase resistant again in line with its behaviour in cycling cells.

To dissect whether mitogenic cues from serum might be important for recruitment of the E4 epitope onto the NM, cells were released into medium containing 0 % serum. The E4 epitope was recruited to the DNase resistant fraction by 1 hour even in the absence of serum, and in remarkably similar proportions of cells between 1 and 4 hours to when serum was present (fig C4 A, B). This suggests release from contact inhibition to be the crucial event. Supporting this, the addition of 10% serum medium to quiescent cells had no effect on the localisation of the E4 epitope, which remained extractable with DNase (fig C4 C). The high percentage of cells with DNase resistant E4 epitope at 1 hour post release suggests this may be an early decision step in cell cycle re-entry, for example, before the requirement for serum at the restriction point (R) which occurs at around 15 hours in this system (Coverley et al., 2002).

Inhibition of proteasome dependent proteolysis or CDKs, or depletion of *CIZ1* does not affect E4 recruitment to the NM

To try to reveal the mechanism for recruitment of the E4 epitope to the NM upon cell cycle release, effects of kinase and proteolysis inhibitors were investigated Neither the use of the proteasome dependent proteolysis inhibitor, MG132, nor the kinase inhibitors Roscovitin or Olomucine, significantly prevented the recruitment of the E4 epitope to the DNase resistant fraction (fig C5). The efficacy of the inhibitors was confirmed by cell death at 24 hours. This suggests recruitment to the NM of the E4 epitope is not controlled by proteolysis or negative phosphorylation of an inhibitor, nor by positive phosphorylation of the E4 epitope, at least by cdk2.

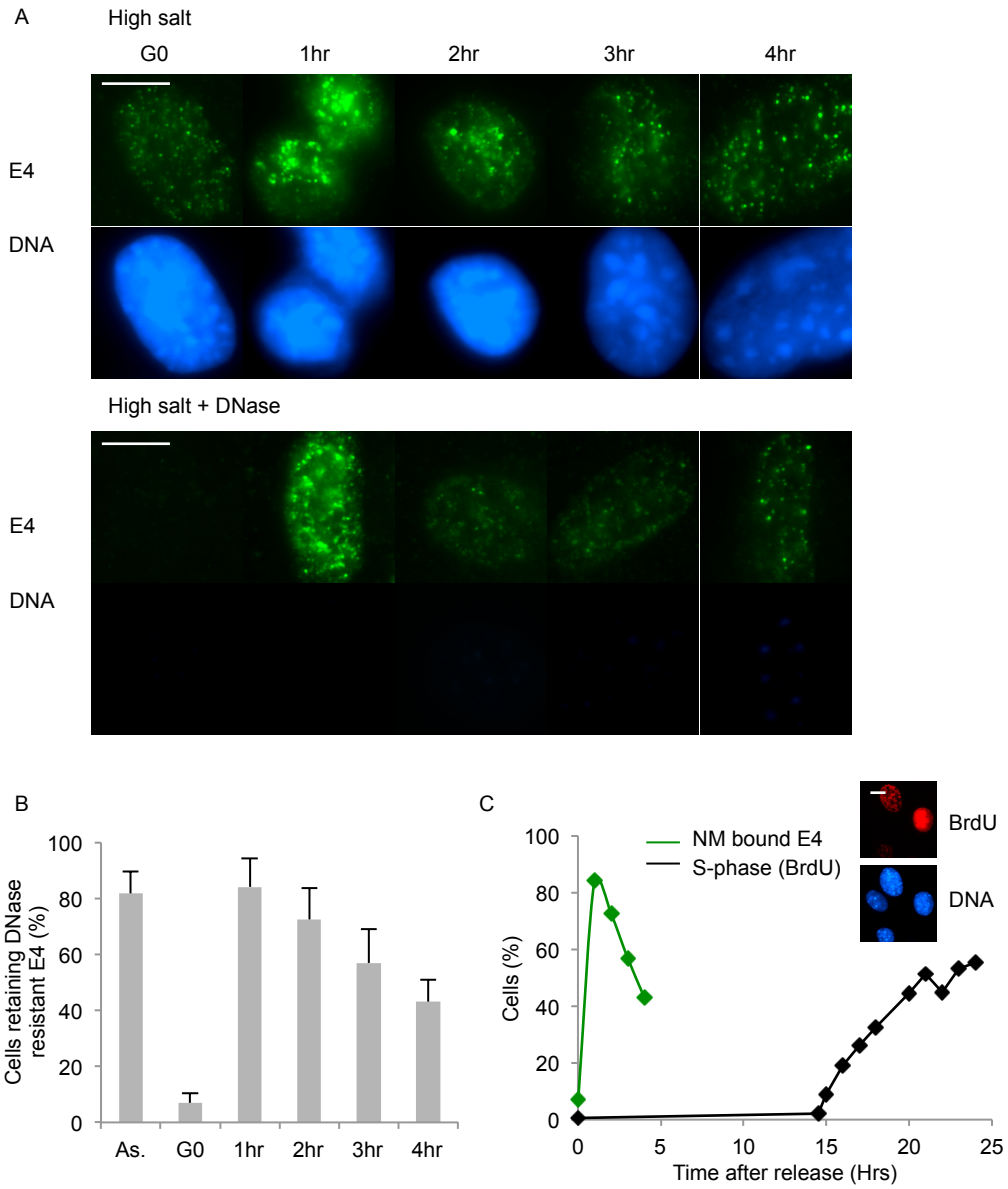

Figure C3: The E4 epitope rebinds to the NM by one hour after release back into the cell cycle. A) Top: E4 foci resist high salt treatment in quiescent populations and cells released back into the cell cycle at the indicated time points. Staining as figure C2. Scale bar is 10 μm. Lower: E4 foci do not resist DNase treatment in quiescent cells but become DNase resistant when cells are released back into the cell cycle at the indicated timepoints. B) Histogram shows percentage of cells retaining DNase resistant E4 foci at indicated timepoints. C) Graph shows percentage of cells in S-phase at indicated timepoints from representative release (black) and percentage retaining NM bound E4 epitope (green). S-phase is determined by BrdU incorporation. Inset: representative images shows BrdU staining. BrdU shown in red, DNA counterstained with Hoechst 33258 (blue). Scale bar is 10 μm.

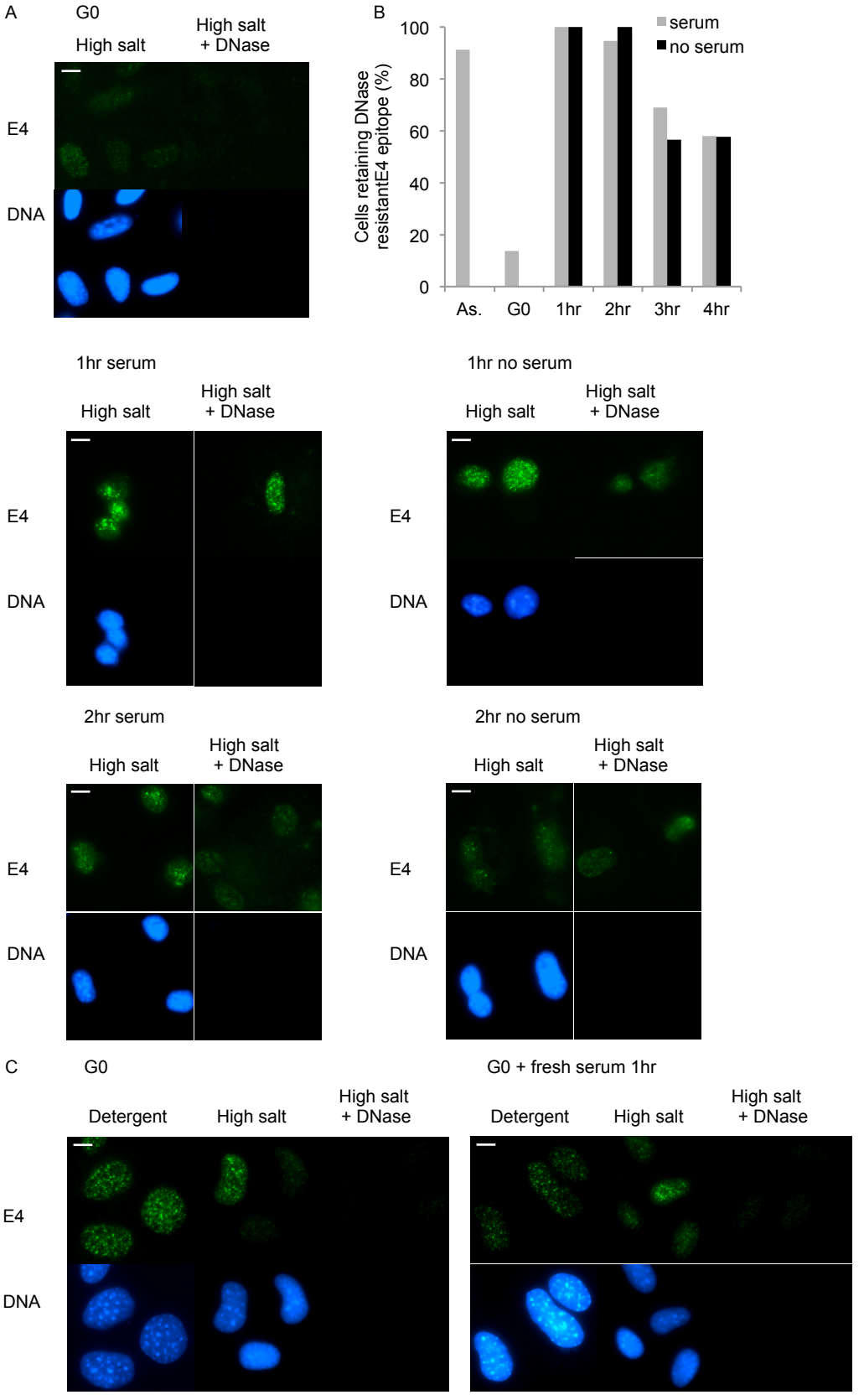
A
G0
High salt
High salt + DNase
E4
DNA
B
Cells retaining DNase resistantE4 epitope (%)
100
80
60
40
20
0
As.
G0
1hr
2hr
3hr
4hr
serum
no serum
1hr serum
1hr no serum
2hr serum
2hr no serum
C
G0
G0 + fresh serum 1hr
Detergent
High salt
High salt + DNase

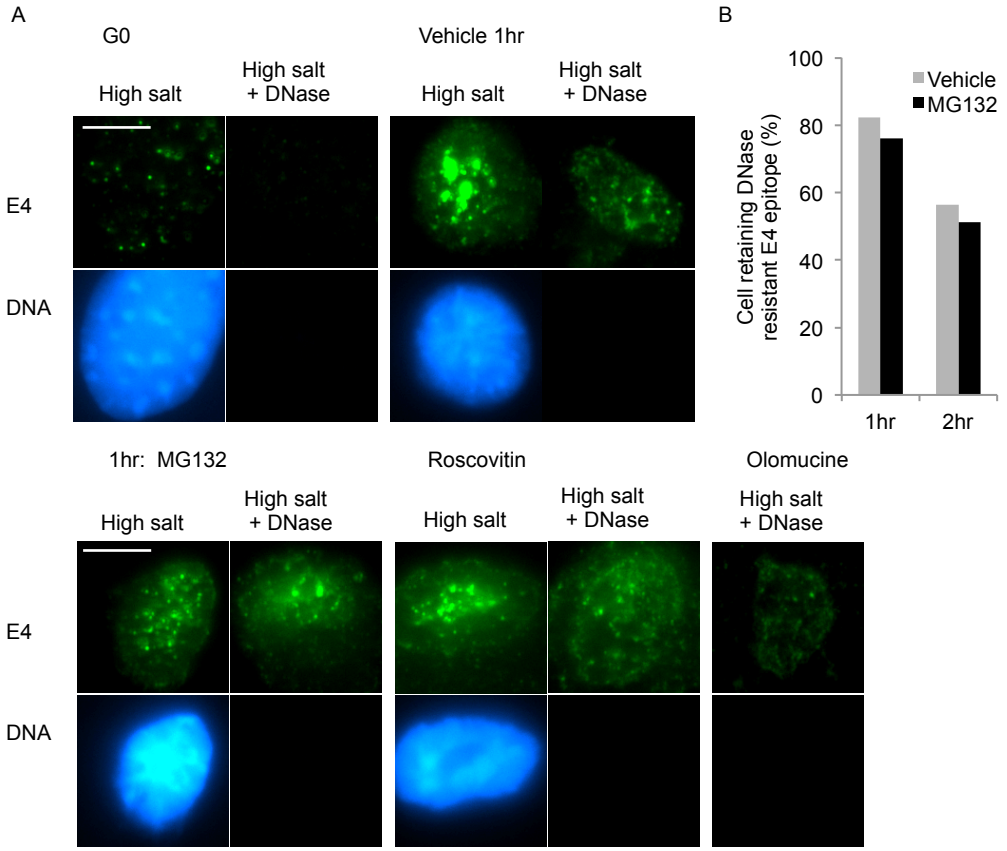

Figure C5: Inhibition of proteasome dependent proteolysis or cdks does not affect E4 epitope recruitment to the NM. A) E4 epitope becomes resistant to DNase by 1 hour after release in the presence of vehicle, MG132, Roscovitin or Olomucine. Staining as figure C2. Scale bar is 10 μm. B) Histogram shows no difference between cells released into media containing vehicle or MG132 in terms of percentage of cells with DNase resistant E4 foci.

Figure C4 (previous page): The recruitment of E4 epitope to the NM is independent of serum. A) Representative images show the E4 epitope becomes resistant to DNase by 1 hour after release whether cells are released into media containing 10 % serum or media containing 0 % serum. Staining as figure C2. Scale bar is 10 μm. B) Histogram shows no difference between cells released into media with or without serum in terms of the percentage of cells with DNase resistant E4 epitope at indicated timepoints. C) Images show E4 does not become recruited to DNase resistant structures if quiescent cells are treated for 1 hour with media containing fresh serum. Scale bar is 10 μm.

The requirement for newly synthesised CIZ1 was investigated by releasing cells from quiescence in the presence of a cocktail of α-*CIZ1* siRNA. Recruitment of E4 to the DNase resistant fraction by 1 hour was unaffected by transfection with *CIZ1* siRNA when compared to either scrambled siRNA control or electroporation only (mock) (fig C6). Presence of E4 in the DNase resistant fraction was also unaffected when newly synthesised CIZ1 was depleted in cycling cells (fig C7). This suggests that recruitment of the E4 epitope is not dependent on CIZ1. The siRNA have been previously validated (Coverley et al., 2005), though confirmation of knock-down for these experiments was not completed.

The above mechanisms were investigated for their effect on the recruitment of the E4 epitope due to their connection to cyclin E. However, these negative results, although allowing us to rule out certain factors, do not shed much light on how the E4 epitope is recruited. Other potential mechanisms that could be investigated include transcription or translation of a potential NM receptor or post-translational modifications (either of the E4 epitope itself or binding partners) such as SUMOylation, ubiquitination or NEDDylation. Identification of the E4 epitope would help to guide experimental direction.

The anti-cyclin E antibody E4 recognises an epitope found in cyclin E1-/- E2-/- cells.

Part way though this project I received WT MEFs and cyclin E1-/- E2-/- MEFs from Prof. Peter Sicinski's group (Geng et al., 2003). A similar nuclear punctate staining pattern to that seen in 3T3 cells was seen in the control MEFs and also in the cyclin E1-/- E2-/- cells. This was confirmed with three batches of E4 (fig C8 A). No staining was observed in coverslips processed without primary antibody (no primary) and staining was proportional to the concentration of E4 used (fig C8 B). Cyclin E1-/- E2-/- status of these cells was confirmed by western blot using a different α-cyclin E antibody, ab7959 (Abcam) (fig C8 C), and was in agreement with published data (Geng et al., 2003). It was also found that E4 foci did not colocalise with CIZ1 foci or CDK2 foci (fig C8 D, DNase treated samples shown only) which might be expected in at least a proportion of cells if E4 recognised cyclin E, as interaction between cyclin E and CIZ1 and CDK2 is established (Copeland et al., 2010; Mitsui et al., 1999). These

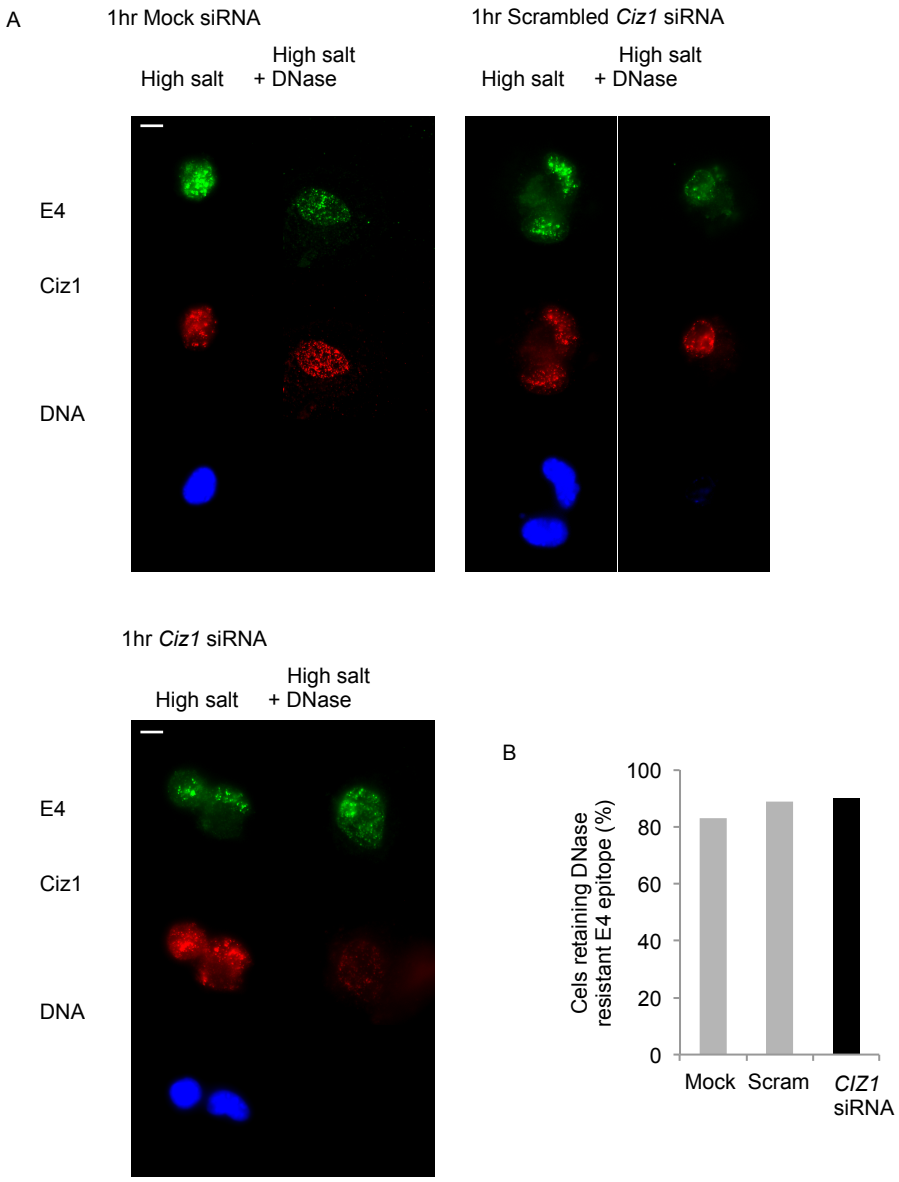

Figure C6: Depletion of *CIZ1* during release from quiescence does not affect E4 epitope recruitment to the NM by 1 hour. A) During release from quiescence, 3T3 cells were treated with no siRNA (electroporation only – mock), scrambled *CIZ1* siRNA or *CIZ1* siRNA. Images show E4 foci become resistant to DNase by 1 hour irrespective of siRNA treatment. E4 shown in green, CIZ1 shown in red, DNA counterstained with Hoechst 33258 (blue). B) Scale bar is 10 μm. Histogram shows percentage of cells with DNase resistant E4 foci after indicated siRNA treatment.

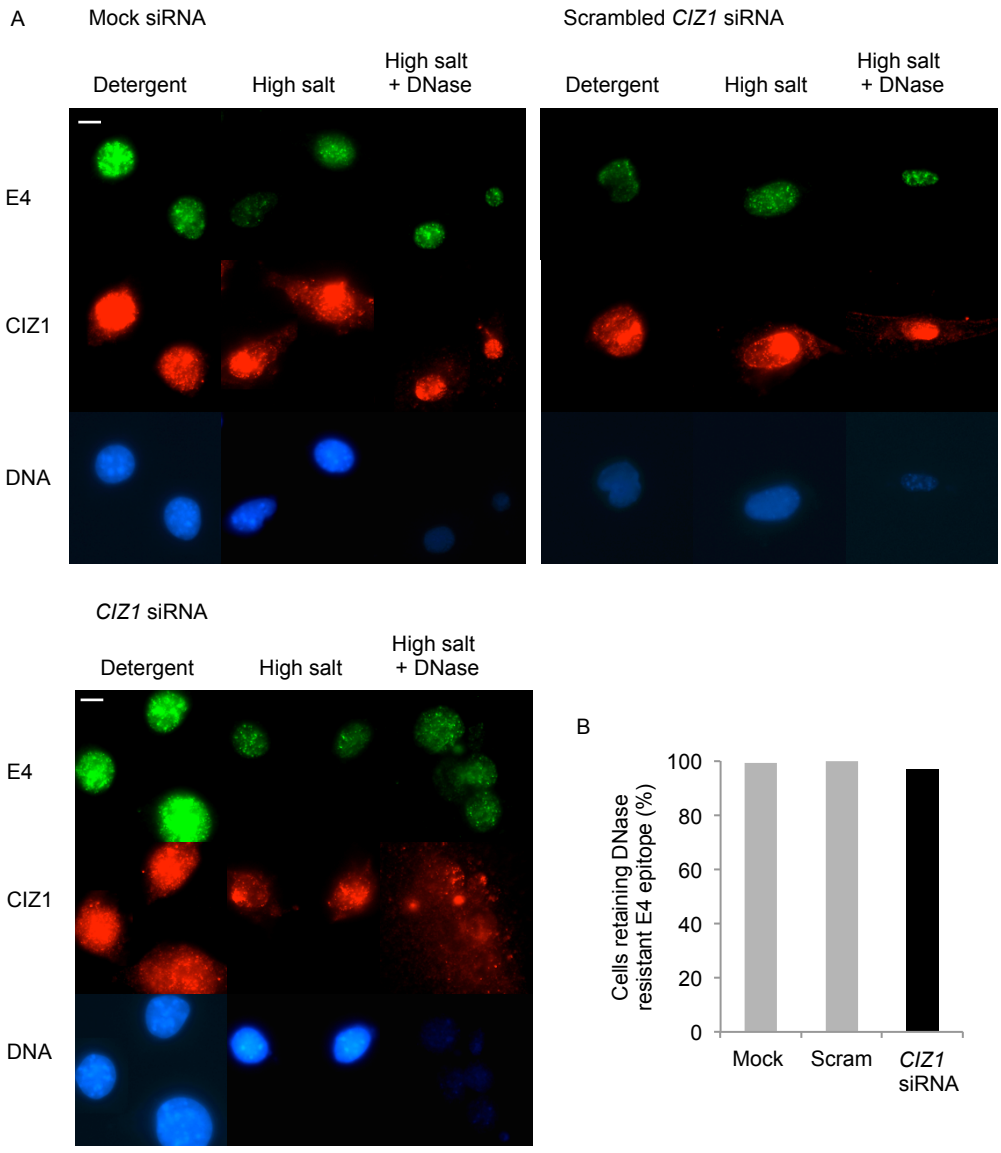

Figure C7: Depletion of *CIZ1* in cycling cells does not affect E4 epitope recruitment to the NM. A) Cycling 3T3 cells were treated with no siRNA (electroporation only – mock), scrambled *CIZ1* siRNA or *CIZ1* siRNA. Images show E4 foci remain resistant to DNase irrespective of siRNA treatment. Staining as figure C6. Scale bar is 10 μm. B) Histogram shows percentage of cells with DNase resistant E4 foci after indicated siRNA treatment.

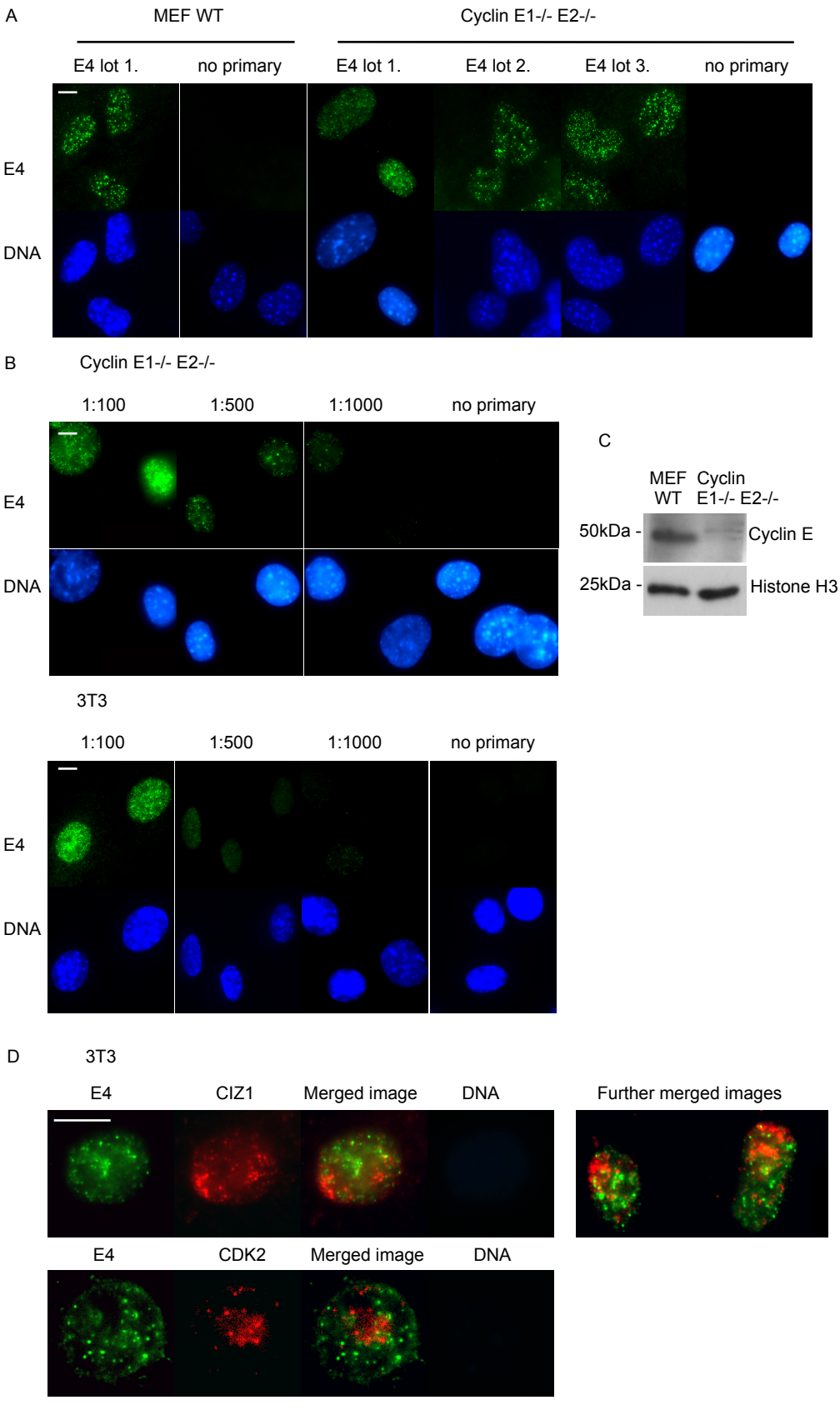
A
MEF WT
Cyclin E1-/- E2-/-
E4 lot 1.
no primary
E4 lot 1.
E4 lot 2.
E4 lot 3.
no primary
E4
DNA
B
Cyclin E1-/- E2-/-
1:100
1:500
1:1000
no primary
E4
DNA
3T3
1:100
1:500
1:1000
no primary
E4
DNA
C
MEF WT
Cyclin E1-/- E2-/-
50kDa -
Cyclin E
25kDa -
Histone H3
D
3T3
E4
CIZ1
Merged image
DNA
Further merged images
E4
CDK2
Merged image
DNA

results show that α-cyclin E antibody E4 recognises another epitope, either instead of or in addition to cyclin E. Therefore, any results using E4 cannot be convincingly attributed to cyclin E. My results with the E4 antibody are included here as they constitute a package of information about an epitope with interesting properties.

Comparison of α-cyclin E antibodies

The Abcam α-cyclin E antibody ab7959 and Upstate α-cyclin E antibody 07-687 both recognise a doublet with approximate mobility of 50 kDa by western blot (fig C9 A, black arrow), consistent with the molecular weight for murine cyclin E of 47kDa. This can be knocked down using α-cyclin E1/E2 siRNAs and is absent from cyclin E null MEFs but present in control MEFs (fig C9 B, C). E4 was also tested by western blot but did not detect a ~50 kDa band absent from the no primary control (fig C9 A). E4 does recognise some bands absent from the no primary control, for example, one at ~75 kDa and one ~60 kDa. (grey arrows) These may be informative in identifying the E4 epitope.

Comment about previous data

This data shows E4 cannot be used to reliably recognise cyclin E. Munkley et al., (2011) presented a small amount of data using E4, however, these data and the overall conclusions were reinforced with other α-cyclin E antibodies in mouse, human and *Xenopus* (Abcam ab7957, Upstate 07-687, Santa Cruz sc247 HE12 and a *Xenopus* antibody from Tim Hunt). Some queries exist in the lab about cyclin E in murine 3T3 cells due to conflicting results. Therefore, as a result of this uncertainty and difficulties with cyclin E antibodies in murine cells, I focussed on other aspects of this project for the rest of my PhD.

Figure C8 (previous page): The α-cyclin E antibody E4 recognises an epitope found in cyclin E1-/- E2-/- cells. A) Images show E4 staining in WT MEF and cyclin E1-/- E2-/- cells with indicated E4 antibody lots or in the absence of primary antibody (no primary) in which only the secondary antibody was used. Staining as figure C2. Scale bar is 10 μm. B) Images show E4 staining using indicated concentrations of antibody. In all other immunofluorescence images a concentration of 1:100 (2μg/ml) was used. C) Western blot showing absence of 50 kDa doublet from cyclin E1-/- E2-/- sample using ab7959 antibody. Samples are total protein extracts from indicated cells. Histone H3 is shown as a loading control. D) Images show an absence of significant co-localisation between either E4 and CIZ1 (staining as figure 6.5) or E4 and CDK2 (E4 shown in green, Cdk2 shown in red, DNA counterstained with Hoechst 33258, shown in blue) for DNase treated cells. Scale bar is 10 μm.

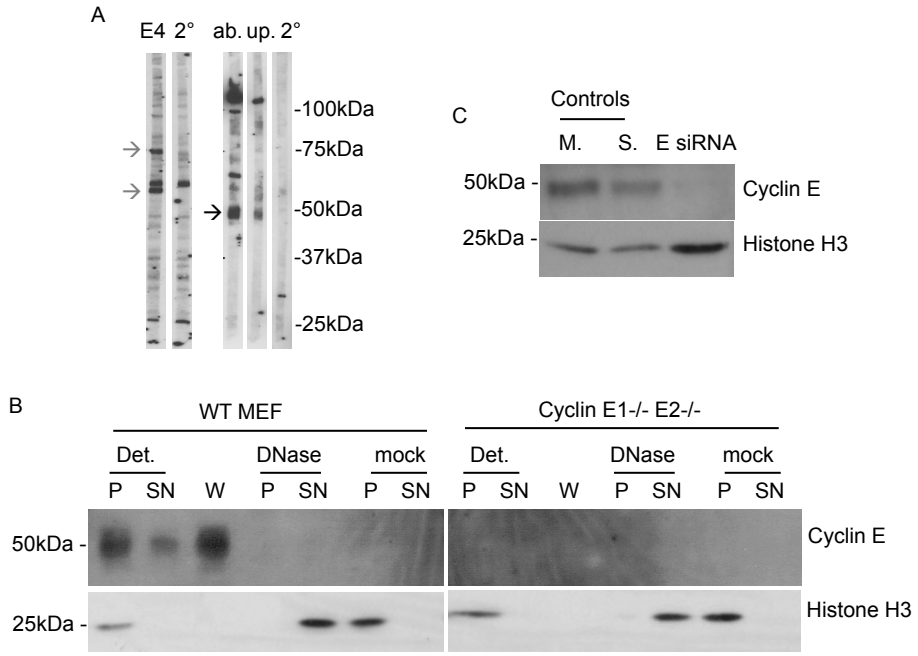

Figure C9: Comparison of α-cyclin E antibodies. A) Western blot strips show long exposures of band pattern from indicated antibodies or secondary antibody only controls (2º). Note absence of E4 specific 50kDa band unlike 50kDa doublet recognised by Abcam ab7959 (ab.) or Upstate 07-687 (up.) indicated by black arrow. Grey arrows mark E4 specific bands. Strips are total protein extracts from 3T3 cells. B) Western blot shows absence of 50kDa cyclin E band in cyclin E1-/- E2-/- cells and that cyclin E in WT MEF cells is detergent resistant but extracted with 0.5 M NaCl (W). For lane descriptions see materials and methods section 2.5.2. All lane contain cellular equivalents except detergent supernatant (Det. SN) which is two fold less. Histone H3 is shown as control for DNase extraction, remaining in the pellet without DNase extraction (mock) but extracted by DNase and present in DNase supernatant. C) Western blot shows absence of 50kDa cyclin E band from 3T3 cells treated with *cyclin E* siRNA (E siRNA) compared to cells treated with no siRNA, electroporation only (M.) or with scrambled *cyclin E* siRNA (S.). Samples are total protein extracts. Histone H3 is shown as loading control.

Discussion

The epitope recognised by E4 is a conditional NM factor. It is NM bound in 82 % of asynchronous 3T3 cells suggesting at least some level of cell cycle regulation. In support of this, the E4 epitope is present but not NM bound in quiescent cells. Surprisingly, the E4 epitope became recruited to the NM within 1 hour of release from quiescence, and this transition was independent of serum. This event is extremely early in terms of known steps that occur during cell cycle re-entry (fig C3 C), for example, R occurs at around 15 hours. In addition, data show it is independent of the cyclin D response to mitogens. Also, the percentage of cells that contained DNase resistant E4 epitope at 1 hour post-release was consistently higher than the percentage of cells that successfully entered S-phase (compare 84 %, with typical release reaching ~ 60 % of cells in S-phase by 24 hr, fig C3 C). This raises the possibility that the recruitment of the E4 epitope to the NM may be a very early step during the process of cell cycle re-entry and that other later steps occur with lower efficiency. Consistent with this, when cells were released into medium without serum the E4 epitope was recruited to the NM but these cells did not successfully enter S-phase. Despite satisfying a potential requirement for NM binding of the E4 epitope they cannot pass through R.

Identity of the E4 epitope

Cyclin E1-/- E2-/- mice were generated by deletion of cyclin E1 exons 2-11 and cyclin E2 exons 1-8 (Geng et al., 2003). As E4 was raised against 1-145 amino acids of cyclin E1, it is possible that the E4 specific signal seen in cyclin E1-/- E2-/- cells lies in exon 1 of cyclin E1. From examination of NCBI Reference Sequence NT_187034.1 (Mus musculus strain C57BL/6J chromosome 7 genomic contig, GRCm38.p1 C57BL/6J MMCHR7_CTG2), exon 1 appears to be 5 amino acids long (MPRER). Potentially this could exist as a fusion protein with the neomycin resistance gene product and thereby enter the nucleus. It would however, be extremely unlikely for the 5 amino acids from exon 1 to contain the epitope for E4 (considering the antibody was raised to a 145 amino acid fragment) and it is therefore, more likely that it recognises a protein either in addition to, or instead of, cyclin E.

A protein blast search of Swissprot database for *Mus musculus* proteins using the immunogen peptide for E4 (1-145aa of Hs cyclin E1) produced top hits of cyclin E1 and Cyclin E2 (table C2). Hits with E values of less than 0.1 are also shown. These hits all had query coverage of less than 32 % but this easily falls within the possible size for epitopes so these may all be considered potential candidates for the identity of the E4 epitope. In contrast, a blast search (same conditions) of *Mus musculus* cyclin E1 produces exclusively cyclins for the top 15 hits (hits with E values of less than 0.1 also shown, table C3). However, cyclins align to the central portion of cyclin E1, containing the conserved cyclin box fold domain, which begins at amino acid 143. Therefore, the identity of the E4 epitope appears unlikely to be another cyclin. It may be possible to identify the epitope by immunoprecipitating proteins that associate with E4, possibly in cyclin E1-/- E2-/- cells. However, as the E4 epitope is predominantly NM bound, this has proved difficult. I began experimentation in this area but decided to focus my time elsewhere.

Table C2: BLASTP hits (Altschul et al., 1997; Altschul et al., 2005) from E4 immunising peptide (Hs cyclin E1 1-145).

BLASTP Hit	Score	E-value
Cyclin E1	305	6e-107
Cyclin E2	55.8	5e-12
Cleavage stimulating factor	28.5	0.013
L-Myc-1	29.9	0.040
MAP7 domain-containing protein 3	26.6	0.056
C->U-editing enzyme APOBEC-1	25.8	0.076
STE20-like serine/threonine-protein kinase	26.2	0.080
Serine/threonine-protein kinase 10	26.2	0.086

Summary

Data presented here show that the 'α-cyclin E antibody' E4 cannot be used to generate reliable information about cyclin E as it most likely recognises another epitope either instead of, or in addition to, cyclin E. However, the location of the E4 epitope is interesting as it varies through the cell cycle and rebinds to the NM extremely early upon cell cycle re-entry.

Table C3: BLASTP hits (Altschul et al., 1997; Altschul et al., 2005) from cyclin E1 (Mus musculus sequence).

BLASTP Hit	Score	E-value
Cyclin E1	848	0.0
Cyclin E2	354	3e-122
Cyclin A2	111	4e-29
Cyclin A1	111	4e-29
Cyclin B2	93.2	7e-23
Cyclin B1	93.2	1e-22
Cyclin B3	79.7	6e-18
Cyclin D2	75.5	3e-17
Cyclin D3	73.6	1e-16
Cyclin D1	70.5	1e-15
Cyclin O	70.1	3e-15
Cyclin I	57.0	6e-11
Cyclin G2	49.3	2e-08
Cyclin F	42.4	4e-06
Cyclin G1	41.2	6e-06
Integrator complex subunit 9	30.4	0.022
tRNA-dihydrouridine(47) synthase [NAD(P)(+)]-like	29.6	0.032
Protein lifeguard 2	29.3	0.041
Trafficking protein particle complex subunit 10	29.3	0.054
Cleavage stimulation factor subunit 3	28.9	0.058
Spartin	28.5	0.081
Heparin cofactor 2	28.1	0.087
Cyclin-J-like protein	28.1	0.097

Appendix D

This draft manuscript is included, as the data within have been referenced in this thesis and have informed our understanding of nuclear matrix attachment in cancer and non-cancer cell lines. They therefore affected experimental choices and conclusions of the experiments presented within this thesis. This draft manuscript was assembled from data collected from a variety of Coverley lab members, including myself, and prepared by Dawn Coverley. We expect to publish these data but the form of the manuscript may change.

Dominant negative function of CIZ1 anchor domain uncouples CIZ1 and CDC6 from the nuclear matrix

Jennifer Munkley[1†], Rosemary H. C. Wilson[1], Emma Hesketh[1], Heather E. Sercombe[1], Elizabeth Klakus[1], Jennifer Southgate[1], Justin F-X. Ainscough[2], and Dawn Coverley[1*]

[1] Department of Biology, University of York, Heslington, York, UK, YO10 5DD
[2] School of Medicine, Leeds University, UK, LS2 9JT

Present address:
[†] Institute of Genetic Medicine, Newcastle University, Newcastle upon Tyne, NE1 3BZ.

* To whom correspondence should be addressed.
Tel: +44 (0)1904 328664; Email: dawn.coverley@york.ac.uk

Key words Nuclear matrix, CIZ1, DNA replication, Cancer.

Word count 5389 (whole manuscript)

Abstract CIZ1 promotes cyclin-dependent initiation of DNA replication via its N-terminal replication domain (RD). A nuclear matrix anchor domain (AD) immobilizes CIZ1 on the nuclear matrix in normal, differentiated cells, but neither AD nor recruitment to the nuclear matrix are essential for CIZ1 to promote DNA replication. We show that, like its interaction partner cyclin E, CIZ1 transitions from the soluble phase to the nuclear matrix during differentiation of murine embryonic stem cells, and that this coincides with complex changes in isoform expression. In cell-based assays recombinant AD interferes with attachment of endogenous CIZ1 to the nuclear matrix, revealing a dominant negative function that also impacts on nuclear matrix-recruitment of CDC6, a key component of the pre-replication complex. Notably, expression of CIZ1 is elevated in a panel of cancer cell lines, but RD and AD are uncoupled giving rise to excess RD protein that is not attached to the nuclear matrix. We suggest that release of CIZ1 RD from the nuclear matrix can be achieved in several ways, including the dominant negative action of AD and expression of isoforms that lack AD. Release may function to relax the spatial constraints normally imposed on initiation of DNA replication in the differentiated nucleus.

Introduction Duplication of the mammalian genome is initiated at thousands of DNA replication origins, whose selection and activation is coordinated with changing patterns of gene expression. Spatial and temporal regulation of DNA replication is underpinned by a dynamic, insoluble protein and RNA-rich framework, referred to as the nuclear matrix (NM) [1,2]. The NM has been implicated in the spatial organisation of DNA replication for nearly forty years [3-5], though analysis in a diverse array of cell types and by multiple methods has led to the emergence of a somewhat confusing picture (reviewed in [6]. However, it is now understood that components of the pre-replication complex (pre-RC) including CDC6 and ORC1 [7,8] and also virally-encoded DNA replication factors [9] can undergo transient, functional NM-association. Similarly, activities that limit initiation of DNA replication to S phase of the cell cycle have also been reported to function in association with the NM [10], while we showed directly that cyclin E, a regulator of pre-RC assembly [11,12], is stably recruited to the NM in normal differentiated somatic cells [13]. Moreover, using three independent experimental models of differentiation, we identified a solubility transition that appears to reflect a change in the structural organisation of DNA replication during cell specification. In undifferentiated, multi-potent cell types cyclin E is not immobilized by association with the NM, but becomes recruited in differentiated cells that have established an identity and associated transcriptional program [13]. This shift implies that initiation of DNA replication becomes spatially constrained as template usage is defined, suggesting that the NM may offer a platform on which pattern is established or a framework for its maintenance. Notably, cyclin E was not immobilized on the NM in a panel of cancer cell lines, suggesting that there are fundamental differences between 'normal' and cancer cells with respect to the spatial organisation of DNA replication. This also raises the possibility that the impact of deregulation of cyclin E on genome stability [14], and pre-RC assembly [15], may in part arise by overriding the organisation imposed by attachment to the NM.

Several proteins have been proposed as potential mediators between the NM and the pre-RC or other regulators of initiation, including MCM2 interacting protein AKAP95 [16], and Cip1-interacting zinc-finger protein 1 (CIZ1) [17,18]. Here we focus on the CIZ1 protein and show that it is not only a NM linker [19], but that variants of CIZ1 have the capacity to modulate the linkage, identifying a mechanism by which changes in anchorage, and potentially therefore in DNA replication pattern, may be effected. CIZ1 appears to function as a platform for cyclin exchange in late G1 phase and has been shown to interact directly with cyclin E and cyclin A through discrete RXL cyclin binding motifs which are essential for its ability to promote DNA replication *in vitro* [20]. These are encoded within exons 3-9, excluding exon 4 [21], which together make up the minimal N-terminal DNA replication domain (RD). Although normally spatially constrained via its C-terminal anchor domain (AD), encoded within exons 13-17 [19], immobilization on the NM is not essential

for the cyclin-dependent function of CIZ1 in initiation (13). Thus, CIZ1 is made up of at least two independent and separable functional domains, RD which promotes initation and AD which spatially constrains this activity. Importanatly, we find that RD and AD are not always expressed together and that in the panel of cancer cell lines we tested there exists excess unconstrained RD protein that is not immobilized on the NM.

Materials and methods

Cell culture and transfection: Cell lines were from ATCC or JCRB, and were cultured as recommended for less than 6 months from receipt, except HeLa cells and NIH3T3 cells which were obtained from R. Laskey, and T24/EJ, RT4 and RT112 cells which were characterised previously [22]. All experiments were performed with sub-confluent cells in the exponential phase of growth. NIH3T3 cells were grown as previously described [11], and transfected with GFP-CIZ1 or GFP-AD (also known as Cterm275 [19], using Amaxa nucleofector kit R. ES cells were cultured and differentiated as described previously [13].

Sub-cellular fractionation: Detergent-soluble and DNase1 soluble proteins were extracted from cells essentially as described [13]. Typically, cells on coverslips were rinsed with cold PBS then fixed with fresh 4% paraformaldehyde ('unextracted'), or washed with cold CSK buffer (10mM Pipes/KOH pH 6.8, 100mM NaCl, 1mM EGTA, 300mM sucrose, 1mM DTT, 0.1% TX100, with protease inhibitor cocktail), then fixed with 4% paraformaldehyde to generate 'detergent-treated' cells. For 'DNase treated' cells, coverslips were incubated in DNase1 buffer (10mM Tris [pH 7.6], 2.5mM $MgCl_2$, 0.5mM $CaCl_2$), for 20 min at 25 °C, as recommended by supplier (Roche) after CSK treatment and prior to fixation. For western blot analysis, fractionation was carried out as described [13], to generate a total cell lysate (T), a detergent pellet (Det. P) and a detergent-soluble supernatant (Det. SN) fraction. By further washing of the detergent pellet with CSK containing 0.5M NaCl, a salt wash (or 'w') fraction is generated, and further treatment of the pellet with DNase1, yields DNase1 P (nuclear matrix and nuclear matrix-bound proteins) and DNase1 SN (chromatin and chromatin bound proteins). Control incubation of Det. P in the absence of enzyme yields mock P and mock SN.

Immuno-detection: CIZ1-RD was detected with anti-CIZ1 polyclonal antibody 1793 raised against recombinant Nterm442 [17,19-21] and CIZ1-AD with polyclonal antibody 2C raised against CIZ1 AD sequences and affinity purified using peptide DEDEEEIEVEEELCKQVRSRDISR (Covalab). DNA was counterstained with Hoechst 33258 (Sigma). CDC6 was detected with sc9964 clone 180.2 (Santa Cruz), ORC4 with ab9641 (abcam), MCM2 with 610700 clone 46/BM28 (BD Transduction Laboratories), and histone H3 with ab179 (Abcam).

Imaging: Images were collected using a Zeiss Axiovert 200 M fitted with a 63x oil immersion objective, and Openlab image acquisition software, using identical exposure parameters within each experiment. Where images were digitally enhanced to remove background fluorescence or increase brightness using Adobe Photoshop, identical manipulations were applied within each experiment, so that the intensity of staining before and after extraction, and with and without transfection is accurately represented. Moreover, constant parameters were used to image different cell lines so that fluorescence intensity represents relative levels of CIZ1. No conclusions should be drawn about relative levels of CIZ1 RD and CIZ1 AD protein, due to possible differences in antibody affinities.

Quantitative RT-PCR: RNA from cell lines was isolated with Trizol (Invitrogen) and cDNA synthesized using Superscript III (Invitrogen) and random hexamers (Promega). Primers and probes used to quantitate CIZ1 RD and AD were described previously [23]. These were primers 13/14 with a probe in exon 7 (RD) and 6/7 with a probe in exon 16 (AD). Relative expression was calculated using the comparative Ct method (2-ΔΔCt). Results were normalised to actin and expressed relative to normal cells as indicated.

Results Analysis of *CIZ1* splice variants using genome-wide expression data indicates considerable transcript diversity, with at least 6 of its 17 exons subject to regulated alternative splicing in humans [24] and mouse [25]. Aceview (accessed on 4/4/13) annotates at least 25 possible translated isoforms but in most cases combinations of splicing events are unconfirmed, and represent the minimal non-redundant assemblies. Exclusion of complete or partial exons has been reported to be associated with disease states but, although impact on protein localization is documented for some, their effect on cellular function is not known [21,23,24,26-28]. Here we show that, like its interaction partner cyclin E [13], CIZ1 is recruited to the DNase1 and high-salt resistant NM fraction upon induction of differentiation in murine embryonic stem (ES) cells (Fig. 1A). However unlike cyclin E, this transition in immobilisation is accompanied by complex changes in isoform expression, revealed by a change in the protein species reactive with polyclonal antibody 1793 (raised against recombinant CIZ1 RD [17]. Notably only two of these isoforms are detected in the NM fraction, with the rest being extracted at different stages of NM isolation. Similar sized isoforms to those detected in the NM fraction in differentiated ES cells are observed in NIH3T3 cells, and one is retained in the NM fraction after extraction (Fig. 1B) [19]. This is observed in sub-nuclear foci after removal of chromatin (Fig. 1C), indicating a spatial arrangement maintained by attachment to the NM. NIH3T3 cells are used in subsequent experiments to investigate immobilization of CIZ1.

Our previous analysis showed that NM attachment is mediated by domains encoded in the C-terminal third of full-length CIZ1 referred to as Cterm275 [19] or anchor domain (AD, [23], though notably this fragment is not sufficient to specify the focal patterning seen with endogenous CIZ1 or full-length recombinant GFP-CIZ1 [17]. Moreover others have reported a contribution to NM binding from sequences encoded by exon 8 [26] which is outside of this region, suggesting that aggregation into nuclear foci may be a complex process that involves more than one immobilization event. Here we show that AD possesses a potent dominant negative capability that interferes with assembly of recombinant GFP-CIZ1 into sub-nuclear foci, while leaving intact its ability to form detergent and high salt-resistant attachments (Fig. 2B). Moreover, within 24 hours of transfection, GFP-AD causes displacement of endogenous CIZ1 foci from the NM (Fig. 2C, D). While endogenous CIZ1 foci remain in the nucleus and intact (albeit against a diffusely stained background that is not present in control cells), extraction with DNase1 reveals that they are no longer attached to the NM and are instead depleted along with chromatin (Fig. 2D). This suggests that sequences encoded within GFP-AD can act to disengage previously formed NM attachments, and might therefore have the capability to facilitate a resetting or remodelling process.

As well as CIZ1 and cyclin E, some of the proteins that play a direct role in initiation of DNA replication as part of the pre-RC are also partially or transiently associated with the NM. This has been reported for ORC1, part of the six subunit origin recognition complex, which appears to support transient NM recruitment of the rest of the ORC complex in G1 phase [8,29], for CDC6 during G1 or early S-phase but not in G2/M [7], and for CDT1 in G1 phase but not S or G2/M [9]. For the mini-chromosome maintenance (MCM) complex the published evidence is not yet convincing. What is emerging clearly from the literature (reviewed in [30], is that reports differ depending on the cell type in which the analysis is carried out. This prompted us to undertake a small survey of a representative set of cell lines derived from tumours and from non-tumour tissue, looking at NM recruitment of CDC6 and MCM2 in asynchronous populations of cells by western blot. Overall, we find that in four cancer cell lines none of these factors are evident in the NM fraction (Table 1), whereas in four non-cancer cell lines at least one of them is detectable, though often only as a small fraction of the total cellular compliment (Table 1 and Fig. 3A). This is consistent with previous reports that support the idea that the pre-RC is normally transiently associated with the NM around the time of initiation of DNA replication, though contrary to the majority of published data which tends to report only on the dominant insoluble fraction, or is carried out in cancer cells. As with our analysis of cyclin E [13] and CIZ1 (below), the partitioning of these pre-RC components suggests a fundamental difference between cancer and non-cancer cells, and is consistent with the idea that the compartment in which they exert their function in DNA replication may be compromised or blocked in the cancer cell nucleus.

Using CDC6 in NIH3T3 cells as a clear and robust output, we tested the effect of CIZ1 AD on NM immobilization of the pre-RC. Transfection with GFP vector had no impact on the location or extractability of CDC6, with DNase 1-resistant protein evident in the nucleus of the late G1/early S phase fraction of a cycling population of cells (21%, Fig. 3B upper panels). However, GFP-AD rendered the nuclear CDC6 in these cells sensitive to extraction (0%, Fig. 3B, lower panels). These findings were confirmed by western blot (Fig. 3C). Thus, the dominant negative effect that CIZ1 AD has on NM attachment of endogenous CIZ1 also applies to CDC6, and possibly therefore the sub-nuclear compartment in which the pre-RC exerts its function in initiation of DNA replication.

Detachment of CDC6 from the NM had no gross effect on cell cycle profile after 24 hours (Fig. 3D). The absence of any detectable effect on S phase progression argues that NM recruitment is not a requirement for initiation or elongation, and is consistent with the facts that i) CIZ1 can promote initiation *in vitro* in the absence of AD [17], and ii) none of the components we have studied (cyclin E, CIZ1, pre-RC) appear to be immobilized in cancer cells. We suggest that the functional consequence of NM attachment is not in facilitating

the initiation process itself, but in maintaining and stabilizing genome configurations within a cell lineage, effectively hardwiring it for its chosen purpose.

Consistent with the idea that immobilization of initiation of DNA replication on the NM is not an obligate function, CIZ1 is not immobilized in cancer cells. Using the RD-specific antibody 1793 [17] we observed a consistent pattern of expression and sub-cellular localization in a panel of cancer cells, that is fundamentally different to cells derived from normal tissues. In normal cells, including human Wi38 (Fig.4A), MRC5, HFL1 and IMR90 (not shown), NIH3T3 (Fig. 1B) and mouse ES cells induced to differentiate *in vitro* (Fig. 1A), a large proportion of RD fractionates with the DNase1-resistant NM, and resides almost exclusively in sub-nuclear foci. However, in all seven cancer cell lines tested, RD protein was highly over-represented compared to non-cancer cells (Fig. 4A); shown for HeLa (cervical carcinoma), H727 (lung carcinoid) and T24/EJ (urothelial cancer) cells. Similar results were obtained for SBC5 (neuroendocrine lung cancer), U2OS (osteosarcoma), and RT4, RT112 (urothelial cancer). More importantly, in the cancer cells RD protein is not anchored to the NM (Fig. 4A, B), and is instead susceptible to extraction with DNase1, either completely (example T24/EJ cells) or leaving behind a small fraction comparable to the total amount in normal cells (example HeLa). Thus, in the cancer cell lines there exists a large pool of CIZ1 RD that is not constrained by attachment to the NM.

Despite this failure to attach to DNase1-resistant structures, the AD domain of CIZ1 is in fact expressed in these cancer cell lines and can be detected with domain-specific antibody 2C, raised against a peptide encoded by exon 14 (Fig. 5A). Critically under conditions where RD protein is fully extracted (for example EJ cells), AD remains immobilized on the NM, indicating that it is present under some circumstances in a form that is uncoupled from RD. This is direct evidence of uncoupled domain expression. Furthermore in contrast to RD, AD protein levels are broadly similar between these example cancer and normal cell lines (Fig. 5B, C) again implying regulation that is independent from RD. Consistent with this protein level information, at the transcript level AD and RD are similarly expressed in non-cancer cells, but are elevated and strikingly uneven in most of the cancer cell lines (Fig. 5D). Thus, uncoupled domain expression also occurs at the transcript level. Transcripts that skip internal sequences that encode RD are notable amongst *CIZ1* expressed sequence tags isolated from tumour tissue (for example BE300131, BF306155, BU538884), suggesting that aberrant splicing may be driving imbalanced expression in the tumour context.

Discussion Despite many of the same players, the specification of replication origins is fundamentally different in higher and lower eukaryotes. In yeast, specific DNA sequences

identify origins of replication from which surrounding DNA is duplicated. In higher eukaryotic cells, replication origins are less precisely defined by DNA sequence, with context having an apparently greater influence. At the simplest level this means chromatin conformation, including epigenetic modification of DNA or associated proteins. However in spatial terms, 'context' may well be specified by the functional relationship between chromatin and the NM. There is also a dichotomy in the mechanism of origin selection during *Xenopus* embryogenesis, where a shift occurs at the mid-blastula transition from frequent, random initiation events at short intervals, to fewer events with preference for particular sites [31]. Our previous analysis of the immobilization of cyclin E in the developing *Xenopus* embryo mirrors this transition [13], and suggests that initiation of DNA replication becomes immobilized on the NM around the time when more precise selection criteria begin to specify origins. Normally in somatic cells initiation from individual origins progresses with a defined spatial and temporal pattern, and in higher eukaryotes there is a strong relationship between this and gene expression [32], or transcription factor binding [33]. If this pattern is maintained by immobilization on the NM, failure to attach could have a chronic destabilizing effect which impacts on the epigenetic control of gene expression.

The picture that emerges from the data presented here, and from the published evidence, is that CIZ1 plays a role in initiation of DNA replication by acting as both a NM anchor and a coordinator of cyclin function at the pre-RC. This has important implications for the spatial organisation of DNA replication and the mechanism by which pattern is stabilised. We suggest that the changes in CIZ1 expression that we have observed in cancer cell lines would give rise to spatially unconstrained DNA replication, and possibly therefore a pathogenic failure to stabilize cell-type specific genome configurations. We already know that RD has the capacity to promote DNA replication when not attached to the NM, because truncated forms that lack AD can function *in vitro* and are actually more effective than CIZ1 forms that posses NM interaction domains, indicating that immobilization is a constraining feature rather than one that is intrinsic to function [17]. Therefore, expression of excess unconstrained RD in tumours could support cyclin-mediated functions at locations that are not specified by attachment to the NM. Notably, the impact of excess AD could be very similar to that of excess RD. When NM-binding domains are expressed in the context of a protein that cannot support cyclin recruitment, such a protein could compete for docking sites on the NM. The present analysis suggests that this may in fact be the case and that CIZ1 AD possesses a dominant negative capability that impinges not only on CIZ1 itself but also the pre-RC. This capability offers a mechanism by which recruitment of replication origins might be regulated during normal differentiation, offering flexibility to detach and re-establish attachments with an altered configuration.

Acknowledgments We would like to thank E. Greaves, G. Higgins, and are grateful to Phil Roberts for graphics.

Funding This work was supported by The Biotechnology and Biological Sciences Research Council, UK (JM, HES, RHCW), the Lister Institute of Preventive Medicine (EK), Yorkshire Cancer Research (EH). JS is funded by York Against Cancer and JA by the British Heart Foundation.

References

1 Belgrader, P., Siegel, A. J. & Berezney, R. A comprehensive study on the isolation and characterization of the HeLa S3 nuclear matrix. *J Cell Sci* **98 (Pt 3)**, 281-291, (1991).

2 Jackson, D. A., Dickinson, P. & Cook, P. R. Attachment of DNA to the nucleoskeleton of HeLa cells examined using physiological conditions. *Nucleic Acids Res* **18**, 4385-4393, (1990).

3 Berezney, R. & Coffey, D. S. Nuclear protein matrix: association with newly synthesized DNA. *Science* **189**, 291-293, (1975).

4 Dijkwel, P. A., Mullenders, L. H. & Wanka, F. Analysis of the attachment of replicating DNA to a nuclear matrix in mammalian interphase nuclei. *Nucleic Acids Res* **6**, 219-230, (1979).

5 Razin, S. V., Kekelidze, M. G., Lukanidin, E. M., Scherrer, K. & Georgiev, G. P. Replication origins are attached to the nuclear skeleton. *Nucleic Acids Res* **14**, 8189-8207, (1986).

6 Wilson, R. H. & Coverley, D. Relationship between DNA replication and the nuclear matrix. *Genes Cells* **18**, 17-31, (2013).

7 Fujita, M., Ishimi, Y., Nakamura, H., Kiyono, T. & Tsurumi, T. Nuclear organization of DNA replication initiation proteins in mammalian cells. *J Biol Chem* **277**, 10354-10361, (2002).

8 Ohta, S., Tatsumi, Y., Fujita, M., Tsurimoto, T. & Obuse, C. The ORC1 cycle in human cells: II. Dynamic changes in the human ORC complex during the cell cycle. *J Biol Chem* **278**, 41535-41540, (2003).

9 Ohsaki, E., Suzuki, T., Karayama, M. & Ueda, K. Accumulation of LANA at nuclear matrix fraction is important for Kaposi's sarcoma-associated herpesvirus replication in latency. *Virus Res* **139**, 74-84, (2009).

10 Radichev, I., Parashkevova, A. & Anachkova, B. Initiation of DNA replication at a nuclear matrix-attached chromatin fraction. *J Cell Physiol* **203**, 71-77, (2005).

11 Coverley, D., Laman, H. & Laskey, R. A. Distinct roles for cyclins E and A during DNA replication complex assembly and activation. *Nature Cell Biology* **4**, 523-528, (2002).

12 Geng, Y. *et al.* Cyclin E ablation in the mouse. *Cell* **114**, 431-443, (2003).

13 Munkley, J. *et al.* Cyclin E is recruited to the nuclear matrix during differentiation, but is not recruited in cancer cells. *Nucleic Acids Res* **39**, 2671-2677, (2011).

14 Spruck, C. H., Won, K.-A. & Reed, S. I. Deregulated cyclin E induces chromosome instability. *Nature* **401**, 297-300, (1999).

15 Ekholm-Reed, S. *et al.* Deregulation of cyclin E in human cells interferes with prereplication complex assembly. *J Cell Biol* **165**, 789-800, (2004).

16 Eide, T. *et al.* Protein kinase A-anchoring protein AKAP95 interacts with MCM2, a regulator of DNA replication. *J Biol Chem* **278**, 26750-26756, (2003).

17 Coverley, D., Marr, J. & Ainscough, J. F.-X. Ciz1 promotes mammalian DNA replication. *J.Cell Sci.* **118**, 101-112, (2005).

18 Mitsui, K., Matsumoto, A., Ohtsuka, S., Ohtsubo, M. & Yoshimura, A. Cloning and characterization of a novel $P21^{Cip1/Waf1}$ interacting zinc finger protein, Ciz1. *Biochemical and Biophysical Research Communications* **264**, 457-464, (1999).

19 Ainscough, J. F. *et al.* C-terminal domains deliver the DNA replication factor Ciz1 to the nuclear matrix. *J Cell Sci* **120**, 115-124, (2007).

20 Copeland, N. A., Sercombe, H. E., Ainscough, J. F. & Coverley, D. Ciz1 cooperates with cyclin-A-CDK2 to activate mammalian DNA replication in vitro. *J Cell Sci* **123**, 1108-1115, (2010).

21 Rahman, F. A., Ainscough, J. F.-X., Copeland, N. & Coverley, D. Cancer-associated missplicing of exon 4 influences the subnuclear distribution of the DNA replication factor Ciz1. *Human Mutation* **28**, 993-1004, (2007).

22 Southgate, J., Proffitt, J., Roberts, P., Smith, B. & Selby, P. Loss of cyclin-dependent kinase inhibitor genes and chromosome 9 karyotypic abnormalities in human bladder cancer cell lines. *British journal of cancer* **72**, 1214-1218, (1995).

23 Higgins, G. *et al.* Variant Ciz1 is a circulating biomarker for early-stage lung cancer. *Proc Natl Acad Sci U S A*, (2012).

24 Rahman, F. A., Aziz, N. & Coverley, D. Differential detection of alternatively spliced variants of Ciz1 in normal and cancer cells using a custom exon-junction microarray. *BMC cancer* **10**, 482, (2010).

25 Greaves, E. A., Copeland, N. A., Coverley, D. & Ainscough, J. F. Cancer-associated variant expression and interaction of CIZ1 with cyclin A1 in differentiating male germ cells. *J Cell Sci* **125**, 2466-2477, (2012).

26 Dahmcke, C. M., Buchmann-Moller, S., Jensen, N. A. & Mitchelmore, C. Altered splicing in exon 8 of the DNA replication factor CIZ1 affects subnuclear distribution and is associated with Alzheimer's disease. *Molecular and cellular neurosciences* **38**, 589-594, (2008).

27 Warder, D. E. & Keherly, M. J. Ciz1, Cip1 interacting zinc finger protein 1 binds the consensus DNA sequence ARYSR(0-2)YYAC. *Journal of Biomedical Science* **10**, 406-417, (2003).

28 Xiao, J. *et al.* Mutations in CIZ1 cause adult onset primary cervical dystonia. *Ann Neurol* **71**, 458-469, (2012).

29 Tatsumi, Y., Tsurimoto, T., Shirahige, K., Yoshikawa, H. & Obuse, C. Association of human origin recognition complex 1 with chromatin DNA and nuclease-resistant nuclear structures. *J Biol Chem* **275**, 5904-5910, (2000).

30 Wilson, R. H. & Coverley, D. Relationship between DNA replication and the nuclear matrix. *Genes Cells*, (2012).

31 Mechali, M. DNA replication origins: from sequence specificity to epigenetics. *Nature reviews. Genetics* **2**, 640-645, (2001).

32 Schubeler, D. *et al.* Genome-wide DNA replication profile for Drosophila melanogaster: a link between transcription and replication timing. *Nat Genet* **32**, 438-442, (2002).

33 Danis, E. *et al.* Specification of a DNA replication origin by a transcription complex. *Nat Cell Biol* **6**, 721-730, (2004).

Figure legends

Fig. 1 CIZ1 is associated with the nuclear matrix in differentiating mouse ES and NIH3T3 cells. A) Western blot of protein fractions derived from murine ES cells before and after differentiation, showing total CIZ1 (T), the proportion that is detergent-resistant (P) and detergent soluble (SN), the products released by a salt wash (w) of the detergent-resistant pellet, prior to digestion with DNase 1 (P, SN), or mock incubation in the absence of DNase 1 (P, SN). The extent of histone H3 released into the DNase 1 SN fraction shows the efficiency of chromatin digestion. CIZ1 is detected with antibody 1793 [17]. Evidence of the differentiation status of these samples was published previously [13]. B) Western blot shows similar analysis for NIH3T3 cells, and images show CIZ1 (red) in unextracted nuclei and after extraction to reveal detergent-resistant or DNase 1-resistant CIZ1, as indicated. Nuclei are counterstained with H33258 (blue). Bar is 10 μm.

Fig. 2 Dominant negative activity of CIZ1 anchor domain. A) Representation of CIZ1, showing exons that encode the fragment used to raise polyclonal antibody 1793 (red), domains that code for DNA replication activity (RD, [17,20], nuclear matrix anchor domain (AD), and two putative nuclear localization sequences predicted by http://wolfpsort.org/ (black stars). The fragment referred to as GFP-AD is shown below (also known as C-term 275 [19]. B) Histograms show the proportion of NIH3T3 cells with nuclear fluorescence (± SEM) after transfection with GFP-CIZ1, GFP-AD or equivalent amounts of each as a co-transfection for 24 hours. 'U' refers to cells that were not extracted prior to fixation, 'Det' refers to cells with detergent-resistant GFP in the nucleus. 'D' denotes defuse pattern and 'F' (red columns) denotes focal pattern. 'S' refers to cells with 0.5 M NaCl-resistant GFP in the nucleus. Images show pattern of nuclear fluorescence after extraction with detergent in individual nuclei at high resolution (upper panels) and in populations of cells. DNA is blue, bar is 10 μm. C) Immunofluorescence analysis of CIZ1 (red, detected with 1793), after transfection with GFP-AD or GFP control, and extraction with detergent or DNase 1 as indicated. DNA is blue. Note the lack of DNase-resistant CIZ1 nuclear foci in cells transfected with GFP-AD. D) High-magnification images of endogenous CIZ1 in cells transfected and extracted as indicated. Bar is 2 μM.

Fig. 3 CIZ1 anchor domain displaces endogenous CDC6 from the nuclear matrix. A) Western blots showing subcellular fractionation of three normal tissue-derived cell lines, and the location of pre-replication complex proteins CDC6 and MCM2. Histone H3 is shown as a control for DNase 1 digestion. Summary results for these and other cell lines are given in Table 1. Labels are defined in Fig.1. B) CDC6 (red) in NIH3T3 cells 24 hours after transfection with GFP-AD or GFP alone (green), after extraction with detergent or DNase 1, as indicated. Nuclei are blue. Bar is 10 μm. The proportion of cells with

DNase1-resistant CDC6 falls from 21% to 0% in cells transfected with GFP-AD. C) Western blot showing the behaviour of the detergent-resistant fraction of CDC6 after extraction with DNase 1, in NIH3T3 cells without and with expression of ectopic GFP-AD as indicated. D) Flow cytometry showing DNA profile of NIH3T3 cells transfected with GFP-AD or GFP, after staining with propidium iodide as described previously [17].

Fig. 4 Cancer cells contain CIZ1 replication domain (RD) that is not immobilized on the nuclear matrix. A) Representative immunofluorescence images of CIZ1 RD (red, detected with 1793) in three cancer cell lines showing total protein in unextracted cells, and antigen remaining after removal of the soluble fraction (Detergent) and chromatin-bound fraction (DNase). A non-cancer lung cell line (WI38) is shown for comparison. DNA is stained with Hoechst 33258 (blue). Bar is 10 μm. Images were collected under identical conditions, so that within and between cell lines the intensity of CIZ1 and DNA reflects the levels remaining in the cell. These cancer cell lines and four others (not shown) contain excess CIZ1 that is not attached to the nuclear matrix. B) Western blot analysis of fractionated cancer cells as described in Fig. 1. Histone H3 is shown as a control for DNase 1 digestion, and the nuclear matrix fraction is indicated.

Fig. 5 Cancer cells express CIZ1 anchor domain that is immobilized on the nuclear matrix. A) Representation of CIZ1 showing the location of the antigenic peptide used to generate anchor domain antibody 2C (green), and two qRT-PCR primer/probe sets in exons 6/7 (red) and exon 16 (green). B) Immunofluorescence images of CIZ1 AD (green, detected with 2C) in two cancer cell lines showing total protein in unextracted cells, and antigen remaining after removal of the soluble fraction (Detergent) and chromatin-bound fraction (DNase). DNA is stained with Hoechst 33258 (blue). Bar is 10 μm. C) Similar analysis of non-cancer line WI38. Anchor domain is present and immobilized to some extent in all cell lines. D) Relative quantification of *CIZ1* RD (red) and *CIZ1* AD transcripts (green), after normalization to actin and calibration to RD in normal cell line Asf1, which is given an arbitrary value of 1. Analysis was performed in triplicate and is shown ± SEM. E) Ways in which uncoupled expression of CIZ1 RD and AD could influence the sub-nuclear localization of its DNA replication activity. The model assumes that nuclear matrix-associated docking sites are limiting, so that uncoupled AD blocks assembly of CIZ1 on the nuclear matrix.

Cell Line (Non-cancer)	Protein	Det. resistant	0.5M NaCl resistant	DNase resistant
ARPE19	CDC6			
	MCM2			
	Cyclin E			
MRC5	CDC6	ND	ND	ND
	MCM2			
	Cyclin E	ND	ND	ND
MCF10a	CDC6			
	MCM2			
	Cyclin E	ND	ND	ND
3T3	CDC6			
	MCM2			
	Cyclin E			

Cell Line (Cancer)	Protein	Det. resistant	0.5M NaCl resistant	DNase resistant
HeLa	CDC6			
	MCM2			
	Cyclin E			
EJ	CDC6			
	MCM2			
	Cyclin E			
H727	CDC6			
	MCM2			
	Cyclin E			
LNCaP	CDC6			
	MCM2			
	Cyclin E			

	high		medium		low		None

Table 1 The location of pre-RC components CDC6 and MCM2, in sub-cellular fractions generated from cancer cell lines (HeLa; cervical carcinoma, EJ; bladder cancer, H727; lung carcinoid, LNCAP; prostate cancer) and non-cancer cell lines (ARPE19, MCF10a, MRC5, 3T3), using the western blot protocol used in Figs. 1, 3, 4. The proportion of protein in key fractions is indicated by the key and is shown in relation to signal intensity in the total fraction (whole cell lysate). 'Chromatin' refers to protein detected in the DNase1 supernatant, and 'nuclear matrix' refers to protein in the DNase1 pellet fraction. Cyclin E results are partly taken from [13]. ND is not determined.

Fig. 1

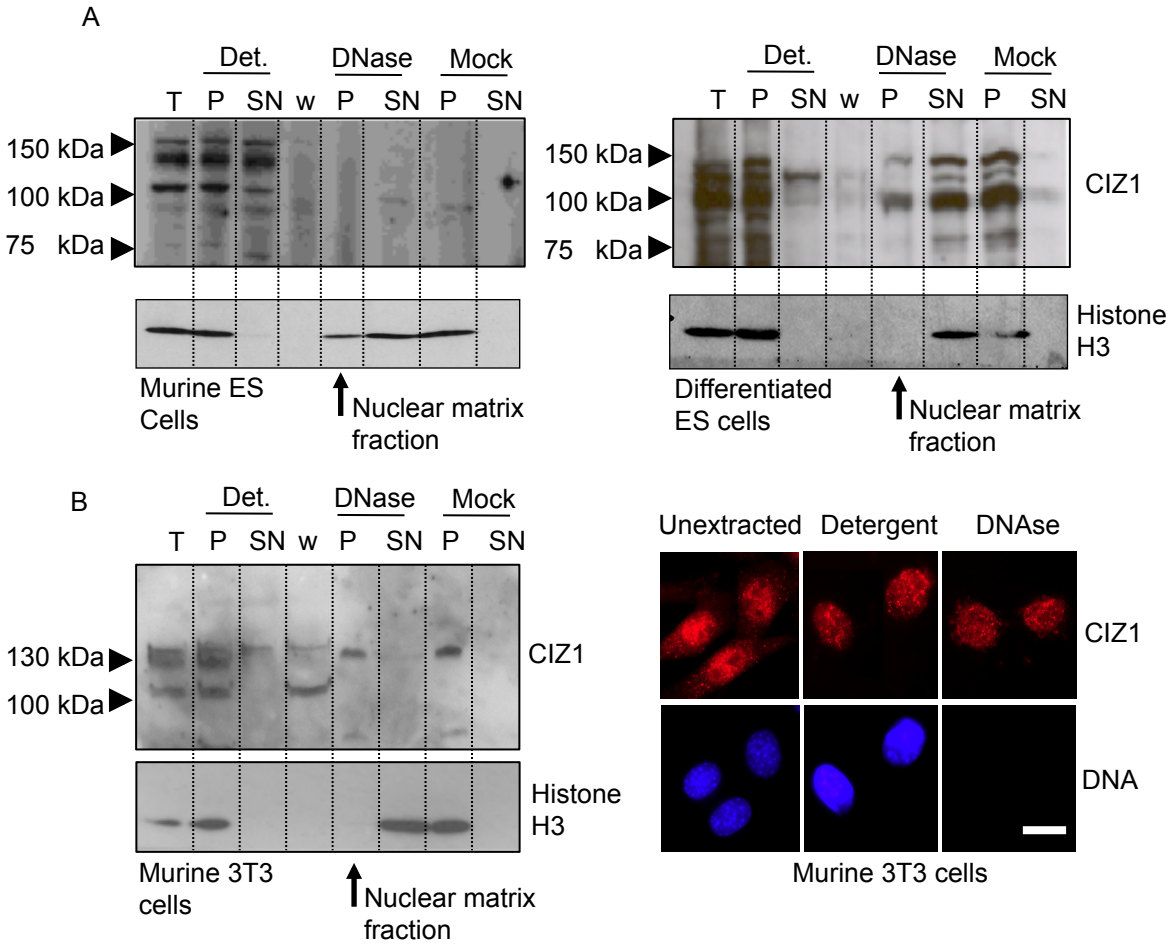
A
Det.
DNase
Mock
T P SN w P SN P SN
150 kDa
100 kDa
75 kDa
Histone H3
Murine ES Cells
Nuclear matrix fraction
Differentiated ES cells
CIZ1
B
130 kDa
100 kDa
Murine 3T3 cells
Unextracted
Detergent
DNAse
DNA
Murine 3T3 cells

Fig. 2

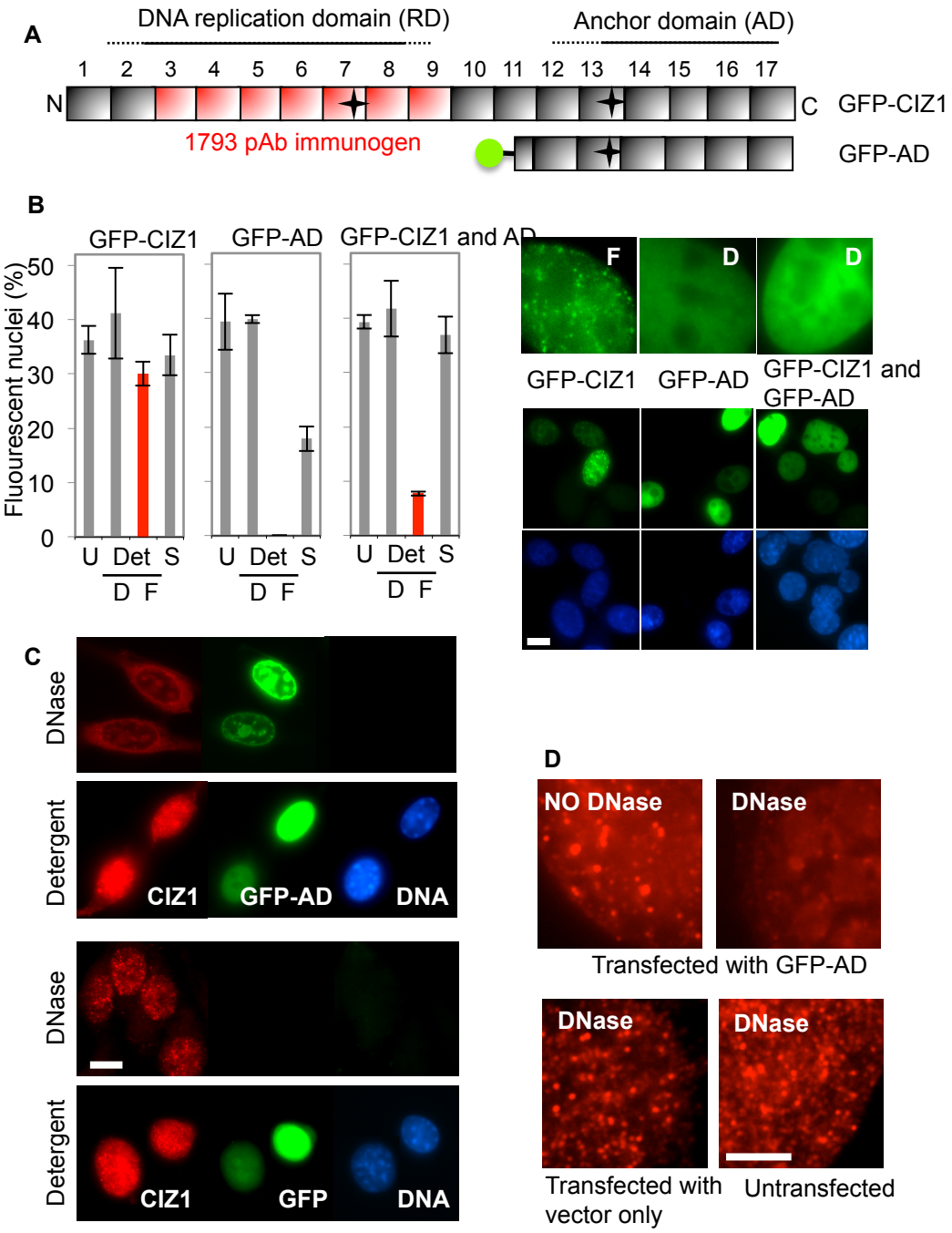
A
DNA replication domain (RD)
Anchor domain (AD)
1 2 3 4 5 6 7 8 9 10 11 12 13 14 15 16 17
N
C
GFP-CIZ1
1793 pAb immunogen
GFP-AD
B
GFP-CIZ1
GFP-AD
GFP-CIZ1 and AD
Fluorescent nuclei (%)
0 10 20 30 40 50
U Det S
D F
F
D
D
GFP-CIZ1
GFP-AD
GFP-CIZ1 and GFP-AD
C
DNase
Detergent
CIZ1
GFP-AD
DNA
DNase
Detergent
CIZ1
GFP
DNA
D
NO DNase
DNase
Transfected with GFP-AD
DNase
DNase
Transfected with vector only
Untransfected

Fig. 3

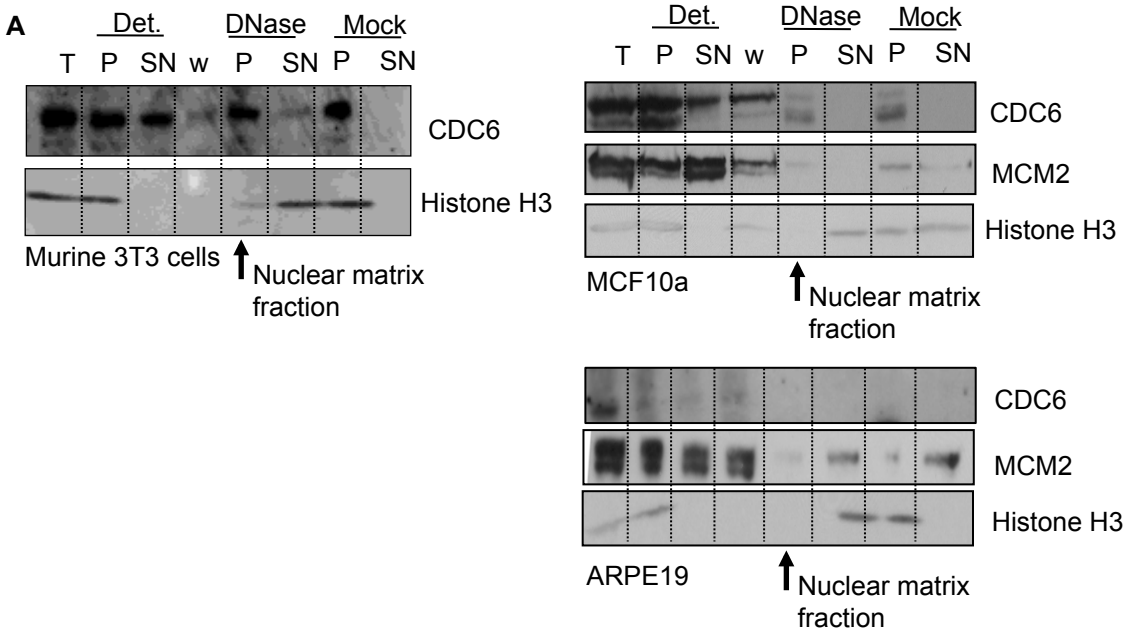
A
Det.
DNase
Mock
T P SN w P SN P SN
CDC6
Histone H3
Murine 3T3 cells
Nuclear matrix fraction
Det.
DNase
Mock
T P SN w P SN P SN
CDC6
MCM2
Histone H3
MCF10a
Nuclear matrix fraction
CDC6
MCM2
Histone H3
ARPE19
Nuclear matrix fraction

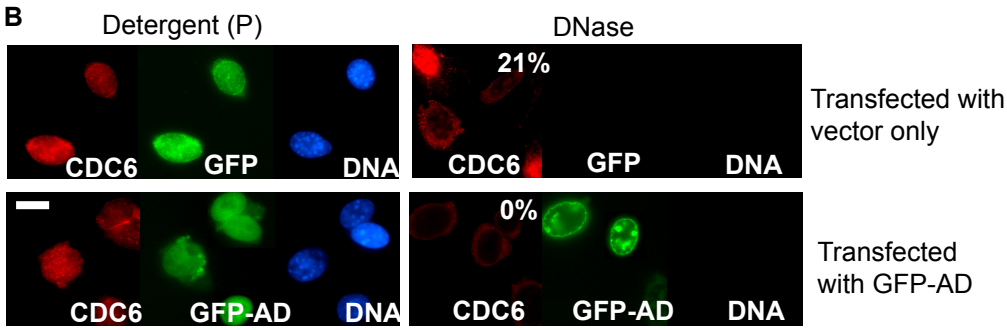
B
Detergent (P)
DNase
21%
CDC6
GFP
DNA
Transfected with vector only
0%
CDC6
GFP-AD
DNA
Transfected with GFP-AD

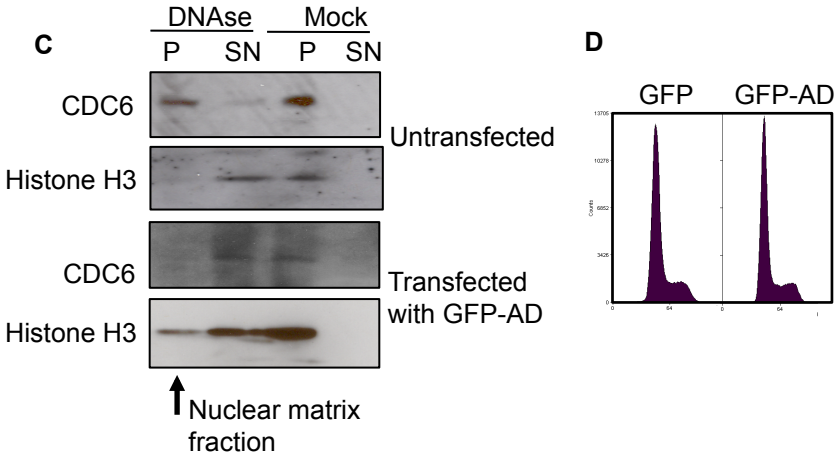
C
DNAse
Mock
P SN P SN
CDC6
Histone H3
Untransfected
CDC6
Histone H3
Transfected with GFP-AD
Nuclear matrix fraction
D
GFP
GFP-AD

Fig. 4

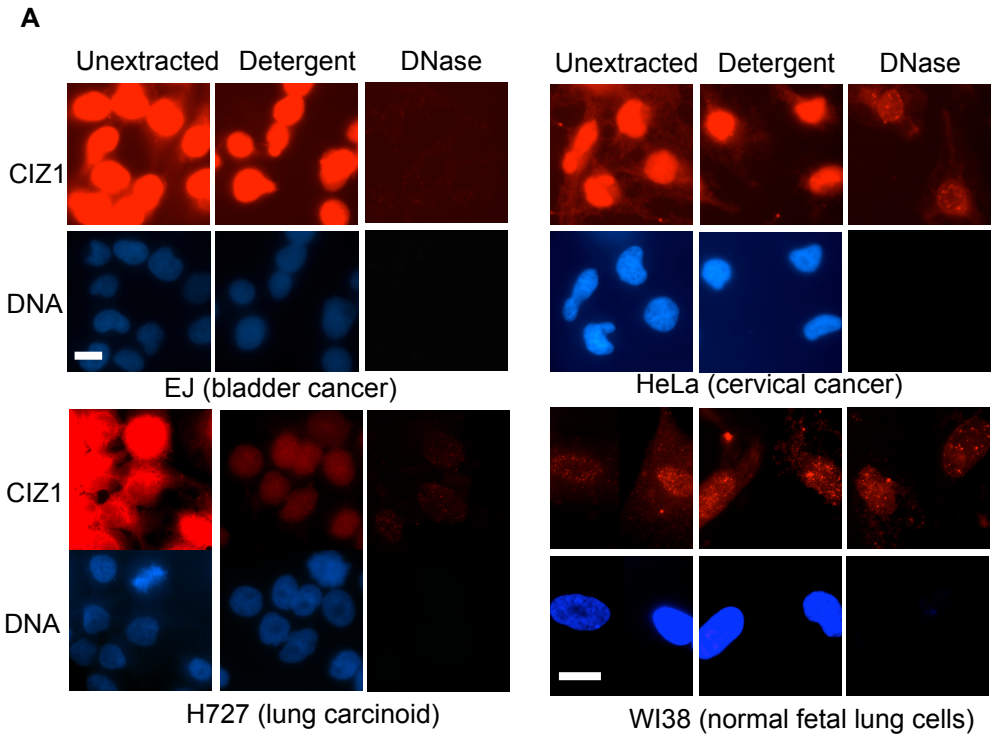
A
Unextracted
Detergent
DNase
CIZ1
DNA
EJ (bladder cancer)
HeLa (cervical cancer)
H727 (lung carcinoid)
WI38 (normal fetal lung cells)

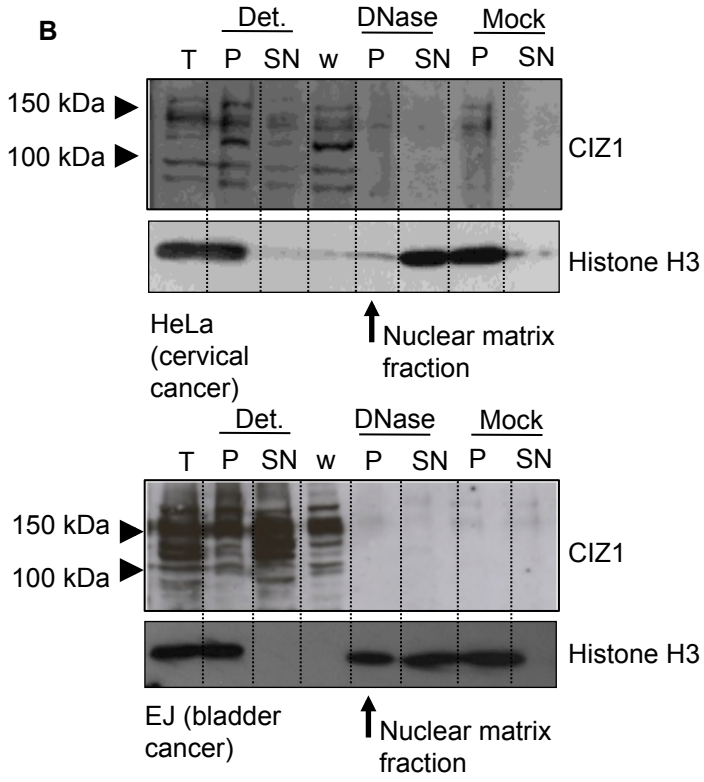
B
Det.
DNase
Mock
T P SN w P SN P SN
150 kDa
100 kDa
CIZ1
Histone H3
HeLa (cervical cancer)
Nuclear matrix fraction
EJ (bladder cancer)

Fig. 5

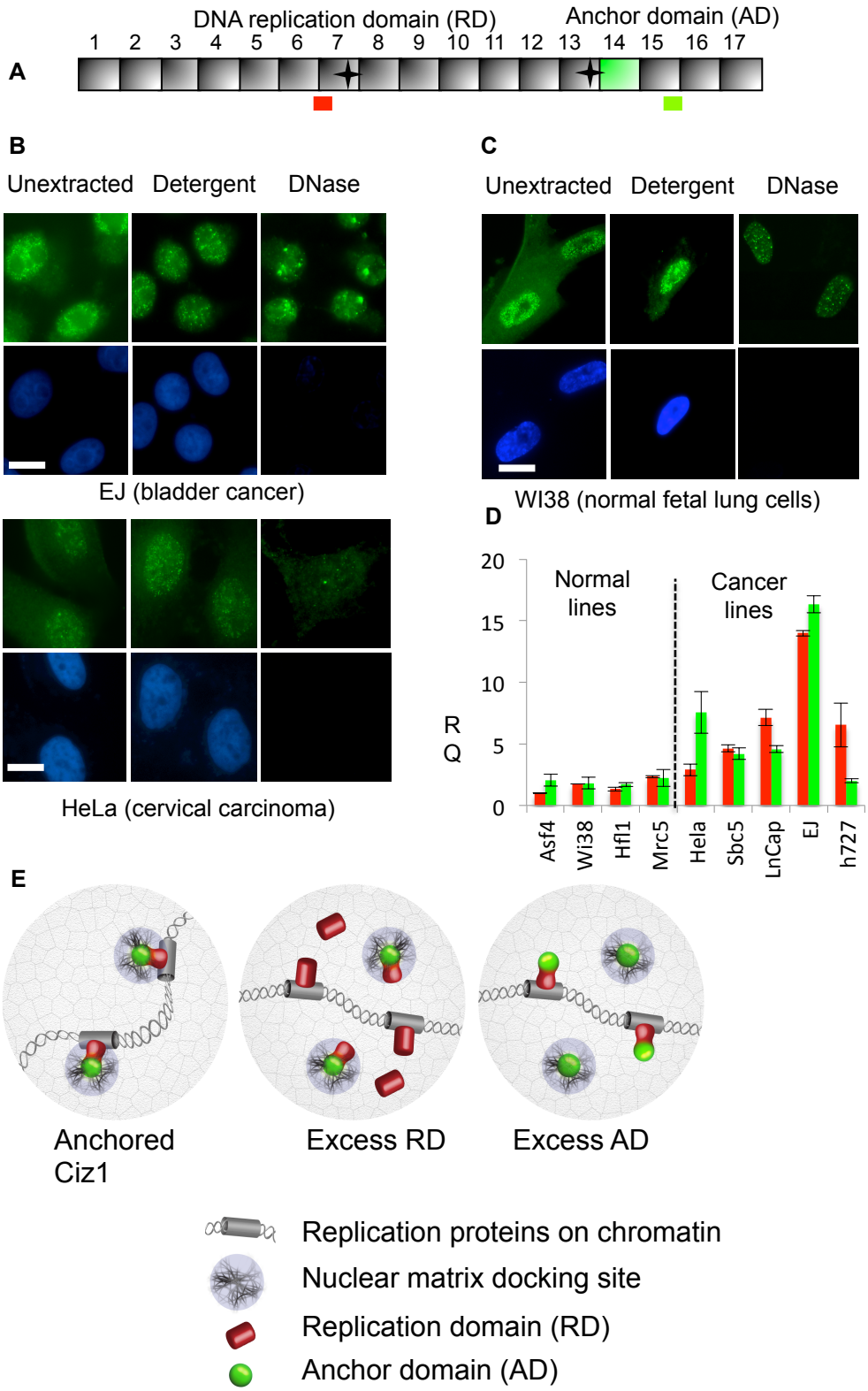
A
DNA replication domain (RD)
Anchor domain (AD)
1 2 3 4 5 6 7 8 9 10 11 12 13 14 15 16 17
B
Unextracted Detergent DNase
EJ (bladder cancer)
HeLa (cervical carcinoma)
C
Unextracted Detergent DNase
WI38 (normal fetal lung cells)
D
RQ
Normal lines
Cancer lines
Asf4 Wi38 Hfl1 Mrc5 Hela Sbc5 LnCap EJ h727
E
Anchored Ciz1
Excess RD
Excess AD
Replication proteins on chromatin
Nuclear matrix docking site
Replication domain (RD)
Anchor domain (AD)

Abbreviations

°C	degrees centigrade
3C	chromosome conformation capture
A	adenine
AB	antibody buffer
AD	acidic domain
AD	anchor domain of CIZ1, EGFP-CIZ1 C-term274
ANOVA	analysis of variance
AoAF	primary aortic adventitial fibroblasts
APS	ammonium persulphate
ARS	autonomous replication sequence
ATCC	American Tissue Culture Collection
ATM	ataxia telangiectasia mutated protein
ATR	ataxia telangiectasia and Rad3-related protein
bp	base-pairs
BrdU	5-bromo-2'-deoxyuridine
BSA	bovine serum albumin
CAK	CDK-activating kinase
CAPS	N-cyclohexyl-3-aminopropanesulfonic acid
CDC6	cell division cycle 6
CDK	cyclin-dependent kinase
CDKi	CDK-dependent kinase inhibitor
CDT1	chromatin licensing and DNA replication factor 1
CHO	Chinese Hamster Ovary
CIN	chromosomal instability
CIP	CDK-interacting protein
CIZ1	$p21^{CIP1}$-interacting zinc finger protein
cm	centimetres
CSK	cytoskeletal buffer
Cy	cyclin binding motif
DAPI	4',6-diamidino-2-phenylindole
DDK	Dbf4-dependent kinase
DDR	DNA damage response

dH_2O	distilled H_2O
DEPC	diethylpyrocarbonate treated
DHFR	dihydrofolate reductase
DLC1	dynein light chain 1
DMEM	Dulbecco's modified Eagle's medium
DMSO	dimethyl sulphoxide
DNp53	dominant negative p53
dNTP	deoxyribonucleotide triphosphate
D-PBS	Dulbecco's phosphate buffered saline
DSB	double strand break
DTT	dithiothreitol
E1	cyclin E1 (*ccne1*)
E2	cyclin E2 (*ccne2*)
EDTA	ethylenediaminetetraacetic acid
EdU	5-ethynyl-2'-deoxyuridine
EGF	epidermal growth factor
EGTA	ethylene glycol tetraacetic acid
EM	electron micrographs
EMEM	Eagle's modified essential medium
ER	oestrogen receptor
ERH	enhancer of rudimentary homologue
ESC	embryonic stem cell
ESI	electron spectroscopic imaging
EST	expressed sequence tag
EtBr	ethidium bromide
FBS	fetal bovine sera
FISH	Fluorescence *In Situ* Hybridisation
FITC	fluorescein isothiocyanate
G	guanine
G0	quiescence
G1	growth 1 phase
$G1^M$	G1 occurring directly after mitosis
$G1^Q$	G1 occurring after release from quiescence
G2	growth 2 phase
HIM	Halo Intensity Macro

hnRNPs	heterogeneous nuclear ribonucleoproteins
HPLC	high-performance liquid chromatography
HPV	Human papilloma virus
hr	hours
HRP	horseradish peroxidase
INK4	inhibitor of CDK4
JCRB	Japanese Collection of Research Biosciences Cell Bank
kbp	kilobase-pairs
kDa	kilodalton
KO	knock-out
KSFM	keratinocyte serum free medium
LIS	lithium 3,5-diiodosalicylate
M	mitosis
MAR	matrix attachment region
MARBP	S/MAR binding protein
Mb	megabases
MCM	mini-chromosome maintenance (complex)
MEF	mouse embryonic fibroblast
MEM	minimum essential medium
MFHR	maximum fluorescence halo radius
MH3	matrin 3 domain
min	minutes
ms	milliseconds
MSC	mesenchymal stem cell
NEAA	non-essential amino acids
NHU	normal human urothelial cell
NLS	nuclear localisation sequence
NM	nuclear matrix
NMPdb	Nuclear Matrix Protein database
O/N	overnight
ODP	origin decision point
ORC	origin recognition complex
PBS	phosphate buffered saline
PCNA	proliferating cell nuclear antigen
PEF	primary mouse embryonic fibroblast

PFA	paraformaldehyde
PI	protease inhibitor tablet
PMSF	phenylmethanesulfonylfluoride
pre-IC	pre-initiation complex
pre-RC	pre-replication complex
PSG	penicillin streptomycin glutamine
QD	glutamine rich domain
qRT-PCR	quantitative real-time polymerase chain reaction
R	restriction point
RB	retinoblastoma protein
RC	replication complex
REC	retinal endothelial cells
RN	residual nucleus
RNAi	RNA interference
ROI	region of interest
rpm	revolutions per minute
RPMI	Roswell Park Memorial Institute medium 1640
RT	room temperature
S	DNA synthesis phase
s	seconds
SAF-A	scaffold attachment factor A
SAF-B	scaffold attachment factor B
SAR	scaffold attached region
SATB1	special AT-rich sequence-binding protein-1
SDS	sodium dodecyl sulphate
shRNA	small hairpin RNA
siRNA	small interfering RNA
S/MAR	scaffold, skeleton or matrix attached region
SSB	single strand break
T	thymidine
TBS	tris buffered saline
TDP	timing decision point
TEMED	tetramethylethylenediamine
TIGM	Texas A&M Institute for Genomic Medicine
TRITC	tetramethylrhodamine isothiocyanate

TTF	tail tip fibroblast
Tx-100	triton X-100
UTR	untranslated region
UV	ultra violet
v/v	volume per volume
w/v	weight per volume
WT	wild type
ZF	zinc finger

References

Ainscough, J.F., Rahman, F.A., Sercombe, H., Sedo, A., Gerlach, B., and Coverley, D. (2007). C-terminal domains deliver the DNA replication factor Ciz1 to the nuclear matrix. J Cell Sci *120*, 115-124.

Allen, C.D., Okada, T., and Cyster, J.G. (2007). Germinal-center organization and cellular dynamics. Immunity *27*, 190-202.

Altschul, S.F., Madden, T.L., Schaffer, A.A., Zhang, J., Zhang, Z., Miller, W., and Lipman, D.J. (1997). Gapped BLAST and PSI-BLAST: a new generation of protein database search programs. Nucleic Acids Res *25*, 3389-3402.

Altschul, S.F., Wootton, J.C., Gertz, E.M., Agarwala, R., Morgulis, A., Schaffer, A.A., and Yu, Y.K. (2005). Protein database searches using compositionally adjusted substitution matrices. FEBS J *272*, 5101-5109.

Alva-Medina, J., Dent, M.A., and Aranda-Anzaldo, A. (2010). Aged and post-mitotic cells share a very stable higher-order structure in the cell nucleus in vivo. Biogerontology *11*, 703-716.

Alva-Medina, J., Maya-Mendoza, A., Dent, M.A., and Aranda-Anzaldo, A. (2011). Continued stabilization of the nuclear higher-order structure of post-mitotic neurons in vivo. PLoS ONE *6*, e21360.

Aranda-Anzaldo, A., and Dent, M.A. (1997). Loss of DNA loop supercoiling and organization in cells infected by herpes simplex virus type 1. Research in virology *148*, 397-408.

Assoian, R.K., and Zhu, X. (1997). Cell anchorage and the cytoskeleton as partners in growth factor dependent cell cycle progression. Curr Opin Cell Biol *9*, 93-98.

Bagnell, R. (2011). Comet Assay. http://wwwmeduncedu/microscopy/resources/imagej-plugins-and-macros/comet-assay, Accessed 11th January 2013.

Baldin, V., Lukas, J., Marcote, M.J., Pagano, M., and Draetta, G. (1993). Cyclin D1 is a nuclear protein required for cell cycle progression in G1. Genes Dev *7*, 812-821.

Bartek, J., and Lukas, J. (2003). Chk1 and Chk2 kinases in checkpoint control and cancer. Cancer Cell *3*, 421-429.

Bartkova, J., Horejsi, Z., Koed, K., Kramer, A., Tort, F., Zieger, K., Guldberg, P., Sehested, M., Nesland, J.M., Lukas, C.*, et al.* (2005). DNA damage response as a candidate anti-cancer barrier in early human tumorigenesis. Nature *434*, 864-870.

Bauer, D.E., Harris, M.H., Plas, D.R., Lum, J.J., Hammerman, P.S., Rathmell, J.C., Riley, J.L., and Thompson, C.B. (2004). Cytokine stimulation of aerobic glycolysis in hematopoietic cells exceeds proliferative demand. Faseb J *18*, 1303-1305.

Bell, S.P., and Dutta, A. (2002). DNA replication in eukaryotic cells. Annu Rev Biochem *71*, 333-374.

Benyajati, C., and Worcel, A. (1976). Isolation, characterization, and structure of the folded interphase genome of Drosophila melanogaster. Cell *9*, 393-407.

Berezney, R., and Buchholtz, L.A. (1981). Dynamic association of replicating DNA fragments with the nuclear matrix of regenerating liver. Exp Cell Res *132*, 1-13.

Berezney, R., and Coffey, D.S. (1974). Identification of a nuclear protein matrix. Biochem Biophys Res Commun *60*, 1410-1417.

Berezney, R., Dubey, D.D., and Huberman, J.A. (2000). Heterogeneity of eukaryotic replicons, replicon clusters, and replication foci. Chromosoma *108*, 471-484.

Berrios, M., Osheroff, N., and Fisher, P.A. (1985). In situ localization of DNA topoisomerase II, a major polypeptide component of the Drosophila nuclear matrix fraction. Proc Natl Acad Sci U S A *82*, 4142-4146.

Berthet, C., Aleem, E., Coppola, V., Tessarollo, L., and Kaldis, P. (2003). Cdk2 knockout mice are viable. Curr Biol *13*, 1775-1785.

Bian, Q., and Belmont, A.S. (2012). Revisiting higher-order and large-scale chromatin organization. Curr Opin Cell Biol *24*, 359-366.

Bickmore, W.A., and Oghene, K. (1996). Visualizing the spatial relationships between defined DNA sequences and the axial region of extracted metaphase chromosomes. Cell *84*, 95-104.

Bito, T., Ueda, M., Ito, A., and Ichihashi, M. (1997). Less expression of cyclin E in cutaneous squamous cell carcinomas than in benign and premalignant keratinocytic lesions. Journal of cutaneous pathology *24*, 305-308.

Bloom, J., and Cross, F.R. (2007). Multiple levels of cyclin specificity in cell-cycle control. Nature Reviews Molecular Cell Biology *8*, 149-160.

Blow, J.J. (2001). Control of chromosome DNA replication in the early *Xenopus* embryo. EMBO J *20*, 3293-3297.

Bode, J., Benham, C., Ernst, E., Knopp, A., Marschalek, R., Strick, R., and Strissel, P. (2000). Fatal connections: when DNA ends meet on the nuclear matrix. J Cell Biochem Suppl *Suppl 35*, 3-22.

Boos, D., Frigola, J., and Diffley, J.F. (2012). Activation of the replicative DNA helicase: breaking up is hard to do. Curr Opin Cell Biol *24*, 423-430.

Booth, C., Harnden, P., Trejdosiewicz, L.K., Scriven, S., Selby, P.J., and Southgate, J. (1997). Stromal and vascular invasion in an human in vitro bladder cancer model. Lab Invest *76*, 843-857.

Bortner, D.M., and Rosenberg, M.P. (1997). Induction of mammary gland hyperplasia and carcinomas in transgenic mice expressing human cyclin E. Mol Cell Biol *17*, 453-459.

Boulikas, T. (1995). Chromatin domains and prediction of MAR sequences. Int Rev Cytol *162A*, 279-388.

Bridger, J.M., Boyle, S., Kill, I.R., and Bickmore, W.A. (2000). Re-modelling of nuclear architecture in quiescent and senescent human fibroblasts. Curr Biol *10*, 149-152.

Brooks, S.C., Locke, E.R., and Soule, H.D. (1973). Estrogen receptor in a human cell line (MCF-7) from breast carcinoma. J Biol Chem *248*, 6251-6253.

Buchkovich, K., Duffy, L.A., and Harlow, E. (1989). The retinoblastoma protein is phosphorylated during specific phases of the cell cycle. Cell *58*, 1097-1105.

Buongiorno-Nardelli, M., Micheli, G., Carri, M.T., and Marilley, M. (1982). A relationship between replicon size and supercoiled loop domains in the eukaryotic genome. Nature *298*, 100-102.

Burhans, W.C., and Weinberger, M. (2007). DNA replication stress, genome instability and aging. Nucleic Acids Res *35*, 7545-7556.

Burkhart, R., Schulte, D., Hu, B., Musahl, C., Gohring, F., and Knippers, R. (1995). Interactions of human nuclear proteins P1Mcm3 and P1Cdc46. Eur J Biochem *228*, 431-438.

Bustany, S., Tchakarska, G., and Sola, B. (2011). Cyclin D1 regulates p27(Kip1) stability in B cells. Cell Signal *23*, 171-179.

Cai, S., and Kohwi-Shigematsu, T. (1999). Intranuclear relocalization of matrix binding sites during T cell activation detected by amplified fluorescence in situ hybridization. Methods (San Diego, Calif *19*, 394-402.

Cailleau, R., Olive, M., and Cruciger, Q.V. (1978). Long-term human breast carcinoma cell lines of metastatic origin: preliminary characterization. In vitro *14*, 911-915.

Capco, D.G., Wan, K.M., and Penman, S. (1982). The nuclear matrix: three-dimensional architecture and protein composition. Cell *29*, 847-858.

Cayrol, C., and Ducommun, B. (1998). Interaction with cyclin-dependent kinases and PCNA modulates proteasome-dependent degradation of p21. Oncogene *17*, 2437-2444.

Cayrou, C., Coulombe, P., and Mechali, M. (2010). Programming DNA replication origins and chromosome organization. Chromosome Res *18*, 137-145.

Cayrou, C., Coulombe, P., Vigneron, A., Stanojcic, S., Ganier, O., Peiffer, I., Rivals, E., Puy, A., Laurent-Chabalier, S., Desprat, R.*, et al.* (2011). Genome-scale analysis of metazoan replication origins reveals their organization in specific but flexible sites defined by conserved features. Genome Res *21*, 1438-1449.

Chavali, P.L., Funa, K., and Chavali, S. (2011). Cis-regulation of microRNA expression by scaffold/matrix-attachment regions. Nucleic Acids Res *39*, 6908-6918.

Chen, G., and Li, G. (2010). Increased Cul1 expression promotes melanoma cell proliferation through regulating p27 expression. Int J Oncol *37*, 1339-1344.

Chiaradonna, F., Sacco, E., Manzoni, R., Giorgio, M., Vanoni, M., and Alberghina, L. (2006). Ras-dependent carbon metabolism and transformation in mouse fibroblasts. Oncogene *25*, 5391-5404.

Coller, H.A. (2007). What's taking so long? S-phase entry from quiescence versus proliferation. Nat Rev Mol Cell Biol *8*, 667-670.

Coller, H.A., Sang, L., and Roberts, J.M. (2006). A new description of cellular quiescence. PLoS Biol *4*, e83.

Cook, J.G., Chasse, D.A., and Nevins, J.R. (2004). The regulated association of Cdt1 with minichromosome maintenance proteins and Cdc6 in mammalian cells. J Biol Chem *279*, 9625-9633.

Cook, J.G., Park, C.-H., Burke, T., Leone, G., DeGregori, J., Engel, A., and Nevins, J. (2002). Analysis of Cdc6 function in the assembly of mammalian prereplication complexes. Proc Natl Acad Sci USA *99*, 1347-1352.

Cook, P.R. (1999). The organization of replication and transcription. Science *284*, 1790-1795.

Copeland, N.A., Sercombe, H.E., Ainscough, J.F., and Coverley, D. (2010). Ciz1 cooperates with cyclin-A-CDK2 to activate mammalian DNA replication in vitro. J Cell Sci *123*, 1108-1115.

Courbet, S., Gay, S., Arnoult, N., Wronka, G., Anglana, M., Brison, O., and Debatisse, M. (2008). Replication fork movement sets chromatin loop size and origin choice in mammalian cells. Nature *455*, 557-560.

Coverley, D., Laman, H., and Laskey, R.A. (2002). Distinct roles for cyclins E and A during DNA replication complex assembly and activation. Nature Cell Biology *4*, 523-528.

Coverley, D., Marr, J., and Ainscough, J. (2005). Ciz1 promotes mammalian DNA replication. J Cell Sci *118*, 101-112.

Coverley, D., Pelizon, C., Trewick, S., and Laskey, R.A. (2000). Chromatin bound Cdc6 persists in S and G2 phases in human cells, while soluble Cdc6 is destroyed in a cyclin A-cdk2 dependent process. J Cell Sci *113*, 1929-1938.

Craig, J.M., Boyle, S., Perry, P., and Bickmore, W.A. (1997). Scaffold attachments within the human genome. J Cell Sci *110 (Pt 21)*, 2673-2682.

Cremer, T., Cremer, M., Dietzel, S., Muller, S., Solovei, I., and Fakan, S. (2006). Chromosome territories--a functional nuclear landscape. Curr Opin Cell Biol *18*, 307-316.

Dahmcke, C.M., Buchmann-Moller, S., Jensen, N.A., and Mitchelmore, C. (2008). Altered splicing in exon 8 of the DNA replication factor CIZ1 affects subnuclear distribution and is associated with Alzheimer's disease. Molecular and cellular neurosciences *38*, 589-594.

Darzynkiewicz, Z., Gong, J., Juan, G., Ardelt, B., and Traganos, F. (1996). Cytometry of cyclin proteins. Cytometry *25*, 1-13.

de Belle, I., Cai, S., and Kohwi-Shigematsu, T. (1998). The genomic sequences bound to special AT-rich sequence-binding protein 1 (SATB1) in vivo in Jurkat T cells are tightly associated with the nuclear matrix at the bases of the chromatin loops. J Cell Biol *141*, 335-348.

den Hollander, P., and Kumar, R. (2006). Dynein light chain 1 contributes to cell cycle progression by increasing cycling-dependent kinase 2 activity in estrogen-stimulated cells. Cancer Research *66*, 5941-5949.

den Hollander, P., Rayala, S.K., Coverley, D., and Kumar, R. (2006). Ciz1, a novel DNA-binding coactivator of the estrogen receptor α, confers hypersensitivity to estrogen action. Cancer Research *66*, 11021-11030.

DePamphilis, M.L. (2003). The 'ORC cycle': a novel pathway for regulating eukaryotic DNA replication. Gene *310*, 1-15.

Diffley, J.F. (2011). Quality control in the initiation of eukaryotic DNA replication. Philos Trans R Soc Lond B Biol Sci *366*, 3545-3553.

Diffley, J.F., and Labib, K. (2002). The chromosome replication cycle. J Cell Sci *115*, 869-872.

Dimitrova, D.S., Prokhorova, T.A., Blow, J.J., Todorov, I.T., and Gilbert, D.M. (2002). Mammalian nuclei become licensed for DNA replication during late telophase. J Cell Sci *115*, 51-59.

Djeliova, V., Russev, G., and Anachkova, B. (2001a). Distribution of DNA replication origins between matrix-attached and loop DNA in mammalian cells. J Cell Biochem *80*, 353-359.

Djeliova, V., Russev, G., and Anachkova, B. (2001b). Dynamics of association of origins of DNA replication with the nuclear matrix during the cell cycle. Nucleic Acids Res *29*, 3181-3187.

Dou, Q.P., Pardee, A.B., and Keyomarsi, K. (1996). Cyclin E -- a better prognostic marker for breast cancer than cyclin D? Nature medicine *2*, 254.

Dutta, A., Chandra, R., Leiter, L.M., and Lester, S. (1995). Cyclins as markers of tumor proliferation: immunocytochemical studies in breast cancer. Proc Natl Acad Sci U S A *92*, 5386-5390.

Edwards, M.C., Tutter, A.V., Cvetic, C., Gilbert, C.H., Prokhorova, T.A., and Walter, J.C. (2002). MCM2-7 complexes bind chromatin in a distributed pattern surrounding the origin recognition complex in Xenopus egg extracts. J Biol Chem *277*, 33049-33057.

Ekholm, S.V., Zickert, P., Reed, S.I., and Zetterberg, A. (2001). Accumulation of cyclin E is not a prerequisite for passage through the restriction point. Mol Cell Biol *21*, 3256-3265.

Ekholm-Reed, S., Mendez, J., Tedesco, D., Zetterberg, A., Stillman, B., and Reed, S.I. (2004a). Deregulation of cyclin E in human cells interferes with prereplication complex assembly. J Cell Biol *165*, 789-800.

Ekholm-Reed, S., Spruck, C.H., Sangfelt, O., van Drogen, F., Mueller-Holzner, E., Widschwendter, M., Zetterberg, A., and Reed, S.I. (2004b). Mutation of hCDC4 leads to cell cycle deregulation of cyclin E in cancer. Cancer Res *64*, 795-800.

Emmerich, J., Meyer, C.A., de la Cruz, A.F., Edgar, B.A., and Lehner, C.F. (2004). Cyclin D does not provide essential Cdk4-independent functions in Drosophila. Genetics *168*, 867-875.

Erlandsson, F., Wahlby, C., Ekholm-Reed, S., Hellstrom, A.C., Bengtsson, E., and Zetterberg, A. (2003). Abnormal expression pattern of cyclin E in tumour cells. Int J Cancer *104*, 369-375.

Erlanson, M., Portin, C., Linderholm, B., Lindh, J., Roos, G., and Landberg, G. (1998). Expression of cyclin E and the cyclin-dependent kinase inhibitor p27 in malignant lymphomas-prognostic implications. Blood *92*, 770-777.

Evans, K., Ott, S., Hansen, A., Koentges, G., and Wernisch, L. (2007). A comparative study of S/MAR prediction tools. BMC Bioinformatics *8*, 71.

Evans, T., Rosenthal, E.T., Youngblom, J., Distel, D., and Hunt, T. (1983). Cyclin: a protein specified by maternal mRNA in sea urchin eggs that is destroyed at each cleavage division. Cell *33*, 389-396.

Fero, M.L., Rivkin, M., Tasch, M., Porter, P., Carow, C.E., Firpo, E., Polyak, K., Tsai, L.H., Broudy, V., Perlmutter, R.M*., et al.* (1996). A syndrome of multiorgan hyperplasia with features of gigantism, tumorigenesis, and female sterility in p27(Kip1)-deficient mice. Cell *85*, 733-744.

Flickinger, R.A., Givens, R., Pine, S., and Sepanik, P. (1986). Factors controlling the size of DNA loops in frog embryos and Friend erythroleukemia cells. Cell differentiation *19*, 59-71.

Fox, C.J., Hammerman, P.S., and Thompson, C.B. (2005). Fuel feeds function: energy metabolism and the T-cell response. Nat Rev Immunol *5*, 844-852.

Frauwirth, K.A., Riley, J.L., Harris, M.H., Parry, R.V., Rathmell, J.C., Plas, D.R., Elstrom, R.L., June, C.H., and Thompson, C.B. (2002). The CD28 signaling pathway regulates glucose metabolism. Immunity *16*, 769-777.

Frouin, I., Montecucco, A., Spadari, S., and Maga, G. (2003). DNA replication: a complex matter. EMBO Rep *4*, 666-670.

Fu, M., Rao, M., Bouras, T., Wang, C., Wu, K., Zhang, X., Li, Z., Yao, T.P., and Pestell, R.G. (2005). Cyclin D1 inhibits peroxisome proliferator-activated receptor gamma-mediated adipogenesis through histone deacetylase recruitment. J Biol Chem *280*, 16934-16941.

Fu, M., Wang, C., Li, Z., Sakamaki, T., and Pestell, R.G. (2004). Minireview: Cyclin D1: normal and abnormal functions. Endocrinology *145*, 5439-5447.

Fudenberg, G., and Mirny, L.A. (2012). Higher-order chromatin structure: bridging physics and biology. Curr Opin Genet Dev *22*, 115-124.

Fuge, E.K., Braun, E.L., and Werner-Washburne, M. (1994). Protein synthesis in long-term stationary-phase cultures of Saccharomyces cerevisiae. Journal of bacteriology *176*, 5802-5813.

Fujita, M. (1999). Cell cycle regulation of DNA replication initiation proteins in mammalian cells. Front Biosci *4*, D816-823.

Fujita, M., Ishimi, Y., Nakamura, H., Kiyono, T., and Tsurumi, T. (2002). Nuclear organization of DNA replication initiation proteins in mammalian cells. J Biol Chem *277*, 10354-10361.

Fujita, M., Kiyono, T., Hayashi, Y., and Ishibashi, M. (1997). In vivo interaction of human MCM heterohexameric complexes with chromatin. Possible involvement of ATP. J Biol Chem *272*, 10928-10935.

Fujita, M., Yamada, C., Goto, H., Yokoyama, N., Kuzushima, K., Inagaki, M., and Tsurumi, T. (1999). Cell cycle regulation of human CDC6 protein. Intracellular localization, interaction with the human mcm complex, and CDC2 kinase-mediated hyperphosphorylation. J Biol Chem *274*, 25927-25932.

Funes, J.M., Quintero, M., Henderson, S., Martinez, D., Qureshi, U., Westwood, C., Clements, M.O., Bourboulia, D., Pedley, R.B., Moncada, S.*, et al.* (2007). Transformation of human mesenchymal stem cells increases their dependency on oxidative phosphorylation for energy production. Proc Natl Acad Sci U S A *104*, 6223-6228.

Geng, Y., Lee, Y.M., Welcker, M., Swanger, J., Zagozdzon, A., Winer, J.D., Roberts, J.M., Kaldis, P., Clurman, B.E., and Sicinski, P. (2007). Kinase-independent function of cyclin E. Mol Cell *25*, 127-139.

Geng, Y., Whoriskey, W., Park, M.Y., Bronson, R.T., Medema, R.H., Li, T., Weinberg, R.A., and Sicinski, P. (1999). Rescue of cyclin D1 deficiency by knockin cyclin E. Cell *97*, 767-777.

Geng, Y., Yu, Q., Sicinska, E., Das, M., Schneider, J.E., Bhattacharya, S., Rideout, W.M., Bronson, R.T., Gardner, H., and Sicinski, P. (2003). Cyclin E ablation in the mouse. Cell *114*, 431-443.

Gerdes, M.G., Carter, K.C., Moen, P.T., Jr., and Lawrence, J.B. (1994). Dynamic changes in the higher-level chromatin organization of specific sequences revealed by in situ hybridization to nuclear halos. J Cell Biol *126*, 289-304.

Gerner, C., Gotzmann, J., Frohwein, U., Schamberger, C., Ellinger, A., and Sauermann, G. (2002). Proteome analysis of nuclear matrix proteins during apoptotic chromatin condensation. Cell Death Differ *9*, 671-681.

Getzenberg, R.H. (1994). Nuclear matrix and the regulation of gene expression: tissue specificity. J Cell Biochem *55*, 22-31.

Greaves, E.A., Copeland, N.A., Coverley, D., and Ainscough, J.F. (2012). Cancer-associated variant expression and interaction of CIZ1 with cyclin A1 in differentiating male germ cells. J Cell Sci *125*, 2466-2477.

Guillou, E., Ibarra, A., Coulon, V., Casado-Vela, J., Rico, D., Casal, I., Schwob, E., Losada, A., and Mendez, J. (2010). Cohesin organizes chromatin loops at DNA replication factories. Genes Dev *24*, 2812-2822.

Hahn, W.C., Counter, C.M., Lundberg, A.S., Beijersbergen, R.L., Brooks, M.W., and Weinberg, R.A. (1999). Creation of human tumour cells with defined genetic elements. Nature *400*, 464-468.

Hahn, W.C., Dessain, S.K., Brooks, M.W., King, J.E., Elenbaas, B., Sabatini, D.M., DeCaprio, J.A., and Weinberg, R.A. (2002). Enumeration of the simian virus 40 early region elements necessary for human cell transformation. Mol Cell Biol *22*, 2111-2123.

Hanahan, D., and Weinberg, R.A. (2000). The Hallmarks of Cancer. Cell *100*, 57-70.

Hanahan, D., and Weinberg, R.A. (2011). Hallmarks of cancer: the next generation. Cell *144*, 646-674.

Hanashiro, K., Kanai, M., Geng, Y., Sicinski, P., and Fukasawa, K. (2008). Roles of cyclins A and E in induction of centrosome amplification in p53-compromised cells. Oncogene *27*, 5288-5302.

Hancock, R. (2000). A new look at the nuclear matrix. Chromosoma *109*, 219-225.

Harper, J.W., and Elledge, S.J. (2007). The DNA damage response: ten years after. Mol Cell *28*, 739-745.

Hayflick, L., and Moorhead, P.S. (1961). The serial cultivation of human diploid cell strains. Exp Cell Res *25*, 585-621.

He, D.C., Nickerson, J.A., and Penman, S. (1990). Core filaments of the nuclear matrix. J Cell Biol *110*, 569-580.

He, S., Dunn, K.L., Espino, P.S., Drobic, B., Li, L., Yu, J., Sun, J.M., Chen, H.Y., Pritchard, S., and Davie, J.R. (2008). Chromatin organization and nuclear microenvironments in cancer cells. J Cell Biochem *104*, 2004-2015.

Hendzel, M.J., Boisvert, F., and Bazett-Jones, D.P. (1999). Direct visualization of a protein nuclear architecture. Mol Biol Cell *10*, 2051-2062.

Heng, H.H., Goetze, S., Ye, C.J., Liu, G., Stevens, J.B., Bremer, S.W., Wykes, S.M., Bode, J., and Krawetz, S.A. (2004). Chromatin loops are selectively anchored using scaffold/matrix-attachment regions. J Cell Sci *117*, 999-1008.

Higgins, G., Roper, K.M., Watson, I.J., Blackhall, F.H., Rom, W.N., Pass, H.I., Ainscough, J.F., and Coverley, D. (2012). Variant Ciz1 is a circulating biomarker for early-stage lung cancer. Proc Natl Acad Sci U S A *109*, E3128-3135.

Hochegger, H., Takeda, S., and Hunt, T. (2008). Cyclin-dependent kinases and cell-cycle transitions: does one fit all? Nature Reviews Molecular Cell Biology *9*, 910-916.

Honda, R., Lowe, E.D., Dubinina, E., Skamnaki, V., Cook, A., Brown, N.R., and Johnson, L.N. (2005). The structure of cyclin E1/CDK2: implications for CDK2 activation and CDK2-independent roles. Embo J *24*, 452-463.

Hozak, P., Hassan, A.B., Jackson, D.A., and Cook, P.R. (1993). Visualization of Replication Factories Attached to the Nucleoskeleton. Cell *73*, 361-373.

Hozak, P., Jackson, D.A., and Cook, P.R. (1994). Replication factories and nuclear bodies: the ultrastructural characterization of replication sites during the cell cycle. J Cell Sci *107 (Pt 8)*, 2191-2202.

Hwang, H.C., and Clurman, B.E. (2005). Cyclin E in normal and neoplastic cell cycles. Oncogene *24*, 2776-2786.

Iarovaia, O.V., Bystritskiy, A., Ravcheev, D., Hancock, R., and Razin, S.V. (2004). Visualization of individual DNA loops and a map of loop domains in the human dystrophin gene. Nucleic Acids Res *32*, 2079-2086.

Imoto, M., Doki, Y., Jiang, W., Han, E.K., and Weinstein, I.B. (1997). Effects of cyclin D1 overexpression on G1 progression-related events. Exp Cell Res *236*, 173-180.

Jackson, D.A., and Cook, P.R. (1985). Transcription occurs at a nucleoskeleton. Embo J *4*, 919-925.

Jackson, D.A., and Cook, P.R. (1986a). Different populations of DNA polymerase alpha in HeLa cells. J Mol Biol *192*, 77-86.

Jackson, D.A., and Cook, P.R. (1986b). Replication occurs at a nucleoskeleton. Embo J *5*, 1403-1410.

Jackson, D.A., and Cook, P.R. (1988). Visualization of a filamentous nucleoskeleton with a 23 nm axial repeat. Embo J *7*, 3667-3677.

Jackson, D.A., Dickinson, P., and Cook, P.R. (1990). The size of chromatin loops in HeLa cells. Embo J *9*, 567-571.

Jacobs, J.P., Jones, C.M., and Baille, J.P. (1970). Characteristics of a human diploid cell designated MRC-5. Nature *227*, 168-170.

Jainchill, J.L., Aaronson, S.A., and Todaro, G.J. (1969). Murine sarcoma and leukemia viruses: assay using clonal lines of contact-inhibited mouse cells. J Virol *4*, 549-553.

Johnson, G.D., Lalancette, C., Linnemann, A.K., Leduc, F., Boissonneault, G., and Krawetz, S.A. (2011). The sperm nucleus: chromatin, RNA, and the nuclear matrix. Reproduction *141*, 21-36.

Jones, H.W., Jr., McKusick, V.A., Harper, P.S., and Wuu, K.D. (1971). George Otto Gey. (1899-1970). The HeLa cell and a reappraisal of its origin. Obstetrics and gynecology *38*, 945-949.

Judex, M., Neumann, E., Lechner, S., Dietmaier, W., Ballhorn, W., Grifka, J., Gay, S., Schölmerich, J., Kullman, F., and Müller-Ladner, U. (2003). Laser-mediated microdissection facilitates analysis of area-specific gene expression in rheumatoid synovium. Arthritis & Rheumatism *48*, 97-102.

Kastan, M.B., and Bartek, J. (2004). Cell-cycle checkpoints and cancer. Nature *432*, 316-323.

Kato, J., Matsushime, H., Hiebert, S.W., Ewen, M.E., and Sherr, C.J. (1993). Direct binding of cyclin D to the retinoblastoma gene product (pRb) and pRb phosphorylation by the cyclin D-dependent kinase CDK4. Genes Dev *7*, 331-342.

Keezer, S.M., and Gilbert, D.M. (2002). Sensitivity of the origin decision point to specific inhibitors of cellular signaling and metabolism. Exp Cell Res *273*, 54-64.

Keyomarsi, K., and Herliczek, T.W. (1997). The role of cyclin E in cell proiliferation, development and cancer. Prog Cell Cycle Res *3*, 171-191.

Kirkman, T.W. (1996). Statistics to use. http://wwwphysicscsbsjuedu/stats/, Accessed 10th January 2013

Kiyokawa, H., Kineman, R.D., Manova-Todorova, K.O., Soares, V.C., Hoffman, E.S., Ono, M., Khanam, D., Hayday, A.C., Frohman, L.A., and Koff, A. (1996). Enhanced growth of mice lacking the cyclin-dependent kinase inhibitor function of p27(Kip1). Cell *85*, 721-732.

Klaus, A.V., McCarrey, J.R., Farkas, A., and Ward, W.S. (2001). Changes in DNA loop domain structure during spermatogenesis and embryogenesis in the Syrian golden hamster. Biol Reprod *64*, 1297-1306.

Koff, A., Cross, F., Fisher, A., Schumacher, J., Leguellec, K., Philippe, M., and Roberts, J.M. (1991). Human cyclin E, a new cyclin that interacts with two members of the CDC2 gene family. Cell *66*, 1217-1228.

Kreitz, S., Ritzi, M., Baack, M., and Knippers, R. (2001). The human origin recognition complex protein 1 dissociates from chromatin during S phase in HeLa cells. J Biol Chem *276*, 6337-6342.

Lagarkova, M.A., Svetlova, E., Giacca, M., Falaschi, A., and Razin, S.V. (1998). DNA loop anchorage region colocalizes with the replication origin located downstream to the human gene encoding lamin B2. J Cell Biochem *69*, 13-18.

Lei, M., and Tye, B.K. (2001). Initiating DNA synthesis: from recruiting to activating the MCM complex. J Cell Sci *114*, 1447-1454.

Lemaitre, J.M., Danis, E., Pasero, P., Vassetzky, Y., and Mechali, M. (2005). Mitotic remodeling of the replicon and chromosome structure. Cell *123*, 787-801.

Lemons, J.M., Feng, X.J., Bennett, B.D., Legesse-Miller, A., Johnson, E.L., Raitman, I., Pollina, E.A., Rabitz, H.A., Rabinowitz, J.D., and Coller, H.A. (2010). Quiescent fibroblasts exhibit high metabolic activity. PLoS Biol *8*, e1000514.

Lever, E., and Sheer, D. (2010). The role of nuclear organization in cancer. J Pathol *220*, 114-125.

Li, C.J., and DePamphilis, M.L. (2002). Mammalian Orc1 protein is selectively released from chromatin and ubiquitinated during the S-to-M transition in the cell division cycle. Mol Cell Biol *22*, 105-116.

Li, F., Chen, J., Solessio, E., and Gilbert, D.M. (2003a). Spatial distribution and specification of mammalian replication origins during G1 phase. J Cell Biol *161*, 257-266.

Li, X., Zhao, Q., Liao, R., Sun, P., and Wu, X. (2003b). The SCF(Skp2) ubiquitin ligase complex interacts with the human replication licensing factor Cdt1 and regulates Cdt1 degradation. J Biol Chem *278*, 30854-30858.

Lieberman-Aiden, E., van Berkum, N.L., Williams, L., Imakaev, M., Ragoczy, T., Telling, A., Amit, I., Lajoie, B.R., Sabo, P.J., Dorschner, M.O*., et al.* (2009). Comprehensive mapping of long-range interactions reveals folding principles of the human genome. Science *326*, 289-293.

Liebich, I., Bode, J., Frisch, M., and Wingender, E. (2002a). S/MARt DB: a database on scaffold/matrix attached regions. Nucleic Acids Res *30*, 372-374.

Liebich, I., Bode, J., Reuter, I., and Wingender, E. (2002b). Evaluation of sequence motifs found in scaffold/matrix-attached regions (S/MARs). Nucleic Acids Res *30*, 3433-3442.

Linnemann, A.K., and Krawetz, S.A. (2009a). Maintenance of a functional higher order chromatin structure: The role of the nuclear matrix in normal and disease states. Gene Ther Mol Biol *13*, 231-243.

Linnemann, A.K., and Krawetz, S.A. (2009b). Silencing by nuclear matrix attachment distinguishes cell-type specificity: association with increased proliferation capacity. Nucleic Acids Res *37*, 2779-2788.

Linnemann, A.K., Platts, A.E., and Krawetz, S.A. (2009). Differential nuclear scaffold/matrix attachment marks expressed genes. Hum Mol Genet *18*, 645-654.

Little, R.D., Platt, T.H., and Schildkraut, C.L. (1993). Initiation and termination of DNA replication in human rRNA genes. Mol Cell Biol *13*, 6600-6613.

Liu, E., Li, X., Yan, F., Zhao, Q., and Wu, X. (2004). Cyclin-dependent kinases phosphorylate human Cdt1 and induce its degradation. J Biol Chem *279*, 17283-17288.

Livak, K.J., and Schmittgen, T.D. (2001). Analysis of relative gene expression data using real-time quantitative PCR and the 2(-Delta Delta C(T)) Method. Methods (San Diego, Calif *25*, 402-408.

Lu, J., Li, F., Murphy, C.S., Davidson, M.W., and Gilbert, D.M. (2010). G2 phase chromatin lacks determinants of replication timing. J Cell Biol *189*, 967-980.

Lukasik, A., Uniewicz, K.A., Kulis, M., and Kozlowski, P. (2008). Ciz1, a p21 cip1/Waf1-interacting zinc finger protein and DNA replication factor, is a novel molecular partner for human enhancer of rudimentary homolog. FEBS J *275*, 332-340.

Ma, H., Siegel, A.J., and Berezney, R. (1999). Association of chromosome territories with the nuclear matrix. Disruption of human chromosome territories correlates with the release of a subset of nuclear matrix proteins. J Cell Biol *146*, 531-542.

Madine, M.A., Sweitlik, M., Pelizon, C., Romanowski, P., Mills, A.D., and Laskey, R.A. (2000). The roles of Mcm, Orc and Cdc6 protein in determining the replication competence of chromatin in quiescent cells. J Structural Biol *129*, 198-210.

Malumbres, M., and Barbacid, M. (2009). Cell cycle, CDKs and cancer: a changing paradigm. Nature reviews *9*, 153-166.

Malyapa, R.S., Wright, W.D., Taylor, Y.C., and Roti Roti, J.L. (1996). DNA supercoiling changes and nuclear matrix-associated proteins: possible role in oncogene-mediated

radioresistance. International journal of radiation oncology, biology, physics *35*, 963-973.

Mancini, M.A., Shan, B., Nickerson, J.A., Penman, S., and Lee, W.H. (1994). The retinoblastoma gene product is a cell cycle-dependent, nuclear matrix-associated protein. Proc Natl Acad Sci U S A *91*, 418-422.

Marsden, M.P., and Laemmli, U.K. (1979). Metaphase chromosome structure: evidence for a radial loop model. Cell *17*, 849-858.

Marshall, C.J., Franks, L.M., and Carbonell, A.W. (1977). Markers of neoplastic transformation in epithelial cell lines derived from human carcinomas. Journal of the National Cancer Institute *58*, 1743-1751.

Martelli, A.M., Falcieri, E., Zweyer, M., Bortul, R., Tabellini, G., Cappellini, A., Cocco, L., and Manzoli, L. (2002). The controversial nuclear matrix: a balanced point of view. Histol Histopathol *17*, 1193-1205.

Matsumoto, Y., and Maller, J.L. (2004). A centrosomal localization signal in cyclin E required for Cdk2-independent S phase entry. Science *306*, 885-888.

Matsuoka, S., Ballif, B.A., Smogorzewska, A., McDonald, E.R.r., Hurov, K.E., Luo, J., Bakalarski, C.E., Zhao, Z., Solimini, N., Lerenthal, Y.*, et al.* (2007). ATM and ATR substrate analysis reveals extensive protein networks responsive to DNA damage. Science *316*, 1160-1166.

Mauck, J.C., and Green, H. (1973). Regulation of RNA synthesis in fibroblasts during transition from resting to growing state. Proc Natl Acad Sci U S A *70*, 2819-2822.

Maya-Mendoza, A., and Aranda-Anzaldo, A. (2003). Positional mapping of specific DNA sequences relative to the nuclear substructure by direct polymerase chain reaction on nuclear matrix-bound templates. Anal Biochem *313*, 196-207.

Maya-Mendoza, A., Hernandez-Munoz, R., Gariglio, P., and Aranda-Anzaldo, A. (2003). Gene positional changes relative to the nuclear substructure correlate with the proliferating status of hepatocytes during liver regeneration. Nucleic Acids Res *31*, 6168-6179.

Maya-Mendoza, A., Hernandez-Munoz, R., Gariglio, P., and Aranda-Anzaldo, A. (2005). Natural ageing in the rat liver correlates with progressive stabilisation of DNA-nuclear matrix interactions and withdrawal of genes from the nuclear substructure. Mech Ageing Dev *126*, 767-782.

McNairn, A.J., Okuno, Y., Misteli, T., and Gilbert, D.M. (2005). Chinese hamster ORC subunits dynamically associate with chromatin throughout the cell-cycle. Exp Cell Res *308*, 345-356.

Mechali, M. (2010). Eukaryotic DNA replication origins: many choices for appropriate answers. Nat Rev Mol Cell Biol *11*, 728-738.

Mehta, I.S., Amira, M., Harvey, A.J., and Bridger, J.M. (2010). Rapid chromosome territory relocation by nuclear motor activity in response to serum removal in primary human fibroblasts. Genome Biol *11*, R5.

Mehta, I.S., Elcock, L.S., Amira, M., Kill, I.R., and Bridger, J.M. (2008). Nuclear motors and nuclear structures containing A-type lamins and emerin: is there a functional link? Biochem Soc Trans *36*, 1384-1388.

Mendelsohn, M.L. (1962). Chronic infusion of tritiated thymidine into mice with tumors. Science *135*, 213-215.

Mendez, J., and Stillman, B. (2000). Chromatin association of human origin recognition complex, cdc6, and minichromosome maintenance proteins during the cell cycle: assembly of prereplication complexes in late mitosis. Mol Cell Biol *20*, 8602-8612.

Mendez, J., Zou-Yang, X.H., Kim, S.Y., Hidaka, M., Tansey, W.P., and Stillman, B. (2002). Human origin recognition complex large subunit is degraded by ubiquitin-mediated proteolysis after initiation of DNA replication. Mol Cell *9*, 481-491.

Mika, S., and Rost, B. (2005). NMPdb: Database of Nuclear Matrix Proteins. Nucleic Acids Res *33*, D160-163.

Milsom, M.D., Jerabek-Willemsen, M., Harris, C.E., Schambach, A., Broun, E., Bailey, J., Jansen, M., Schleimer, D., Nattamai, K., Wilhelm, J.*, et al.* (2008). Reciprocal relationship between O6-methylguanine-DNA methyltransferase P140K expression level and chemoprotection of hematopoietic stem cells. Cancer Res *68*, 6171-6180.

Minn, A.J., Kang, Y., Serganova, I., Gupta, G.P., Giri, D.D., Doubrovin, M., Ponomarev, V., Gerald, W.L., Blasberg, R., and Massague, J. (2005). Distinct organ-specific metastatic potential of individual breast cancer cells and primary tumors. The Journal of clinical investigation *115*, 44-55.

Mirkovitch, J., Gasser, S.M., and Laemmli, U.K. (1988). Scaffold attachment of DNA loops in metaphase chromosomes. J Mol Biol *200*, 101-109.

Mirkovitch, J., Mirault, M.E., and Laemmli, U.K. (1984). Organization of the higher-order chromatin loop: specific DNA attachment sites on nuclear scaffold. Cell *39*, 223-232.

Mitsui, K., Matsumoto, A., Ohtsuka, S., Ohtsubo, M., and Yoshimura, A. (1999). Cloning and characterization of a novel $P21^{Cip1/Waf1}$- interacting zinc finger protein, Ciz1. Biochemical and Biophysical Research Communications *264*, 457-464.

Mitulovic, G., Stingl, C., Smoluch, M., Swart, R., Chervet, J.P., Steinmacher, I., Gerner, C., and Mechtler, K. (2004). Automated, on-line two-dimensional nano liquid chromatography tandem mass spectrometry for rapid analysis of complex protein digests. Proteomics *4*, 2545-2557.

Monneron, A., and Bernhard, W. (1969). Fine structural organization of the interphase nucleus in some mammalian cells. Journal of ultrastructure research *27*, 266-288.

Montazer-Torbati, M.B., Hue-Beauvais, C., Droineau, S., Ballester, M., Coant, N., Aujean, E., Petitbarat, M., Rijnkels, M., and Devinoy, E. (2008). Epigenetic modifications and chromatin loop organization explain the different expression profiles of the Tbrg4, WAP and Ramp3 genes. Exp Cell Res *314*, 975-987.

Moroy, T., and Geisen, C. (2004). Cyclin E. International Journal of Biochemistry & Cell Biology *36*, 1424-1439.

Munkley, J., Copeland, N.A., Moignard, V., Knight, J.R., Greaves, E., Ramsbottom, S.A., Pownall, M.E., Southgate, J., Ainscough, J.F., and Coverley, D. (2011). Cyclin E is recruited to the nuclear matrix during differentiation, but is not recruited in cancer cells. Nucleic Acids Res *39*, 2671-2677.

Murray, A.W. (2004). Recycling the cell cycle: cyclins revisited. Cell *116*, 221-234.

Nadel, B., de Lara, J., Finkernagel, S.W., and Ward, W.S. (1995). Cell-specific organization of the 5S ribosomal RNA gene cluster DNA loop domains in spermatozoa and somatic cells. Biol Reprod *53*, 1222-1228.

Nakayama, K., Ishida, N., Shirane, M., Inomata, A., Inoue, T., Shishido, N., Horii, I., Loh, D.Y., and Nakayama, K. (1996). Mice lacking p27(Kip1) display increased body size, multiple organ hyperplasia, retinal dysplasia, and pituitary tumors. Cell *85*, 707-720.

Nakayasu, H., and Berezney, R. (1989). Mapping replicational sites in the eucaryotic cell nucleus. J Cell Biol *108*, 1-11.

Nelson, W.G., Pienta, K.J., Barrack, E.R., and Coffey, D.S. (1986). The role of the nuclear matrix in the organization and function of DNA. Annu Rev Biophys Biophys Chem *15*, 457-475.

Nickerson, J. (2001). Experimental observations of a nuclear matrix. J Cell Sci *114*, 463-474.

Nickerson, J.A., Krockmalnic, G., Wan, K.M., and Penman, S. (1997). The nuclear matrix revealed by eluting chromatin from a cross-linked nucleus. Proceedings of the National Academy of Sciences of the United States of America *94*, 4446-4450.

Nieduszynski, C.A., Knox, Y., and Donaldson, A.D. (2006). Genome-wide identification of replication origins in yeast by comparative genomics. Genes Dev *20*, 1874-1879.

Nielsen, N.H., Arnerlov, C., Cajander, S., and Landberg, G. (1998). Cyclin E expression and proliferation in breast cancer. Analytical cellular pathology : the journal of the European Society for Analytical Cellular Pathology *17*, 177-188.

Nishibe, R., Watanabe, W., Ueda, T., Yamasaki, N., Koller, R., Wolff, L., Honda, Z., Ohtsubo, M., and Honda, H. (2013). CIZ1, a p21(Cip1/Waf1)-interacting protein, functions as a tumor suppressor in vivo. FEBS Lett *587*, 1529-1535.

Nishitani, H., Sugimoto, N., Roukos, V., Nakanishi, Y., Saijo, M., Obuse, C., Tsurimoto, T., Nakayama, K.I., Nakayama, K., Fujita, M.*, et al.* (2006). Two E3 ubiquitin ligases, SCF-Skp2 and DDB1-Cul4, target human Cdt1 for proteolysis. Embo J *25*, 1126-1136.

Ohsaki, E., Suzuki, T., Karayama, M., and Ueda, K. (2009). Accumulation of LANA at nuclear matrix fraction is important for Kaposi's sarcoma-associated herpesvirus replication in latency. Virus Res *139*, 74-84.

Ohta, S., Tatsumi, Y., Fujita, M., Tsurimoto, T., and Obuse, C. (2003). The ORC1 cycle in human cells: II. Dynamic changes in the human ORC complex during the cell cycle. J Biol Chem *278*, 41535-41540.

Ohtsubo, M., and Roberts, J.M. (1993). Cyclin-dependent regulation of G1 in mammalian fibroblasts. Science *259*, 1908-1912.

Ohtsubo, M., Theodoras, A.M., Schumacher, J., and Roberts, J.M. (1995). Human cyclin E, a nuclear protein essential for the G1-to-S phase transition. Mol Cell Biol *15*, 2612-2624.

Ortega, J.M., and DePamphilis, M.L. (1998). Nucleoskeleton and initiation of DNA replication in metazoan cells. J Cell Sci *111 (Pt 24)*, 3663-3673.

Ortega, S., Prieto, I., Odajima, J., Martin, A., Dubus, P., Sotillo, R., Barbero, J.L., Malumbres, M., and Barbacid, M. (2003). Cyclin-dependent kinase 2 is essential for meiosis but not for mitotic cell division in mice. Nat Genet *35*, 25-31.

Osborne, C.K., Hobbs, K., and Clark, G.M. (1985). Effect of estrogens and antiestrogens on growth of human breast cancer cells in athymic nude mice. Cancer Res *45*, 584-590.

Ottaviani, D., Lever, E., Mitter, R., Jones, T., Forshew, T., Christova, R., Tomazou, E.M., Rakyan, V.K., Krawetz, S.A., Platts, A.E.*, et al.* (2008a). Reconfiguration of genomic anchors upon transcriptional activation of the human major histocompatibility complex. Genome Res *18*, 1778-1786.

Ottaviani, D., Lever, E., Takousis, P., and Sheer, D. (2008b). Anchoring the genome. Genome Biol *9*, 201.

Panneerselvam, J., Park, H.K., Zhang, J., Dudimah, F.D., Zhang, P., Wang, H., and Fei, P. (2012). FAVL impairment of the Fanconi anemia pathway promotes the development of human bladder cancer. Cell Cycle *11*, 2947-2955.

Pardee, A.B. (1974). A restriction point for control of normal animal cell proliferation. Proc Natl Acad Sci U S A *71*, 1286-1290.

Pardoll, D.M., Vogelstein, B., and Coffey, D.S. (1980). A fixed site of DNA replication in eucaryotic cells. Cell *19*, 527-536.

Parisi, T., Beck, A.R., Rougier, N., McNeil, T., Lucian, L., Werb, Z., and Amati, B. (2003). Cyclins E1 and E2 are required for endoreplication in placental trophoblast giant cells. Embo J *22*, 4794-4803.

Pascreau, G., Eckerdt, F., Churchill, M.E., and Maller, J.L. (2010). Discovery of a distinct domain in cyclin A sufficient for centrosomal localization independently of Cdk binding. Proc Natl Acad Sci U S A *107*, 2932-2937.

Paulson, J.R., and Laemmli, U.K. (1977). The structure of histone-depleted metaphase chromosomes. Cell *12*, 817-828.

Pederson, T. (1998). Thinking about a nuclear matrix. J Mol Biol *277*, 147-159.

Petersen, B.O., Wagener, C., Marinoni, F., Kramer, E.R., Melixetian, M., Lazzerini Denchi, E., Gieffers, C., Matteucci, C., Peters, J.M., and Helin, K. (2000). Cell cycle- and cell growth-regulated proteolysis of mammalian CDC6 is dependent on APC-CDH1. Genes Dev *14*, 2330-2343.

Pienta, K.J., Getzenberg, R.H., and Coffey, D.S. (1992). Characterization of nuclear morphology and nuclear matrices in ageing human fibroblasts. Mech Ageing Dev *62*, 13-24.

Pines, J. (1991). Cyclins: wheels within wheels. Cell growth & differentiation : the molecular biology journal of the American Association for Cancer Research *2*, 305-310.

Pines, J. (1999). Four-dimensional control of the cell cycle. Nat Cell Biol *1*, E73-79.

Pines, J., and Hunt, T. (1987). Molecular cloning and characterization of the mRNA for cyclin from sea urchin eggs. Embo J *6*, 2987-2995.

Platts, A.E., Quayle, A.K., and Krawetz, S.A. (2006). In-silico prediction and observations of nuclear matrix attachment. Cell Mol Biol Lett *11*, 191-213.

Porter, P.L., Malone, K.E., Heagerty, P.J., Alexander, G.M., Gatti, L.A., Firpo, E.J., Daling, J.R., and Roberts, J.M. (1997). Expression of cell-cycle regulators p27Kip1 and cyclin E, alone and in combination, correlate with survival in young breast cancer patients. Nature medicine *3*, 222-225.

Qiao, F., Moss, A., and Kupfer, G.M. (2001). Fanconi anemia proteins localize to chromatin and the nuclear matrix in a DNA damage- and cell cycle-regulated manner. J Biol Chem *276*, 23391-23396.

Radichev, I., Parashkevova, A., and Anachkova, B. (2005). Initiation of DNA replication at a nuclear matrix-attached chromatin fraction. J Cell Physiol *203*, 71-77.

Rahman, F.A., Ainscough, J.F.-X., Copeland, N., and Coverley, D. (2007). Cancer-associated missplicing of exon 4 influences the subnuclear distribution of the DNA replication factor Ciz1. Human Mutation *28*, 993-1004.

Rahman, F.A., Aziz, N., and Coverley, D. (2010). Differential detection of alternatively spliced variants of Ciz1 in normal and cancer cells using a custom exon-junction microarray. BMC cancer *10*, 482.

Rangarajan, A., Hong, S.J., Gifford, A., and Weinberg, R.A. (2004). Species- and cell type-specific requirements for cellular transformation. Cancer Cell *6*, 171-183.

Remeseiro, S., and Losada, A. (2013). Cohesin, a chromatin engagement ring. Curr Opin Cell Biol *25*, 63-71.

Remus, D., and Diffley, J.F. (2009). Eukaryotic DNA replication control: lock and load, then fire. Curr Opin Cell Biol *21*, 771-777.

Resnitzky, D., Gossen, M., Bujard, H., and Reed, S.I. (1994). Acceleration of the G1/S phase transition by expression of cyclins D1 and E with an inducible system. Mol Cell Biol *14*, 1669-1679.

Revuelta-Cervantes, J., Mayoral, R., Miranda, S., Gonzalez-Rodriguez, A., Fernandez, M., Martin-Sanz, P., and Valverde, A.M. (2011). Protein Tyrosine Phosphatase 1B (PTP1B) deficiency accelerates hepatic regeneration in mice. Am J Pathol *178*, 1591-1604.

Reyes, J.C., Muchardt, C., and Yaniv, M. (1997). Components of the human SWI/SNF complex are enriched in active chromatin and are associated with the nuclear matrix. J Cell Biol *137*, 263-274.

Rigby, C.C., and Franks, L.M. (1970). A human tissue culture cell line from a transitional cell tumour of the urinary bladder: growth, chromosone pattern and ultrastructure. British journal of cancer *24*, 746-754.

Rivera-Mulia, J.C., and Aranda-Anzaldo, A. (2010). Determination of the in vivo structural DNA loop organization in the genomic region of the rat albumin locus by means of a topological approach. DNA research : an international journal for rapid publication of reports on genes and genomes *17*, 23-35.

Rivera-Mulia, J.C., Hernandez-Munoz, R., Martinez, F., and Aranda-Anzaldo, A. (2011). DNA moves sequentially towards the nuclear matrix during DNA replication in vivo. BMC Cell Biol *12*, 3.

Roper, K.M. (2011). Identifying a role for CIZ1 in the DNA damage response. PhD thesis, University of York.

Roti Roti, J.L., and Wright, W.D. (1987). Visualization of DNA loops in nucleoids from HeLa cells: assays for DNA damage and repair. Cytometry *8*, 461-467.

Saha, P., Chen, J., Thome, K.C., Lawlis, S.J., Hou, Z.H., Hendricks, M., Parvin, J.D., and Dutta, A. (1998). Human CDC6/Cdc18 associates with Orc1 and cyclin-cdk and is selectively eliminated from the nucleus at the onset of S phase. Mol Cell Biol *18*, 2758-2767.

Sakaguchi, T., Watanabe, A., Sawada, H., Yamada, Y., Yamashita, J., Matsuda, M., Nakajima, M., Miwa, T., Hirao, T., and Nakano, H. (1998). Prognostic value of cyclin E and p53 expression in gastric carcinoma. Cancer *82*, 1238-1243.

Sambasivan, R., Pavlath, G.K., and Dhawan, J. (2008). A gene-trap strategy identifies quiescence-induced genes in synchronized myoblasts. J Biosci *33*, 27-44.

Sasaki, T., Ramanathan, S., Okuno, Y., Kumagai, C., Shaikh, S.S., and Gilbert, D.M. (2006). The Chinese hamster dihydrofolate reductase replication origin decision point follows activation of transcription and suppresses initiation of replication within transcription units. Mol Cell Biol *26*, 1051-1062.

Schraml, P., Bucher, C., Bissig, H., Nocito, A., Haas, P., Wilber, K., Seelig, S., Kononen, J., Mihatsch, M.J., Dirnhofer, S.*, et al.* (2003). Cyclin E overexpression and amplification in human tumours. J Pathol *200*, 375-382.

Sclafani, R.A., and Holzen, T.M. (2007). Cell cycle regulation of DNA replication. Annu Rev Genet *41*, 237-280.

Sherr, C.J., and Roberts, J.M. (1995). Inhibitors of mammalian G1 cyclin-dependent kinases. Genes Dev *9*, 1149-1163.

Sherr, C.J., and Roberts, J.M. (1999). CDK inhibitors: positive and negative regulators of G1-phase progression. Genes Dev *13*, 1501-1512.

Singh, G.B., Kramer, J.A., and Krawetz, S.A. (1997). Mathematical model to predict regions of chromatin attachment to the nuclear matrix. Nucleic Acids Res *25*, 1419-1425.

Sorlie, T., Perou, C.M., Tibshirani, R., Aas, T., Geisler, S., Johnsen, H., Hastie, T., Eisen, M.B., van de Rijn, M., Jeffrey, S.S.*, et al.* (2001). Gene expression patterns of breast carcinomas distinguish tumor subclasses with clinical implications. Proc Natl Acad Sci U S A *98*, 10869-10874.

Southgate, J., Hutton, K.A., Thomas, D.F., and Trejdosiewicz, L.K. (1994). Normal human urothelial cells in vitro: proliferation and induction of stratification. Lab Invest *71*, 583-594.

Southgate, J., Proffitt, J., Roberts, P., Smith, B., and Selby, P. (1995). Loss of cyclin-dependent kinase inhibitor genes and chromosome 9 karyotypic abnormalities in human bladder cancer cell lines. British journal of cancer *72*, 1214-1218.

Spruck, C.H., Won, K.-A., and Reed, S.I. (1999). Deregulated cyclin E induces chromosome instability. Nature *401*, 297-300.

Stoeber, K., Mills, A.D., Kubota, Y., Krude, T., Romanowski, P., Marheineke, K., Laskey, R.A., and Williams, G.H. (1998). Cdc6 protein causes premature entry into S phase in a mammalian cell-free system. Embo J *17*, 7219-7229.

Stolfi, C., Sarra, M., Caruso, R., Fantini, M.C., Fina, D., Pellegrini, R., Palmieri, G., Macdonald, T.T., Pallone, F., and Monteleone, G. (2010). Inhibition of colon carcinogenesis by 2-methoxy-5-amino-N-hydroxybenzamide, a novel derivative of mesalamine. Gastroenterology *138*, 221-230.

Su, Y., Meador, J.A., Calaf, G.M., Proietti De-Santis, L., Zhao, Y., Bohr, V.A., and Balajee, A.S. (2010). Human RecQL4 helicase plays critical roles in prostate carcinogenesis. Cancer Res *70*, 9207-9217.

Tada, S., Li, A., Maiorano, D., Mechali, M., and Blow, J.J. (2001). Repression of origin assembly in metaphase depends on inhibition of RLF-B/Cdt1 by geminin. Nat Cell Biol *3*, 107-113.

Tait, L., Soule, H.D., and Russo, J. (1990). Ultrastructural and immunocytochemical characterization of an immortalized human breast epithelial cell line, MCF-10. Cancer Res *50*, 6087-6094.

Takisawa, H., Mimura, S., and Kubota, Y. (2000). Eukaryotic DNA replication: from pre-replication complex to initiation complex. Curr Opin Cell Biol *12*, 690-696.

Tan, M., Davis, S.W., Saunders, T.L., Zhu, Y., and Sun, Y. (2009). RBX1/ROC1 disruption results in early embryonic lethality due to proliferation failure, partially rescued by simultaneous loss of p27. Proc Natl Acad Sci U S A *106*, 6203-6208.

Tatsumi, Y., Ohta, S., Kimura, H., Tsurimoto, T., and Obuse, C. (2003). The ORC1 cycle in human cells: I. cell cycle-regulated oscillation of human ORC1. J Biol Chem *278*, 41528-41534.

Taylor, Y.C., Zhang, X.F., Parsian, A.J., and Duncan, P.G. (1991). Image analysis-based measurement of DNA supercoiling changes in transformed and nontransformed human cell lines. Exp Cell Res *197*, 222-228.

Thierry-Mieg, D., and Thierry-Mieg, J. (2006). AceView: a comprehensive cDNA-supported gene and transcripts annotation. Genome Biol *7 Suppl 1*, S12 11-14.

Thomas, E.A., and Thomas, C.A., Jr. (1989). Nucleoid halo expansion indirectly measures DNA damage in single cells. Exp Cell Res *183*, 149-158.

Todorov, I.T., Attaran, A., and Kearsey, S.E. (1995). BM28, a human member of the MCM2-3-5 family, is displaced from chromatin during DNA replication. J Cell Biol *129*, 1433-1445.

Tokuriki, A., Iyoda, T., Inaba, K., Ikuta, K., Fujimoto, S., Kumakiri, M., and Yokota, Y. (2009). Dual role for Id2 in chemical carcinogen-induced skin tumorigenesis. Carcinogenesis *30*, 1645-1650.

Trent, S., Yang, C., Li, C., Lynch, M., and Schmidt, E.V. (2007). Heat shock protein B8, a cyclin-dependent kinase-independent cyclin D1 target gene, contributes to its effects on radiation sensitivity. Cancer Res *67*, 10774-10781.

Trevilla-Garcia, C., and Aranda-Anzaldo, A. (2011). Cell-type-specific organization of nuclear DNA into structural looped domains. J Cell Biochem *112*, 531-540.

Varma, P., and Mishra, R.K. (2011). Dynamics of nuclear matrix proteome during embryonic development in Drosophila melanogaster. J Biosci *36*, 439-459.

Vassetzky, Y.S., Hair, A., and Razin, S.V. (2000). Rearrangement of chromatin domains in cancer and development. J Cell Biochem Suppl *Suppl 35*, 54-60.

Veiga-Fernandes, H., and Rocha, B. (2004). High expression of active CDK6 in the cytoplasm of CD8 memory cells favors rapid division. Nat Immunol *5*, 31-37.

Vermeulen, K., Van Bockstaele, D.R., and Berneman, Z.N. (2003). The cell cycle: a review of regulation, deregulation and therapeutic targets in cancer. Cell proliferation *36*, 131-149.

Vogelstein, B., Pardoll, D.M., and Coffey, D.S. (1980). Supercoiled loops and eucaryotic DNA replicaton. Cell *22*, 79-85.

Wang, C., Pattabiraman, N., Zhou, J.N., Fu, M., Sakamaki, T., Albanese, C., Li, Z., Wu, K., Hulit, J., Neumeister, P., *et al.* (2003). Cyclin D1 repression of peroxisome proliferator-activated receptor gamma expression and transactivation. Mol Cell Biol *23*, 6159-6173.

Wang, J., Gu, Q., Li, M., Zhang, W., Yang, M., Zou, B., Chan, S., Qiao, L., Jiang, B., Tu, S., *et al.* (2009). Identification of XAF1 as a novel cell cycle regulator through modulating G(2)/M checkpoint and interaction with checkpoint kinase 1 in gastrointestinal cancer. Carcinogenesis *30*, 1507-1516.

Wang, J.C. (1979). Helical repeat of DNA in solution. Proc Natl Acad Sci U S A *76*, 200-203.

Warder, D.E., and Keherly, M.J. (2003). Ciz1, Cip1 interacting zinc finger protein 1 binds the consensus DNA sequence ARYSR(0-2)YYAC. Journal of Biomedical Science *10*, 406-417.

Watson, J.D., and Crick, F.H. (1953). Molecular structure of nucleic acids; a structure for deoxyribose nucleic acid. Nature *171*, 737-738.

Wilson, R.H., and Coverley, D. (2013). Relationship between DNA replication and the nuclear matrix. Genes Cells *18*, 17-31.

Wilson, R.H.C., Hesketh, E.L., and Coverley, D. (Submitted by request to Cold Spring Harbour Laboratory Protocols). The nuclear matrix: preparation for microscopic and biochemical analysis.

Wimmel, A., Lucibello, F., Sewing, A., Adolph, S., and Muller, R. (1994). Inducible acceleration of G1 progression through tetracycline-regulated expression of human cyclin E. Oncogene *9*, 995-997.

Wohlschlegel, J.A., Dwyer, B.T., Dhar, S.K., Cvetic, C., Walter, J.C., and Dutta, A. (2000). Inhibition of eukaryotic DNA replication by geminin binding to Cdt1. Science *290*, 2309-2312.

Wu, J.R., and Gilbert, D.M. (1996). A distinct G1 step required to specify the Chinese hamster DHFR replication origin. Science *271*, 1270-1272.

Wu, J.R., and Gilbert, D.M. (1997). The replication origin decision point is a mitogen-independent, 2-aminopurine-sensitive, G1-phase event that precedes restriction point control. Mol Cell Biol *17*, 4312-4321.

Xiao, J., Uitti, R.J., Zhao, Y., Vemula, S.R., Perlmutter, J.S., Wszolek, Z.K., Maraganore, D.M., Auburger, G., Leube, B., Lehnhoff, K., *et al.* (2012). Mutations in CIZ1 cause adult onset primary cervical dystonia. Ann Neurol *71*, 458-469.

Yamazaki, S., Ishii, A., Kanoh, Y., Oda, M., Nishito, Y., and Masai, H. (2012). Rif1 regulates the replication timing domains on the human genome. Embo J *31*, 3667-3677.

Zaidi, S.K., Young, D.W., Javed, A., Pratap, J., Montecino, M., van Wijnen, A., Lian, J.B., Stein, J.L., and Stein, G.S. (2007). Nuclear microenvironments in biological control and cancer. Nature reviews *7*, 454-463.

Zambrowicz, B.P., Abuin, A., Ramirez-Solis, R., Richter, L.J., Piggott, J., BeltrandelRio, H., Buxton, E.C., Edwards, J., Finch, R.A., Friddle, C.J., *et al.* (2003). Wnk1 kinase deficiency lowers blood pressure in mice: a gene-trap screen to identify potential targets for therapeutic intervention. Proc Natl Acad Sci U S A *100*, 14109-14114.

Zeitlin, S., Parent, A., Silverstein, S., and Efstratiadis, A. (1987). Pre-mRNA splicing and the nuclear matrix. Mol Cell Biol *7*, 111-120.

Zhou, B.B., and Elledge, S.J. (2000). The DNA damage response: putting checkpoints in perspective. Nature *408*, 433-439.

Zink, D., Bornfleth, H., Visser, A., Cremer, C., and Cremer, T. (1999). Organization of early and late replicating DNA in human chromosome territories. Exp Cell Res *247*, 176-188.

Zink, D., Fischer, A.H., and Nickerson, J.A. (2004). Nuclear structure in cancer cells. Nature reviews *4*, 677-687.

Zwijsen, R.M., Wientjens, E., Klompmaker, R., van der Sman, J., Bernards, R., and Michalides, R.J. (1997). CDK-independent activation of estrogen receptor by cyclin D1. Cell *88*, 405-415.

Genes to Cells

REVIEW

Relationship between DNA replication and the nuclear matrix

Rosemary H. C. Wilson and Dawn Coverley*

Department of Biology, University of York, Heslington, York YO10 5DD, UK

There is an extensive list of primary published work related to the nuclear matrix (NM). Here we review the aspects that are required to understand its relationship with DNA replication, while highlighting some of the difficulties in studying such a structure, and possible differences that arise from the choice of model system. We consider NM attachment regions of DNA and discuss their characteristics and potential function before reviewing data that deal specifically with functional interaction with DNA replication factors. Data have long existed indicating that newly synthesized DNA is associated with a nuclease-resistant NM, allowing the conclusion that the elongation step of DNA synthesis is immobilized within the nucleus. We review in more detail the emerging data that suggest that prereplication complex proteins and origins of replication are transiently recruited to the NM during late G1 and early S-phase. Collectively, these data suggest that the initiation step of the DNA replication process is also immobilized by attachment to the NM. We outline models that discuss the possible spatial relationships and highlight the emerging evidence that suggests there may be important differences between cell types.

Introduction

The nuclear matrix

Descriptions of an insoluble proteinaceous nuclear substructure, in some ways analogous to the cytoskeleton, have existed for at least 40 years. However, the difficulties associated with studying this nuclear fraction mean that there are still many unanswered questions about structure and function; and even some residual controversy about its very existence. However, there is now a large and growing body of evidence in favor of such a nuclear substructure. Here we review the published work on its relationship with DNA replication.

The nuclear substructure has been termed the nuclear matrix (NM), the nuclear scaffold or the nuclear skeleton (or nucleoskeleton) depending on the technique used to reveal it. These are, respectively, extraction with high salt (2.0 M NaCl) (Berezney & Coffey 1974), lithium 3,5-diiodosalicylate (LIS) (Mirkovitch *et al.* 1984) or after encapsulation in agarose under physiologically relevant salt concentrations and electrophoresis (Jackson & Cook 1988). A protein is termed part of the nuclear substructure if it resists extraction. However, there are also many variations of these techniques (reviewed in Martelli *et al.* 2002), and this means that interpretation is not always straightforward. Here we use the term NM as an overarching term and aim to consolidate the reported observations to outline some general phenomena. Depending on extraction technique, the residual protein fraction varies slightly in composition but the core components revealed by several large-scale screens are similar (Albrethsen *et al.* 2009; Varma & Mishra 2011; and references therein). These include lamins, matrins, hnRNPs, other 'structural' proteins, and various proteins involved in DNA metabolism, many of which are listed and categorized in a database of NM Proteins, NMPdb (Mika & Rost 2005).

Very early work described a proportion of nuclear proteins as unextractable with high salt (reviewed in Martelli *et al.* 2002) however, the idea of a NM really began with electron micrographs (EM) showing

Communicated by: Mitsuhiro Yanagida
**Correspondence:* dawn.coverley@york.ac.uk

DOI: 10.1111/gtc.12010

a network of fibers that remain within the nucleus after extraction (Berezney & Coffey 1974). The controversy associated with NM research appears to be attributable to two key reasons. First, it has proved difficult to show such a framework as that seen by EM using immunofluorescence methods in unextracted cells. Instead immunofluorescence against candidate NM proteins usually reveals a pattern of punctate spots (reviewed in Martelli *et al.* 2002). One study used electron spectroscopic imaging (ESI) to view unextracted nuclei by electron microscopy with the aim of identifying areas as protein and/or nucleic acid rich. Using paraformaldehyde fixed sections, this showed inter chromosomal areas to be composed of protein rich but nucleic acid poor structures, consistent with the description of a NM (Hendzel *et al.* 1999). Also worth consideration when thinking about the NM is the idea that there may exist multiple local NMs (Martelli *et al.* 2002) that are dynamic and capable of altering characteristics and composition based on the nuclear processes occurring at that point in time and space (Nelson *et al.* 1986). Therefore, we might not expect to see filamentous structures composed of a small number of specific proteins, but instead transient associations between functional proteins and a 'core'. The use of nonphysiological conditions, in particular high salt extraction, has been criticized as potentially causing aggregation of such protein assemblies (Pederson 1998). To address this, the LIS and physiologically relevant buffer techniques were developed, which give very similar results.

The second major reason that appears to have added complexity and contributed to the controversy in the NM field is the widespread use of systems that now appear to lack or possess a different kind of NM, such as *Xenopus* eggs, cancer cell lines, and progenitor cells. Recent research suggests that the NM changes as cells differentiate or become transformed (reviewed in Zink *et al.* 2004; Munkley *et al.* 2011, and discussed in more detail below).

We will not review evidence for the NM as this has been extensively evaluated elsewhere (Pederson 1998; Hancock 2000; Nickerson 2001; Martelli *et al.* 2002). Instead we consider its functional significance. The NM has been proposed as an anchor for DNA structure, the site of transcription (Jackson & Cook 1985), DNA repair (Qiao *et al.* 2001), splicing (Zeitlin *et al.* 1987), chromatin remodeling (Reyes *et al.* 1997), and DNA replication (Jackson & Cook 1986b). Here, we aim to describe how a NM could support DNA replication and discuss proposed mechanisms and models.

Structural organization of DNA

In order to fit approximately 2 m of DNA within a mammalian nucleus of the order of 10 μm in diameter, it is clear that there must be multiple levels of organization. The extremes of packing of DNA, from wrapping the double helix around histone octamers to form nucleosomes, to compartmentalization into chromosome territories (reviewed in Cremer *et al.* 2006) are now as accepted as the helix itself. However, intermediate levels of organization incur more debate (reviewed in Bian & Belmont 2012).

One model is that nucleosomes are organized into a 30 nm fiber. However, existence of this structure *in vivo* is still hotly contested as the evidence is largely from *in vitro* work (Bian & Belmont 2012). An alternative model is that of fractal globules (reviewed in Fudenberg & Mirny 2012), in which short regions of DNA are proposed to 'crumple' (condense) together to form a series of globules (or domains). These then further crumple together to form larger globules, repeating until they achieve the size of chromosome territories. Some key points of this model are that DNA is not knotted as it would be in an equilibrium globule model (random compaction of DNA), and that it includes all the required levels of compaction. In this model, spatially segregated domains would suggest flexible access to each region of DNA. There are supportive data for the idea of domains within domains, from Fluorescence *In Situ* Hybridisation (FISH) and Chromosome Conformation Capture techniques (Lieberman-Aiden *et al.* 2009). Consistent with both of the above, chromatin loops are thought to periodically attach to the NM. It is likely that the true state of chromatin is a combination of these proposed higher order structures and is likely to be highly dynamic. Here we focus primarily on the organization inherent in attachment to the NM.

Attachment of DNA to the nuclear matrix

Attachment to a proteinaceous structure was first observed by electron microscopy in the 1970s (Paulson & Laemmli 1977). Various methods have been used to study the DNA : NM attachment points (Mirkovitch *et al.* 1984) including imaging by FISH and Maximum Fluorescence Halo Radius (MFHR) (Fig. 1), and biochemical (digestion of loop DNA with restriction enzymes, DNase I or topoisomerase II). Early studies showing attachment of DNA to the NM led to the idea of periodic attachments and the

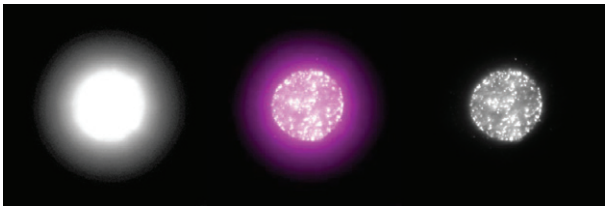

Figure 1 Newly synthesized DNA (A) Left: example of Maximum Fluorescence Halo Radius image from NIH3T3 cell showing DNA loops stained with DAPI emanating out from the nuclear matrix (NM) (MFHR method described in Buongiorno-Nardelli *et al.* 1982; Guillou *et al.* 2010). Right: newly synthesized DNA is observed at the NM but not visible in loop DNA. Cells were pulsed for 30 min with BrdU and visualized with α-BrdU. Centre: merged image showing BrdU (newly synthesized DNA) in white and DNA in magenta.

concept of intervening chromatin loops (Benyajati & Worcel 1976; Marsden & Laemmli 1979) (Fig. 2A). Subsequent work has led to a modification to include loops of different sizes (Fig. 2B) and likely different functions (described in more detail below).

Attachments are termed MARs (matrix attached region), which are resistant to extraction with high salt, scaffold attached region (SARs), which are resistant to extraction with LIS, or skeleton-attached sequences, which are resistant to physiological buffers after encapsulation in agarose, all coupled with enzymatic digestion of DNA. The attachment points revealed by different extraction methods have significant overlap but some are method specific. For example, only approximately half of sequences revealed as MARs on chromosomes 14–18 were also identified as SARs (Linnemann *et al.* 2009). It is likely that the total attachment points in a cell comprise a combination of those revealed by these techniques. We first discuss general features of attachment regions, for which we use the overarching term S/MAR, before highlighting some differences between MARs, SARs and skeleton-attached sequences.

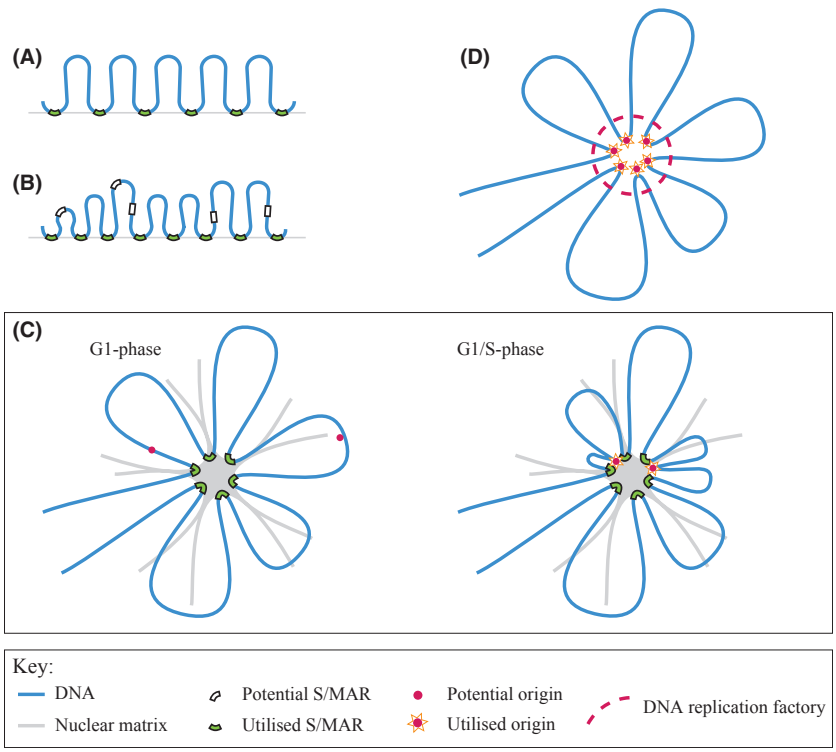

Figure 2 Possible relationships between DNA replication and the nuclear matrix (NM). (A) DNA is thought to be periodically attached to the NM at S/MARs forming intervening chromatin loops. (B) Refined model illustrating variable loop sizes and complex S/MAR usage including utilized S/MARs and function-related alternative potential S/MARs. (C) Our preferred model showing attachment to the NM via nonorigin S/MARs, and recruitment of DNA replication origins at G1/S-phase with possible impact on loop size. (D) Alternative representation of chromatin loops showing replication origin clustering within a DNA replication factory, with no representation of NM attachments.

The length of DNA that is associated with the NM at each attachment point is variously reported as between 100 and 1000 bp with individual loops ranging from 4 to 200 kbp (Vogelstein *et al.* 1980; Buongiorno-Nardelli *et al.* 1982; Singh *et al.* 1997; Bode *et al.* 2003). From our data, we calculate an average loop size of 70 kbp in noncancer differentiated mammalian cells (Wilson, R.H.C., and Coverley, D., our unpublished observation), which ties in closely with several of the previous estimates in the 60–86 kbp range (Vogelstein *et al.* 1980; Jackson *et al.* 1990). With a human haploid genome of ~3 billion bp, this would suggest that ~86 000 attachment points exist at any one time per diploid, G1 cell. As different S/MARs exist in different cell types, and most likely in different phases of the cell cycle and transcriptional programmes, the total number of potential S/MARs is likely to be much more than this (Fig. 2B). Boulikas (1995) predicted approximately 100 000 potential S/MARs based on (i) a loop size of 60 kbp, (ii) an estimated genome size of 3.6 billion bp, and (iii) the fact that some S/MARs are facultative (Boulikas 1995). As we will discuss, predictive tools for S/MARs have their limitations, but it is interesting to note that all tools appear to overpredict S/MARs (Platts *et al.* 2006). While we cannot currently differentiate between false positives and facultative S/MARs, a surplus of potential S/MAR regions would allow for flexibility in usage and imply some form of selection. Consistent with these ideas, it has been shown that a sequence that has the potential to be a functional S/MAR is not always recruited to the NM (Heng *et al.* 2004).

Features of S/MARs

Many of the S/MARs that have been identified arise from studies at a particular gene or locus, and there have been few chromosome or genome wide investigations. The collation of S/MARs identified by individual groups into the S/MAR database (Liebich *et al.* 2002a) has allowed comparison of potential S/MAR motifs (Liebich *et al.* 2002b). However, other than an over-representation of As and Ts, the authors found little sequence similarity. Instead, structural motifs are thought to play a greater role in determining the potential for NM attachment. One predictive tool, 'MAR finder' uses combinations of the following structural motifs to predict S/MARs; origins of replication, TG-rich sequences (commonly in 3′ UTRs), curved DNA, kinked DNA, topoisomerase II sites, and AT-rich sequences (Singh *et al.* 1997). Other suggested characteristics include transcription factor binding sites and other regulatory sequences linked with promoter function (Singh *et al.* 1997). However, some reports are contradictory and motif enrichment may depend on the method used to remove loop DNA. Moreover, the predictive power of tools that use a combination of structural motifs and AT-rich DNA is little better than prediction based on AT-content alone (Evans *et al.* 2007). One of the reasons for the lack of a good predictive model is that only a few S/MARs have been identified by different methods, which appear to identify different populations. So while a particular motif may appear common to one set of identified S/MARs, it may not be hugely predictive of S/MARs in general. It may also be that many motifs can increase the probability of a region forming NM attachment with each increasing the probability only slightly. Therefore, the identification of more S/MARs and a better understanding of their function will be necessary in order to develop better predictive tools.

Functions of S/MARs

In spite of difficulties identifying and predicting S/MARs, several different functions have been suggested for these NM attachments. Constitutive attachments, which do not vary by cell type, are suggested to have a structural role in anchoring the DNA and maintaining nuclear architecture. Consistent with this organizational function, territories have been shown to remain after extraction to reveal the NM but be lost when the NM is disrupted with RNase (Ma *et al.* 1999). In contrast, other S/MARs appear to be transient and facultative in their attachment to the NM. Some vary by cell type and are thought to be involved in maintaining the transcriptional programe, and others vary with external signals and the subsequent change in transcriptional programe. These include S/MARs associated with transcription units, enhancers, and transcription factor binding sites. Furthermore S/MARs vary by cell cycle stage and include regions at potential origins of replication. We describe below, evidence that both transcription and replication occur at the NM. The facultative S/MARs that are implicated in these processes are likely to be involved in the recruitment of specific regions to the NM. Consistent with the idea of constitutive and facultative S/MARs, some proteins which bind S/MARs (MARBPs) are core components of the NM, such as matrins and lamins, topoisomerase II and high-mobility group proteins,

while others are cell type or signal specific, such as Scaffold Attachment Factors A (SAF-A) and B (SAF-B) and SATB1 (reviewed in Wang *et al.* 2010).

Attachment regions could be grouped by characteristics, namely motif composition, extraction method or function. For example, some investigators have advocated a classification of S/MARs into the following four groups based on: regulatory elements including origins and enhancers (class I), somatic cell boundary elements (class II), haploid genome boundary elements observed in sperm (class III), and those with intermediate affinity with the NM (class IV) (Kramer & Krawetz 1996). Although this scheme does not appear to be in widespread use, it effectively classifies S/MARs by motif or structure and by context dependent factor binding.

It is possible that classification by motif or extraction method reveals the same groups. For example, matrix attachment regions (MARs) may contain specific motifs and be related to a specific function. Alternatively, one feature may be more important and, using this example, MARs may encompass regions with different function. We now describe reports from two groups that investigated whether the attachments revealed by different methods specify function.

One study used chromosome paints to compare MARs, SARs, and skeleton-attached sequences genome-wide in human lymphoblasts (Craig *et al.* 1997). Cells were extracted with either 25 mM LIS, 2.0 M NaCl or physiological buffers after agarose encapsulation, and loop fragments released using restriction enzyme digestion. Loop and attached DNA fragments were separated and fluorescently labeled and then used in combination as FISH chromosome paints. It is important to note that the resolution for this study is in the megabase range and that metaphase chromosomes were used. Nevertheless, the study found MARs to be slightly enriched in gene poor regions and relatively absent from transcriptional promoters, and SARs were also enriched in gene poor regions, whereas skeleton-attached sequences were associated with gene rich regions and CpG islands. The authors found little change in SARs between mitotic and interphase chromatin but considerable difference when looking at MARs or skeleton-attached sequences. Overall, the data suggest that SARs are constitutive and structural. In contrast, MARs appear to vary by cell cycle phase but not transcriptional status, whereas skeleton-attached sequences varied by cell cycle phase and in addition appear to be linked to transcription.

In other studies, MARs and SARs of chromosomes 14–18 of HeLa and primary aortic adventitial fibroblasts (AoAF) were compared using a microarray approach with much finer resolution than imaging approaches (Linnemann & Krawetz 2009b; Linnemann *et al.* 2009). Regions enriched in the attached DNA fraction relative to loop fraction were designated as MARs or SARs depending on the method of extraction. For both types of cell, MARs were generally found in intergenic and gene poor regions and were strongly associated with silenced genes, comparing well with data from Craig *et al.* In comparison, SARs density did not depend on gene density but tended to overlap genes and be associated with expressed genes. Linnemann *et al.* propose MARs to be structural with a subset of intragenic MARs providing silencing attachments, and SARs to be facultative and related to function, especially transcription. This suggests that control of gene expression is achieved through multiple mechanisms which include MAR attachment and histone modifications and other epigenetic marks (Linnemann & Krawetz 2009b).

The lack of more genome wide studies makes definitive statements about subgroups of S/MARs and their function difficult. However, general conclusions from these studies suggest MARs to include structural and silencing attachment points, SARs to perhaps be important for cell type determination and maintenance, and SARs and/or skeleton-attached sequences to be important for gene expression.

DNA replication and the nuclear matrix

Various lines of evidence suggest that DNA replication occurs in association with the NM. Origins of replication are recruited to the NM, but as yet there is little indication which subgroup they are likely to fall into. Both newly synthesized DNA and termination structures exist within NM fractions, DNA replication origins appear to be facultative S/MARs, and a number of key proteins involved in replication are themselves associated with the NM. We will discuss evidence for elongation, termination, and initiation of DNA replication.

Elongation of DNA replication

Biochemical fractionation of nuclei to localize nascent DNA, or visualization after labeling with short pulses of nucleotide analogues, has shown newly synthesized DNA and replication intermediates to be located at

the NM and crucially not in the loops (Fig. 1). Furthermore, pulse-chase experiments show that when newly synthesized DNA is observed at later timepoints, it has migrated from the NM fraction into loop regions (Pardoll *et al.* 1980; Vogelstein *et al.* 1980; Jackson & Cook 1986b; Nakayasu & Berezney 1989; Gerdes *et al.* 1994). This collection of studies indicates that the DNA synthesis step and presumably therefore also replication forks are located at the NM. Consistent with this, S-phase cells possess both proliferating cell nuclear antigen (PCNA) and DNA polymerase α in the nuclear skeleton fraction (Hozak *et al.* 1993, 1994). Moreover, this population of polymerase α showed *in vitro* activity that was comparable to that *in vivo*, and nascent DNA remained associated with the skeleton (Jackson & Cook 1986a,b). Similar conclusions were drawn from analysis of NM preparations (Nakayasu & Berezney 1989).

Termination of DNA replication

Relatively little is known about the termination of DNA replication; however, there are data that suggest an association with the NM. First, topoisomerase II is located at the NM (Berrios *et al.* 1985) and appears to be required for resolving replication intermediates. More direct evidence comes from analysis of NM attached DNA, by 2D agarose gel electrophoresis, which revealed termination structures in addition to replication intermediates. Patterns were consistent with both termination at specific points and as a consequence of the convergence of forks (Little *et al.* 1993).

Initiation of DNA replication

The most direct evidence that initiation of DNA replication is located at the NM makes use of synchronised late G1-phase cells treated with DNase I to remove chromatin loops (Radichev *et al.* 2005). When incubated in soluble extract from S-phase cells (which contains regulatory protein kinases that induce initiation) more DNA synthesis occurred on the residual NM-associated chromatin than in control incubations that only support elongation. This indicates that NM-attached chromatin from late G1 cells can undergo initiation. Because this was found to be both located within characteristic foci and dependent on protein kinase activity, these data support the idea that the initiation step of DNA replication occurs in chromatin that is protected by association with a nuclease-resistant structure.

Interestingly, under the same conditions, chromatin-depleted early G1 nuclei did not undergo kinase dependent initiation. This may be due to incomplete assembly of all required factors of the preinitiation complex (pre-IC) or because origins are not located at the NM during early G1. Data described below do indeed suggest that origins are recruited to the NM only during late G1. However, we cannot assume that all origins are recruited to the NM together, as this may occur in conjunction with their activation.

Origins of replication as S/MARs

In human cells, between 30 000 and 50 000 replication origins are thought to be activated per cell cycle in a spatially and temporally ordered fashion. *Saccharomyces cerevisiae* origins of replication are defined by DNA sequence, the autonomous replication sequence (ARS). However, similar short sequences do not specify origins in higher eukaryotes. Instead, structural information and epigenetic marks that can be stably inherited by daughter cells play a role in specification. These include promoter status, CpG methylation, nucleosome positioning, DNase I sensitive sites, DNA topology, and chromatin loop architecture (reviewed in Mechali 2010). For example, there is a higher probability of initiation occurring just before or after transcription start sites, with and without CpG-rich regions (Cayrou *et al.* 2011). Even in *S. cerevisiae* the ARS, though required, is not sufficient to specify origin use as contextual features are known to play a role (Nieduszynski *et al.* 2006). The apparently weak dependence on primary sequence has made it difficult to predict higher eukaryote origins, although S/MARs have been identified in the vicinity of origins of replication for a handful of exemplar genes (reviewed in Cayrou *et al.* 2010).

Early experiments suggested that mammalian cell origins were permanently associated with the NM (Lagarkova *et al.* 1998; and references therein). Furthermore, the similarity in size between replication units and chromatin loops reported in the 1980s (Buongiorno-Nardelli *et al.* 1982) suggested that they might be one and the same, with all attachment points being origins. In apparent support of this conclusion, regions of DNA labeled in early S-phase by incorporation of nucleotide analogues are observed at the NM fraction.

More recent evidence, however, suggests that recruitment of origins of replication to the NM occurs only transiently in late G1 and S-phase. Attachment to the NM and nucleoskeleton has been

investigated for the well-studied origin of replication, *oriB*, at the *dihydrofolate reductase* (DFHR) locus in Chinese Hamster Ovary (CHO) cells (Ortega & DePamphilis 1998; Djeliova *et al.* 2001a,b). In one study, DNA from CHO cells was separated into loop and NM attached fractions (Djeliova *et al.* 2001a) and then probed with the *oriB* sequence or with nascent DNA from early S-phase (the collective origin fraction). No enrichment of origins, either *oriB* or the collective origin fraction, was observed in the NM attached DNA from asynchronous cells (Djeliova *et al.* 2001a). However, *oriB* was enriched in the NM attached DNA (Djeliova *et al.* 2001b) and nucleoskeleton attached DNA (Ortega & DePamphilis 1998) from late G1 phase cells (but not early G1), and lost from this fraction as cells progressed through S-phase (Djeliova *et al.* 2001b). In contrast to this early replicating origin, the late replicating origin from the *β-globin* gene was investigated in HeLa cells, where the NM association was maintained through S-phase (Djeliova *et al.* 2001b). Origins from other exemplar genes have also been described to temporally associate with the NM (reviewed in Ottaviani *et al.* 2008). Collectively, these studies show that origins have the potential to reside close to the NM, but that their association is not constitutive, being recruited during late G1 (Fig. 2C) and lost during S-phase.

Prereplication complex components

Potential DNA replication origins are marked by the origin recognition complex (ORC1-6), then licensed by recruitment of the rest of the prereplication complex components (pre-RC), including cell division cycle 6 (CDC6), chromatin licensing and DNA replication factor 1 (CDT1) and the mini-chromosome maintenance complex (MCM2-7), and reviewed in more detail elsewhere (Takisawa *et al.* 2000; Bell & Dutta 2002). Additional proteins associate with the pre-RC to form the pre-IC, which recruits the DNA replication machinery itself (RC) (summarized in Boos *et al.* 2012). We are not aware of any published investigations of pre-IC components in relation to the NM, but several report findings for pre-RC and RC components.

Consistent with their role in the regulation of temporally restricted events, pre-RC proteins have tightly controlled temporal expression and degradation, as well as restricted subnuclear localization. Unfortunately, many researchers limit their analysis by failing to include a nuclease digestion step in cellular extraction protocols, allowing only generalized conclusions about association with chromatin and/or NM. Furthermore, the cell cycle context of potential NM recruitment means that the fraction detected may be small and their recruitment to the NM may in fact be cell-type specific making the overall picture difficult to interpret. An important consideration to highlight here is that pre-RCs are laid down at potential origins (origin licensing) during late telophase in the mitotic cell cycle (Dimitrova *et al.* 2002), but lost if cells become quiescent (Madine *et al.* 2000; Tatsumi *et al.* 2003; Cook *et al.* 2004) necessitating their re-synthesis and recruitment following cell cycle re-entry. Therefore, the timing of both pre-RC formation and their NM recruitment is likely to be different for the G1 after release from quiescence compared to the G1-phase in the mitotic cell cycle. However, the accumulation of increasingly sophisticated reports on NM attachment of pre-RC components is beginning to support the idea that some core components become attached to the NM, possibly in particular combinations and only around the time of initiation of DNA replication.

The most widely used method to determine NM recruitment of pre-RC proteins uses cytoskeletal buffer (10 mM Pipes pH 6.8, 100 mM NaCl, 300 mM sucrose, 1 mM $MgCl_2$, 1 mM EGTA, 1 mM DTT) and fractionation by centrifugation (Ainscough *et al.* 2007). Soluble and insoluble proteins are recovered following treatment with 0.1% Triton X-100, and chromatin bound proteins are released by inclusion of 0.5 M or 2.0 M NaCl or subsequent treatment with DNase I. NM bound proteins are defined as those which are not released by any of these treatments. This method can be carried out on cell populations, for western blot analysis, and is also compatible with immunofluorescence-based imaging. A further distinction can be made between those proteins that are released from native cells but retained by those treated with a protein cross-linker such as DTSP. Chromatin bound proteins such as histones do not remain in the DNase I resistant fraction in the presence of cross-linker but NM associated proteins do, indicating direct interaction with a component of the NM (Fujita *et al.* 2002).

Origin recognition complex

Data show stable levels of ORC subunits 2–5 throughout the mitotic cell cycle (Madine *et al.* 2000; Fujita *et al.* 2002; Ohta *et al.* 2003; Tatsumi *et al.* 2003; McNairn *et al.* 2005), and one report suggests this is also true for ORC1 (McNairn *et al.* 2005).

However, the majority of reports show ORC1 to peak in G1 phase with subsequent proteolysis during S-phase and mitosis (Tatsumi *et al.* 2003). This 'ORC cycle' has been extensively reviewed elsewhere (DePamphilis 2003).

Several studies have looked at the relationship between ORC subunits and the NM. ORC1 has been detected in the NM fraction of asynchronous populations of HeLa, BJAB, and BC3 cells (Kreitz *et al.* 2001; Fujita *et al.* 2002; Ohta *et al.* 2003; Tatsumi *et al.* 2003; Ohsaki *et al.* 2009) and in *Drosophila melanogaster* cells (Varma & Mishra 2011). Several investigators have temporally resolved this NM association by cell cycle phase, which revealed ORC1 to be enriched in the NM fraction in G1, BJAB and BC3 cells, and G1 or from late G1 in HeLa cells (Kreitz *et al.* 2001; Fujita *et al.* 2002; Ohta *et al.* 2003; Tatsumi *et al.* 2003; Ohsaki *et al.* 2009). This suggests that when ORC1 is expressed it becomes NM bound. However, it should be borne in mind that NM attachment of ORC1 might be cell type dependent as one report shows ORC1 as sensitive to extraction with DNase I in proliferating NIH3T3 cells (Madine *et al.* 2000).

Other ORC subunits have also been detected in NM fractions, specifically ORC2-5 in asynchronous HeLa cells (Kreitz *et al.* 2001; Fujita *et al.* 2002; Ohta *et al.* 2003) and ORCs 2, 4, 5, and 6 in *Drosophila melanogaster* cells (Varma & Mishra 2011), although again this may be cell type specific as little ORC2 was NM bound in Raji cells (Mendez & Stillman 2000).

Where temporal resolution was attempted, ORC2-5 were enriched in the NM fraction in G1 (Kreitz *et al.* 2001) or from late G1, in HeLa cells (Ohta *et al.* 2003). In both cases, this was at the same time as ORC1 was expressed and NM bound. Furthermore investigation in HeLa cells showed that when ORC1 was depleted by RNAi, ORC2 was no longer enriched in the NM fraction (Ohta *et al.* 2003). Therefore, NM binding of ORC may well be dependent on ORC1.

Cell division cycle 6

The majority of investigations into the subnuclear localization of the CDC6 protein have revealed a proportion that is attached to the NM. This has been noted in asynchronous HeLa cells, BJAB, BC3, and HEK293 cells and is somewhat depleted in the absence of ORC1 in FT210 cells (Fujita 1999; Fujita *et al.* 2002; Ohta *et al.* 2003; Ohsaki *et al.* 2009). However, little CDC6 was found to be NM bound in NIH3T3 cells (Madine *et al.* 2000) or Raji cells (Mendez & Stillman 2000). Where cell cycle phases were investigated, CDC6 was present in the NM fraction during G1 or early S-phase but not in G2/M cells (Fujita *et al.* 1999; Ohsaki *et al.* 2009). Therefore, it is clear that independent groups, using different methods and cell lines, have shown ORC and CDC6 to be at least transiently attached to the NM.

Chromatin licensing and DNA replication factor 1

Along with CDC6, CDT1 is essential for the functional assembly of the MCM helicase complex and replication origin licensing (Cook *et al.* 2004). Few investigators have looked at NM attachment but one report described recovery of CDT1 in the NM fraction for BJAB, BC3, and HEK293 cells; this occurred specifically in G1 phase but not S or G2/M phases (Ohsaki *et al.* 2009). This suggests that CDT1 may be recruited to the NM but there is not enough information available to draw generalized conclusions.

Mini chromosome maintenance complex

The heterohexameric MCM complex is believed to be the helicase responsible for unwinding DNA during replication (Takisawa *et al.* 2000), but its relationship with the NM is not as clear as for other pre-RC components. The majority of MCM3 and MCM2 is not NM bound in asynchronous HeLa cells (Todorov *et al.* 1995; Fujita *et al.* 1997) with similar results for MCM2, MCM3, and MCM5/7 in REF52 cells (Cook *et al.* 2002), MCM3 in Raji cells (Mendez & Stillman 2000), and MCM5 in NIH3T3 cells (Stoeber *et al.* 1998). However, Burkhart *et al.* (1995) report a small but significant fraction of MCM3 in HeLa cells, which is not released by nuclease or high salt extraction. There are also several reports identifying MCM4, MCM2, MCM3, and MCM7 in NM proteomic screens in human or *Drosophila melanogaster* cell lines (Gerner *et al.* 2002; Mitulovic *et al.* 2004; Varma & Mishra 2011). Although the majority of the MCM complex does not appear to be NM bound it is possible that the small amount of MCM protein in NM preparations reflects a weak, transient association, which is easily missed in bulk preparations from asynchronous cells. Some circumstantial support for the idea that attachment to the NM may be important for MCM function comes from ORC1 or CDC6 depletion studies, in which immobilization of MCM (on chromatin or NM) is prevented (Ohta *et al.*

2003). Similarly, immobilization of ORC2-5 complexes on chromatin is not sufficient for MCM2 loading in the absence of ORC1 (Ohta *et al.* 2003). As ORC1 appears to recruit the rest of the ORC complex to the NM, this begins to suggest that loading of MCM2 occurs in that fraction.

Coordinators and regulators

A few proteins involved in the regulation of initiation of DNA replication and cell cycle progression have been studied in the context of the NM, including cyclin E (Munkley *et al.* 2011), Rb (Mancini *et al.* 1994), and CIZ1 (Ainscough *et al.* 2007).

Our study of cyclin E has been revealing, because it seeks to compare NM recruitment at different developmental stages (Munkley *et al.* 2011). In fact the NM attachment of cyclin E, a key regulator of initiation of DNA replication, may serve as a case study that goes some way to explain the differing reports of NM attachment of other replication proteins. We showed that a proportion of cyclin E is NM bound in differentiated, noncancer primary and established cell lines. However, in all but one of eight cancer cell lines we investigated, no cyclin E was observed in the NM fraction (Munkley *et al.* 2011). A similar distinction was seen between differentiated cells and undifferentiated cells in mouse, human, and *Xenopus* model systems, so that in all cases cyclin E was easily extracted from progenitor cells but resistant to extraction in differentiated derivatives. This suggests that cyclin E is recruited to the NM as cells differentiate, and that cancer cells either originate from cells that have not recruited cyclin E, or that cyclin E is released from the NM as a consequence of one of the events that lead to transformation. In fact, failure to recruit cyclin E (and by implication, initiation) to the NM in undifferentiated and cancer cells may be one of the factors that promote plasticity in response to extrinsic or intrinsic signals.

Overall, the work outlined here suggests that all three phases of DNA replication can occur in association with the NM. However, this may not be true for all cell types, making choice of experimental system crucial when planning further work. For various practical reasons, much of the analysis of DNA replication is undertaken with *Xenopus* eggs, or cancer cell lines such as HeLa, sometimes leading to the conclusion that NM immobilization may not be important for DNA replication. We would argue that the reported differences in nuclear organization in terms of proteins and loop attachments between embryonic systems and cancer cell lines on the one hand, and noncancer, differentiated cells on the other, offers a clear path forward.

Models

Here we consider models that attempt to explain how DNA replication may be organized in relation to the NM. Template DNA and DNA replication enzymes must move relative to each other during synthesis. It is still common to see depictions that show the DNA replication machinery as an entity that moves along the DNA strand. However, consideration of the evidence (below) has lead to the suggestion that the DNA replication machinery is static and instead the DNA moves through these fixed sites (Pardoll *et al.* 1980).

Replication factories

Replication foci or 'factories' can be visualized by immuno-detection of replication enzymes, or by following incorporation of nucleotide analogues into nascent DNA. They are believed to be macromolecular assemblies populated by the enzymes that replicate DNA, forming several hundred efficient factories representing clusters of origins and that are activated at the same time. The number of origins is thought to be highly heterogeneous but to be an average of 5–6 per factory (Berezney *et al.* 2000; Frouin *et al.* 2003; and references therein). There is some reason to think that clustering of origins may offer an energy saving, as activation in near space may enable more efficient processing due to locally higher concentrations of factors (Frouin *et al.* 2003) (Fig. 2D). However, not all origins are activated at the same time in S-phase. Some areas of the genome are replicated early in S-phase while others are replicated later. Replication foci from all temporal stages of S-phase have been shown to be NM associated (Nakayasu & Berezney 1989) complete with nascent DNA which gradually moves out from each focus (Hozak *et al.* 1993, 1994), consistent with the concept of emanating loops. Cohesin is thought to help hold loops together because it is present at origins, interacts with the pre-RC, and its absence slows S-phase (Guillou *et al.* 2010). These data indicate that the replication machinery is located at NM attachment points at the base of chromatin loops.

Organization of chromatin loops

Chromatin loops were first thought to be purely structural, giving way to more complex models with functionality at the base of loops. Depending on which direction researchers have approached this problem, models tend to appear in one of two forms, either a flower shaped factory of loops with little consideration of the NM (Frouin *et al.* 2003), or attachment to a NM at loop bases without representation of how these may come together into a factory (Cook 1999; Ottaviani *et al.* 2008) (Fig. 2B,D).

We, and others (Cook 1999; Ottaviani *et al.* 2008; Rivera-Mulia *et al.* 2011), hypothesize that recruitment of origins to the NM is part of the process of initiation (Fig. 2C). Recruitment appears to occur after pre-RC formation, as much of this is laid down at telophase in the mitotic cell cycle, yet origins appear to be recruited later in G1-phase (Djeliova *et al.* 2001b). When incorporating origin recruitment into models, several show an origin located distally on a loop, being recruited to the NM in late G1/S-phase. As DNA is spooled through replication factories, newly synthesized DNA is extruded as two new loops, with their origins returning to their original location (Cook 1999; Ottaviani *et al.* 2008). This implies a transient shortening of loops as origin attachments are made and a further transient shortening as DNA is reeled through replication machinery following origin activation. To understand the impact this would have on average loop size, and we must consider whether origins are all recruited at the same time because if this is not synchronous the effect on loop size could be minimal. Djeliova *et al.* (2001a,b) report that both an early and a late origin were recruited to the NM during late G1 (described in more detail above), suggesting that recruitment to the NM is synchronous rather than temporally distributed as for replication factory activation. However, analysis of chromatin loop size by MFHR has revealed no global loop remodeling between different phases of the cell cycle (Jackson *et al.* 1990).

To reconcile the model with these observations, we considered the consequences of recruitment of origins that are more proximal to existing attachment points, as proposed elsewhere (Rivera-Mulia *et al.* 2011). Recruitment of origins at the 'top' of loops would cause a reduction in loop size by up to 50%, but this would be the maximum observed. Recruitment of origins closer to the existing S/MAR would have less of an effect on loop size. For example, recruitment of origins a quarter of the way 'up' a loop would initially cause only a maximum of 12.5% drop in loop size (Fig. 2C), and the closer the origin is to an existing S/MAR the less the effect would be. Recruitment of origins close to existing S/MARs may preferentially occur, in which case a small decrease in global loop size may be difficult to observe and may explain why no decrease is reported for late G1-phase.

Similarly, no decrease in loop size is reported for S-phase despite a theoretical decrease, as the DNA is reeled in towards the replication machinery at the NM. This is perhaps not surprising given that origins are not all activated at the same time but as part of an organized temporal programe. Taken together, these arguments go some way to explaining little global impact on average chromatin loop size in either late G1 or S-phase.

Similarities to transcription

Briefly, we highlight the data suggesting a role of the NM in transcription, as conclusions from this similar mechanism can be informative. There is a large array of published work implicating the NM as the site for transcription (summarised in Razin *et al.* 2011). Nuclear skeleton preparations showed nascent RNA, active RNA polymerase, and active genes in the resistant fraction, with similar results from NM preparations (Jackson & Cook 1985; and references therein). Consistent with this, several reports suggest that attachment points are enriched at transcribed genes (Jackson *et al.* 1996; Craig *et al.* 1997), with loops of ~4 kb, in contrast to ~200 kb loops of inactive chromatin (Bode *et al.* 2003), suggesting the attachments have functional significance. A proteomics screen of NM proteins returned many transcription factors (Albrethsen *et al.* 2009), which have been suggested to be MARBPs with binding sites potentially increasing the probability of a S/MAR. FISH to various genes showed transcriptionally active genes exhibited a spot at the NM (increased attachment) whereas transcriptionally inactive genes were extended on loops (Gerdes *et al.* 1994). However, this separation was less clear during S-phase when it was suggested that the attachment pattern was then a combination of effects of transcriptional status and transient NM attachment during replication with both gain and loss of attachments during this period (Gerdes *et al.* 1994). Models proposed for transcription, like replication, involve loops forming factories (Cook 1999; Sutherland & Bickmore 2009), implying

a degree of commonality in mechanisms, but also a potential conflict of organization.

Nuclear changes in cancer and disease

As a common feature of cancer cells, changes in nuclear architecture and morphology have long been the basis for cancer diagnoses (reviewed in Zink *et al.* 2004). However, without a complete understanding of nuclear architecture in normal cells it is difficult to consider whether such changes are cause or consequence of the dysregulation of cancer cells. In addition to genetic and epigenetic changes, there are many other recorded changes in the organization of genes, subnuclear domains, nonlinear DNA associations, and regulatory and macromolecular complexes in cancer cells (reviewed extensively elsewhere, for example, in Zaidi *et al.* 2007). This is also true for several other diseases (reviewed in Bode *et al.* 2000; Linnemann & Krawetz 2009a), including the thalassaemias where deletions often correspond with S/MAR sites suggesting that a change in chromatin loop attachment is a contributory factor (Bode *et al.* 2000). Changes in NM composition have been described for cancer cells compared to noncancer cells, with some exploited as the basis of diagnostic tests (Zink *et al.* 2004; He *et al.* 2008; Albrethsen *et al.* 2009; Lever & Sheer 2010; Munkley *et al.* 2011; and references therein). For example, a splice variant of the NM protein CIZ1 is associated with and can be detected in the blood of individuals with early stage disease (Higgins *et al.* 2012). Splice variants or altered expression of CIZ1 have also been reported to be associated with other cancers, including medulloblastoma, breast cancer, and Ewing's sarcoma (Warder & Keherly 2003; den Hollander & Kumar 2006; Rahman *et al.* 2007) and with other disorders including Alzheimer disease, rheumatoid arthritis, and cervical dystonia (Judex *et al.* 2003; Dahmcke *et al.* 2008; Xiao *et al.* 2012), many of which report alteration in subnuclear localization. The MARBP SATB1 is linked to aggressive breast cancers, (reviewed in Lever & Sheer 2010) while SAF-B is inversely correlated with the proliferative rate of tumors (reviewed in Lever & Sheer 2010). A number of NM proteins (for example, RUNX, CIZ1 and cyclin E) have been reported to have an altered localization in cancer cells, sometimes due to failure to be recruited to the NM (Zaidi *et al.* 2007; Munkley *et al.* 2011; Higgins *et al.* 2012).

We suggest that some of the dysregulation of cancer cells may be a direct result of events such as these, with DNA replication and transcription no longer spatially constrained by attachment to the NM. NM composition and loop attachments have been observed to change during differentiation and development (Getzenberg 1994; Munkley *et al.* 2011; Varma & Mishra 2011), leading to the idea that this may serve to 'fix' the developmental programe (Vassetzky *et al.* 2000; Munkley *et al.* 2011). We suggest this fixing of cell type specific characteristics such as transcriptional programe and replication timing is defective in cancer cells, resulting in a partial reversal to a less specified, embryonic-like organization of chromatin.

Conclusions

The replication of DNA is fundamental to all cells, but is often deregulated in cancer cells with dramatic consequences. Data are amassing that suggest all stages of DNA replication are located at the NM at least in some cell types, and it is becoming clear that immobilization of DNA machinery and the resultant mechanisms of replication are likely to be an important method of regulating DNA synthesis. DNA replication should therefore not be considered alone, but in the context of nuclear architecture, with many other processes occurring at the same time and in the same space, in connection with a nuclear substructure. The NM can appear mysterious and elusive in detail, which we suggest may reflect the model system of choice.

The available published work suggests that in differentiated, noncancer cells, attachment of DNA and proteins involved in DNA replication to a NM occurs at specific times in the preparation for and during DNA replication. This is likely to constrain the process in time and space and possibly help to establish a heritable pattern of DNA replication. Attachment to a spatially constrained structure would also promote efficient use of required factors, with locally high concentrations at specific sites rather than diffusely spread throughout the nucleus. However, using the behavior of cyclin E as an indicator, we suggest that in undifferentiated or cancer cells initiation of DNA replication is less fixed in space. We suggest that failure to constrain initiation may allow greater flexibility and plasticity in these cell types, and that such flexibility may be lost with the imposition of spatial constraint as cells differentiate. This idea echoes the change in origin usage recorded as cells differentiate, with random and more frequent origin usage in early embryonic cell cycles, giving way to fewer and more specified origin usage in later cell cycles. Many other fundamental processes also appear

to occur at the NM, such as transcription, DNA repair and epigenetic remodeling. Therefore, it is likely that these may also be subject to a similar level of regulation as DNA replication and their disregulation in cancer may similarly be in part due to compromised attachment to the NM.

As well as these potential differences between cell types we should also bear in mind that there may well be different mechanisms occurring within one cell. While there appears a universal process of DNA synthesis, it is likely that there will be differences in the initiation process. For example, there may be slightly different mechanisms used to select and initiate origins that govern replication through euchromatin compared to heterochromatin.

In conclusion we suggest that the relationship between the NM and DNA replication is important and complex, providing organization in many forms as well as anchoring key processes. However, this relationship cannot at the moment be generalized with differences occurring between cell types, and we hypothesize different types of chromatin within the same cell.

Acknowledgements

We thank G. Higgins, O. Jackson for critical comment and P. Roberts for graphics. Work in authors' laboratory was supported in part by grants from the BBSRC, UK and Yorkshire Cancer Research, UK.

References

Ainscough, J.F., Rahman, F.A., Sercombe, H., Sedo, A., Gerlach, B. & Coverley, D. (2007) C-terminal domains deliver the DNA replication factor Ciz1 to the nuclear matrix. *J. Cell Sci.* **120**, 115–124.

Albrethsen, J., Knol, J.C. & Jimenez, C.R. (2009) Unravelling the nuclear matrix proteome. *J. Proteomics* **72**, 71–81.

Bell, S.P. & Dutta, A. (2002) DNA replication in eukaryotic cells. *Ann. Rev. Biochem.* **71**, 333–374.

Benyajati, C. & Worcel, A. (1976) Isolation, characterization, and structure of the folded interphase genome of Drosophila melanogaster. *Cell* **9**, 393–407.

Berezney, R. & Coffey, D.S. (1974) Identification of a nuclear protein matrix. *Biochem. Biophys. Res. Commun.* **60**, 1410–1417.

Berezney, R., Dubey, D.D. & Huberman, J.A. (2000) Heterogeneity of eukaryotic replicons, replicon clusters, and replication foci. *Chromosoma* **108**, 471–484.

Berrios, M., Osheroff, N. & Fisher, P.A. (1985) In situ localization of DNA topoisomerase II, a major polypeptide component of the Drosophila nuclear matrix fraction. *Proc. Natl Acad. Sci. USA* **82**, 4142–4146.

Bian, Q. & Belmont, A.S. (2012) Revisiting higher-order and large-scale chromatin organization. *Curr. Opin. Cell Biol.* **24**, 359–366.

Bode, J., Benham, C., Ernst, E., Knopp, A., Marschalek, R., Strick, R. & Strissel, P. (2000) Fatal connections: when DNA ends meet on the nuclear matrix. *J. Cell. Biochem. Suppl.* **35** (Suppl.), 3–22.

Bode, J., Goetze, S., Heng, H., Krawetz, S.A. & Benham, C. (2003) From DNA structure to gene expression: mediators of nuclear compartmentalization and dynamics. *Chromosome Res.* **11**, 435–445.

Boos, D., Frigola, J. & Diffley, J.F. (2012) Activation of the replicative DNA helicase: breaking up is hard to do. *Curr. Opin. Cell Biol.* **24**, 423–430.

Boulikas, T. (1995) Chromatin domains and prediction of MAR sequences. *Int. Rev. Cytol.* **162A**, 279–388.

Buongiorno-Nardelli, M., Micheli, G., Carri, M.T. & Marilley, M. (1982) A relationship between replicon size and supercoiled loop domains in the eukaryotic genome. *Nature* **298**, 100–102.

Burkhart, R., Schulte, D., Hu, B., Musahl, C., Gohring, F. & Knippers, R. (1995) Interactions of human nuclear proteins P1Mcm3 and P1Cdc46. *Eur. J. Biochem.* **228**, 431–438.

Cayrou, C., Coulombe, P. & Mechali, M. (2010) Programming DNA replication origins and chromosome organization. *Chromosome Res.* **18**, 137–145.

Cayrou, C., Coulombe, P., Vigneron, A., Stanojcic, S., Ganier, O., Peiffer, I., Rivals, E., Puy, A., Laurent-Chabalier, S., Desprat, R. & Mechali, M. (2011) Genome-scale analysis of metazoan replication origins reveals their organization in specific but flexible sites defined by conserved features. *Genome Res.* **21**, 1438–1449.

Cook, J.G., Chasse, D.A. & Nevins, J.R. (2004) The regulated association of Cdt1 with minichromosome maintenance proteins and Cdc6 in mammalian cells. *J. Biol. Chem.* **279**, 9625–9633.

Cook, J.G., Park, C.-H., Burke, T., Leone, G., DeGregori, J., Engel, A. & Nevins, J. (2002) Analysis of Cdc6 function in the assembly of mammalian prereplication complexes. *Proc. Natl Acad. Sci. USA* **99**, 1347–1352.

Cook, P.R. (1999) The organization of replication and transcription. *Science* **284**, 1790–1795.

Craig, J.M., Boyle, S., Perry, P. & Bickmore, W.A. (1997) Scaffold attachments within the human genome. *J. Cell Sci.* **110** (Pt 21), 2673–2682.

Cremer, T., Cremer, M., Dietzel, S., Muller, S., Solovei, I. & Fakan, S. (2006) Chromosome territories–a functional nuclear landscape. *Curr. Opin. Cell Biol.* **18**, 307–316.

Dahmcke, C.M., Buchmann-Moller, S., Jensen, N.A. & Mitchelmore, C. (2008) Altered splicing in exon 8 of the DNA replication factor CIZ1 affects subnuclear distribution and is associated with Alzheimer's disease. *Mol. Cell. Neurosci.* **38**, 589–594.

DePamphilis, M.L. (2003) The 'ORC cycle': a novel pathway for regulating eukaryotic DNA replication. *Gene* **310**, 1–15.

Dimitrova, D.S., Prokhorova, T.A., Blow, J.J., Todorov, I.T. & Gilbert, D.M. (2002) Mammalian nuclei become licensed for DNA replication during late telophase. *J. Cell Sci.* **115**, 51–59.

Djeliova, V., Russev, G. & Anachkova, B. (2001a) Distribution of DNA replication origins between matrix-attached and loop DNA in mammalian cells. *J. Cell. Biochem.* **80**, 353–359.

Djeliova, V., Russev, G. & Anachkova, B. (2001b) Dynamics of association of origins of DNA replication with the nuclear matrix during the cell cycle. *Nucleic Acids Res.* **29**, 3181–3187.

Evans, K., Ott, S., Hansen, A., Koentges, G. & Wernisch, L. (2007) A comparative study of S/MAR prediction tools. *BMC Bioinformatics* **8**, 71.

Frouin, I., Montecucco, A., Spadari, S. & Maga, G. (2003) DNA replication: a complex matter. *EMBO Rep.* **4**, 666–670.

Fudenberg, G. & Mirny, L.A. (2012) Higher-order chromatin structure: bridging physics and biology. *Curr. Opin. Genet. Dev.* **22**, 115–124.

Fujita, M. (1999) Cell cycle regulation of DNA replication initiation proteins in mammalian cells. *Front. Biosci.* **4**, D816–D823.

Fujita, M., Ishimi, Y., Nakamura, H., Kiyono, T. & Tsurumi, T. (2002) Nuclear organization of DNA replication initiation proteins in mammalian cells. *J. Biol. Chem.* **277**, 10354–10361.

Fujita, M., Kiyono, T., Hayashi, Y. & Ishibashi, M. (1997) In vivo interaction of human MCM heterohexameric complexes with chromatin. Possible involvement of ATP. *J. Biol. Chem.* **272**, 10928–10935.

Fujita, M., Yamada, C., Goto, H., Yokoyama, N., Kuzushima, K., Inagaki, M. & Tsurumi, T. (1999) Cell cycle regulation of human CDC6 protein. Intracellular localization, interaction with the human mcm complex, and CDC2 kinase-mediated hyperphosphorylation. *J. Biol. Chem.* **274**, 25927–25932.

Gerdes, M.G., Carter, K.C., Moen, P.T. Jr & Lawrence, J. B. (1994) Dynamic changes in the higher-level chromatin organization of specific sequences revealed by in situ hybridization to nuclear halos. *J. Cell Biol.* **126**, 289–304.

Gerner, C., Gotzmann, J., Frohwein, U., Schamberger, C., Ellinger, A. & Sauermann, G. (2002) Proteome analysis of nuclear matrix proteins during apoptotic chromatin condensation. *Cell Death Differ.* **9**, 671–681.

Getzenberg, R.H. (1994) Nuclear matrix and the regulation of gene expression: tissue specificity. *J. Cell. Biochem.* **55**, 22–31.

Guillou, E., Ibarra, A., Coulon, V., Casado-Vela, J., Rico, D., Casal, I., Schwob, E., Losada, A. & Mendez, J. (2010) Cohesin organizes chromatin loops at DNA replication factories. *Genes Dev.* **24**, 2812–2822.

Hancock, R. (2000) A new look at the nuclear matrix. *Chromosoma* **109**, 219–225.

He, S., Dunn, K.L., Espino, P.S., Drobic, B., Li, L., Yu, J., Sun, J.M., Chen, H.Y., Pritchard, S. & Davie, J.R. (2008) Chromatin organization and nuclear microenvironments in cancer cells. *J. Cell. Biochem.* **104**, 2004–2015.

Hendzel, M.J., Boisvert, F. & Bazett-Jones, D.P. (1999) Direct visualization of a protein nuclear architecture. *Mol. Biol. Cell* **10**, 2051–2062.

Heng, H.H., Goetze, S., Ye, C.J., Liu, G., Stevens, J.B., Bremer, S.W., Wykes, S.M., Bode, J. & Krawetz, S.A. (2004) Chromatin loops are selectively anchored using scaffold/matrix-attachment regions. *J. Cell Sci.* **117**, 999–1008.

Higgins, G., Roper, K.M., Watson, I.J., Blackhall, F.H., Rom, W.N., Pass, H.I., Ainscough, J.F. & Coverley, D. (2012) Variant Ciz1 is a circulating biomarker for early stage lung cancer. *Proc. Natl Acad. Sci. USA* (in press).

den Hollander, P. & Kumar, R. (2006) Dynein light chain 1 contributes to cell cycle progression by increasing cyclin-dependent kinase 2 activity in estrogen-stimulated cells. *Cancer Res.* **66**, 5941–5949.

Hozak, P., Hassan, A.B., Jackson, D.A. & Cook, P.R. (1993) Visualization of replication factories attached to the nucleoskeleton. *Cell* **73**, 361–373.

Hozak, P., Jackson, D.A. & Cook, P.R. (1994) Replication factories and nuclear bodies: the ultrastructural characterization of replication sites during the cell cycle. *J. Cell Sci.* **107** (Pt 8), 2191–2202.

Jackson, D.A., Bartlett, J. & Cook, P.R. (1996) Sequences attaching loops of nuclear and mitochondrial DNA to underlying structures in human cells: the role of transcription units. *Nucleic Acids Res.* **24**, 1212–1219.

Jackson, D.A. & Cook, P.R. (1985) Transcription occurs at a nucleoskeleton. *EMBO J.* **4**, 919–925.

Jackson, D.A. & Cook, P.R. (1986a) Different populations of DNA polymerase alpha in HeLa cells. *J. Mol. Biol.* **192**, 77–86.

Jackson, D.A. & Cook, P.R. (1986b) Replication occurs at a nucleoskeleton. *EMBO J.* **5**, 1403–1410.

Jackson, D.A. & Cook, P.R. (1988) Visualization of a filamentous nucleoskeleton with a 23 nm axial repeat. *EMBO J.* **7**, 3667–3677.

Jackson, D.A., Dickinson, P. & Cook, P.R. (1990) The size of chromatin loops in HeLa cells. *EMBO J.* **9**, 567–571.

Judex, M., Neumann, E., Lechner, S., Dietmaier, W., Ballhorn, W., Grifka, J., Gay, S., Schölmerich, J., Kullman, F. & Müller-Ladner, U. (2003) Laser-mediated microdissection facilitates analysis of area-specific gene expression in rheumatoid synovium. *Arthritis Rheum.* **48**, 97–102.

Kramer, J.A. & Krawetz, S.A. (1996) Nuclear matrix interactions within the sperm genome. *J. Biol. Chem.* **271**, 11619–11622.

Kreitz, S., Ritzi, M., Baack, M. & Knippers, R. (2001) The human origin recognition complex protein 1 dissociates from chromatin during S phase in HeLa cells. *J. Biol. Chem.* **276**, 6337–6342.

Lagarkova, M.A., Svetlova, E., Giacca, M., Falaschi, A. & Razin, S.V. (1998) DNA loop anchorage region colocalizes

with the replication origin located downstream to the human gene encoding lamin B2. *J. Cell. Biochem.* **69**, 13–18.

Lever, E. & Sheer, D. (2010) The role of nuclear organization in cancer. *J. Pathol.* **220**, 114–125.

Lieberman-Aiden, E., van Berkum, N.L., Williams, L., *et al.* (2009) Comprehensive mapping of long-range interactions reveals folding principles of the human genome. *Science* **326**, 289–293.

Liebich, I., Bode, J., Frisch, M. & Wingender, E. (2002a) S/MARt DB: a database on scaffold/matrix attached regions. *Nucleic Acids Res.* **30**, 372–374.

Liebich, I., Bode, J., Reuter, I. & Wingender, E. (2002b) Evaluation of sequence motifs found in scaffold/matrix-attached regions (S/MARs). *Nucleic Acids Res.* **30**, 3433–3442.

Linnemann, A.K. & Krawetz, S.A. (2009a) Maintenance of a functional higher order chromatin structure: the role of the nuclear matrix in normal and disease states. *Gene Ther. Mol. Biol.* **13**, 231–243.

Linnemann, A.K. & Krawetz, S.A. (2009b) Silencing by nuclear matrix attachment distinguishes cell-type specificity: association with increased proliferation capacity. *Nucleic Acids Res.* **37**, 2779–2788.

Linnemann, A.K., Platts, A.E. & Krawetz, S.A. (2009) Differential nuclear scaffold/matrix attachment marks expressed genes. *Hum. Mol. Genet.* **18**, 645–654.

Little, R.D., Platt, T.H.K. & Schildkraut, C.L. (1993) Initiation and termination of DNA replication in human rRNA genes. *Mol. Cell. Biol.* **13**, 6600–6613.

Ma, H., Siegel, A.J. & Berezney, R. (1999) Association of chromosome territories with the nuclear matrix. Disruption of human chromosome territories correlates with the release of a subset of nuclear matrix proteins. *J. Cell Biol.* **146**, 531–542.

Madine, M.A., Sweitlik, M., Pelizon, C., Romanowski, P., Mills, A.D. & Laskey, R.A. (2000) The roles of Mcm, Orc and Cdc6 protein in determining the replication competence of chromatin in quiescent cells. *J. Struct. Biol.* **129**, 198–210.

Mancini, M.A., Shan, B., Nickerson, J.A., Penman, S. & Lee, W.H. (1994) The retinoblastoma gene product is a cell cycle-dependent, nuclear matrix-associated protein. *Proc. Natl Acad. Sci. USA* **91**, 418–422.

Marsden, M.P. & Laemmli, U.K. (1979) Metaphase chromosome structure: evidence for a radial loop model. *Cell* **17**, 849–858.

Martelli, A.M., Falcieri, E., Zweyer, M., Bortul, R., Tabellini, G., Cappellini, A., Cocco, L. & Manzoli, L. (2002) The controversial nuclear matrix: a balanced point of view. *Histol. Histopathol.* **17**, 1193–1205.

McNairn, A.J., Okuno, Y., Misteli, T. & Gilbert, D.M. (2005) Chinese hamster ORC subunits dynamically associate with chromatin throughout the cell-cycle. *Exp. Cell Res.* **308**, 345–356.

Mechali, M. (2010) Eukaryotic DNA replication origins: many choices for appropriate answers. *Nat. Rev. Mol. Cell Biol.* **11**, 728–738.

Mendez, J. & Stillman, B. (2000) Chromatin association of human origin recognition complex, Cdc6 and minichromosome maintenance proteins during the cell cycle: assembly of the pre-replication complex in late mitosis. *Mol. Cell. Biol.* **20**, 8602–8612.

Mika, S. & Rost, B. (2005) NMPdb: database of nuclear matrix proteins. *Nucleic Acids Res.* **33**, D160–D163.

Mirkovitch, J., Mirault, M.E. & Laemmli, U.K. (1984) Organization of the higher-order chromatin loop: specific DNA attachment sites on nuclear scaffold. *Cell* **39**, 223–232.

Mitulovic, G., Stingl, C., Smoluch, M., Swart, R., Chervet, J. P., Steinmacher, I., Gerner, C. & Mechtler, K. (2004) Automated, on-line two-dimensional nano liquid chromatography tandem mass spectrometry for rapid analysis of complex protein digests. *Proteomics* **4**, 2545–2557.

Munkley, J., Copeland, N.A., Moignard, V., Knight, J.R., Greaves, E., Ramsbottom, S.A., Pownall, M.E., Southgate, J., Ainscough, J.F. & Coverley, D. (2011) Cyclin E is recruited to the nuclear matrix during differentiation, but is not recruited in cancer cells. *Nucleic Acids Res.* **39**, 2671–2677.

Nakayasu, H. & Berezney, R. (1989) Mapping replicational sites in the eucaryotic cell nucleus. *J. Cell Biol.* **108**, 1–11.

Nelson, W.G., Pienta, K.J., Barrack, E.R. & Coffey, D.S. (1986) The role of the nuclear matrix in the organization and function of DNA. *Annu. Rev. Biophys. Biophys. Chem.* **15**, 457–475.

Nickerson, J. (2001) Experimental observations of a nuclear matrix. *J. Cell Sci.* **114**, 463–474.

Nieduszynski, C.A., Knox, Y. & Donaldson, A.D. (2006) Genome-wide identification of replication origins in yeast by comparative genomics. *Genes Dev.* **20**, 1874–1879.

Ohsaki, E., Suzuki, T., Karayama, M. & Ueda, K. (2009) Accumulation of LANA at nuclear matrix fraction is important for Kaposi's sarcoma-associated herpesvirus replication in latency. *Virus Res.* **139**, 74–84.

Ohta, S., Tatsumi, Y., Fujita, M., Tsurimoto, T. & Obuse, C. (2003) The ORC1 cycle in human cells: II. Dynamic changes in the human ORC complex during the cell cycle. *J. Biol. Chem.* **278**, 41535–41540.

Ortega, J.M. & DePamphilis, M.L. (1998) Nucleoskeleton and initiation of DNA replication in metazoan cells. *J. Cell Sci.* **111** (Pt 24), 3663–3673.

Ottaviani, D., Lever, E., Takousis, P. & Sheer, D. (2008) Anchoring the genome. *Genome Biol.* **9**, 201.

Pardoll, D.M., Vogelstein, B. & Coffey, D.S. (1980) A fixed site of DNA replication in eucaryotic cells. *Cell* **19**, 527–536.

Paulson, J.R. & Laemmli, U.K. (1977) The structure of histone-depleted metaphase chromosomes. *Cell* **12**, 817–828.

Pederson, T. (1998) Thinking about a nuclear matrix. *J. Mol. Biol.* **277**, 147–159.

Platts, A.E., Quayle, A.K. & Krawetz, S.A. (2006) In-silico prediction and observations of nuclear matrix attachment. *Cell. Mol. Biol. Lett.* **11**, 191–213.

Qiao, F., Moss, A. & Kupfer, G.M. (2001) Fanconi anemia proteins localize to chromatin and the nuclear matrix in a DNA damage- and cell cycle-regulated manner. *J. Biol. Chem.* **276**, 23391–23396.

Radichev, I., Parashkevova, A. & Anachkova, B. (2005) Initiation of DNA replication at a nuclear matrix-attached chromatin fraction. *J. Cell. Physiol.* **203**, 71–77.

Rahman, F.A., Ainscough, J.F.-X., Copeland, N. & Coverley, D. (2007) Cancer-associated missplicing of exon 4 influences the subnuclear distribution of the DNA replication factor Ciz1. *Hum. Mutat.* **28**, 993–1004.

Razin, S.V., Gavrilov, A.A., Pichugin, A., Lipinski, M., Iarovaia, O.V. & Vassetzky, Y.S. (2011) Transcription factories in the context of the nuclear and genome organization. *Nucleic Acids Res.* **39**, 9085–9092.

Reyes, J.C., Muchardt, C. & Yaniv, M. (1997) Components of the human SWI/SNF complex are enriched in active chromatin and are associated with the nuclear matrix. *J. Cell Biol.* **137**, 263–274.

Rivera-Mulia, J.C., Hernandez-Munoz, R., Martinez, F. & Aranda-Anzaldo, A. (2011) DNA moves sequentially towards the nuclear matrix during DNA replication in vivo. *BMC Cell Biol.* **12**, 3.

Singh, G.B., Kramer, J.A. & Krawetz, S.A. (1997) Mathematical model to predict regions of chromatin attachment to the nuclear matrix. *Nucleic Acids Res.* **25**, 1419–1425.

Stoeber, K., Mills, A.D., Kubota, Y., Krude, T., Romanowski, P., Marheineke, K., Laskey, R.A. & Williams, G.H. (1998) Cdc6 protein causes premature entry into S phase in a mammalian cell-free system. *EMBO J.* **17**, 7219–7229.

Sutherland, H. & Bickmore, W.A. (2009) Transcription factories: gene expression in unions? *Nat. Rev.* **10**, 457–466.

Takisawa, H., Mimura, S. & Kubota, Y. (2000) Eukaryotic DNA replication: from pre-replication complex to initiation complex. *Curr. Opin. Cell Biol.* **12**, 690–696.

Tatsumi, Y., Ohta, S., Kimura, H., Tsurimoto, T. & Obuse, C. (2003) The ORC1 cycle in human cells: I. Cell cycle-regulated oscillation of human ORC1. *J. Biol. Chem.* **278**, 41528–41534.

Todorov, I.T., Attaran, A. & Kearsey, S.E. (1995) BM28, a human member of the MCM2-3-5 family, is displaced from chromatin during DNA replication. *J. Cell Biol.* **129**, 1433–1445.

Varma, P. & Mishra, R.K. (2011) Dynamics of nuclear matrix proteome during embryonic development in Drosophila melanogaster. *J. Biosci.* **36**, 439–459.

Vassetzky, Y.S., Hair, A. & Razin, S.V. (2000) Rearrangement of chromatin domains in cancer and development. *J. Cell. Biochem. Suppl.* **35**(Suppl.), 54–60.

Vogelstein, B., Pardoll, D.M. & Coffey, D.S. (1980) Supercoiled loops and eucaryotic DNA replicaton. *Cell* **22**, 79–85.

Wang, T.Y., Han, Z.M., Chai, Y.R. & Zhang, J.H. (2010) A mini review of MAR binding proteins. *Molecular Biology Reports* **37**, 3553–3560.

Warder, D.E. & Keherly, M.J. (2003) Ciz1, Cip1 interacting zinc finger protein 1 binds the consensus DNA sequence ARYSR(0-2)YYAC. *J. Biomed. Sci.* **10**, 406–417.

Xiao, J., Uitti, R.J., Zhao, Y., Vemula, S.R., Perlmutter, J.S., Wszolek, Z.K., Maraganore, D.M., Auburger, G.D.M., Leube, B.D.M., Lehnhoff, K. & Ledoux, M.S. (2012) Mutations in CIZ1 cause adult onset primary cervical dystonia. *Ann. Neurol.* **71**, 458–469.

Zaidi, S.K., Young, D.W., Javed, A., Pratap, J., Montecino, M., van Wijnen, A., Lian, J.B., Stein, J.L. & Stein, G.S. (2007) Nuclear microenvironments in biological control and cancer. *Nat. Rev. Cancer* **7**, 454–463.

Zeitlin, S., Parent, A., Silverstein, S. & Efstratiadis, A. (1987) Pre-mRNA splicing and the nuclear matrix. *Mol. Cell. Biol.* **7**, 111–120.

Zink, D., Fischer, A.H. & Nickerson, J.A. (2004) Nuclear structure in cancer cells. *Nat. Rev. Cancer* **4**, 677–687.

Received: 20 July 2012
Accepted: 10 September 2012

Chapter

The nuclear matrix: preparation for microscopy and biochemical analysis

Topic introduction

The nuclear matrix: fractionation techniques and analysis

Short title: Nuclear matrix fractionation

Wilson, R. H. C.[1*] Hesketh, E.[1] and Coverley, D.[1]

[1] Department of Biology, University of York, Wentworth Way, York, YO10 5DD, UK

[*] Corresponding author: Wilson, R. H. C. rhcw500@york.ac.uk, 01904 328569

The first descriptions of an insoluble nuclear structure appeared more than 70 years ago, but it is only in recent years that a sophisticated picture of its significance has begun to emerge. In this article we explain multiple methods for the study of the nuclear matrix. These have led to the understanding that the nuclear matrix consists of core components that are consistently present, such as matrins, lamins, hnRNPs and other 'structural' proteins, and conditional proteins that are recruited into the nuclear matrix to facilitate specific processes (Mika and Rost 2005). These include components of the DNA replication machinery (reviewed in Wilson & Coverley 2013), transcription machinery (Jackson and Cook 1985), DNA repair (Qiao et al. 2001; Boisvert et al. 2005; Campalans et al. 2007), splicing (Zeitlin et al. 1987; Jagatheesan et al. 1999) and chromatin remodelling (Reyes et al. 1997) as well as a catalogue of proteins identified by proteomic analysis (Albrethsen et al. 2009). In most cases the functional significance of their immobilisation remains an area of study, nevertheless, a number of nuclear matrix proteins are already gaining credibility as clinically useful biomarkers (Keesee et al. 1999; Subong et al. 1999; Van Le et al. 2004; Higgins et al. 2012).

A brief history

Descriptions of a protein fraction that is resistant to extraction under high salt conditions were first made in 1942 (reviewed in Pederson 1998). However, the term 'nuclear matrix' was first used in 1974 to refer to those proteins resistant to extraction with 2.0 M NaCl (Berezney and Coffey 1974). 'Nuclear matrix' has become widely adopted as an overarching term for the proteins that resist aggressive methods of extraction, and we use it as such here. The 2.0 M NaCl method has been criticised because of its potential to cause aggregation of proteins. This led to the development of more refined extraction methods including lithium 3,5-diiodosalicylate (LIS), which was first used by Mirkovitch et al. (1984) to reveal a protein fraction termed the nuclear scaffold, and extraction after encapsulation in agarose under physiologically relevant salt concentrations (Jackson and Cook 1988) to reveal a substructure known as the nuclear skeleton (or nucleoskeleton). Further variations and refinement of these techniques have also been used (reviewed in Martelli et al. 2002). A modification of the original nuclear matrix method was developed by Capco et al (1982), which reduced the potential for aggregation by using more physiologically relevant buffers with lower salt (0.5 M NaCl) and used nucleases (DNase I or other enzymes) to digest chromatin into small diffusible fragments. This was termed the 'in situ nuclear matrix' as the cytoskeleton is also maintained under these conditions. Extraction with 2.0 M NaCl has subsequently been termed the 'core nuclear matrix'.

A simple picture?

Despite the range of approaches used, some controversies have remained and reviews of the evidence for and against the nuclear matrix have come to conflicting conclusions (Pederson 1998; Hancock 2000; Nickerson 2001; Martelli et al. 2002). It has proved difficult to visualise the filamentous structure revealed by electron microscopy, using immunofluorescence-light microscopy, which typically reveal punctate foci for most of the 100s of nuclear matrix proteins that have been described. However it should be bourn in mind that the proteins which fractionate with the nuclear matrix and are identified by proteomic analysis may in fact make up highly dynamic 'local' matrices rather than one large static structure (Martelli et al. 2002).

One fundamental biological reason for the debate surrounding existence and nature of the nuclear matrix may in fact be that it exists in different forms in different cell types and may even be absent in some instances. We and others have shown that nuclear matrix composition varies dramatically with differentiation and disease status and that some proteins are actively recruited as part of normal cellular transitions (Getzenberg 1994; Zink et al. 2004; Munkley et al. 2011; Varma and Mishra 2011). Thus a lot of work previously undertaken on cancer cell lines, embryonic cells or Xenopus eggs must now be interpreted in this light to avoid clouding the picture in normal somatic cells (Munkley et al. 2011). There remains a need for a resurgence in nuclear matrix investigation that includes comparative analysis, the protocols that we use for this purpose accompany this topic introduction (The nuclear matrix: preparation protocol for parallel microscopy and biochemical analysis, Wilson et al. 2013).

Approaches to functional analysis (for schematic see figure 1)

Electron microscopy

The resolution of the electron microscope has allowed detailed visualisation of the fibrilar protein network within the nucleus of higher eukaryotic cells (Capco et al. 1982; Fey et al. 1986; Jackson and Cook 1988). It has been viewed after RNase digestion (Berezney and Coffey 1974), DNase digestion (Capco et al. 1982), removal of chromatin by electroelution (Jackson and Cook 1988) and in a range of buffer conditions designed to minimise artefacts (Mirkovitch et al. 1984; Jackson and Cook 1988; Nickerson et al. 1997; Engelhardt 1999; Wan et al. 1999). The nuclear matrix has also been viewed in paraformaldehyde fixed sections of unextracted nuclei, identifying protein rich inter chromosomal areas consistent with the description of a NM (Hendzel et al. 1999).

Proteomic analysis

Studies to identify the component parts of the nuclear matrix were compiled in a database of Nuclear Matrix Proteins, NMPdb (Mika and Rost 2005). Since then, large-scale proteomic screens have been undertaken which compare nuclear matrix components enriched in tumour cells and at different developmental stages (Albrethsen et al. 2009; Albrethsen et al. 2010; Varma & Mishra 2011 and references therein for methods).

Analysis of attached DNA

The proteinaceous structure isolated by nuclear matrix extraction protocols is associated with residual DNA as well as RNA. Attachment of DNA was first observed by electron microscopy in the 1970s (Paulson and Laemmli 1977). Various methods have since been used to study the attached DNA, including digestion of chromatin loops with restriction enzymes, DNase I or topoisomerase II to

reveal the attachment points (Mirkovitch et al. 1984; Djeliova et al. 2001; Linnemann et al. 2009; Rivera-Mulia et al. 2011), followed by isolation and sequencing, labelling by FISH, or by incorporation of nucleotide analogues. DNA that remains attached after extraction with high salt are termed MARs (matrix attached region), and those remaining following extraction for the scaffold or skeleton are known respectively, as SARs (scaffold attached region), or skeleton-attached sequences. The possible functional significance of these classes of attachment has been reviewed previously (Wilson & Coverley 2013).

Related protocols (Maximum Fluorescence Halo Radius) that extract histones and loosely attached proteins, but which leave chromatin undigested have been used to study the DNA loops that emanate from the attachment points on the nuclear matrix (Vogelstein et al. 1980; Gerdes et al. 1994; Lemaitre et al. 2005; Guillou et al. 2010). A method combining nuclear matrix extraction with chromosome conformation capture (3C) has also recently been developed, termed M3C (Gavrilov et al. 2010).

Analysis by CSK protocol

The following method describes the protocol that we prefer to use for the analysis of nuclear matrix related functions. This incorporates serial extraction with non-ionic detergent (Triton–X-100) to remove membranes and soluble proteins under physiologically relevant salt concentrations, followed by 0.5 M NaCl, then DNase I digestion and removal of fragmented DNA. Complimentary analysis by immunoblotting and immunofluorescence reveals information on isoforms and on spatial organisation. The protocol uses cytoskeletal (CSK) buffer to stabilise the cytoskeleton and nuclear matrix in relatively gentle conditions. CSK was first used by Lenk et al. (1977) and later by Capco et al. (1982) for electron microscopy. Others have used it for immuno-detection of individual nuclear matrix components (Nickerson et al. 1992; Grondin et al. 1996; Huang et al. 2004; Boisvert et al. 2005; Ainscough et al. 2007; Campalans et al. 2007), identification of protein domains required for nuclear matrix binding (Ainscough et al. 2007), analysis of temporally regulated recruitment (Fujita 1999; Fujita et al. 2002; Miccoli et al. 2003; Samaniego et al. 2006; Sree et al. 2012), and to compare recruitment between developmental or differentiation stages and between disease states (Munkley et al. 2011). The benefits of this method include the relatively gentle buffer conditions, potential to generate robust results by using imaging and biochemical analysis in parallel, and its flexibility to incorporate high salt to reveal the core nuclear matrix, or pre-treatment with a protein-protein crosslinker to reveal those proteins only weakly associated with the nuclear matrix. It can also be combined with other cellular manipulations for specific questions, such as cell synchrony protocols, depletion by RNAi and expression of ectopic proteins. Together, these offer the potential to uncover the functional relevance of recruitment to the nuclear matrix.

Acknowledgements:

Work in this laboratory is supported by the Biotechnology and Biological Sciences Research Council, UK and Yorkshire Cancer Research, UK.

References:

Ainscough JF, Rahman FA, Sercombe H, Sedo A, Gerlach B, Coverley D. 2007. C-terminal domains deliver the DNA replication factor Ciz1 to the nuclear matrix. *J Cell Sci* **120**: 115-124.

Albrethsen J, Knol JC, Jimenez CR. 2009. Unravelling the nuclear matrix proteome. *J Proteomics* **72**: 71-81.

Albrethsen J, Knol JC, Piersma SR, Pham TV, de Wit M, Mongera S, Carvalho B, Verheul HM, Fijneman RJ, Meijer GA et al. 2010. Subnuclear proteomics in colorectal cancer: identification of

proteins enriched in the nuclear matrix fraction and regulation in adenoma to carcinoma progression. *Mol Cell Proteomics* **9**: 988-1005.

Berezney R, Coffey DS. 1974. Identification of a nuclear protein matrix. *Biochem Biophys Res Commun* **60**: 1410-1417.

Boisvert FM, Hendzel MJ, Masson JY, Richard S. 2005. Methylation of MRE11 regulates its nuclear compartmentalization. *Cell Cycle* **4**: 981-989.

Campalans A, Amouroux R, Bravard A, Epe B, Radicella JP. 2007. UVA irradiation induces relocalisation of the DNA repair protein hOGG1 to nuclear speckles. *Journal of Cell Science* **120**: 23-32.

Capco DG, Wan KM, Penman S. 1982. The nuclear matrix: three-dimensional architecture and protein composition. *Cell* **29**: 847-858.

Djeliova V, Russev G, Anachkova B. 2001. Distribution of DNA replication origins between matrix-attached and loop DNA in mammalian cells. *J Cell Biochem* **80**: 353-359.

Engelhardt M. 1999. Demonstration of a DNase-sensitive network associated with the nuclear pore complexes in rat liver nuclei. *Chromosoma* **108**: 64-71.

Fey EG, Krochmalnic G, Penman S. 1986. The nonchromatin substructures of the nucleus: the ribonucleoprotein (RNP)-containing and RNP-depleted matrices analyzed by sequential fractionation and resinless section electron microscopy. *J Cell Biol* **102**: 1654-1665.

Fujita M. 1999. Cell cycle regulation of DNA replication initiation proteins in mammalian cells. *Front Biosci* **4**: D816-823.

Fujita M, Ishimi Y, Nakamura H, Kiyono T, Tsurumi T. 2002. Nuclear organization of DNA replication initiation proteins in mammalian cells. *J Biol Chem* **277**: 10354-10361.

Fujita M, Kiyono T, Hayashi Y, Ishibashi M. 1997. In vivo interaction of human MCM heterohexameric complexes with chromatin. Possible involvement of ATP. *J Biol Chem* **272**: 10928-10935.

Gavrilov AA, Zukher IS, Philonenko ES, Razin SV, Iarovaia OV. 2010. Mapping of the nuclear matrix-bound chromatin hubs by a new M3C experimental procedure. *Nucleic Acids Res* **38**: 8051-8060.

Gerdes MG, Carter KC, Moen PT, Jr., Lawrence JB. 1994. Dynamic changes in the higher-level chromatin organization of specific sequences revealed by in situ hybridization to nuclear halos. *J Cell Biol* **126**: 289-304.

Getzenberg RH. 1994. Nuclear matrix and the regulation of gene expression: tissue specificity. *J Cell Biochem* **55**: 22-31.

Grondin B, Bazinet M, Aubry M. 1996. The KRAB zinc finger gene ZNF74 encodes an RNA-binding protein tightly associated with the nuclear matrix. *Journal of Biological Chemistry* **271**: 15458-15467.

Guillou E, Ibarra A, Coulon V, Casado-Vela J, Rico D, Casal I, Schwob E, Losada A, Mendez J. 2010. Cohesin organizes chromatin loops at DNA replication factories. *Genes Dev* **24**: 2812-2822.

Hancock R. 2000. A new look at the nuclear matrix. *Chromosoma* **109**: 219-225.

Hendzel MJ, Boisvert F, Bazett-Jones DP. 1999. Direct visualization of a protein nuclear architecture. *Mol Biol Cell* **10**: 2051-2062.

Higgins G, Roper KM, Watson IJ, Blackhall FH, Rom WN, Pass HI, Ainscough JF, Coverley D. 2012. Variant Ciz1 is a circulating biomarker for early-stage lung cancer. *Proc Natl Acad Sci U S A*.

Huang JY, Shen BJ, Tsai WH, Lee SC. 2004. Functional interaction between nuclear matrix-associated HBXAP and NF-kappa B. *Experimental cell research* **298**: 133-143.

Jackson DA, Cook PR. 1985. Transcription occurs at a nucleoskeleton. *Embo J* **4**: 919-925.

-. 1988. Visualization of a filamentous nucleoskeleton with a 23 nm axial repeat. *Embo J* **7**: 3667-3677.

Jagatheesan G, Thanumalayan S, Muralikrishna B, Rangaraj N, Karande AA, Parnaik VK. 1999. Colocalization of intranuclear lamin foci with RNA splicing factors. *Journal of Cell Science* **112**: 4651-4661.

Keesee SK, Meyer JL, Hutchinson ML, Cibas ES, Sheets EE, Marchese J, Oreper A, Potz D, Wu YJ. 1999. Preclinical feasibility study of NMP179, a nuclear matrix protein marker for cervical dysplasia. *Acta Cytol* **43**: 1015-1022.

Lemaitre JM, Danis E, Pasero P, Vassetzky Y, Mechali M. 2005. Mitotic remodeling of the replicon and chromosome structure. *Cell* **123**: 787-801.

Lenk R, Ransom L, Kaufmann Y, Penman S. 1977. A cytoskeletal structure with associated polyribosomes obtained from HeLa cells. *Cell* **10**: 67-78.

Linnemann AK, Platts AE, Krawetz SA. 2009. Differential nuclear scaffold/matrix attachment marks expressed genes. *Hum Mol Genet* **18**: 645-654.

Martelli AM, Falcieri E, Zweyer M, Bortul R, Tabellini G, Cappellini A, Cocco L, Manzoli L. 2002. The controversial nuclear matrix: a balanced point of view. *Histol Histopathol* **17**: 1193-1205.

Miccoli L, Biard DSF, Frouin I, Harper F, Maga G, Angulo JF. 2003. Selective interactions of human kin17 and RPA proteins with chromatin and the nuclear matrix in a DNA damage- and cell cycle-regulated manner. *Nucleic Acids Research* **31**: 4162-4175.

Mika S, Rost B. 2005. NMPdb: Database of Nuclear Matrix Proteins. *Nucleic Acids Res* **33**: D160-163.

Mirkovitch J, Mirault ME, Laemmli UK. 1984. Organization of the higher-order chromatin loop: specific DNA attachment sites on nuclear scaffold. *Cell* **39**: 223-232.

Munkley J, Copeland NA, Moignard V, Knight JR, Greaves E, Ramsbottom SA, Pownall ME, Southgate J, Ainscough JF, Coverley D. 2011. Cyclin E is recruited to the nuclear matrix during differentiation, but is not recruited in cancer cells. *Nucleic Acids Res* **39**: 2671-2677.

Nickerson J. 2001. Experimental observations of a nuclear matrix. *J Cell Sci* **114**: 463-474.

Nickerson JA, Krockmalnic G, Wan KM, Penman S. 1997. The nuclear matrix revealed by eluting chromatin from a cross-linked nucleus. *Proceedings of the National Academy of Sciences of the United States of America* **94**: 4446-4450.

Nickerson JA, Krockmalnic G, Wan KM, Turner CD, Penman S. 1992. A normally masked nuclear matrix antigen that appears at mitosis on cytoskeleton filaments adjoining chromosomes, centrioles, and midbodies. *J Cell Biol* **116**: 977-987.

Paulson JR, Laemmli UK. 1977. The structure of histone-depleted metaphase chromosomes. *Cell* **12**: 817-828.

Pederson T. 1998. Thinking about a nuclear matrix. *J Mol Biol* **277**: 147-159.

Qiao F, Moss A, Kupfer GM. 2001. Fanconi anemia proteins localize to chromatin and the nuclear matrix in a DNA damage- and cell cycle-regulated manner. *J Biol Chem* **276**: 23391-23396.

Reyes JC, Muchardt C, Yaniv M. 1997. Components of the human SWI/SNF complex are enriched in active chromatin and are associated with the nuclear matrix. *J Cell Biol* **137**: 263-274.

Rivera-Mulia JC, Hernandez-Munoz R, Martinez F, Aranda-Anzaldo A. 2011. DNA moves sequentially towards the nuclear matrix during DNA replication in vivo. *BMC Cell Biol* **12**: 3.

Samaniego R, Jeong SY, de la Torre C, Meier I, de la Espina SMD. 2006. CK2 phosphorylation weakens 90 kDa MFP1 association to the nuclear matrix in Allium cepa. *Journal of Experimental Botany* **57**: 113-124.

Sree NK, Anesh R, Radha V. 2012. Dynamic changes in nuclear localization of a DNA-binding protein tyrosine phosphatase TCPTP in response to DNA damage and replication arrest. *Cell Biology and Toxicology* **28**: 409-419.

Subong EN, Shue MJ, Epstein JI, Briggman JV, Chan PK, Partin AW. 1999. Monoclonal antibody to prostate cancer nuclear matrix protein (PRO:4-216) recognizes nucleophosmin/B23. *Prostate* **39**: 298-304.

Van Le TS, Myers J, Konety BR, Barder T, Getzenberg RH. 2004. Functional characterization of the bladder cancer marker, BLCA-4. *Clin Cancer Res* **10**: 1384-1391.

Varma P, Mishra RK. 2011. Dynamics of nuclear matrix proteome during embryonic development in Drosophila melanogaster. *J Biosci* **36**: 439-459.

Vogelstein B, Pardoll DM, Coffey DS. 1980. Supercoiled loops and eucaryotic DNA replicaton. *Cell* **22**: 79-85.

Wan KM, Nickerson JA, Krockmalnic G, Penman S. 1999. The nuclear matrix prepared by amine modification. *Proc Natl Acad Sci U S A* **96**: 933-938.

Wilson RH, Coverley D. 2013. Relationship between DNA replication and the nuclear matrix. *Genes Cells* **18**: 17-31.

Zeitlin S, Parent A, Silverstein S, Efstratiadis A. 1987. Pre-mRNA splicing and the nuclear matrix. *Mol Cell Biol* **7**: 111-120.

Zink D, Fischer AH, Nickerson JA. 2004. Nuclear structure in cancer cells. *Nature reviews* **4**: 677-687.

Figure legends:

Figure 1. Schematic to show available methods for analysis of the nuclear matrix and its functional significance.

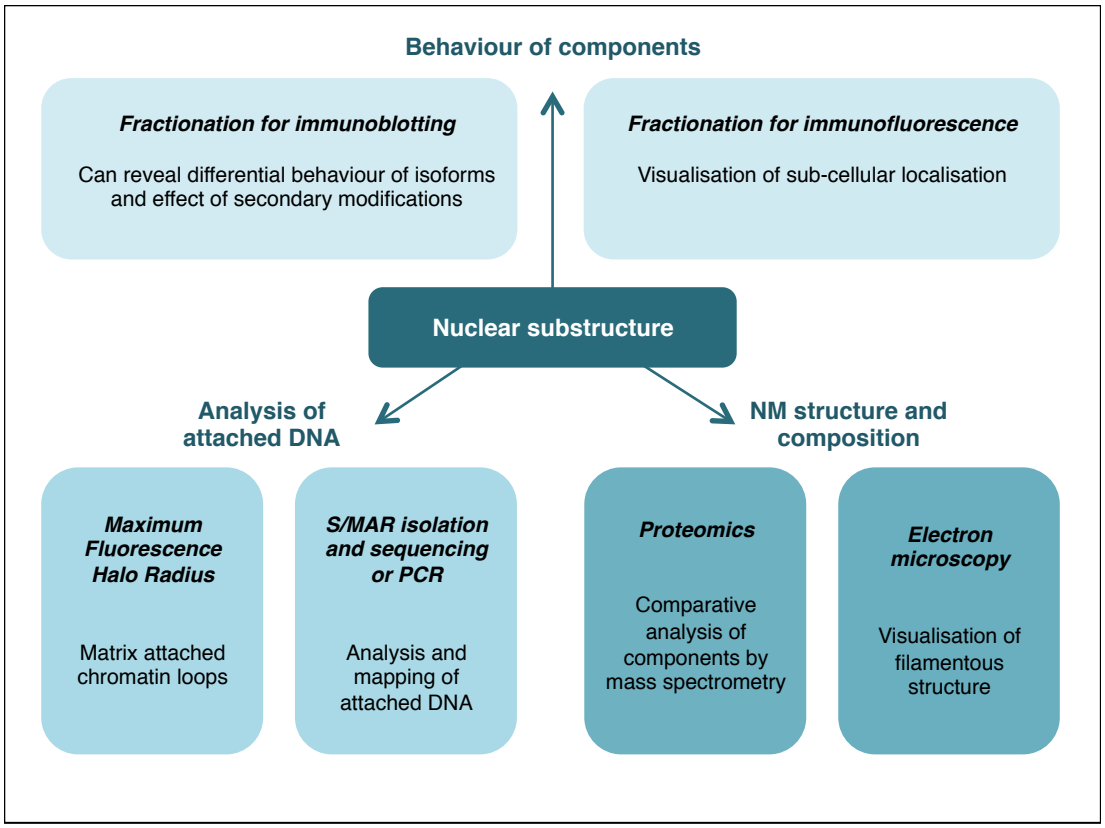
Behaviour of components
Fractionation for immunoblotting
Can reveal differential behaviour of isoforms and effect of secondary modifications
Fractionation for immunofluorescence
Visualisation of sub-cellular localisation
Nuclear substructure
Analysis of attached DNA
NM structure and composition
Maximum Fluorescence Halo Radius
Matrix attached chromatin loops
S/MAR isolation and sequencing or PCR
Analysis and mapping of attached DNA
Proteomics
Comparative analysis of components by mass spectrometry
Electron microscopy
Visualisation of filamentous structure

Protocol

The nuclear matrix: preparation protocol for parallel microscopy and biochemical analysis

Short title: Nuclear matrix protocol

Wilson, R. H. C.[1*], Hesketh, E.[1] and Coverley, D.[1]

[1] Department of Biology, University of York, Wentworth Way, York, YO10 5DD, UK

[*] Corresponding author: Wilson, R. H. C. rhcw500@york.ac.uk, 01904 328569

Abstract

The immobilisation of nuclear proteins is usually investigated using extraction with detergent to reveal attachment to insoluble structures. This is often assumed to be chromatin and is described as such in many studies. However, the detergent resistant protein fraction consists of both chromatin-bound and nuclear matrix-bound proteins. To further separate these fractions DNA should be removed and the remaining proteins visualised in comparison to those in unextracted cells. We describe two related protocols that identify nuclear matrix proteins by immunofluorescence (IF) or immuoblotting (IB). IB has the advantage of resolving different forms of a protein of interest and includes analysis of soluble fractions excluded by the IF protocol. IF analysis has the advantage of allowing individual cells to be monitored rather than homogenised populations and can be performed on very low quantity samples. Analysis by IF will also reveal the spatial arrangement of proteins bound to residual nuclear structures. These methods have been used by many labs to study nuclear matrix proteins (Nickerson et al. 1992; Blencowe et al. 1994; Fujita et al. 1997) and by our laboratory to determine protein domains required for nuclear matrix binding (Ainscough et al. 2007), shifts in protein localisation during biological transitions (Munkley et al. 2011), and absence from the nuclear matrix fraction in diseased states (Munkley et al. 2011).

Reagents

Cells grown on coverslips or cytospun onto slides (IF), or one 15 cm plate of adherent cells at > 50% confluent density (IB)

For transfected cells, first evaluate the transfection protocol for destabilizing effects on the nuclear matrix.

Cytoskeletal buffer (CSK) and derivatives. Filter sterilise and store basic buffer in 50 ml aliquots at -20°C <R>

DNase I, and buffer recommended by supplier

Determine optimal concentration, digestion time and temperature using release of DNA (IF) or chromatin bound proteins such as histone (IB) as indicator. This will vary with cell type, is unlikely to be 100% efficient and will not release MAR DNA. DNase must be RNase free (eg Roche, 04716728001). Test by incubation with prepared RNA and visualisation of products after electrophoresis.

Hoechst or DAPI DNA counterstain (IF)

Use at 0.1 µg/ml and keep constant to allow establishment of imaging conditions.

Mounting medium (IF)

Paraformaldehyde (PFA) 4% <R> (IF)

Phosphate buffered saline (PBS)

PMSF – 200 mM stock in ethanol, stored at -20°C (IB)

Primary antibody to protein of interest and secondary antibody for detection.

Concentration and conditions should be established using cells extracted with detergent. These represent a mid-point between unextracted and chromatin-depleted cells with which imaging parameters can be determined.

SDS loading buffer (4x) – standard Laemmli recipe (IB)

Sodium chloride – 5 M stock

Triton X-100 – at 1%

Equipment

13 mm glass coverslips (IF)

15 cm culture plates (IB)

24 well culture plates (IF)

Cell scraper (IB)

Fine forceps and hooked needle for moving coverslips (IF)

Fluorescent microscope with 63 x oil immersion objective and image capture system (IF)

Gel electrophoresis and Western blotting equipment (IB)

Glass slides (IF)

Heat block at 95°C (IB)

Humidified chamber such as a plastic box with sealable lid (IF)

Incubator at 37°C

Parafilm (IF)

Refridgerated microcentrifuge (IB)

Vortex (IB)

Method

1. Thaw CSK, add supplements as required. See table 1 for volumes <R>. Keep all buffers on ice. DNase I should be kept at -20°C until required.

A. Immunofluorescence

2A. Transfer cells on coverslips to PBS in 24 well plates (3-4 per sample).

Coverslips are processed throughout with cells uppermost. Coverslips can be moved between wells to change buffer, or buffers can be gently changed by pipette.

Coverslips are processed to reveal i) total protein (no extraction), ii) detergent-resistant proteins (immobilised by attachment to insoluble structures), iii) high-salt and DNase resistant proteins (bound to the nuclear matrix), iv) optional high-salt resistant proteins (tightly bound to chromatin or the nuclear matrix). For a summary of the method see figure 1A.

3A. Transfer coverslip i into 4% PFA (10 minutes, RT). Move to PBS and store at 4°C.

4A. Move remaining coverslips to CSKb (1 minute, RT). Move ii to PBS and prepare for IF as 3A.

5A. Move remaining coverslips to CSKc (1 minute, RT).

6A. Wash coverslips twice in DNase buffer (1 minute, RT).

Wash step reduces salt concentration in preparation for DNase treatment.

7A. Place coverslips on parafilm in humidified chamber. For iii add DNase I in DNase buffer, or for iv buffer only (20 µl per coverslip). Seal and incubate using optimised time and temperature.

Humidify chamber to prevent drying out by including a reservoir of sterile water (e.g. damp tissue).

8A. Move coverslips to CSKc (1 minute, RT), then PBS and prepare for IF as 3A.

9A. Coverslips should be processed as soon as possible using standard immunofluorescence protocols, and imaged using high-resolution fluorescence microscopy and appropriate image capture system.

Blocking agents such as BSA should be of ELISA grade and protease and RNase free (eg. Jackson 001-000-162). The contrast between treated and untreated samples should be verified by imaging, using the minimum effective concentration of DNA counterstain and constant image capture parameters (e.g. 10-20 ms). A dramatic reduction in DNA counterstain should be evident for DNase treated coverslips, though a small amount of DNA will remain. Immunostaining conditions and imaging should be kept constant across a sample set (e.g. 200-400 ms). DNase treated nuclei from which the protein of interest is also extracted can be hard to spot. In these cases use an RNA counterstain such as propidium iodide or co-stain for a nuclear structure protein, such as lamin B2. An example image is shown in figure 1B.

B. Immunoblotting

2B. Rinse plate with PBS, then twice with CSKa. Remove and drain plates for 2 mins at 45° on ice. Remove excess buffer then scrape harvest cells (recover ~200 µl per 15 cm plate). Measure the volume, add 2 mM PMSF and TX100 to 0.1% final concentration. Divide equally between four 500 µl eppendorfs (i, ii, iii, iv) and record volume (1 x vol).

Samples will be processed to reveal cell equivalents of 'T' total protein, 'det P' detergent-resistant pellet (proteins immobilised by attachment to insoluble structures), 'det SN' detergent-soluble supernatant, 'w' 0.5 M NaCl-soluble supernatant, 'DNase P' DNase-resistant pellet (bound to the

nuclear matrix), 'DNase SN' DNase-sensitive supernatant (bound to chromatin), 'mock P', high-salt resistant pellet (tightly bound to chromatin or the nuclear matrix) and 'mock SN' (released during control incubation). For a summary of the method see figure 1A.

3B. To i (T), add 1/3 volume of 4 x SDS loading buffer. Vortex, heat to 95°C for 5 minutes and store at -20°C.

4B. After 2 minutes on ice, centrifuge ii, iii and iv at 6800g (2 minutes, 4 °C). Transfer supernatant from ii to a fresh tube (det SN) and resuspend pellet ii in 1 x vol CSKb (det P). Prepare both for SDS-PAGE as 3B.

5B. Discard supernatant from iii and iv. Resuspend pellets in 1 x vol CSKc (2 minutes on ice) and centrifuge at 6800g (3 minutes, 4 °C). Recover supernatant from iii to a fresh tube (w). Prepare for SDS-PAGE as 3B. Discard supernatant from iv.

6B. Resuspend pellets iii and iv in ~ 100 µl DNase buffer. Centrifuge 9500g, (3 minutes, 4 °C). Discard supernatants.

7B. Resuspend pellets iii and iv in 1 x vol DNase buffer, add DNase I to iii and incubate both tubes using optimised amount, time and temperature.

8B. Add 1/10 volume 5 M NaCl to both tubes and incubate for 5 minutes. Centrifuge 9500g (5 minutes, 4 °C), transfer supernatants from tubes iii and iv to fresh tubes (DNase SN and mock SN). Resuspend pellets in 1 x vol DNase buffer (DNase P and mock P). Prepare these samples for SDS-PAGE as 3B.

Pellets iii and iv are very 'sticky' and can get stuck in the pipette tip. Resuspend by vortexing.

9B. Samples can be processed using standard SDS-PAGE and western blotting protocols.

In addition to the protein of interest, blots should be probed with a control antibody against a chromatin bound protein that is released when chromatin is digested (eg. histone H3). If studying a protein that is not normally nuclear matrix-bound a second control antibody should be used that detects an insoluble component of the nucleus (eg. lamin B2). A successful DNase extraction would be expected to release >75% of histone H3 into the DNase supernatant fraction, while retaining all histone H3 in the pellet fraction of the mock treated sample. Loss of histone from this fraction indicates contamination of buffers, or loss or degradation of residual nuclei. An example image is shown in figure 1C.

Troubleshooting

Problem: DNA or protein is not released from DNase treated sample

Solution: Optimise DNase conditions and take care to remove high-salt buffer prior to digestion. For IB, mix digestion reaction periodically during incubation to ensure resuspension of pellet, and take care to mix after NaCl addition (step 8B).

Problem: Absence of expected antigen in DNase treated samples.

Solution: Buffers may be contaminated with proteases or RNases, both of which will degrade (part of) the nuclear matrix. Buffers should be remade, possibly with RNase inhibitors and equipment cleaned. Check for presence of a protein known to be nuclear matrix bound such as lamin B2.

Related Information

The nuclear matrix can also be revealed by the use of 2.0 M NaCl – the 'core' nuclear matrix. The protocol can be adapted to use high-salt treatments instead of DNase extraction. Keeping all the cell lysate in a single tube, follow Immunoblot protocol to step 2B, then proceed by resuspending pellet in CSKb supplemented with increasing NaCl. Repeat with 100mM stepwise increases in NaCl up to 1M, collecting each supernatant and the final pellet as separate samples (Ainscough et al. 2007).

Alternatively, the protocol can be adapted to reveal proteins associated with the nuclear matrix but less tightly bound. In this case a protein-protein cross-linker such as DTSP can be used before extraction to preserve protein complexes. For method see (Fujita et al. 1999).

For further information regarding alternative methods for extracting the nuclear matrix, see The nuclear matrix: fractionation techniques and analysis (Wilson et al. 2013).

Recipes:

<R>		Components	Recipe (per 50ml)	*Vol per 3 sets of 4 coverslips* (IF)	*Vol per 3 15cm plates* (IB)
Cyto-skeletal buffer (CSK)	a	10mM PIPES/KOH pH 6.8 100mM NaCl 300mM Sucrose 1mM EGTA 1mM $MgCl_2$ Immediately before use add:- 1mM DTT Protease inhibitor cocktail (eg Roche, 05 056 489 001)	0.5ml of 1M 1ml of 5M 5.135g 0.2ml of 250mM 50µl of 1M 50ul of 1M 1 tablet	50ml	100ml
CSK 0.1% TX100	b	Add 0.1% Triton X-100	0.5ml of 10% TX100	5ml	1ml
CSK 0.1% TX100 high-salt	c	Add 0.1% Triton X-100 0.5M NaCl	0.5ml of 10% TX100 4ml of 5M	2ml	1ml
PFA		4% paraformaldehyde 50mM HEPES/KOH 7.8	2g 2.5ml of 1M stock	6ml	-

Acknowledgements

Work in this laboratory is supported by the Biotechnology and Biological Sciences Research Council, UK and Yorkshire Cancer Research, UK.

References:

Ainscough JF, Rahman FA, Sercombe H, Sedo A, Gerlach B, Coverley D. 2007. C-terminal domains deliver the DNA replication factor Ciz1 to the nuclear matrix. *J Cell Sci* **120**: 115-124.

Albrethsen J, Knol JC, Jimenez CR. 2009. Unravelling the nuclear matrix proteome. *J Proteomics* **72**: 71-81.

Albrethsen J, Knol JC, Piersma SR, Pham TV, de Wit M, Mongera S, Carvalho B, Verheul HM, Fijneman RJ, Meijer GA et al. 2010. Subnuclear proteomics in colorectal cancer: identification of proteins enriched in the nuclear matrix fraction and regulation in adenoma to carcinoma progression. *Mol Cell Proteomics* **9**: 988-1005.

Berezney R, Coffey DS. 1974. Identification of a nuclear protein matrix. *Biochem Biophys Res Commun* **60**: 1410-1417.

Blencowe BJ, Nickerson JA, Issner R, Penman S, Sharp PA. 1994. Association of nuclear matrix antigens with exon-containing splicing complexes. *J Cell Biol* **127**: 593-607.

Boisvert FM, Hendzel MJ, Masson JY, Richard S. 2005. Methylation of MRE11 regulates its nuclear compartmentalization. *Cell Cycle* **4**: 981-989.

Campalans A, Amouroux R, Bravard A, Epe B, Radicella JP. 2007. UVA irradiation induces relocalisation of the DNA repair protein hOGG1 to nuclear speckles. *Journal of Cell Science* **120**: 23-32.

Capco DG, Wan KM, Penman S. 1982. The nuclear matrix: three-dimensional architecture and protein composition. *Cell* **29**: 847-858.

Coverley D, Marr J, Ainscough J. 2005. Ciz1 promotes mammalian DNA replication. *J Cell Sci* **118**: 101-112.

Djeliova V, Russev G, Anachkova B. 2001. Distribution of DNA replication origins between matrix-attached and loop DNA in mammalian cells. *J Cell Biochem* **80**: 353-359.

Engelhardt M. 1999. Demonstration of a DNase-sensitive network associated with the nuclear pore complexes in rat liver nuclei. *Chromosoma* **108**: 64-71.

Fey EG, Krochmalnic G, Penman S. 1986. The nonchromatin substructures of the nucleus: the ribonucleoprotein (RNP)-containing and RNP-depleted matrices analyzed by sequential fractionation and resinless section electron microscopy. *J Cell Biol* **102**: 1654-1665.

Fujita M. 1999. Cell cycle regulation of DNA replication initiation proteins in mammalian cells. *Front Biosci* **4**: D816-823.

Fujita M, Ishimi Y, Nakamura H, Kiyono T, Tsurumi T. 2002. Nuclear organization of DNA replication initiation proteins in mammalian cells. *J Biol Chem* **277**: 10354-10361.

Fujita M, Kiyono T, Hayashi Y, Ishibashi M. 1997. In vivo interaction of human MCM heterohexameric complexes with chromatin. Possible involvement of ATP. *J Biol Chem* **272**: 10928-10935.

Fujita M, Yamada C, Goto H, Yokoyama N, Kuzushima K, Inagaki M, Tsurumi T. 1999. Cell cycle regulation of human CDC6 protein. Intracellular localization, interaction with the human mcm complex, and CDC2 kinase-mediated hyperphosphorylation. *J Biol Chem* **274**: 25927-25932.

Gavrilov AA, Zukher IS, Philonenko ES, Razin SV, Iarovaia OV. 2010. Mapping of the nuclear matrix-bound chromatin hubs by a new M3C experimental procedure. *Nucleic Acids Res* **38**: 8051-8060.

Gerdes MG, Carter KC, Moen PT, Jr., Lawrence JB. 1994. Dynamic changes in the higher-level chromatin organization of specific sequences revealed by in situ hybridization to nuclear halos. *J Cell Biol* **126**: 289-304.

Getzenberg RH. 1994. Nuclear matrix and the regulation of gene expression: tissue specificity. *J Cell Biochem* **55**: 22-31.

Grondin B, Bazinet M, Aubry M. 1996. The KRAB zinc finger gene ZNF74 encodes an RNA-binding protein tightly associated with the nuclear matrix. *Journal of Biological Chemistry* **271**: 15458-15467.

Guillou E, Ibarra A, Coulon V, Casado-Vela J, Rico D, Casal I, Schwob E, Losada A, Mendez J. 2010. Cohesin organizes chromatin loops at DNA replication factories. *Genes Dev* **24**: 2812-2822.

Hancock R. 2000. A new look at the nuclear matrix. *Chromosoma* **109**: 219-225.

Hendzel MJ, Boisvert F, Bazett-Jones DP. 1999. Direct visualization of a protein nuclear architecture. *Mol Biol Cell* **10**: 2051-2062.

Higgins G, Roper KM, Watson IJ, Blackhall FH, Rom WN, Pass HI, Ainscough JF, Coverley D. 2012. Variant Ciz1 is a circulating biomarker for early-stage lung cancer. *Proc Natl Acad Sci U S A*.

Huang JY, Shen BJ, Tsai WH, Lee SC. 2004. Functional interaction between nuclear matrix-associated HBXAP and NF-kappa B. *Experimental cell research* **298**: 133-143.

Jackson DA, Cook PR. 1985. Transcription occurs at a nucleoskeleton. *Embo J* **4**: 919-925.

-. 1988. Visualization of a filamentous nucleoskeleton with a 23 nm axial repeat. *Embo J* **7**: 3667-3677.

Jagatheesan G, Thanumalayan S, Muralikrishna B, Rangaraj N, Karande AA, Parnaik VK. 1999. Colocalization of intranuclear lamin foci with RNA splicing factors. *Journal of Cell Science* **112**: 4651-4661.

Keesee SK, Meyer JL, Hutchinson ML, Cibas ES, Sheets EE, Marchese J, Oreper A, Potz D, Wu YJ. 1999. Preclinical feasibility study of NMP179, a nuclear matrix protein marker for cervical dysplasia. *Acta Cytol* **43**: 1015-1022.

Lemaitre JM, Danis E, Pasero P, Vassetzky Y, Mechali M. 2005. Mitotic remodeling of the replicon and chromosome structure. *Cell* **123**: 787-801.

Lenk R, Ransom L, Kaufmann Y, Penman S. 1977. A cytoskeletal structure with associated polyribosomes obtained from HeLa cells. *Cell* **10**: 67-78.

Linnemann AK, Platts AE, Krawetz SA. 2009. Differential nuclear scaffold/matrix attachment marks expressed genes. *Hum Mol Genet* **18**: 645-654.

Martelli AM, Falcieri E, Zweyer M, Bortul R, Tabellini G, Cappellini A, Cocco L, Manzoli L. 2002. The controversial nuclear matrix: a balanced point of view. *Histol Histopathol* **17**: 1193-1205.

Miccoli L, Biard DSF, Frouin I, Harper F, Maga G, Angulo JF. 2003. Selective interactions of human kin17 and RPA proteins with chromatin and the nuclear matrix in a DNA damage- and cell cycle-regulated manner. *Nucleic Acids Research* **31**: 4162-4175.

Mika S, Rost B. 2005. NMPdb: Database of Nuclear Matrix Proteins. *Nucleic Acids Res* **33**: D160-163.

Mirkovitch J, Mirault ME, Laemmli UK. 1984. Organization of the higher-order chromatin loop: specific DNA attachment sites on nuclear scaffold. *Cell* **39**: 223-232.

Munkley J, Copeland NA, Moignard V, Knight JR, Greaves E, Ramsbottom SA, Pownall ME, Southgate J, Ainscough JF, Coverley D. 2011. Cyclin E is recruited to the nuclear matrix during differentiation, but is not recruited in cancer cells. *Nucleic Acids Res* **39**: 2671-2677.

Nickerson J. 2001. Experimental observations of a nuclear matrix. *J Cell Sci* **114**: 463-474.

Nickerson JA, Krockmalnic G, Wan KM, Penman S. 1997. The nuclear matrix revealed by eluting chromatin from a cross-linked nucleus. *Proceedings of the National Academy of Sciences of the United States of America* **94**: 4446-4450.

Nickerson JA, Krockmalnic G, Wan KM, Turner CD, Penman S. 1992. A normally masked nuclear matrix antigen that appears at mitosis on cytoskeleton filaments adjoining chromosomes, centrioles, and midbodies. *J Cell Biol* **116**: 977-987.

Paulson JR, Laemmli UK. 1977. The structure of histone-depleted metaphase chromosomes. *Cell* **12**: 817-828.

Pederson T. 1998. Thinking about a nuclear matrix. *J Mol Biol* **277**: 147-159.

Qiao F, Moss A, Kupfer GM. 2001. Fanconi anemia proteins localize to chromatin and the nuclear matrix in a DNA damage- and cell cycle-regulated manner. *J Biol Chem* **276**: 23391-23396.

Reyes JC, Muchardt C, Yaniv M. 1997. Components of the human SWI/SNF complex are enriched in active chromatin and are associated with the nuclear matrix. *J Cell Biol* **137**: 263-274.

Rivera-Mulia JC, Hernandez-Munoz R, Martinez F, Aranda-Anzaldo A. 2011. DNA moves sequentially towards the nuclear matrix during DNA replication in vivo. *BMC Cell Biol* **12**: 3.

Samaniego R, Jeong SY, de la Torre C, Meier I, de la Espina SMD. 2006. CK2 phosphorylation weakens 90 kDa MFP1 association to the nuclear matrix in Allium cepa. *Journal of Experimental Botany* **57**: 113-124.

Sree NK, Anesh R, Radha V. 2012. Dynamic changes in nuclear localization of a DNA-binding protein tyrosine phosphatase TCPTP in response to DNA damage and replication arrest. *Cell Biology and Toxicology* **28**: 409-419.

Subong EN, Shue MJ, Epstein JI, Briggman JV, Chan PK, Partin AW. 1999. Monoclonal antibody to prostate cancer nuclear matrix protein (PRO:4-216) recognizes nucleophosmin/B23. *Prostate* **39**: 298-304.

Van Le TS, Myers J, Konety BR, Barder T, Getzenberg RH. 2004. Functional characterization of the bladder cancer marker, BLCA-4. *Clin Cancer Res* **10**: 1384-1391.

Varma P, Mishra RK. 2011. Dynamics of nuclear matrix proteome during embryonic development in Drosophila melanogaster. *J Biosci* **36**: 439-459.

Vogelstein B, Pardoll DM, Coffey DS. 1980. Supercoiled loops and eucaryotic DNA replicaton. *Cell* **22**: 79-85.

Wan KM, Nickerson JA, Krockmalnic G, Penman S. 1999. The nuclear matrix prepared by amine modification. *Proc Natl Acad Sci U S A* **96**: 933-938.

Wilson RH, Coverley D. 2013. Relationship between DNA replication and the nuclear matrix. *Genes Cells* **18**: 17-31.

Zeitlin S, Parent A, Silverstein S, Efstratiadis A. 1987. Pre-mRNA splicing and the nuclear matrix. *Mol Cell Biol* **7**: 111-120.

Zink D, Fischer AH, Nickerson JA. 2004. Nuclear structure in cancer cells. *Nature reviews* **4**: 677-687.

Figure legends:

Figure 1. A. Flow diagram to represent *in situ* nuclear matrix extraction using Immunofluorescence and Immunoblot (P = pellet, SN = supernatant). **B.** Images show CIZ1 protein (red, detected with α-CIZ1 1793, Coverley et al. 2005) in unextracted nuclei from murine 3T3 cells (total) and after extraction to reveal detergent resistant, or DNase I resistant fractions. Nuclei are counterstained with Hoechst H33258 (blue). Bar=10 mm. **C.** Western blot of protein fractions derived from murine 3T3 cells showing total protein (T), and detergent resistant (P), detergent soluble (SN), 0.5M salt sensitive (w), DNase I resistant (P), DNase I soluble fractions (SN), and mock incubation in the absence of DNase I. CIZ1 (Novus Biologicals 74623) is detected in the DNase pellet fraction revealing it to be a nuclear matrix protein. The presence of lamin B2 (Abcam: ab151735) in DNase pellet confirms the nuclear matrix fraction, and extent of histone H3 release (Abcam: ab1791) into the DNase I SN fraction shows the efficiency of chromatin digestion.

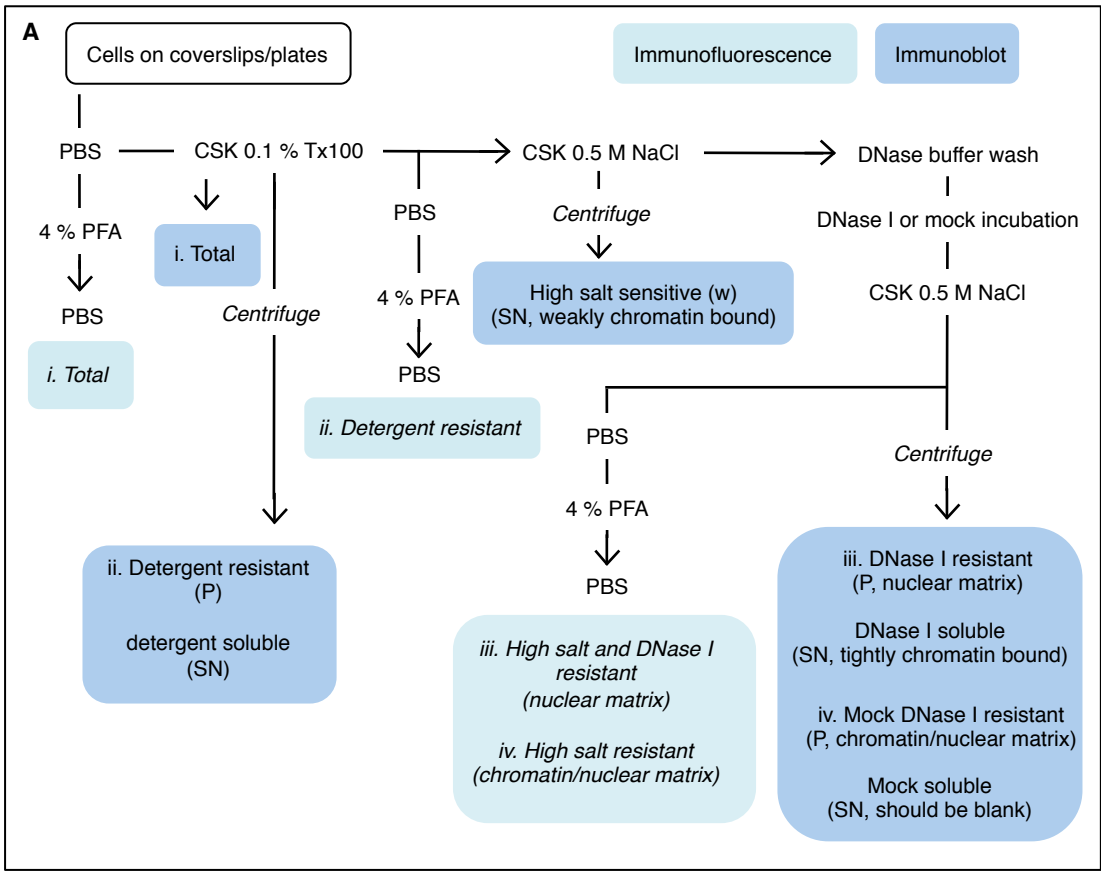
A
Cells on coverslips/plates
Immunofluorescence
Immunoblot
PBS
CSK 0.1 % Tx100
CSK 0.5 M NaCl
DNase buffer wash
4 % PFA
i. Total
PBS
Centrifuge
DNase I or mock incubation
i. Total
Centrifuge
4 % PFA
High salt sensitive (w)
(SN, weakly chromatin bound)
CSK 0.5 M NaCl
PBS
ii. Detergent resistant
PBS
Centrifuge
4 % PFA
ii. Detergent resistant
(P)
detergent soluble
(SN)
PBS
iii. DNase I resistant
(P, nuclear matrix)
DNase I soluble
(SN, tightly chromatin bound)
iii. High salt and DNase I resistant
(nuclear matrix)
iv. High salt resistant
(chromatin/nuclear matrix)
iv. Mock DNase I resistant
(P, chromatin/nuclear matrix)
Mock soluble
(SN, should be blank)

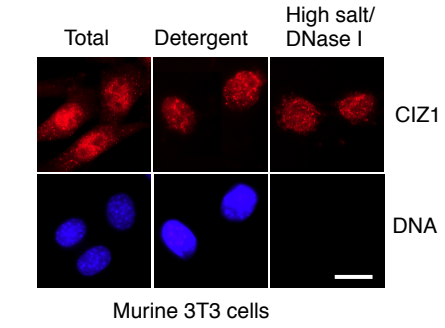
B
Total
Detergent
High salt/
DNase I
CIZ1
DNA
Murine 3T3 cells

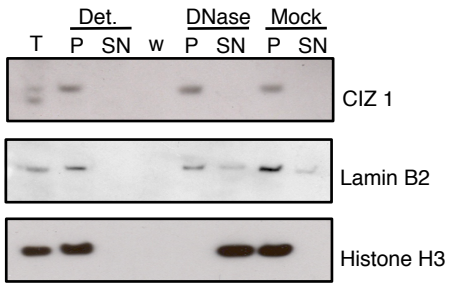
C
Det.
DNase
Mock
T
P
SN
w
P
SN
P
SN
CIZ 1
Lamin B2
Histone H3